UNIVERSITA' DEGLI STUDI DI PARMA

Dottorato di ricerca in Scienze Chimiche

Ciclo XXV (2010-2012)

Innovative metal-based catalytic systems for ecofriendly processes

Coordinatore:
Chiar.mo Prof. Predieri Giovanni

Tutor:
Chiar.mo Prof. Moggi Pietro

Dottorando: Frittella Valerio

2013

Ad Alessandra

ed alla mia famiglia

Contents

Introduction

Catalysts are very important components in industrial plants, in almost all productive processes. The catalysis science can be divided in homogeneous or heterogeneous catalysis. In biological systems, catalysts known as enzymes make process to assure the life in all living organisms. In this work we focused on the synthesis of metal-based heterogeneous catalysts for ecocompatible processes, with particular attention on Fischer-Tropsch synthesis. Fischer-Tropsch synthesis is a process to obtain hydrocarbons in a wide range in alternative to fossil reserves. Many catalysts are synthesized, characterized and tested in order to found the best procedure that brings to a very active catalyst by avoiding as much as possible undesirable byproducts.

The techniques of synthesis, the methods of characterization, the plants for catalytic tests and the raw materials are so similar to those for ammonia synthesis that it seems to be natural to expand the research also in this section.

In the synthesis of catalysts, many techniques can be used, as vapour phase deposition, precipitation and co-precipitation, impregnation, sol-gel techniques and others. We used sol-gel techniques, in comparison with impregnation methods, in order to obtain metal nanoparticles dispersed over different supports. The advantage of the sol-gel technique is the simplicity, the rapidity and reproducibility, and the low cost of raw materials (in general metal alkoxides).

By this method we realized a wide range of inorganic supports, such as alumina, silica, titania or magnesia, on which we deposited the active phases, after their formation, with impregnation methods, or during the synthesis, with bulk sol-gel or anchoring methods.

Characterizations of produced catalysts were made by using many techniques as: Temperature Programmed Reduction (TPR), Temperature Programmed Oxidation (TPO), Hydrogen Temperature Programmed Desorption (H_2-TPD), BET Surface Area (single point), X-Ray Diffraction (XRD) and Infrared Spectroscopy (FT-IR). Also Scanning Electronic Microscopy (SEM) and Transmission Electron Microscopy (TEM) were used for the characterization, according to our collaboration with other laboratories, in particular with the Department of Physics of “Università degli Studi di Perugia”.

All catalytic tests were carried out in our laboratory plants, at low pressure or at atmospheric pressure, at different temperatures.

Section 1: General

Chapter 1 – Catalysts

1.1 – Catalysis

With the name of "Catalysis" chemists intend a complex of phenomena finalized to increase of several order of magnitude the rate of a general chemical process. The term "catalysis" was invented in 1835 by Berzelius, following the observation that some chemical reactions were accelerated by the addition of substances that do not seem to participate to the reaction. Further studies of successive years demonstrated that catalysis is fundamental in biology. This type of catalysts were called enzymes. Usually a catalyst is defined as a substance that accelerates the reaction but remains unaltered after the reaction. We think that the right definition of catalyst is the following:

"a *catalyst is a substance, or a mix of substances, that change the rate of a chemical reaction or process providing an alternative reaction path but it does not modify thermodynamic factors. The catalyst usually returns at the original state after the reaction".*

In FIG. 1.1[1] the reactive path is represented for a generic reaction without (black line) and with the help of catalyst (red line).

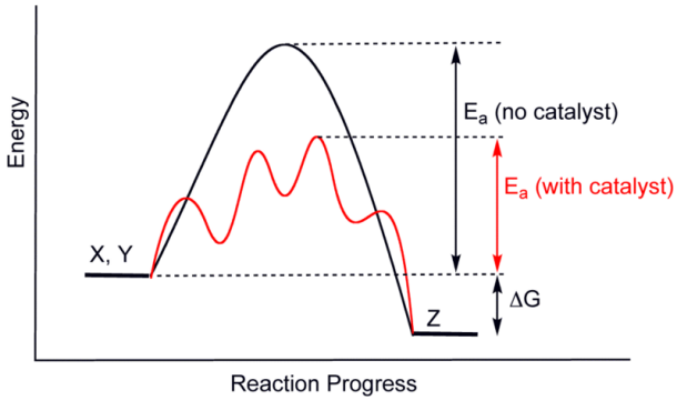

FIG. 1.1: Different paths of catalyzed and uncatalyzed reaction.

There are a lot of applications that use catalytic systems; in chemical industries almost all processes are catalyzed[2]:

- in basic chemistry, for the synthesis of organic and inorganic compounds;

- in petrochemistry, for the synthesis of intermediates and polymers;
- in refining, for catalytic cracking and hydrotreatments;
- in environmental technologies, for the abatement of pollutants and emissions from vehicles;
- in fine chemical industries, for the synthesis of intermediates and final products.

There are two main type of catalysis: heterogeneous and homogeneous catalysis. In the homogeneous catalysis the catalyst and the reagents are in the same phase; typical homogeneous catalysts are acids, bases, salts or organometallic compounds. In the heterogeneous catalysis reagents, products and catalysts are in different phases; usually heterogeneous catalysts are inorganic solids (as oxides, sulphur compounds, metals), or organic solids (as polymers).

The two type of catalysis present different advantages and disadvantages. In the homogeneous catalysis there is generally a more complete utilization of catalysts, higher selectivity for desired products with respect to the heterogeneous process, better temperature control and mild reaction conditions. However, the separation and recovery of catalysts is often difficult, there can be problems of corrosion and contamination of products and treatment of effluent is often an expensive step. On the other hand, in the field of heterogeneous catalysis the separation between catalyst and products is easier than the homogeneous one, problems of corrosion and problems for the effluent treatment are absent. Indeed, problems for the control of highly exothermic reactions can be observed; furthermore this type of catalysis requires high mechanical resistance.

The criteria for the choise of a catalyst are in general based on the same properties:

- activity: a catalyst must show high conversion and reaction rate;
- selectivity: the catalysts must lead to the desired products, avoiding as much as possible the byproducts;
- life: longer life of a catalyst assures an abatement of costs;
- regenerability;
- low toxicity;
- low costs.

In the case of Fischer-Tropsch synthesis and also in the ammonia production plants, industries use different kind of catalysts: for example in Fischer-Tropsch synthesis Cobalt and Iron are usually used as catalysts[3] as well as Iron and, in recent years, Ruthenium in the ammonia production

factory are used as active phases. However, in both case the catalysts are in solid phase while the reagents are gaseous; these experimental conditions correspond to the case of heterogeneous catalysis.

In general, in heterogeneous catalysts different components can be observed. The most important are the active phases, which are the parts that really catalyze the reactions by its interaction with reagents. The support is in general the massive part of the catalyst and it has a lot of functions, but the main is the structural one. Often also a promoter can be used. It stabilizes physical properties (physical promoters) or it helps the active phase for the conversion or selectivity (chemical promoters).

1.2 – Sol-gel technique

Sol-gel process is the technique choosen for the preparation of most our catalysts. This choice was driven by the intrinsic characteristics of this method. These characteristics can be summarized as follows:

- easy procedures of synthesis;
- high purity of products;
- control of final properties;
- control of homogeneity of composition;
- operations at room temperature;
- possibility of “single-step” synthesis
- possibilitiy of different final forms.

The sol-gel process involves at first the formation of a sol, that is a liquid suspension of solid particles with size between 1 nm and 1 micron, obtained by partial hydrolysis and condensation of opportune precursors (ex. metal alkoxides). Further condensation between particles brings to the formation of a tridimensional network that encapsulates the solvent. This biphasic system is the gel[3]. The solvent can be removed by evaporation or by supercritical drying; the final product is called xerogel or aerogel, respectively. The sol-gel technique requires four main steps in order to obtain a powder useful in catalysis:

1. gelification;

2. aging;
3. drying;
4. calcination.

The passage from sol to gel takes place by reactions of hydrolysis and condensation. Usual precursors for these reactions are metal alkoxides, that permit to obtain the gel in form of metal oxide and release the alcohol correspondent to the alkoxide.

When the sol is formed, the addition of water causes the gelification through reactions of hydrolysis and condensation as can be seen in the following schemes:

Hydrolysis:

$$M(OR)_n + nH_2O \rightarrow M(OH)_n + nROH$$

Condensation:

$$-MOH + -MOH \rightarrow -MOM- + H_2O$$

$$-MOH + MOR \rightarrow -MOM- + ROH$$

$$-MOR + -MOR \rightarrow -MOM- + ROR$$

These reactions can take place also under different conditions, for example with the help of acids or basis as catalysts.

In the case of acid catalysts, the reaction of hydrolysis follows the path illustrated in the FIG. 1.2

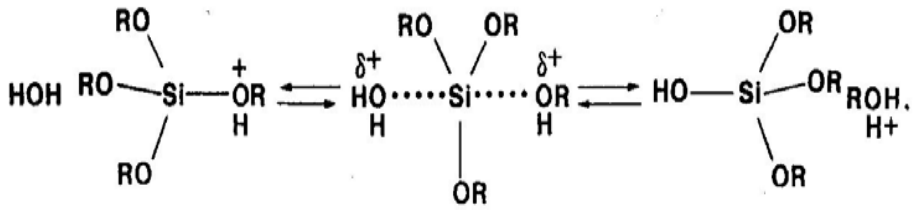

FIG. 1.2: Acid catalyzed hydrolysis for $Si(OR)_4$ compounds

If the hydrolysis is carried out with the help of basic catalysts, the reaction follows the mechanism reported in FIG. 1.3

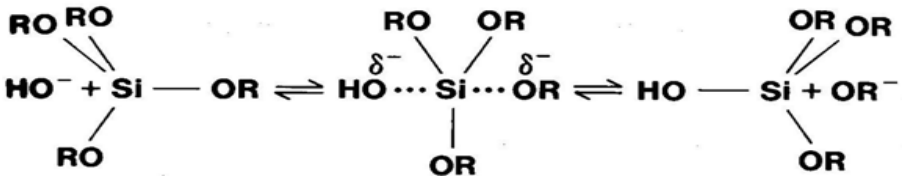

FIG. 1.3: Base catalyzed hydrolysis for $Si(OR)_4$ compounds

The use of acid or basic catalysts during the gel formation drives the formation of gel to different final structures of network. In fact, the control of pH of the solution is very important. We must consider that under basic conditions, at high pH values, the rate of hydrolysis is slow while the rate of condensation is high. This is reflected in the formation of a network with short chains and higher number of branching. On the contrary, in the case of conditions of lower pH values, the rate of hydrolysis is faster and the rate of condensation decreases, as well as the degree of substitution is decreased. The gel formed under these conditions results more linear and less branched than the other one. In FIG. 1.4 is showed the path of sol-gel process under basic and acid conditions respectively. In our work, most of sol-gel synthesis were carried out at neutral conditions, avoiding the help of catalysts for the gelification.

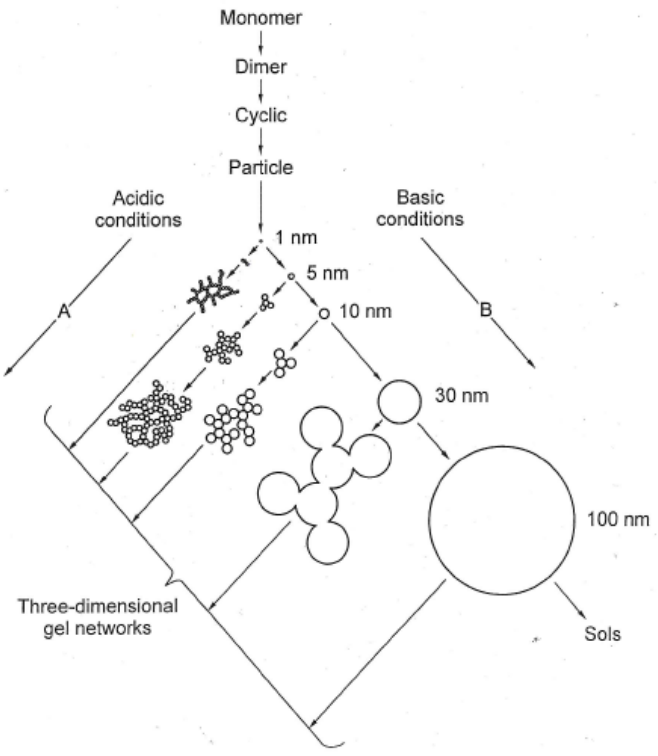

FIG. 1.4: Structural development of gel

Other factors can play an important role in the gelification process. An increase of temperature, for example, leads to an high increase in the speed of the hydrolysis and condensation reactions, that is reflected in an high increase of the rate of gel formation.

Another important factor is the ratio (R) between the water used for the gelification and the number of alkoxide groups.

$$R = \frac{moles\ of\ water}{number\ of\ alkoxides\ groups} \qquad (1)$$

This ratio is very important because the amount of water influences the hydrolysis step. Three general cases can be taken into consideration in order to describe this factor:

A) R<1: in this case the number of moles of water is smaller than that of the alkoxide groups. Then water molecules are not enough for a complete hydrolysis of –OR groups. Under these conditions the condensation is favoured with respect to hydrolysis and not all metal alkoxide molecules are able to gelificate without the help of an excess of water.
B) R=1: this case reflects the ideal ratio but, although the polymerization can be carried out by the hydrolysis steps, the branching is disfavoured and the reaction drives to the formation of linear products.
C) R>1: this case occurs when water is added in excess with respect to alkoxide groups. The water excess helps the formation of the inorganic polymer, with an high number of branching. The powder formed in this case results better for the use as support, by the high surface area resulting from the evaporation of solvent that assure an high porosity of the material. However, it is good to remember that the effect of an excess of water is related to the decrease of the gelification rate.

In this research project, for all the syntheses of catalysts using the sol-gel method, the water/alkoxide ratio was choosen as R = 2.

Two other factors are considered during the catalyst synthesis: the nature of the solvent and the nature of the precursors. About the nature of the solvent, the choice was driven in each synthesis by the type of alkoxide groups. In general, we have chosen the alcohol correspondent or more similar to the alkoxide group. The exchange of alkyl group between solvent and metal alkoxide often occurs and this fact can change the velocity of the process. Our choice is driven by the avoiding of this fact as much as possible. Another consideration must be made for the proticity of

the solvents. The hydrolysis and condensation reactions are nucleophilic, and the use of aprotic solvents can boost those processes. However, in our case, only protic solvents (alcohol) are used. By the consideration that both reactions of hydrolysis and condensation are nucleophilic substitutions, it is clear that the reactivity of systems is strongly dependent on the partial positive charge and on the metal. In the case of gelification of multiple metal alkoxides, it is important to consider that the preferred reaction is that one which involves the condensation between the same metal alkoxide, caused by the different hydrolytic velocities. The preferred polymer is therefore the result of an homopolymerization with respect to the heteropolymerization. Also the alkoxide groups can play an important role. The difference in the length of hydrocarbon chains is critical during hydrolysis and condensation reactions, by the capacity of stabilizing the positive charge on metal atom. The gelification with precursors with short hydrocarbon chains takes place with higher velocity than a gelification with longer chain precursors.

The passage from a viscous fluid to an elastic solid is the gelation step. After that, the network of the gel is formed with the solvent encapsulated inside the structure. At this point the step known as “aging” takes place. Despite the gel is formed, other reactions can occur by some sites not yet utilized. This fact gives a further poly-condensation and increases the branching and the connectivity of the network. Furthermore, the drying process of gel follows the gelification. The solvent begins to evaporate from the system. Now it is important to consider that the pores of the network are emptied from the solution, but the emptying takes place with a different rate in relation to their diameter, as can be seen from the equation (2):

$$ln\frac{P}{P_0} = -\frac{V2\sigma cos\theta}{rRT} \qquad (2)$$

where:

P = vapor pressure;

P_0 = saturation vapor pressure;

V = molar volume of the liquid;

σ = surface tension of the liquid;

θ = contact angle between liquid and solid;

r = pore radius.

By defining that P_c is the capillary pressure:

$$P_c = \frac{2\sigma cos\theta}{r} \quad (3)$$

the equation (2) becomes:

$$\ln \frac{P}{P_0} = - \frac{VP_c}{RT} \quad (4)$$

This equation gives as result that the evaporation (called syneresis) is faster in the bigger pores with respect to the smaller ones. Under this conditions, the network of inorganic polymer starts to crash because the capillary pressure of smaller pores causes the breaking of the walls of larger pores. The tridimensional network starts to collapse until the gel is transformed into a fine powder.

The last step of sol-gel procedure is the thermal treatment called “calcination”. The powder obtained after the drying of the gel is completely recovered by hydroxide groups, and sometimes by alkoxide groups. These groups are able to give other condensation reactions. This last step is required in order to assure the chemical stabilization of the system. The powder is heated in an oven at high temperatures (up to 350°C) in air and the –OH functions, as well as –OR groups eventually remained, are transformed in oxygen bonds with the expulsion of water (or alcohol) molecules.

Bibliography

[1] en.wikipedia.org/wiki/Catalysis

[2] F. Cavani; F. Trifirò; **"The catalytic process from laboratory to the industrial plant"** *Chapter 1: Classification of industrial catalysts and catalysis for the petrochemical industry; Ed. D. Sanfilippo, 1994*

[3] E.I. Ko; **"Preparation of solid catalysts"**; *Capter 3.5: Sol-Gel Process Ed. G. Ertl, H. Knözinger, J. Weitkamp*

Chapter 2 – Catalyst preparation methods

2.1 – Impregnation

The impregnation is the most used method[1,2,3] in the preparation of heterogeneous catalysts. By this technique the active species are transported by diffusion motions into the pores of the surface of the supporting material. The transport and the deposition on the surface of the support are carried out through a solvent in which the precursors of the active species are dissolved. The advantage of this method is that the active species are completely dispersed on the surface of the support.

There can be applied two types of impregnation: impregnation in bulk and to incipient wetness. The impregnation in bulk is used when the support is able to establish some interactions with the precursors of active phases dissolved in the solvent. On the contrary, the other method is used when the absorbing capacity of the support is very low. In this case, before the addition of the active species, the incipient wetness point must be determined. This is defined as: the amount of solution needed to wet all the support avoiding the separation of a liquid phase from the surface. Usually the incipient wetness point is calculated over a little amount of support by the addition of the solvent and it is expressed as the volume, in ml of liquid, that wet 1 g of support.

However, in our case most of supports have been prepared by a sol-gel technique.

2.2 – Bulk sol-gel

This method of preparation of the catalyst is a simple gelification[1,2,4,5], as described in the previous chapter. The precursors of the metals used as active phases are added to the sol, before starting the process. The metals are added often as salts, or sometimes as metallic clusters. The metal precursor added to the sol remains into the network when gelification occurs; then, after the further step, the metal is situated inside the pores on the surface of the powder formed. The procedure is probably the most rapid and easiest among the various techniques of catalyst preparation but there is the risk that a few amount of metal is encapsulate inside the structure of the support, then losing its activity for catalysis. In our case, metal nitrates were used as

precursors for the synthesis from metal salts. By this method, a solution of the metal salt usually dissolved in an alcohol, is added to the sol. The gelification step involves the metal alkoxides precursors of the support and the metal salts precursors of the active species. After the gelification the further steps proceed as described into the previous chapter.

2.3 – Anchoring

The anchoring technique[6] requires the setting up of chemical bonds between the support surface and the deposited precursors of the active phase. Inorganic matrices made by sol-gel techniques are often used as support for the anchorage. The support is usually thermally pre-treated, (for instance, heated in an oven), in order to be sure that the system is dry. When the support, with functional groups available on the surface, is kept in contact with the precursor of the metal, a chemical interaction is established and the active phase is then chemically bonded over the surface of the support by reactions of condensation or oxidative addition, as can be seen in the following equations.

$$Y[supp - OH] + MX_n \rightarrow [supp - O]_y MX_{n-y} + yHX$$

$$[supp - OH] + M_3CO_{12} \rightarrow [supp - O]M_3H(CO)_{10} + 2CO$$

The precursor is partially transformed. The system is then activated in order to obtain the active phase in the desired form.

An interesting application of this method is the preparation of “egg-shell” catalysts. This method requires that the support is preliminarly prepared by asol-gel method, but without the calcination step. This part of the supporting surface is called “core”. By avoiding the last step of chemical stabilization, a large amount of hydroxide groups remains over the surface of the core. At this point, a sol, containing the same or another metal alkoxide, is added to the preformed core. The sol also contains the precursor of the active phase. Under these conditions, the second sol is able to react by condensation with the hydroxide groups present on the surface of the core. Then it occurs a second gelification over the support already prepared by sol-gel. The metal precursor remains encapsulate into the structure of the gel, but only in the upper layer. Further steps of

aging, drying and calcination proceed following the same steps of the sol-gel method. By this procedure we can obtain an upper layer called “egg-shell” over the supporting core. The active phase is then deposited by a sol-gel method, but avoiding the loss of material inside the structure, typical in the classic bulk sol-gel techniques.

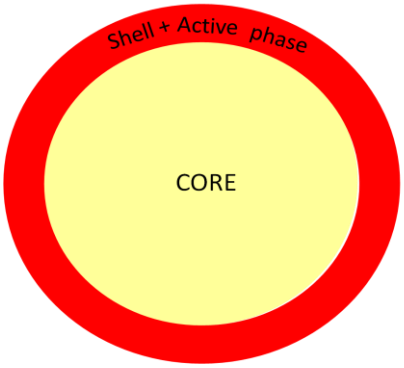

FIG. 2.1: active phase encapsulated in the shell layer

2.4 – Sonochemistry

Sonochemistry is a technique that uses ultrasound waves to obtain chemical reactions or similar effects[7,8]. For example, the ultrasound waves are ableto generate free radicals, to increase the surface area of a solid, to accelerate the dissolution of a chemical compound in the solvent or to renew the catalytic effects of a deactivated catalyst. However, the ultrasound waves formed in a liquid system have wavenumbers between microns and centimeters, which are not of molecular or atom size. The ultrasound waves instead, when they pass into a liquid system, cause an abatement into the pressure of the liquid itself, down to its vapor pressure and the gas dissolved inside is released. This fact is reflected in the formation and the growth of microbubbles into the liquid. This phenomenon is called acoustic cavitation. Inside the bubbles there occurs the development of very high pressures, up to 1000 atm, and very high temperatures that can reach 5000 K. Under these conditions the bubbles collapse. If inside the liquid there are some metal particles, for example dissolved as metal carbonyls, the implosion of the bubbles causes the break-up of bigger metal particles that are crumbled in microparticles and shot away. By this method, the metals can be deposited on a support with a minimal particle size, that corresponds to a large dispersion.

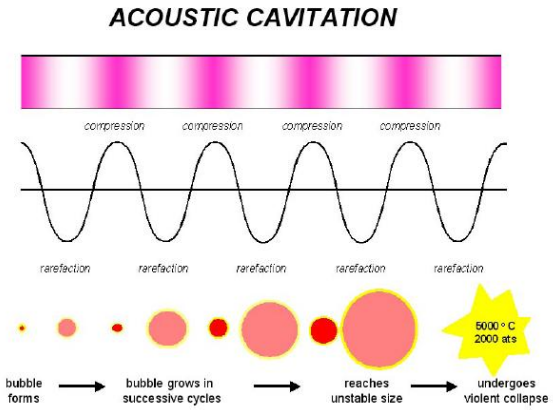

FIG 2.2: Scheme of acoustic cavitation

2.5 – Precipitation

Precipitation (or co-precipitation)[1,2,3] is still a method widely used for the preparation of catalysts. Despite the problems due to the large volumes necessary for this technique, the advantages are the capability of preparation of high pure final products and the flexibility of the process related to the amount of the desired final product. By this method, the precursor of the catalyst is dissolved in a solvent. In order to obtain the precipitation of a solid from the solution, it requires the formation of a nucleus. This event is driven by the condition of saturation of the solution. For the formation of the nucleus it is necessary to attain a condition of oversaturation. Until the concentration has attained the condition of oversaturation, the formation of the nucleus continues. The formation of a nucleus impoverishes the solution of the precursors of the solid phase. When the concentration decreases in a metastable zone (between the saturation and oversaturation) the formation of the nucleus is stopped but it can grow. The oversaturation condition can be obtained with various method, for example by cooling, by evaporation of the solvent, by a change of the pH, by introducing some precipitating agents or specific additives.

The process of precipitation is then governed by the phenomenon of nucleation and the curve of growth of particles. Many factors influence the properties of the final product. The most important are: nature of precursor, nature of the solvent, temperature, concentration, pH of the solution and the eventual presence of additives. In the case of co-precipitation, it is very important to consider the difference between the solubilities of the components in the solution, to avoid as much as possible a gradient of concentration between the two precursors.

2.6 CVD

The Chemical Vapor Deposition (CVD)[1,9,10,11] is another method used for the synthesis of supported catalysts. It is a process in which one or more precursors react on a substrate where they areadsorbed. The precursors must be stable at room temperature but they must have an high volatility. Precursors are often formed from the desired elements bonded with organic groups. This fact assures that the bonds between the desired products are stronger than between elements and theirs ligands into the precursor. This technique allows to obtain high degrees of purity of the final products and a clean reaction over the support, that avoiding the formation of undesired reactions. This technique is often used in coupling with other systems. Some examples are:

- PE CVD (plasma enhanced CVD);
- LA CVD (laser assisted CVD);
- ALD (atomic layer deposition).

Bibliography

[1] A. Y. Khodakov, W. Chu, P. Fongarland; *Chem. Rev.* ***2007****. 107, 1692*

[2] C. Perego, P. Villa; *Catalysis Today.* ***1997****. 34, 281*

[3] I. Chorkendorff, J.W. Niemantsverdriet; **"Concept of modern catalysis and kinetics"** *Chapter 5: Solid Catalysts; Ed. Wiley, 2003*

[4] C. L. Bianchi, F. Martini, P. Moggi; *Catal. Lett.* ***2001****. 76 (1-2), 65*

[5] P. Moggi, G. Predieri, F. Di Silvestri, A. Ferretti; *Appl. Catal. A.* ***1999****. 182, 257.*

[6] I. Louis, M. Che; **"Preparation of solid catalysts"** *Chapter 4.1: Deposition of active components; Ed. Wiley, 1999.*

[7] A. Di Michele; PhD Thesis: **"Sonochemical synthesis of metal nanoclusters and their application in the Fischer-Tropsch process"**; 2007

[8] A.N. Sona; PhD Thesis: **"New catalytic systems based on nano-dispersed metals in inorganic matrices prepared using the sol-gel techniques"**; 2010

[9] A. Dittmar, H. Kosslick, J.-P. Muller, M. Pohl; Surf. Coatings Technol. **2004.** 182, 35.

[10] M. Baerns, S. Temath, M. Reiche; **"Advnaced catalysis and nanostructured materials"** *Chapter 18:---; Ed.W.R. Moser, 1996.*

[11] Y. Iwasawa; **"Preparation of solid catalysts"** *Chapter 4.5: Supported catalysts from chemical vapor deposition and related techniques; Ed. Wiley, 1999.*

Chapter 3 – Characterization

The catalysts were characterized by using different methods, described in this chapter.

3.1 TPR (Temperature Programmed Reduction)

Temperature Programmed Reduction[1,2,3,4,5] (TPR) is one of the most important techniques used when metals are active phases. A known amount of sample is put into a sample-holder and hydrogen diluted in an inert gas flows over the sample, while the temperature is increased with programmed method. The concentration of hydrogen is around 10%. A thermal conductivity detector (TCD) is used to measure the change of hydrogen concentration in the mixture. A calibration line calculated with a known sample of Ag_2O permits to obtain the amount of hydrogen consumed by the reaction with the sample. The integration of the signal gives the amount of hydrogen consumed for a generic reaction:

The catalysts were characterized using different methods, described in this chapter.

$$M_xO_y + yH_2 \leftrightharpoons xM + yH_2O$$

Important informations that can be obtained by this analysis are the temperature of reduction of the sample and the amount of metal reduced with respect to the total. In the figure the calibration line used for our catalysts is reported. Three samples of different amounts of Ag_2O were used for the construction of this curve.

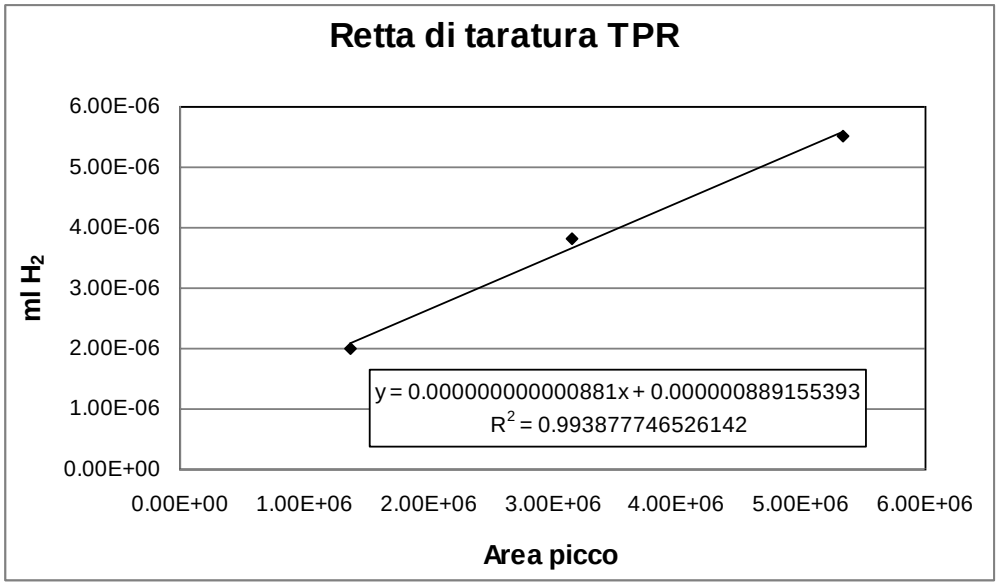

FIG. 3.1: Calibration Line for TPR analysis

The instrument used for the analysis is a MICROMERITICS PulseChemiSorb 2705.

3.2 TPO (Temperature Programmed Oxidation)

Temperature Programmed Oxidation[2,3,4] (TPO) is another method of characterization of metal supported catalysts. The technique is analogue to TPR, but the sample is put in a flow of oxygen diluted at 3% in helium during the programmed heating. The analysis is done after a pre-treatment of activation, performed according to the same procedure of activation used in the plant (usually at 400°C under hydrogen flow). In this case, the active phase of the catalyst is in the metal state. The TC Detector measures the impoverishment of oxygen in the flowing gas due to its use for the oxidation of the sample during the heating step. Also in this case, the signal is integrated to measure the amount of metal oxidized, with the help of a calibration line. This calibration line is reported in figure and is obtained with three standard samples of zinc, of known weight, that are oxidized by the mixture O_2/He.

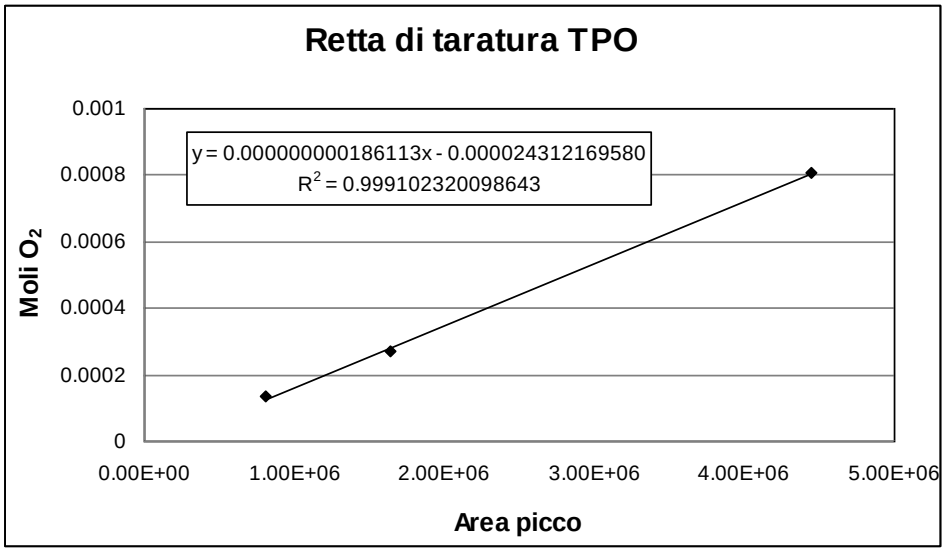

FIG. 3.2: Calibration Line for TPO analysis

The amount of metal oxidized is then calculated according to the following reaction:

$$xM + \frac{y}{2}O_2 \leftrightharpoons M_xO_y$$

This analysis gives as result the amount of metal really active during the catalytic process.

Also in this case, the instrument used for the analysis is the MICROMERITICS PulseChemiSorb 2705.

3.3 H_2-TPD (Hydrogen Temperature Programmed Desorption)

The instrument used for the Hydrogen Temperature Programmed Desorption is again the MICROMERITICS PulseChemiSorb 2705.

H_2-TPD is a technique that permits to measure the hydrogen chemically and physically adsorbed[1,4,6] on the surface of the catalyst.

During the test, the catalyst is activated under the same conditions used in the plant, as already seen for TPO analysis. At the end of the activation treatment, the sample is cooled at 200°C under hydrogen for 30 min and then it is cooled at room temperature then cooled again at -80°C for 5 min (using a slurry of isopropyl alcohol and liquid nitrogen). The flowing gas is changed with an

inert gas such as argon and the sample desorbs at room temperature the hydrogen physically adsorbed. The sample is then heated up to 400°C in order to desorb the chemically adsorbed hydrogen. The calibration is done with pulses of a standard gas mixture of hydrogen diluted in argon. By the area corresponding to this pulse, the hydrogen adsorbed is calculated.

From this analysis it is possible to determine the number of active sites of the sample, the percentage of dispersion and it is also possible to estimate the average diameter of the metal particles, by the following relations (5), (6) and (7) respectively:

$$n_{active\ sites} = \frac{2 \cdot mol_{H_2} \cdot N_A}{W} \qquad (5)$$

where N_A is the Avogadro number and W is the weight of the sample;

$$Dispersion\ (\%) = \frac{n_{active\ sites}}{n_{total\ sites}} \cdot 100 \qquad (6)$$

where n of active sites is the data obtained by (5) and n of total sites is the number of metal atoms in 1 g of the sample;

$$Diameter\ (nm) = \frac{96{,}2}{Dispersion} \qquad (7)$$

3.4 B.E.T. Surface Area

Also the surface area of the samples was measured with the MICROMERITICS PulseChemiSorb 2705.

The surface area is defined as the total area of 1 g of the particles of the samples. It was measured by the B.E.T. (Brunauer-Emmett-Teller) technique[4,7,8] at single point.

For the measurement, it is supposed that a single layer of nitrogen recovers the total surface of the particles, at the temperature of liquid nitrogen (-196°C). The detector (TCD) reveals the change of concentration of nitrogen in a mixture of gases constituted by 30% nitrogen diluted with helium. Before the analysis, the instrument was calibrated by determination of the area recovered by one ml of gaseous hydrogen, under the room conditions of pressure and temperature. The measurement is made under adsorbing conditions (when the nitrogen is adsorbed on the surface) and after under desorbing conditions (when the gas is released). At the temperature of liquid

nitrogen, the nitrogen condenses over the porous surface, forming a uniform monolayer of adsorbed gas. The weight W_m of the monolayer is determined following the B.E.T. equation, by applying the Brunauer-Emmett-Teller theory:

$$\frac{1}{W[(\frac{P_0}{p}-1)]} = \frac{1}{W_m C} + \frac{(C-1)}{W_m C} \left({}^{P}/_{P_0}\right) \qquad (8)$$

where:

W = weight of gas adsorbed at relative pressure P/P_0;

C = constant;

P_0 = saturation pressure of the gas;

By drawing the graph of $1/W[(P_0/P)-1]$ versus P_0/P, for a minimum of three points, a straight line is obtained. From the measure of the intercept and the slope of the straight line, it is possible to determine W_m. This is the multipoint B.E.T. method.

A simplification of this method (single point B.E.T. method) was used for the determination of surface areas of our samples. The equation (9) is:

$$W_m = W\left(1 - {}^{P}/_{P_0}\right) \qquad (9)$$

and the area A is calculated from (11):

$$A = \frac{W_m N_A S}{V} \qquad (10)$$

where:

N_A = Avogadro number;

S = area recovered by a single molecule of the gas;

V = molecular volume of the gas.

3.5 XRD

XRD spectra were acquired by using a diffractometer PHILIPS X'PERT PRO MPD, with scans every 20 s, between 2θ = 5° and 2θ = 80°. X-ray diffraction gives information on the structure of the sample[1,2,3,4] and it is based on a monochromatic radiation, usually using the Kα of Copper, and uses the Bragg (11) law, that describes the interference phenomena due to the reflections of an electromagnetic wave by different parallel planes.

$$n\lambda = 2dsin\theta \qquad (11)$$

where:

λ = width of electromagnetic wave;

d = distance between two crystallographic planes;

θ = angle between incident/reflected radiation and the normal of crystallographic plane.

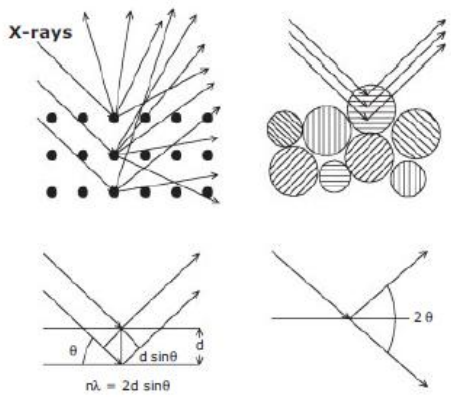

FIG 3.3: X-Ray scattered by atoms in an ordered lattice interfere constructively in directions given by Bragg's law.

The resulting spectra show several peaks, assignable to the structure of the sample, recognizable by comparison with tabulated data. It is possible to analyze powder samples and, in the case of big crystals, the direct analysis on single crystal is also possible. In our case, the powder analysis was used.

The resulting spectra show several peaks, assignable to the structure of the sample, recognizable by comparison with tabulated data. It is possible to analyze powder samples and, in the case of big crystals, the direct analysis on single crystal is also possible. In our case, the powder analysis was used.

3.6 FT-IR

The IR spectra[2,3,9] were acquired following the ATR technique, with a spectrophotometer NICOLET 5 PC at single ray by the help of Fourier Transform.

The attenuated total reflectance (ATR) technique uses the reflection of ray that passes through the sample under analysis. The sample is in contact with a refractive element with high reflection index (usually a diamond crystal).

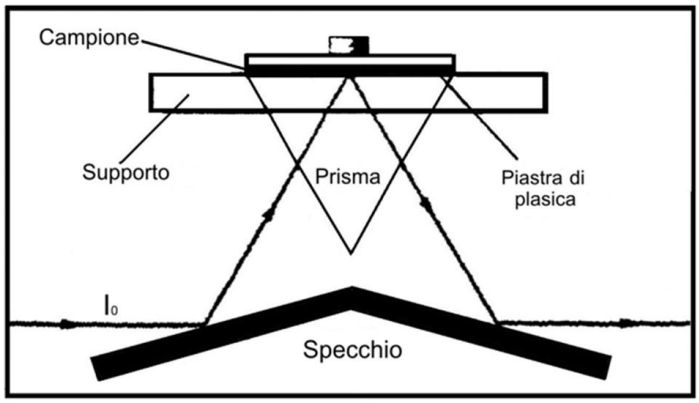

FIG. 3.4: Scheme of ATR

The IR ray passes through this element and, when the incident angle is major than critical angle, there is a phenomenon of total reflection. When this ray passes through the sample, the intensity can be attenuated by the interaction with the analyzed sample. This attenuation can be revealed. In our case, a Michelson interferometer gives response as a function of time. The Fourier Transform converts the signal from time dominium to frequency dominium.

3.7 Electronic microscopies[1,2,3,10]

SEM images are collected by an electronic microscope PHILIPS XL-30CP with RBS as detector and an EDS analyzer to determine the composition of the sample surface.

In this apparatus, a beam of electrons hits the sample. The sample acts by emitting several particles. Among these particles there are electrons that come from the sample (and from the beam). These electrons are revealed by a Faraday detector and converted in an electric impulse. The incident beam is not fixed, but it scans all the surface of the sample. The resulting image is a

black and white image similar to a picture. The sample must be under high vacuum because the air interferes with the electron beam. The Energy Dispersive X-Ray analysis (EDX) can give information about the surface composition of the sample.

SEM and TEM apparatus are showed in the figure FIG. 3.5

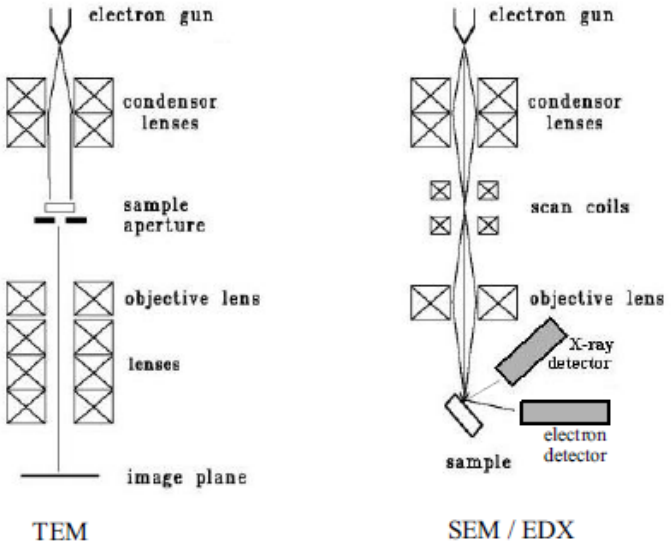

FIG. 3.5: Scheme of TEM and SEM apparatus.

SEM apparatus is composed by:

- an electronic column, where the electron beam is generated;
- a vacuum chamber, where the sample is hit by the electron beam;
- detectors, that acquire the signals and send them to the elaborator;
- a monitor, in which the image is reconstructed.

The Transmission Electron Microscope (TEM) used to study the morphology of catalysts is a PHILIPS 208 instrument.

Also this instrument is maintained under high vacuum because the radiation is again an electron beam. This electron beam is focused on the sample.

The electron beam passes through the sample, that was put on a grid with a reticulated structure. The electrons form the image of the surface of the sample, visible on a fluorescent monitor.

3.8 TGA

Thermal Gravimetric Analysis[4,11] (TGA) is a technique that permits to study the decomposition of the sample during the heating under controlled atmosphere. The technique is carried out by measuring the variation of the weight of the sample as a function of the temperature. The instrument is composed by 4 main parts:

- a thermobalance, where the sample is weighted;
- an oven, that assures the heating;
- a system of controlling gas, in order to control the atmosphere of analysis;
- an elaborator that acquires the signals and controls the conditions of analysis.

In our case, the measure ares carried out in order to obtain informations about the decomposition of precursors in an inert ambient (nitrogen atmosphere).

The instrument used for this analysis is a Perkin Elmer TGA7.

Bibliography

[1] A. Y. Khodakov, W. Chu, P. Fongarland; *Chem. Rev.* ***2007****. 107, 1692*

[2] I. Chorkendorff, J.W. Niemantsverdriet; **"Concept of modern catalysis and kinetics"** *Chapter 4: Catalyst Characterization; Ed. Wiley, 2003*

[3] G. Leofanti, G. Tozzola, M. Padovan, G. Petrini S. Bordiga, A. Zecchina; *Catalysis Today.* ***1997****. 34, 307*

[4] A.N. Sona; PhD Thesis: **"New catalytic systems based on nano-dispersed metals in inorganic matrices prepared using the sol-gel techniques"**; 2010

[5] S. D. Robertson, B. D. McNicol, J. H. De Baas, S. C. Kloet, J. W. Jenkins; *J. Catal.* ***1975.*** *37, 424*

[6] D. J. Richard, C. H. Bartholomew; *Applied Catalysis.* ***1988****. 39, 77*

[7] www.reolab.unimore.it/bet/index.htm

[8] en.wikipedia.org/wiki/BET_theory

[9] en.wikipedia.org/wiki/IR_spectroscopy

[9] en.wikipedia.org/wiki/Electronic_microscope

[9] en.wikipedia.org/wiki/Thermogravimetric_Analysis

Chapter 4 – Plants

Three plants were used in order to evaluate the catalytic activity of the prepared samples. One of the plants works at 20 bar pressure and was used for Fischer-Tropsch synthesis. The others work at room pressure and one was used for the Fischer-Tropsch synthesis and the other for the synthesis of ammonia at room pressure. These plants are described in the following paragraphs.

4.1 Scheme of plant for Fischer-Tropsch synthesis at 20 bar

In the figure the Fischer-Tropsch plant[1,2] is shown, that works at 20 bar of pressure.

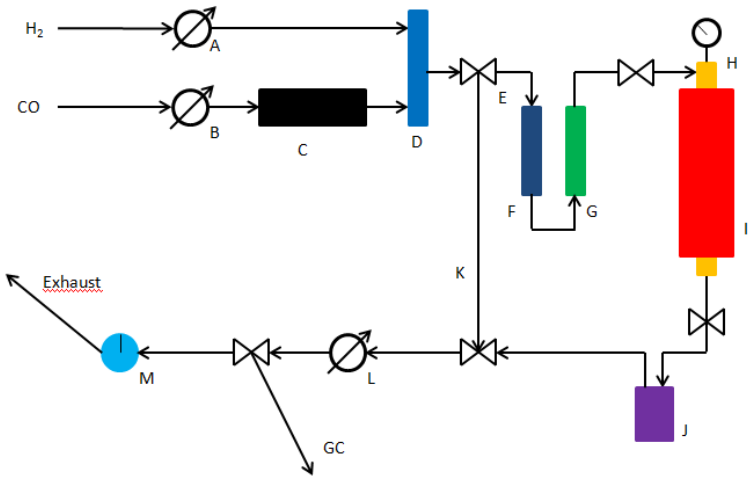

FIG 4.1: Scheme of plant for Fischer-Tropsch synthesis at 20 bar

The inlet flows of the gases (hydrogen and carbon monoxide) are determined and regulate by a pc that controls the electrovalves (A) and (B).

Before mixing with hydrogen in (D), carbon monoxide passes through a trap (C) containing active carbon, that eliminates the impurity traces eventually present together with CO.

The valve (E) is a 3 ways-valve that permits to exclude the feed to the reactor and drives the gas to the exit for the inlet analysis.

Before the reactor (H), two other traps, (F) and (G), assure that neither humidity and oxygen come inside the reactor.

The temperature is controlled by the same pc that controls the flows and, it is assured by an oven, illustrated as (I) in the scheme.

The condensable products (water and liquid hydrocarbons) are collected in the trap (J).

The pressure of the system is controlled by another electrovalve (L) at the end of the path.

Another valve is present to switch the pass by a flowmeter (M) or in the direction of analysis (GC: gas-chromatograph).

4.2 Scheme of laboratory plant for Fischer-Tropsch synthesis at room pressure

The plant used at room pressure for the Fischer-Tropsch synthesis is shown in the following figure.

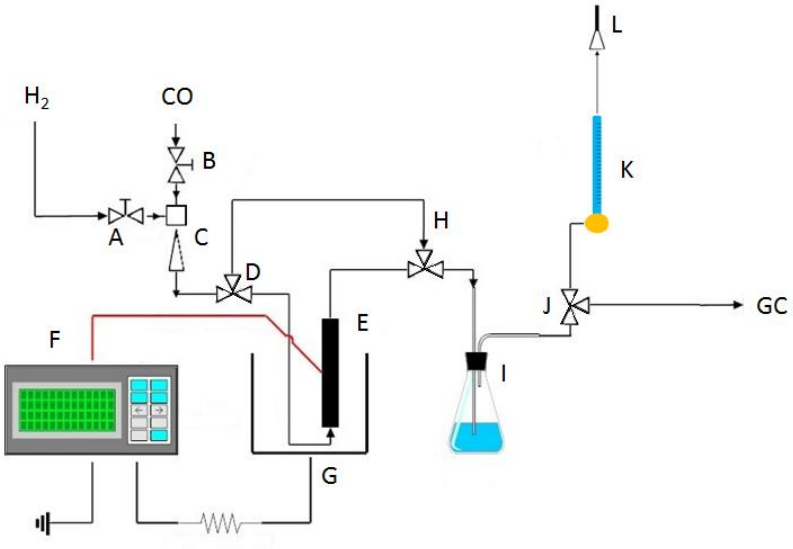

FIG 4.2: Scheme of plant for Fischer-Tropsch synthesis at room pressure

In this plant, H_2 and CO are fed and the relative flows are controlled by two needle valves (A and B) before mixing (C).

Before the reactor (E) there is a line of bypass (from D to H).

The temperature is regulated by a controller (F) that acts on the oven (G).

A trap with water (I) is placed after the reactor; its role is to trap eventually condensed products.

At the end of the plant a switch (J) that permits to drive the flow through a flowmeter (K) or to the GC for analysis, is present.

The outlet gases are collected under hood (L).

4.3 Evaluation of catalytic tests for Fischer-Tropsch synthesis

Both plants use the same equations in order to estimate the catalytic activity of samples.

The conversion is given by:

$$Conversion\ (\%) = \frac{mol_{CO\ in} - mol_{CO\ out}}{mol_{CO\ in}} \cdot 100$$

$$= \frac{A_{CO\ in} - [A_{CO\ out} \cdot F_{out}/F_{in}]}{A_{CO in}} \cdot 100 \qquad (12)$$

where:

mol $_{CO\ in}$ = moles of fed CO;

mol $_{CO\ out}$ = moles of unreacted CO;

$A_{CO\ in}$ = chromatographic area of fed CO;

$A_{CO\ out}$ = chromatographic area of unreacted CO;

F_{in} = flow inlet;

F_{out} = flow exit from the reactor.

The selectivity S_x calculated for each product is given by the equation:

$$S_x = \frac{mol_x \cdot n_C^o}{mol_{CO\ in} - mol_{CO\ out}} \cdot 100 \qquad (13)$$

where:

mol_x = moles of product;

$n°_C$ = number of carbon atoms in the product.

The moles of each product are calculated by the relation:

$$mol_x = \frac{mol_{CO\ out} \cdot A_x \cdot G_x}{A_{CO\ out}} \text{c} \qquad (14)$$

where:

A_x = chromatographic area of product;

G_x = response factor of the product with respect to the internal standard (CO).

The moles of CO inlet are calculated by the equation of an ideal gas:

$$mol_{CO\ in} = \frac{Flux_{CO\ in}\left(\frac{L}{h}\right) \cdot P\ (atm)}{0{,}0821 \cdot T\ (K)} \qquad (15)$$

while the moles of CO outlet are given by:

$$mol_{CO\ out} = mol_{CO\ in} \cdot (1 - {Conversion}/{100}) \qquad (16)$$

The response factors of products are calculated with respect to the CO (choosen as internal standard). These are determined by an injection of a mixture gas containing the products with known percentages. The relation is the following:

$$G_x = \frac{X\ (\%) \cdot A_{CO}}{A_x \cdot CO(\%)} \qquad (17)$$

where:

A_{CO} = is the chromatographic area of CO;

CO(%) = is the percentage amount of CO;

X(%) = is the percentage amount of product;

A_x = is the chromatographic area of product.

4.4 Scheme of laboratory plant for ammonia synthesis

The lab plant for the ammonia synthesis at room pressure is shown in figure[1]:

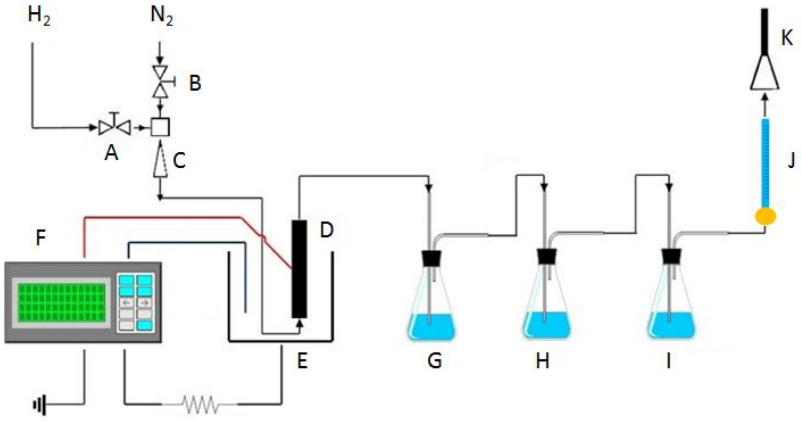

FIG 4.2: Scheme of laboratory plant for ammonia production

The reagent gases, H_2 and N_2 are fed at the beginning of the plant and the relative fluows are controlled by two needle valves (A and B) before mixing (C).

The temperature of the reactor (D) is regulated by a controller (F) that actos on the oven (E).

Three traps are placed at the end of the plant. The first and the second trap (G and H) contains a known amounts as moles of HCl, to adsorb the produced ammonia as ammonium chloride. The third trap (I) contains water and phenolphthalein as indicator to control that all ammonia produced has been is captured. The flow is controlled by a flowmeter (J) before to be collected under the hood (K).

The produced ammonia is compared with the equilibrium curves obtained from thermodinamical data by Gillespie and Beattie[3], showed in Table 4.1

Temperature °C	% mol of NH_3
200	13.304
210	10.803
220	8.827
230	7.214
240	5.903
250	4.842
260	3.984
280	2.727
290	2.27
300	1.898

Temperature °C	% mol of NH_3
310	1.594
320	1.344
330	1.139
340	0.969
350	0.828
360	0.71
370	0.612
380	0.529
390	0.459
400	0.4

Table 4.1: Equilibrium curve at room pressure for a mix of 3:1 hydrogen:nitrogen calculated from Gillispie and Bettie

Bibliography

[1] A.N. Sona; PhD Thesis: **"New catalytic systems based on nano-dispersed metals in inorganic matrices prepared using the sol-gel techniques"**; 2010

[2] A. Di Michele; PhD Thesis: **"Sonochemical synthesis of metal nanoclusters and their application in the Fischer-Tropsch process"**; 2007

[3] L. J. Gillespie, J. A. Beattie; *Physical Review **1930.** 36, 743*

Section 2: Fischer-Tropsch

Chapter 5: Fischer –Tropsch synthesis: General

5.1 History

The history of Fischer-Tropsch synthesis began in 1902, when Sabatier and Senderens synthesized methane from a mixture of CO and H_2 with a catalyst of Nikel[1]. In 1923 Hans Fischer and Franz Tropsch obtained a large amount of liquid hydrocarbons from the syngas by using Fe and Co-based catalysts[2,3]. During the years ’30 and ’40 in Germany there was a rapid development of this synthesis in order to obtain gasoline from carbon (CTL: coal to liquid process). Further developments were carried out in South Africa after the second world war[1]. An increasing of the price of petroleum in the ’70, caused by the wars in the Middle East, awake a renovation of interest on this synthesis. Then, the Fischer-Tropsch synthesis was developed also from natural gas (GTL: gas to liquid). The advantage of the use of this process is the possibility to obtain products and fuels free from nitrogen or sulfur. In the last years, the possibility to obtain syn-gas from the gasification of biomasses drove the research to the development of “ecofriendly” fuels [4,5].

5.2 Reactions and products of FTS

Several reactions are involved in the Fischer-Tropsch Synthesis. The products are principally a large series of hydrocarbons, that starts with methane and chains with more than 40 atoms of carbon can also be reached. The production of hydrocarbons is always accompanied by the formation of water as by-product. The main reactions are the following:

formation of paraffins:

$$(2n+1)H_2 + nCO \rightarrow C_nH_{2n+2} + nH_2O$$

formation of olefins:

$$2nH_2 + nCO \rightarrow C_nH_{2n} + nH_2O$$

formation of alcohols:

$$2nH_2 + nCO \rightarrow C_nH_{2n+1}OH + (n-1)H_2O$$

Beside those reactions, a large number of secondary reactions can occur during the synthesis. The secondary reactions are the driving reason of the deactivation of catalysts.

The most important are:

water gas shift (WGS) reaction:

$$H_2O + CO \leftrightharpoons CO_2 + H_2$$

formation of polycyclic hydrocarbons over the catalytic system:

$$(x + y/2)\,H_2 + xC \rightarrow C_xH_y + H_2O$$

disproportionation of Boudouard:

$$2CO \rightarrow CO_2 + C$$

oxidation of active phases:

$$xM + yH_2O \leftrightharpoons M_xO_y + yH_2$$

$$xM + yCO_2 \leftrightharpoons M_xO_y + yCO$$

formation of metallic carbides:

$$yC + xM \leftrightharpoons M_xC_y$$

Important thermodynamical informations can be obtained by the Francis diagram (Graph 5.1), where the standard free energies of formation are shown as a function of the temperature.

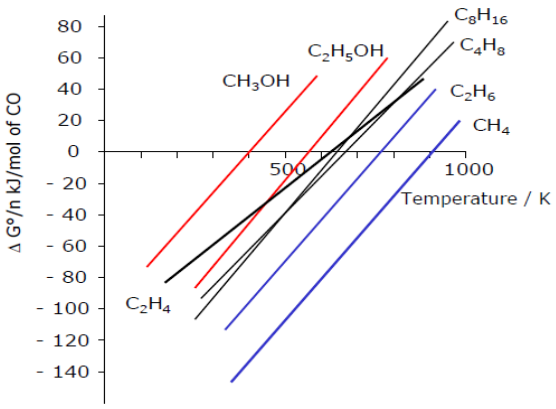

Graph. 5.1: Francis diagram for hydrocarbons

According to this diagram, the formation of methane is favoured with respect to the other compounds and, in general, lighter hydrocarbons are thermodynamically favoured with respect to the heavier ones. The formation of alcohols is the less favoured reaction. Hence, the Fischer-Tropsch synthesis permits to obtain a large variety of compounds. A mathematical model proposed by Anderson, Schulz and Flory (ASF)[6] is used in order to describe the distribution of products. This model was used at first to describe the polymerization and polycondensation reactions, but now it is applied for Fischer-Tropsch synthesis. It is based over the assumption that the chain growth happens by the addition of one carbon atom at time and the probability of growth is independent from the chain' length. The equation is:

$$W_n = n \cdot (1-\alpha)^2 \cdot \alpha^{(n-1)} \qquad (18)$$

where:

Wn = weight fraction of product with n number of carbon atoms;

α = the chain growth probability factor. It is defined as:

$$\alpha = \frac{r_p}{r_p + r_t} \qquad (19)$$

where rp and rt are respectively the rate of chain propagation and the rate of chain termination. The final products of the Fischer-Tropsch synthesis are highly dependent from the value of α (that

can be between 0 and 1), as it can be seen by the Graph 5.2, where the weight of products is shown as a function of α (or the polymerization degree D = 1/(1-α)).

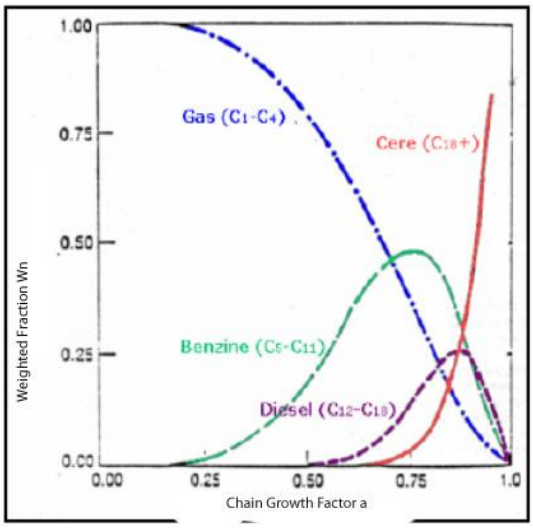

Graph 5.2: Product distribution as a function of chain growth

It is important to remember that α is dependent on many factors. For example, α increases when the temperature or the pressure decrease, or again when H_2/CO ratio decreases.

The equation 5.3 can be linearized as follows:

$$\log (W_n/n) = \log[(1-\alpha)^2/\alpha] + n \cdot \log \alpha \qquad (20)$$

5.3 Mechanism of FTS

There is still discussion on the mechanism of Fischer-Tropsch synthesis, because not all experimental data can be explained by only a mechanism. Mainly, there are three proposed mechanisms: via surface carbide, via hydroxycarbene and via carbonyl insertion. Nowadays, it is accepted that the real mechanism is a combination of the three.

The following mechanism is the via surface carbide:

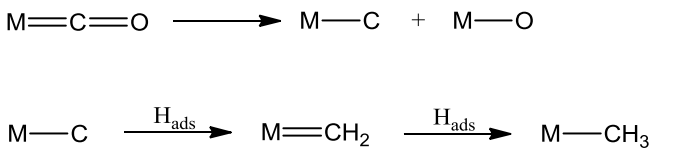

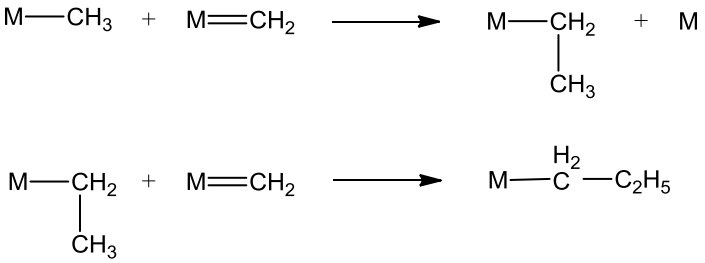

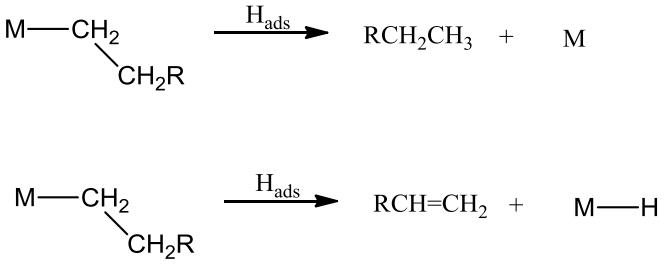

This mechanism starts from the dissociative chemisorption of CO[7] with the formation of a carbide that is transformed with hydrogenation steps to methylene-metal (monomer)[8]. The termination occurs by the addition of hydrogen that leads to the release of the hydrocarbon molecule from the metal site of the catalyst surface.

The second mechanism is that via hydroxycarbene:

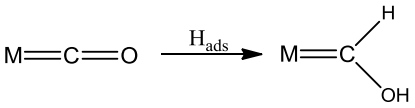

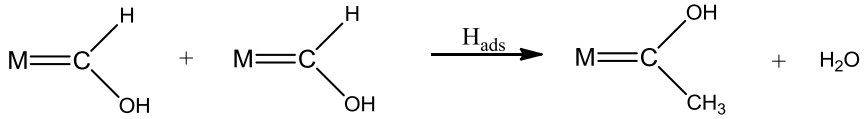

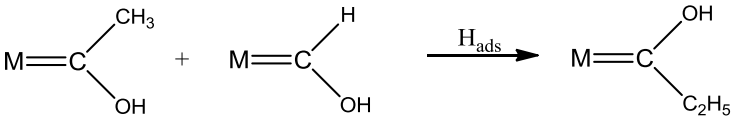

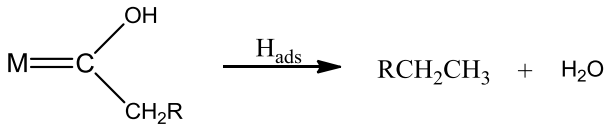

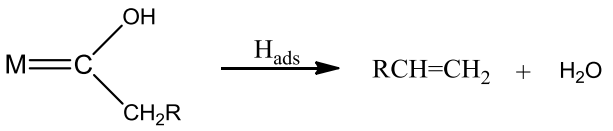

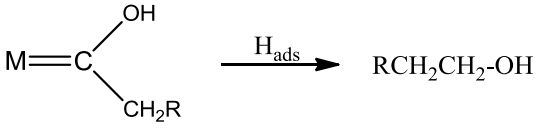

In this case, the reaction starts with the adsorption of molecular CO[9]. A metal carbonyl species is formed and further hydrogenation gives the hydroxycarbene group. This species is the initiator but also the monomer species. The propagation of reaction happens by a further hydrogenation step

with elimination of water. The C – O bond is broken only at the end. The further addition of hydrogen causes the termination of the reaction with the formation of paraffins, olefins or oxygenate species.

The last mechanism is that via carbonyl insertion:

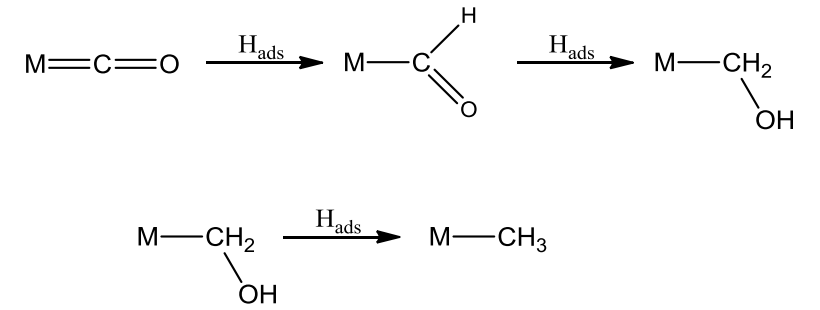

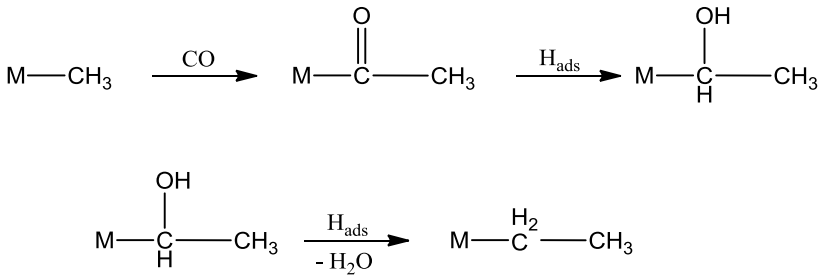

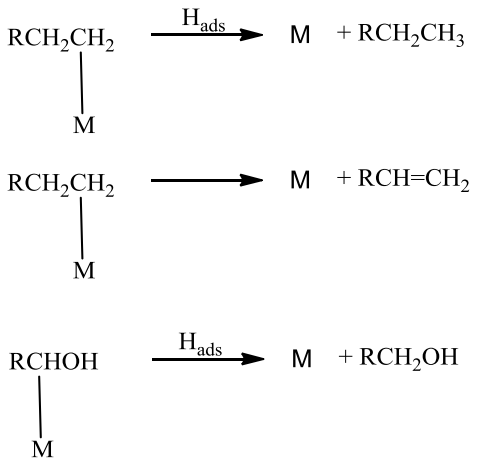

For this mechanism the not dissociative adsorption of CO is required. During the propagation of reaction, the CO molecule is inserted inside the metal-alkyl bond. The monomer species are formed from CO and H_2. The addition of CO transforms the metal-alkyl species into the metal-acyl species. The addition of hydrogen and the loss of water bring to the chain' growth. In the termination step, the addition of hydrogen causes the production of paraffins and oxygenated species or, in the case of hydrogen loss, the formation of olefins.

5.4 Active phases and supports

In the Fischer-Tropsch synthesis, the active phases are transition metals as: Ru, Rh, Co, Fe and Ni[1,10] (FIG. 5.1). The cost of these metals follows the order:

Rh > Ru > Co > Ni > Fe

By considering that the product obtained when Ni is used is almost only methane, only Iron and Cobalt have found industrial applications.

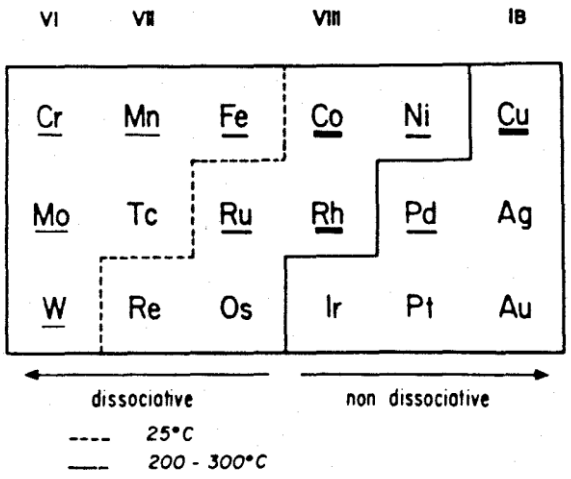

FIG. 5.1: Active metals in Fischer-Tropsch synthesis

The main difference between various metals is the kind of CO adsorption. The metals at the left side of the dashed line can dissociate CO already at room temperature. At 200°C - 300°C (usual operative temperatures of Fischer-Tropsch process), this line is shifted on the right hand (continuum line). The metal situated on the right hand of the line can produce only compounds in which the bond between carbon and oxygen remains unbroken (ketons, alcohols, acids).

Another important component of the catalyst is the support. In Fischer-Tropsch synthesis supports often used are SiO_2, Al_2O_3 and TiO_2, thanks to their ability to give chemical stability and to improve the surface area of the catalyst. Also promoters can be present. Their function is to give electrons to the metal in order to grow the hydrocarbon chain length, by reinforcing the metal – carbon bond.

The use of cobalt with respect to iron, despite its cost, is justified by its advantages:

longer chains;

longer lifetime;

less branched products;

absence of water gas shift reaction.

By the ability of cobalt to produce longer and linear chains, it is preferred when diesel-type fuels are desired, while iron is preferably used for the synthesis of gasoline-type fuels.

The cobalt-based catalyst is usually promoted with ruthenium, that makes cobalt precursors more easily reducible.

Bibliography

[1] A. Y. Khodakov, W. Chu, P. Fongarland; *Chem. Rev.* ***2007.*** *107, 1692*

[2] F. Fischer, H. Tropsch; *Brennst. Chem.* ***1926.*** *7, 97*

[3] F. Fischer, H. Tropsch; *Ber.* Dtsch. Chem. Ges. **1926.** 59, 830

[4] D. Unruh, K. Pabst, G. Schaub; Energy Fuels **2010.** 24, 2634

[5] C. Medina, R. Garcia, P. Reyes, J.L.G. Fierro, N. Escalona; Appl. Cat. A: Gen. **2010.** 373, 71

[6] C. G. Visconti, E. Tronconi, L. Lietti, P. Forzatti, S. Rossini, R. Zennaro; Top. Catal. **2011.** 54, 786

[7] M. E. Dry; **"The Fischer-Tropsch Process-Commercial aspects"**, Eseviever Science Publishers B. V. 1990. 183

[8] E. van Steen, H. Schulz; App. Catal. A: General **1999.** 186, 309

[9] B. Eisenberg, R. A. Fiato, C. H. Mouldin, G. R. Say; Stud. Surf. Sci. Catal. **1998.** 119, 943

[10] M. A. Vannice; *J. Catal.* ***1975.*** *37, 449*

Chapter 6 – Alumina supported catalysts

6.1 - Introduction

In this chapter, four catalysts are compared. The support for all these catalysts is the same: alumina[1,2,3,4,5,6]. The amount of active phase for all catalysts is 13% by weight. The active phase for the first catalyst, called FT01, is Cobalt, with the addition of Ruthenium as promoter. The cobalt is added as cobalt nitrate. The second catalyst, FT02, has the same composition of FT01 but it is prepared by the sonochemical method. The active phases of FT03 and FT04, indeed, are composed by 9,75% (weight) of Cobalt and 3,25% (weight) of Iron. In the case of FT03, the precursors are nitrate salts. The active phase of FT04 is provided by a cluster containing both metals. Table 6.1 summarize all these characteristics for the four catalysts.

SAMPLE	SUPPORT	ACTIVE PHASE	RAW MATERIAL	METHOD OF PREPARATION
FT01	alumina	13% Co - 0,5% Ru	Nitrate	Bulk sol-gel
FT02	alumina	13% Co - 0,5% Ru	Carbonyl clusters	Sonochemical
FT03	alumina	9,75% Co - 3,25% Fe	Nitrate	Bulk sol-gel
FT04	alumina	9,75% Co - 3,25% Fe	Bimetallic cluster	Bulk sol-gel

Table 6.1: method of preparation and precursors for alumina supported catalysts.

6.2 Preparation

FT01

This catalyst was prepared by sol-gel technique. 52.6 g of $Al(Sec\text{-}OBu)_3$ were dissolved in 300 mL of isopropyl alcohol under dry atmosphere. In a flask, 7.38 g of $Co(NO_3)_2{\cdot}6H_2O$ were dissolved in 60 mL of isopropyl alcohol. 0.108 g of $Ru_3(CO)_{12}$ were dissolved in a THF solution. The solutions of $Co(NO_3)_2{\cdot}6H_2O$ and $Ru_3(CO)_{12}$ were mixed and then added drop by drop at the solution of Al(Sec-

$OBu)_3$. The formation of a precipitate can be observed during the addition of metal precursor solution: this is the start of gelification caused by the water of crystallization of cobalt salt. At the end, the right amount of water (20,3 mL) to complete the gelification was added drop by drop to the solution. After, the solution was left under hood to evaporate the solvent, then put in an oven at 110°C for one night to dry the solid. The dried product was finally calcinated at 250°C for 2 hours and at 500°C for one night.

FT02

The catalyst FT02 was prepared at the "Università degli Studi di Perugia", by Dott. A. Di Michele, using the sonochemical method for the deposition of metal[7]. Precursors of the active phase were carbonyl clusters of Cobalt and Ruthenium. The support was commercial alumina. The composition is the same of FT01. The catalyst was finally calcinated for 10 hours at 300°C.

FT03

This catalyst was prepared by the sol-gel technique. 51 g of $Al(Sec\text{-}OBu)_3$ were dissolved in 300 mL of isopropyl alcohol under dry atmosphere. In a flask, 5.6084 g of $Co(NO_3)_2 \cdot 6H_2O$ and 2.7341 g of $Fe(NO_3)_3 \cdot 9H_2O$ were dissolved in 80 mL of isopropyl alcohol. The solutions of nitrates were added drop by drop to the solution of $Al(Sec\text{-}OBu)_3$. 19 mL of water was then added to complete the gelification. The solvent was left to evaporate and then the sample was dried in an oven at 110°C for one night. The dried product was finally calcinated at 250°C for 2 hours and at 500°C for one night.

FT04

The catalyst was prepared by the bulk sol-gel method. The composition is the same of FT03, but the precursor of the active phase is the cluster $HFeCo_3(CO)_{12}$ prepared by Dott. Deborah Vidick. The catalyst was not calcinated to not destroy the cluster structure.

6.3 Characterization

6.3.1 TPR profiles

The TPR profile for FT01 (FIG. 6.1) shows three peaks at 206°C, 404°C and 745°C respectively. The first peak is caused by the reduction of ruthenium oxides formed during the sol-gel process; the

second is the combination of reduction of steps cobalt oxides (CoO and Co_2O_3). The third peak shows the presence of species not easy reducibly in the plant, probably due to the Cobalt-alumina strong interaction, verified during the calcinations process. The reducibility degree up to 400°C is 7.4%; the total reducibility is 39.4%.

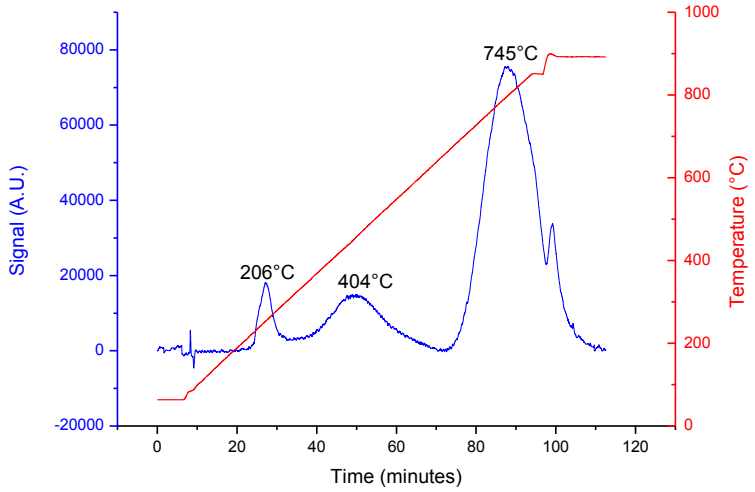

FIG. 6.1: TPR profile for FT01

The TPR profile for FT02 (FIG. 6.2) shows three peaks partially overlapped due to the reduction of metal oxides. In this case, the preparation method entails that the active phase is completely dispersed over the surface of the support. Indeed, the TPR profile shows the absence of peaks at high temperature, to confirm the absence of species derived from metal-support interactions, then hardly reducible. The percentage of reduction in this case is 76%.

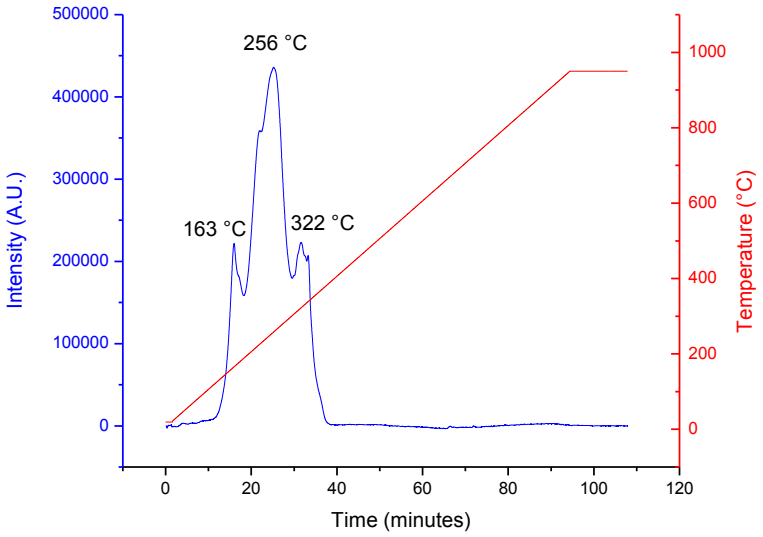

FIG. 6.2: TPR profile FT02

The TPR profile for FT03 (FIG. 6.3) shows a peak at 402°C, imputable to the reduction of Cobalt oxides and Iron oxides, and a peak at 852°C due to the formation of aluminates, that cannot be reduced during the activation procedure before the catalytic tests. The percentage of reduction is 11.3% for the first peak and 31.7% for the total.

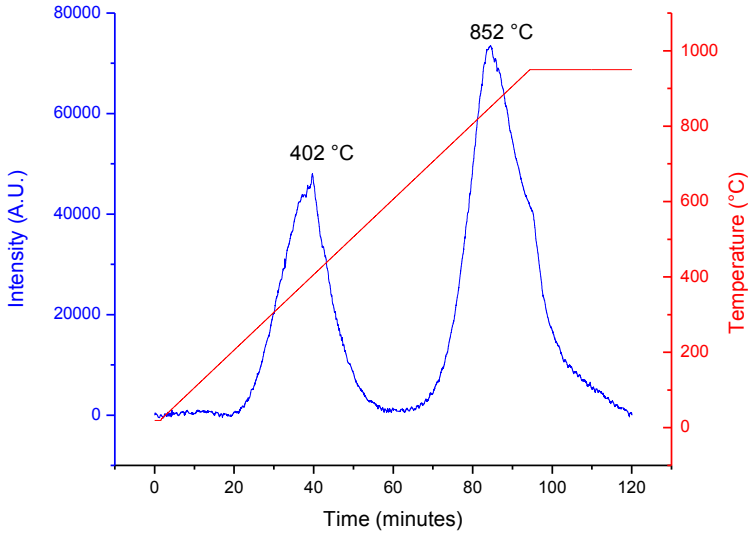

FIG. 6.3: TPR profile for FT03

The TPR profile for FT04 (FIG. 6.4) was obtained after a thermal treatment at 400°C under hydrogen flow for 6 h because the sample was not calcinated. A negative peak at 189°C is probably

due to the release of CO. from the carbonyl groups of the cluster. At 544°C it can be observed a peak due to the reduction of Iron and Cobalt oxidizes species, while the last peak at 840°C is attributable to the formation of aluminate compounds.

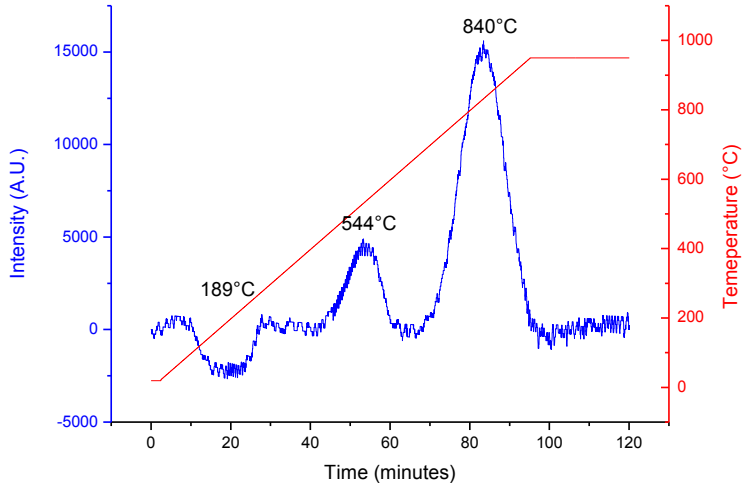

Fig. 6.4: TPR profile for FT04

6.3.2 TPO profiles

All TPO profiles have been acquired after an activation treatment under hydrogen at 400°C for 4h. This activation treatment simulates the activation of catalyst in the plant.

The TPO analysis done on the FT01 catalyst (FIG. 6.5) shows a little broad peak centered at 250°C. The amount of re-oxidation of metal under 400°C was 7.4%.

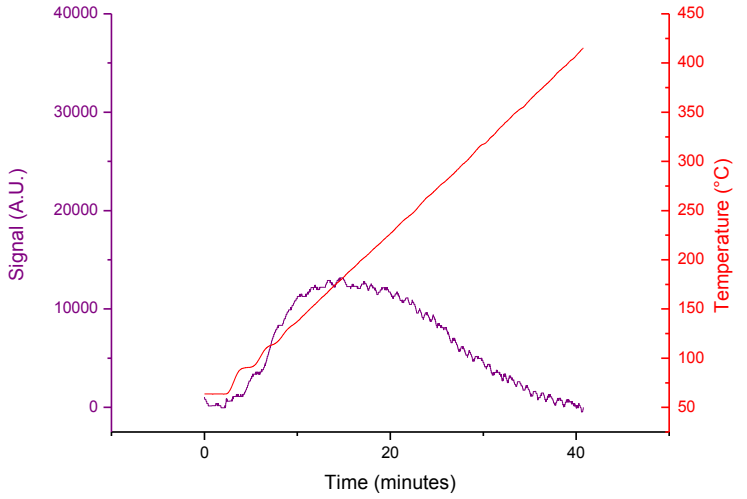

FIG. 6.5: TPO profile for FT01

The TPO profile for FT02 (FIG. 6.6) shows a peak that starts at 200°C and attains the maximum below 400°C. The reoxidation, as well as the activated metal during the test, is quite complete.

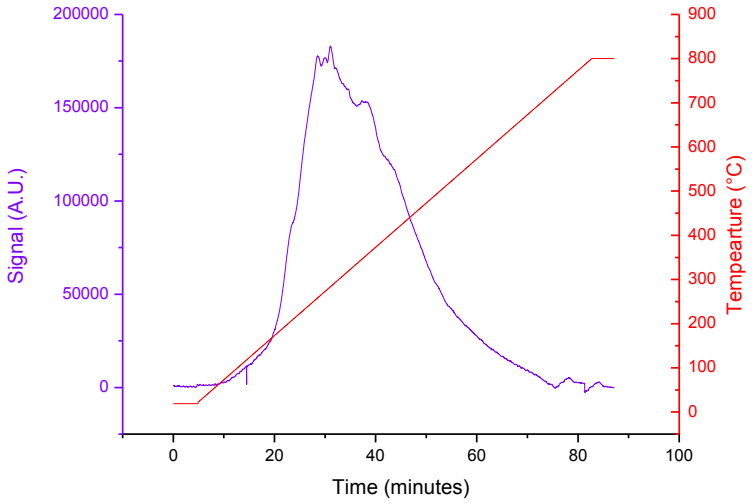

Fig. 6.6: TPO profile FT02

The TPO analysis on the FT03 catalyst (FIG. 6.7) shows a little broad peak centered at 250°C. The amount of re-oxidation of metal under 400°C was 7.4%.

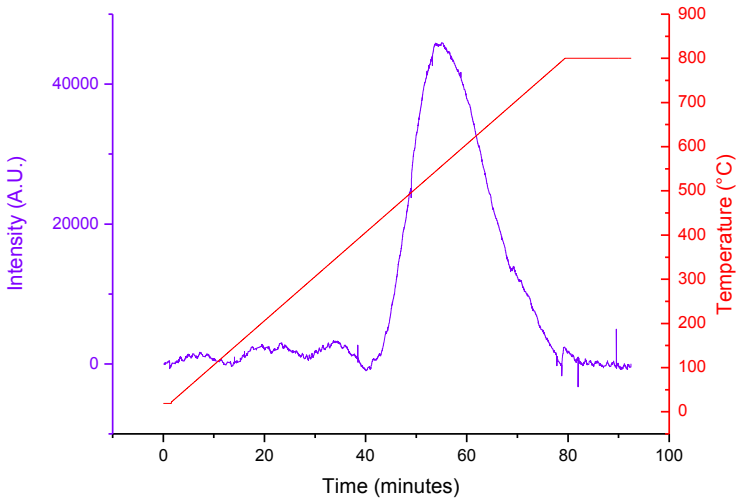

FIG. 6.7: TPO profile for FT03

The TPO profile of the FT04 catalyst (FIG. 6.8) shows a large peak centered at 250°C, that can be due to the reduction of iron oxides.

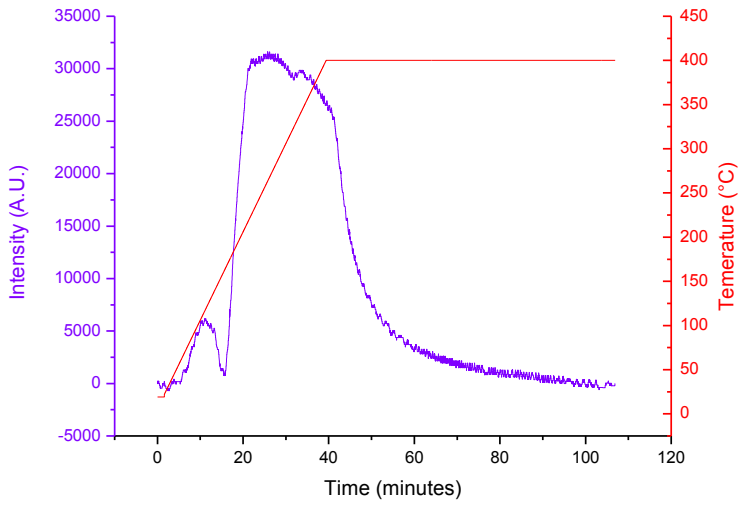

FIG. 6.8: TPO profile for FT04

6.3.3 H_2-TPD profiles

All profiles of desorption of Hydrogen are measured, as well as TPO profiles, after an activation procedure under hydrogen at 400°C for 4h, in order to put the sample at the same condition of the plant tests.

The H_2-TPD profile of the sample FT01 (FIG. 6.9) shows a peak at 400°C. From this profile the resulting dispersion degree resulting is 1.7% and the number of active sites per gram of catalyst in $2.3x10^{19}$. The size of the particles seems to be around 57 nm.

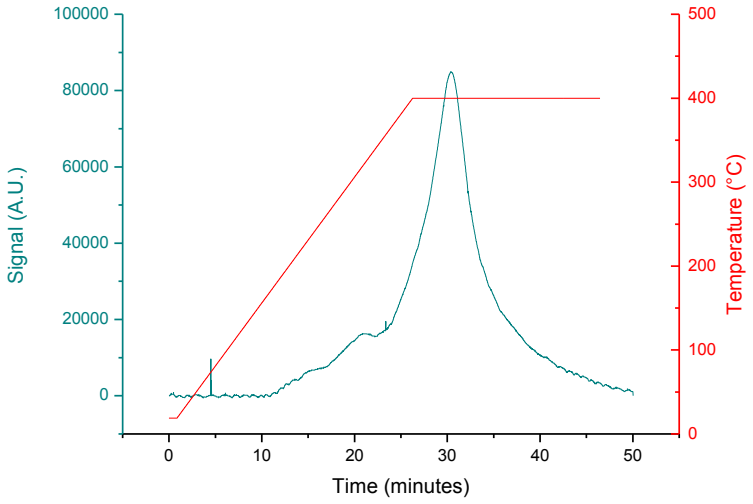

FIG. 6.9: H_2-TPD profile for FT01

The H_2-TPD profile of the sample FT02 (FIG. 6.10) shows a peak at room temperature due to the desorption of hydrogen physically adsorbed. Then, we can observe three other peaks assignable to different active sites for chemical absorption of hydrogen. The number of active sites for this catalyst is 3.91×10^{19}, the dispersion is 2.87% and the size of particles is 33 nm.

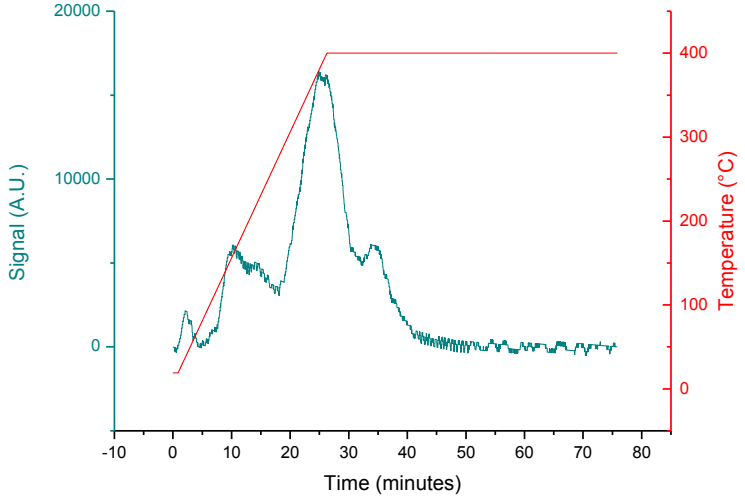

FIG. 6.10: H_2-TPD profile FT02

The H_2-TPD profile of the sample FT03 (FIG. 6.11) shows the peak for desorption of hydrogen chemisorbed at 400 °C. From the H_2-TPD data, the number of active sites for this sample is 2.4×10^{19}, the dispersion is 1.5% and the size of particles is 63 nm.

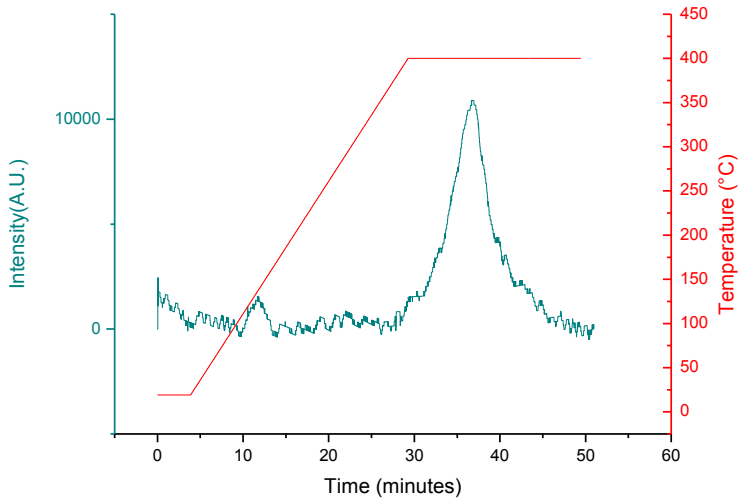

FIG. 6.11: H_2-TPD profile for FT03

The H_2-TPD profile of the sample FT04 (FIG. 6.12) shows that the hydrogen is chemisorbed with different strength. Three peaks partially overlapped can be observed between 106°C and 450 °C. From the data, the number of active sites for this sample is $5.8x10^{19}$, the dispersion degree is 3.7%% and the size of particles is 26 nm.

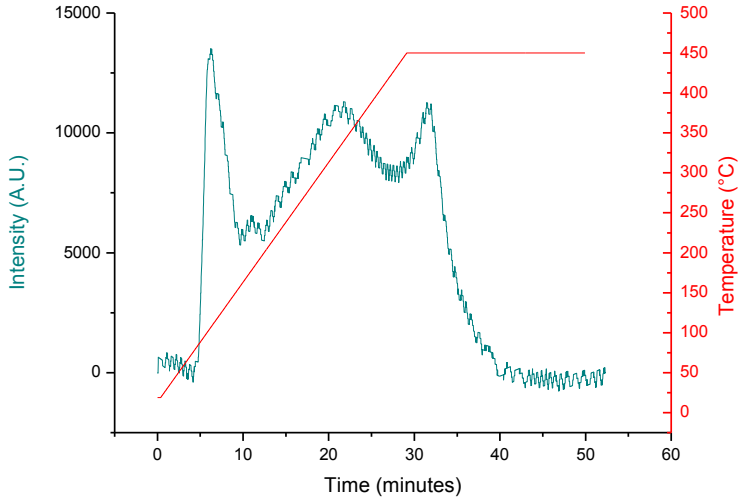

FIG. 6.12: H_2-TPD profile for FT04

6.3.4 Surface area

The surface area of the catalysts, determined with the B.E.T. method at single point, are shown in the table 6.2.

SAMPLE	SURFACE AREA (m^2/g)
FT01	241
FT02	100
FT03	264
FT04	423

Table 6.2: surface area of the samples

6.3.5 XRD

The XRD analysis (FIG. 6.13) of FT01 catalyst shows that the material is completely amorphous, that not surprising by using the sol-gel technique.

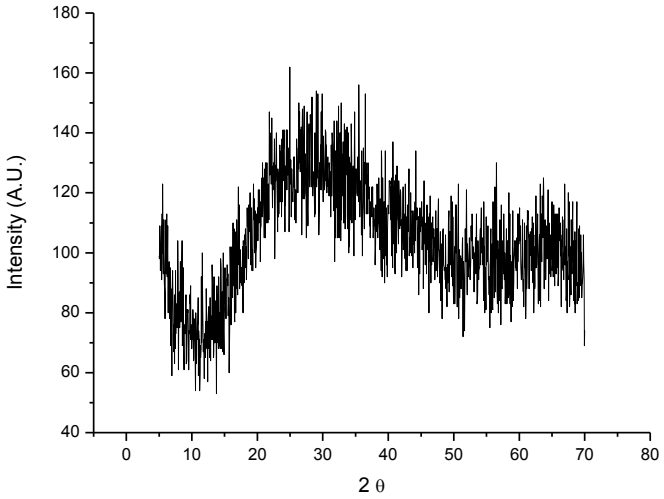

FIG. 6.13: XRD spectrum for FT01

The XRD analysis of FT02 catalyst (FIG. 6.14) shows the presence of peaks at 18.9°, 31.2°, 36.8°, 44.8°, 59° and 65°. These peaks are associated to the cubic structure of Co_3O_4[8].

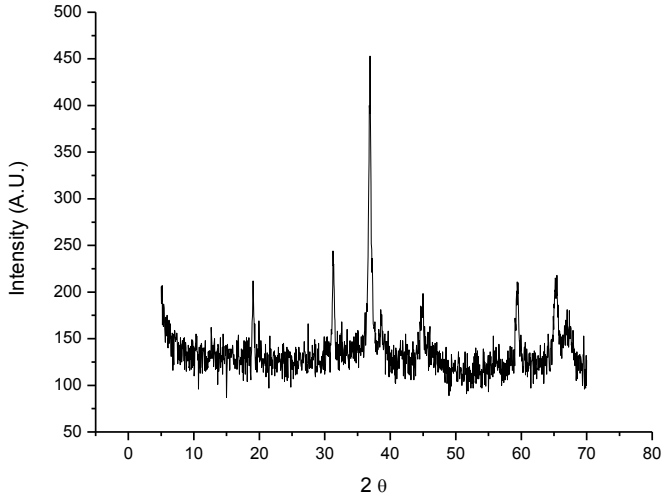

FIG. 6.14: XRD spectrum for FT02

The XRD spectrum for FT03 catalyst (FIG. 6.15) shows again that the sample is completely amorphous.

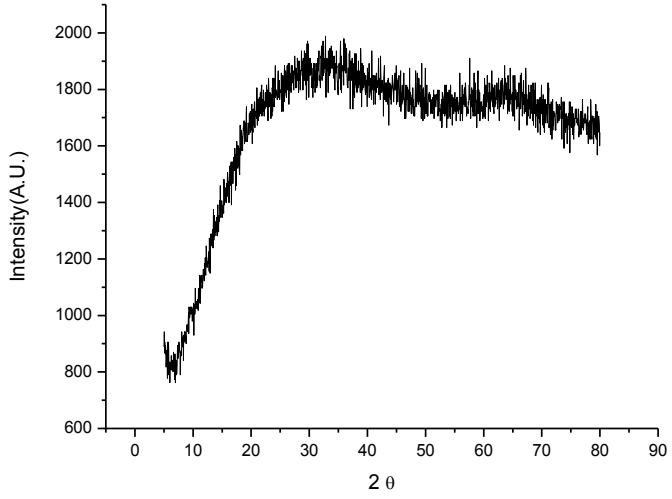

FIG. 6.15: XRD spectrum for FT03

The XRD spectrum for FT04 catalyst (FIG. 6.16) is again a typical spectrum of a completely amorphous material.

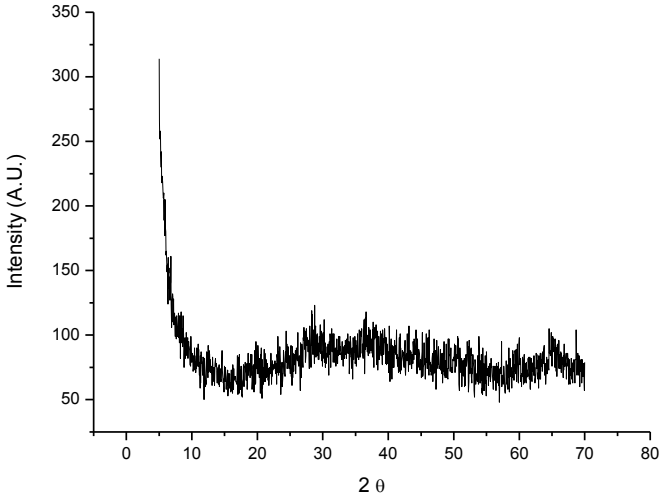

FIG. 6.16: XRD spectrum for FT04

6.3.6 FT-IR

The FT-IR spectra for FT01 catalyst were acquired before (blue line) and after the calcination treatment (red line). We can observe in the figure (FIG 6.17) an high decrease of the intensity of the band at wavenumbers up to 3000 cm^{-1} associated to the –OH groups, caused by the disappearance of water and to the decrease of hydroxide groups on the surface. An intense peak associated to the precursor of metal (nitrate) at 1380 cm^{-1} disappears after the calcination, because the metal salts transforms itself into oxides. The large band between 600 and 800 cm^{-1} is due to the interaction between metal and support, and it becomes less defined after calcination.

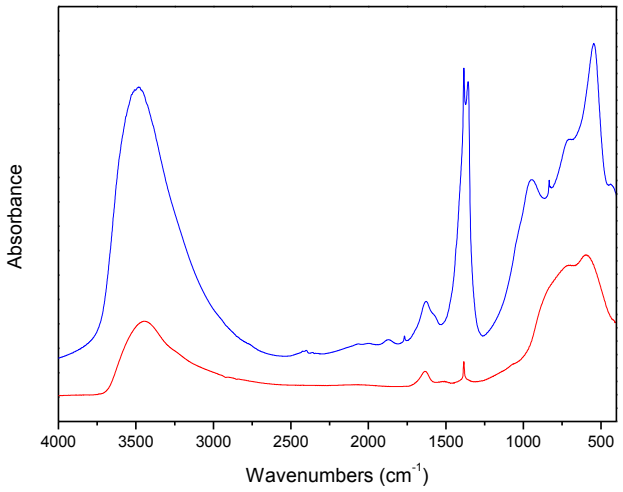

FIG. 6.17: FT-IR spectra for FT01

In the FT-IR spectrum of FT02, in FIG 6.18, besides to the presence of water, we can observe two peaks a 663 cm^{-1} and 572 cm^{-1} due to Co-O bond in present in Co_3O_4. The peak at 1634 cm^{-1} can be associated to the presence of carbonyl species of the precursors.

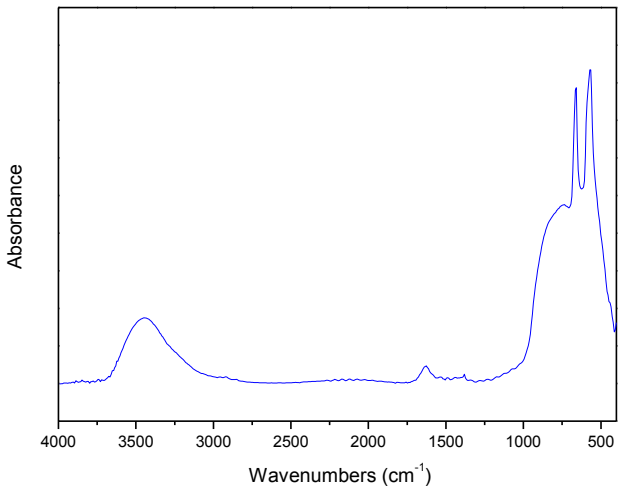

FIG. 6.18: FT-IR spectrum for FT02

In the FT-IR spectrum of FT02 catalyst, in FIG 6.19, besides to the presence of water, we can observe two peaks at 663 cm^{-1} and 572 cm^{-1} due to Co-O bonds present in Co_3O_4.

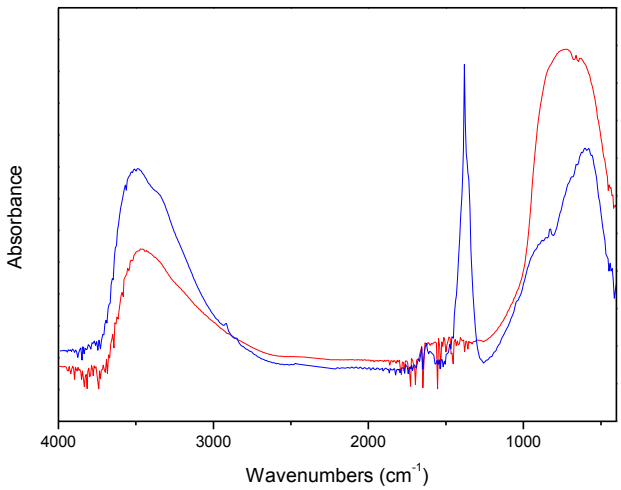

FIG. 6.19: FT-IR spectra for FT03

The FT-IR spectra for FT04 catalyst (FIG. 6.20) were acquired before (blue line) and after activation (red line) under hydrogen. The spectrum of the activated catalyst shows only an homogenization

of the band under 1200 cm^{-1}, with respect to the at not activated sample. This fact is due to the interactions between clusters and support.

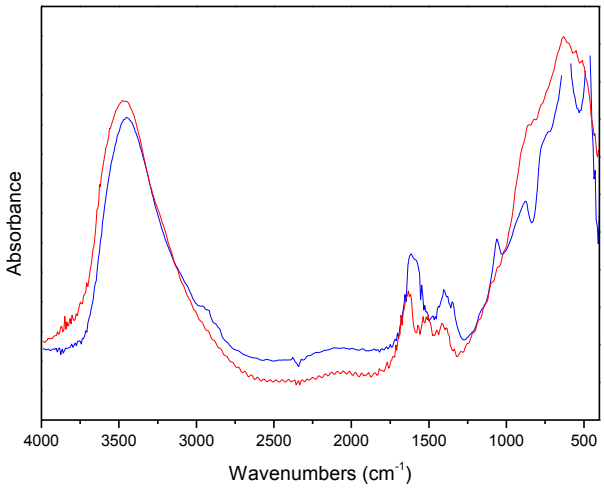

FIG. 6.20: FT-IR spectra for FT04

6.3.7 SEM images

The SEM images of the sample FT01 (FIG. 6.21) show a good covering of the surface, but a large dishomogeneity. The elemental analysis indeed indicates an amount of Cobalt of the 20% instead of 15%. The Ruthenium seems not to be present but the amount was so little that probably it cannot be seen by this technique.

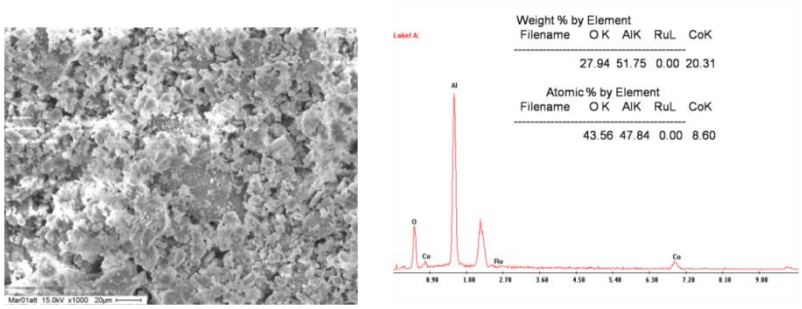

FIG. 6.21 SEM image for FT01

Also in the case of FT02 catalyst the SEM images of the sample (FIG 6.22) show a good covering of the surface, but a large dishomogeneity. The elemental analysis shows that the amount of Cobalt calculated by EDX analysis is 10% instead of 15%.

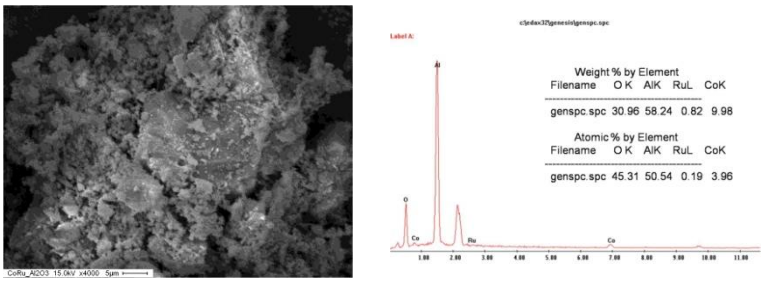

FIG. 6.22 SEM image for FT02

The SEM image of FT03 catalyst is shown in FIG 6.23. It shows a good covering of the surface but the EDX data give different values from the estimated one (18% instead 11% for the Cobalt). This fact can be explained also in this case by the dishomogeneity of surface covering.

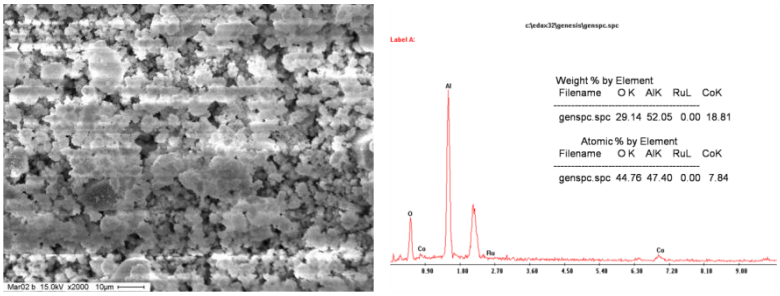

FIG. 6.23 SEM image for FT03

The SEM image and the EDX data of FT04 catalyst (FIG 6.24) show also in this case a surface not very homogeneous but EDX data confirm the presence of Cobalt and Iron.

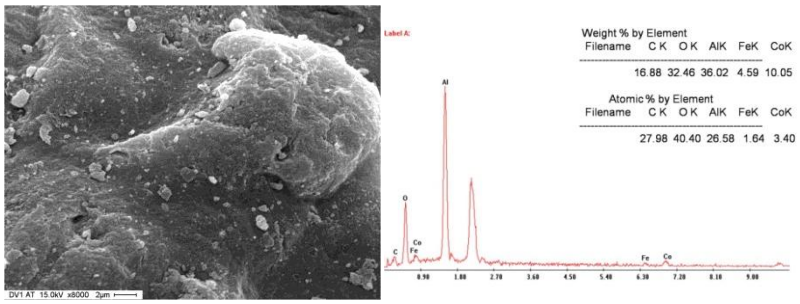

FIG. 6.24: SEM image for FT04

6.4 Catalytic tests

FT01 was tested in a fixed bed reactor. 5 gram of catalyst were charged into the reactor and activated under hydrogen flow at 400°C. After activation, a mixture of H_2 and CO, with molar ratio 2:1 was fed in the reactor. The catalyst was tested under pressure of 20 bar at different temperatures. The results (Graph 6.1) indicate a low conversion, with the maximum around 30% at 210°C; at higher temperatures we can observe a decrease of the conversion due to the deactivation of the catalyst.

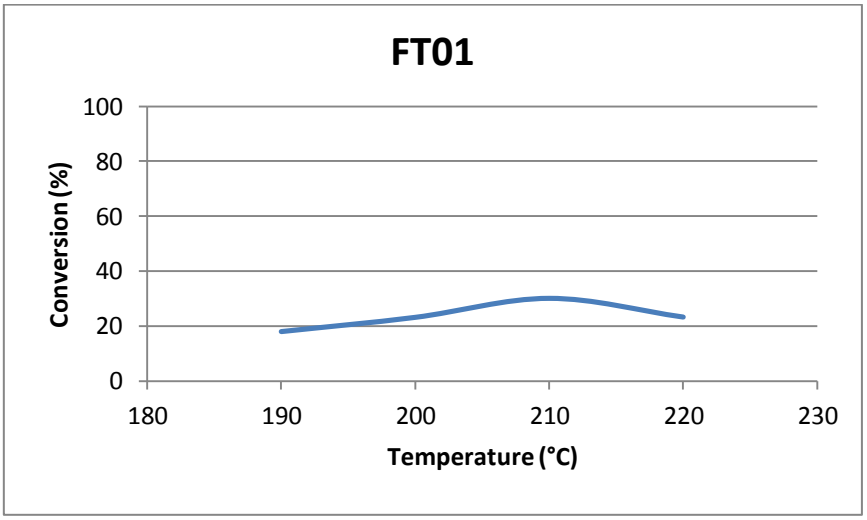

Graph 6.1: Conversion vs temperature for FT01

A test to evaluate the behaviour during the time was carried out at 220°C. This test shows a rapid deactivation, hypothesized also in the previous test, and high formation of methane (over 30%), that remains stable during the test, as well as other products not desiderable like CO_2 (6-8%) and light hydrocarbons (8-10%).

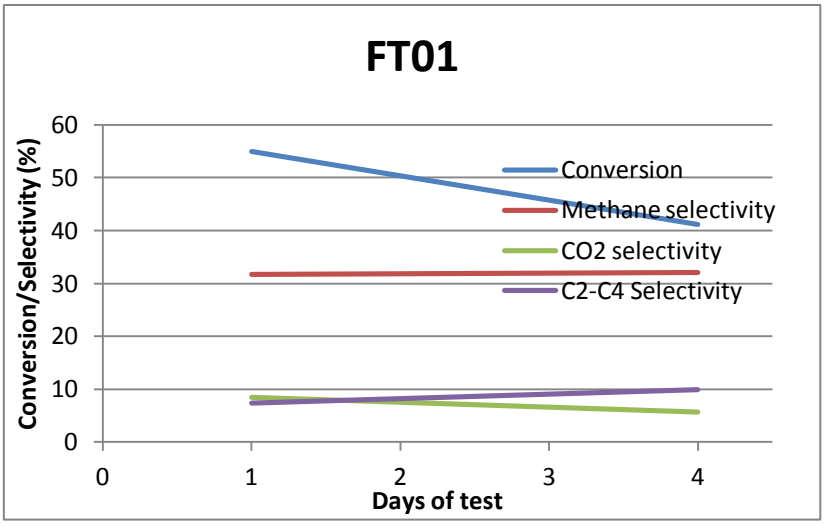

Graph 6.2: Conversion vs time and selectivity of lighter products for FT01

The condensed products after this test were analyzed to obtain the ASF distribution (GRAPH 6.3). From this analysis, the value of α results to be 0.65.

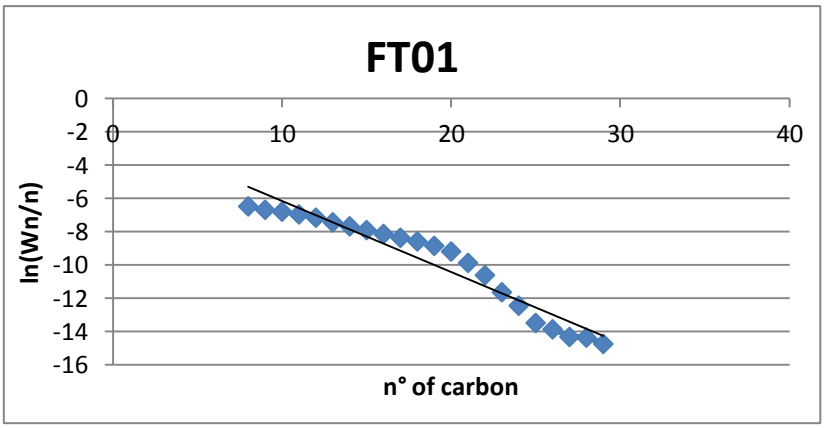

Graph 6.3: linearized distribution of condensed products for FT01

5 gram of catalyst FT02 was charged into a fixed bed reactor and activated under hydrogen flow at 400°C. For the reaction a mixture of H_2 and CO, with molar ratio 2:1 was fed to the reactor. The catalyst was tested at 20 bar of pressure between 200°C and 220°C. The results (Graph 6.4) show a good conversion value, around 60%, at 220°C.

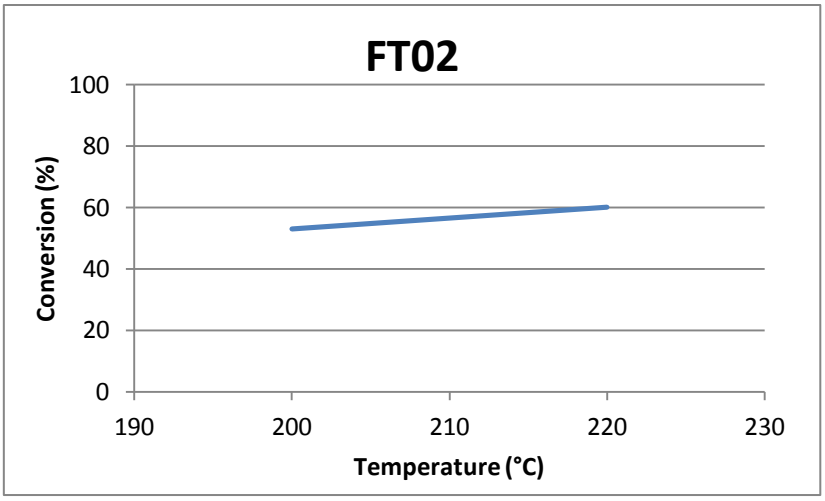

Graph 6.4: Conversion vs temperature for FT02

The test of the catalytic activity during the time was carried out at 220°C. Initially, the conversion was good, around 50%, but it decreased rapidly under 30%. This decrease of activity is due to the formation of waxes that remain on the active sites. The selectivity to methane is about 20%. The selectivity to CO_2 is under 5% and the selectivity to lighter hydrocarbons is lower than 10%. After the test, 10 g of waxes were extracted from the catalyst. The deactivation can be explained with the recovering of active sites from waxes. This fact is also supported by the low selectivity to lighter hydrocarbons.

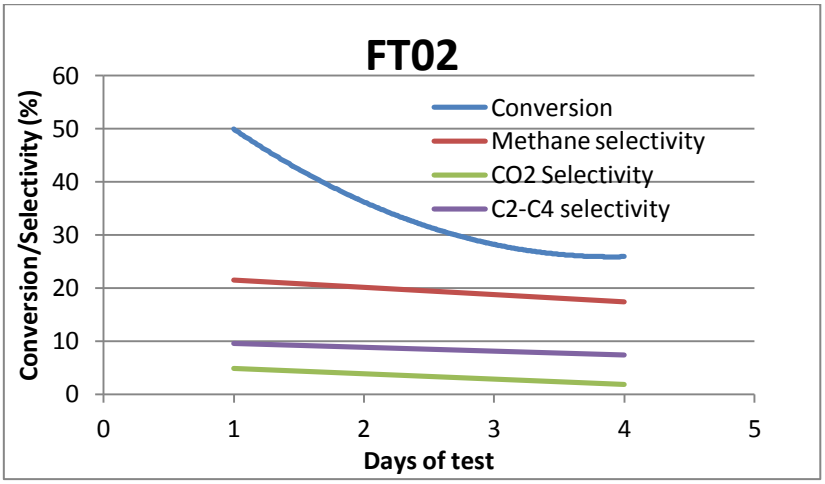

Graph 6.5: Conversion vs time for FT02

From the analysis of condensed products for FT02, the value of α in ASF distribution was 0.79.

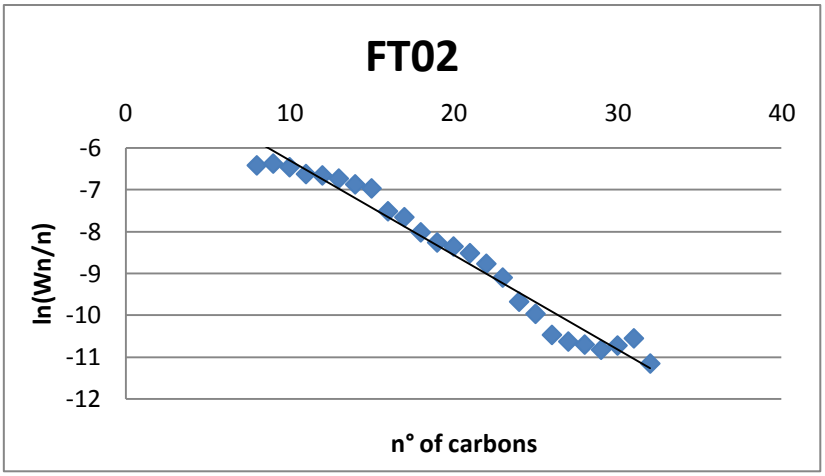

Graph 6.6: linearized distribution of condensed products for FT02

Also in this case, 5 gram of FT03 catalyst were charged into a fixed bed reactor and activated under hydrogen flow at 400°C. After that, the mixture of H_2/CO with 2/1 molar ratio was fed to the reactor. The catalyst was tested at 20 bar of pressure between 290°C and 340°C. The results (Graph 6.7) show that the conversion increases at increasing temperatures until the 80% of conversion is reached at 340°C.

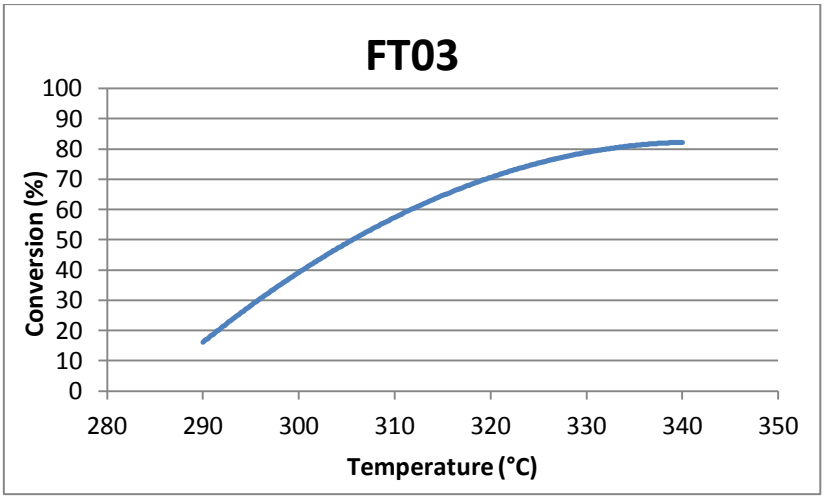

Graph 6.7: Conversion vs temperature for FT03

The test of the catalytic activity during the time was carried out at 300°C. Initially the conversion was good, around 50%, but it decreased rapidly under 30%. This decrease of activity is due to the formation of waxes that remain on the active sites. The selectivity to methane is about 20%. The selectivity to CO_2 is under 5% and the selectivity to lighter hydrocarbons is lower than 10%. After the test, 10 g of waxes were extracted from the catalyst. The deactivation can be explained with

the covering of the active sites from waxes. This fact is also supported by the low selectivity to lighter hydrocarbons. In this case the catalyst did not produce heavy hydrocarbons and it was not possible to calculate the α value.

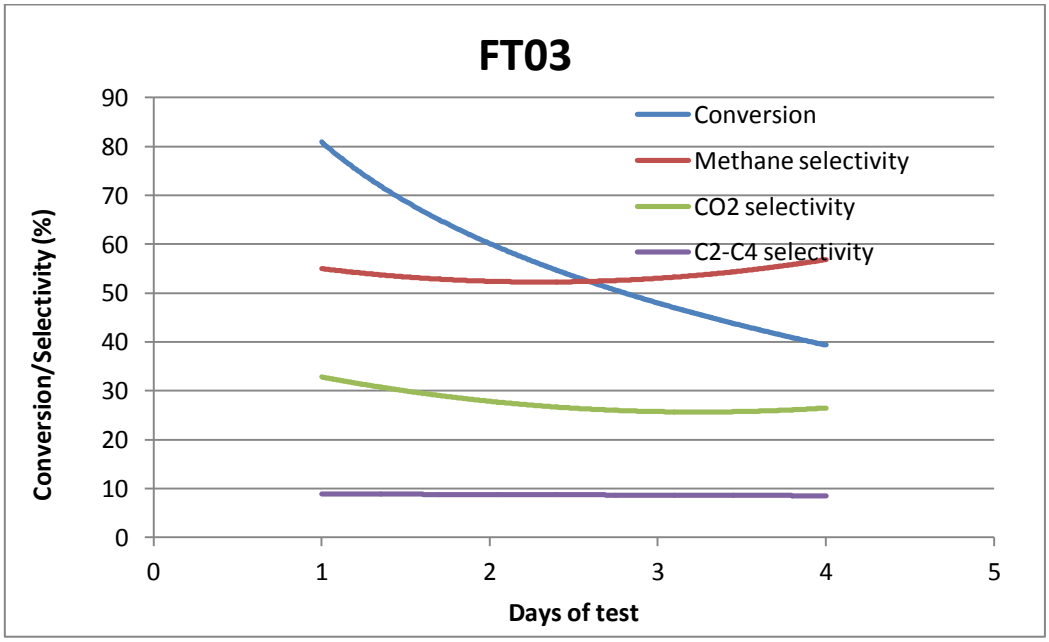

Graph 6.8: Conversion vs time for FT03

5 gram of sample FT04 were charged into a fixed bed reactor and activated under hydrogen flow at 400°C. A mixture of H2 and CO, 2/1 molar ratio, was fed to the reactor. The catalyst was tested at 20 bar of pressure between 225°C and 265°C. The results (Graph 6.9) show that the conversion is around 40% and grows very slowly at increasing temperatures; at 265°C the conversion is about 50%.

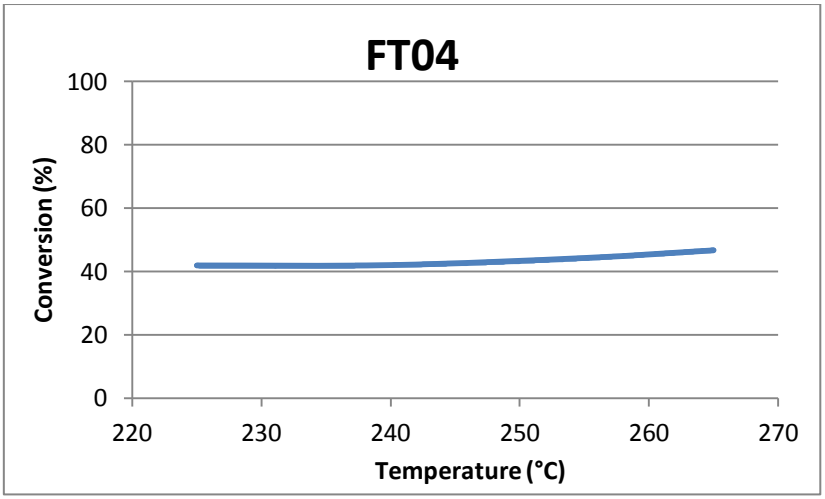

Graph 6.9: Conversion vs temperature for FT04

A productivity test (Graph 6.10) was carried on at 265°C. The catalyst shows a rapid decrease of conversion during the test, as well as the increasing of methane production with the progress of the test. CO_2 and lighter products show a slight growth and they are around 20%. Also in this case, as for FT03 sample, the catalyst does not produce heavy hydrocarbons.

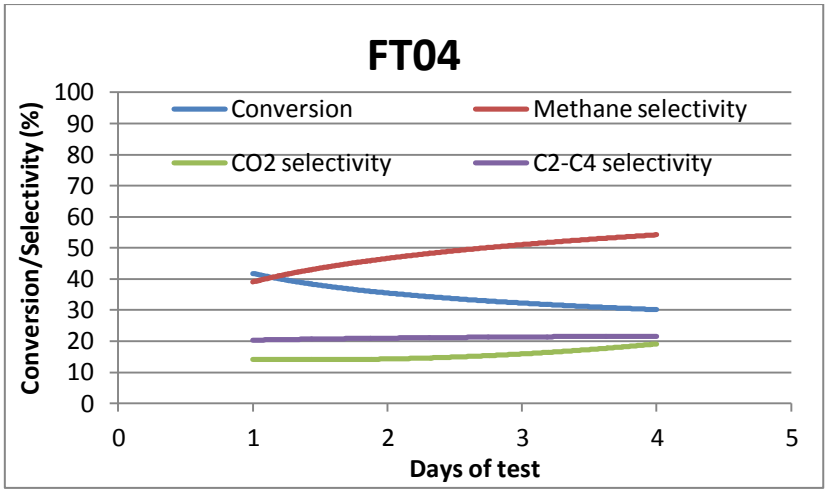

Graph 6.10: Conversion vs time for FT04

6.5 Conclusions

The characterization of FT01 showed the common characteristics of bulk sol-gel catalysts: low reducibility, low surface area and low dispersion. The analysis of structure does not show crystalline phases. On the contrary, the sonochemical method used for the synthesis of FT02 seems better than bulk sol-gel one if the reducibility of the systems is considered. Also the catalytic tests confirm this trend, but the differences in the behaviour are not so strong as expected.

The other catalysts (FT03 and FT04) were obtained both from a bulk sol-gel method and the results of characterization are very similar to FT01.

However, the catalytic behaviour was very different between FT03 and FT04. The operating range is very different; FT03 works well at around 300°C and it is highly affected by changing the temperature while for FT04 the operative range is at 240 - 260°C and its activity is less affected by the temperature. In both cases, the production of liquid hydrocarbons is absent. These systems seem not very good for industrial applications.

Bibliography

[1] A. Y. Khodakov, W. Chu, P. Fongarland; *Chem. Rev.* ***2007.*** *107, 1692*

[2] W. J. Wang, Y.W. Chen; *Appl. Catal.* ***1991.*** *77, 223*

[3] R. L. Chin, D. M. Hercules; *J. Phis. Chem.* ***1982.*** *86, 360*

[4] R. Bechara, D. Balloy, D. Vanhove; *Appl. Catal.* ***2001.*** *207, 343*

[5] H. Xiong, Y. Zhang, S. Wang, J. Li; *Catal. Commun.* ***2005.*** *6, 512*

[6] W. Ma, G. Jacobs, D. E. Sparks, M. K. Gnanamani, V. Ramana, R. Pendyala, C. H. Yen, J. L.S. Klettlinger, T. M. Tomsik, B. H. Davis; *Fuel* ***2011.*** *90, 756*

[7] A. Di Michele; PhD Thesis: **"Sonochemical synthesis of metal nanoclusters and their application in the Fischer-Tropsch process"**; 2007

[8] C. Chen, H. Yuuda, X. Li; *Appl. Catal. A* ***2011.*** *396, 116*

Chapter 7 – Effect of gelification

7.1 - Introduction

In this section, three catalysts are compared. For all these catalysts the support, the active phase and the promoter are the same. The active phase is composed by 9,75% by weight of Cobalt and 3,25% by weight of Iron[1], promoted with 0,5% by weight of Ruthenium[2,3]. The support is alumina[2,4,5,6,7,8]. For the three catalysts the preparation followed the bulk sol-gel method. FT05 and FT06 are prepared from metal nitrates. FT07 was prepared from a bimetallic cluster: $(C_2H_5)_4N[FeCo_3(CO)_{12}]$[9]. The difference between FT05 and FT06 is due to the rate of gelification. In Table 7.1 the characteristics of these catalysts are summarized.

SAMPLE	SUPPORT	ACTIVE PHASE	RAW MATERIAL	METHOD OF PREPARATION
FT05	alumina	9,75% Co - 3,25% Fe - 0,5% Ru	Nitrate	Bulk sol-gel
FT06	alumina	9,75% Co - 3,25% Fe - 0,5% Ru	Nitrate	Bulk sol-gel
FT07	alumina	9,75% Co - 3,25% Fe - 0,5% Ru	Carbonyl clusters	Bulk sol-gel

Table 7.1: method of preparation and precursors for these catalysts.

7.2 Preparation

FT05

The composition of this catalyst is: 9,75% Co – 3,25% Fe – 0,5% Ru; it was prepared by the bulk sol-gel technique. 50 g of $Al(Sec\text{-}OBu)_3$ were dissolved in 300 mL of isopropyl alcohol under dry atmosphere. In a flask 5.6088 g of $Co(NO_3)_2 \cdot 6H_2O$ and 2.7335 g of $Fe(NO_3)_3 \cdot 9H_2O$ were dissolved in 80 mL of isopropyl alcohol. In another flask, 0.106 g of $Ru_3(CO)_{12}$ were dissolved in dried THF. The Ruthenium solution was mixed and then added drop by drop to the aluminium alkoxide solution. To have the right amount of water for the gelification, 19 mL of water were then added drop by

drop very slowly. The system was left to evaporate and the sample was dried in an oven at 110°C for one night. The powder was finally calcinated at 200°C for one night and at 400°C for one day.

FT06

The catalyst FT06 was prepared with the bulk sol-gel method. The composition corresponds to a molar ratio 3:1 between Cobalt and Iron. The support is alumina. A little percentage (0,5%) of ruthenium was added in order to promote the catalytic activity. To obtain 10 g of alumina, 48.155 g of aluminium tri-sec.butoxide were dissolved in 300 ml of isopropyl alcohol. To this solution a solution was added of 5.5488 g of $Co(NO_3)_2 \cdot 6H_2O$ dissolved in 50 ml of isopropyl alcohol and a solution of 2.7089 g of $Fe(NO_3)_3 \cdot 9H_2O$ also dissolved in 50 ml of isopropyl alcohol. The ruthenium was added by a solution of 0.110 g of $Ru_3(CO)_{12}$ dissolved in THF. Then, water was added to the mixture of solutions in one pot and the gelification was instantaneous. The gel was aged under hood for 6 days, then it was dried at 110°C for 1 night. The sample was finally calcinated at 500°C for one night.

FT07

The composition of this catalyst is the same than for FT5 and FT06, but the active phase is coming from a bimetallic cluster instead of a mixture of nitrate solutions. The cluster is $(C_2H_5)_4N[FeCo_3(CO)_{12}]$ and it was synthesized by Dott. Deborah Viddick, at the "Universitè Catholique de Louvain-la-Neuve". 41.8 g of aluminium $(sec\text{-}OBu)_3$ were dissolved in 300 ml of isopropyl alcohol. 4.5 g of cluster were dissolved in THF and another solution was prepared by the dissolution of 0.105 g of triruthenium dodecacarbonyl in THF. The solutions were mixed and 22 ml of water were added to obtain the gelification, that started immediately. The gel was left to dry until a powder was obtained.

7.3 – Characterization

7.3.1 – TPR

Three peaks are observed in the TPR profile for FT05 (FIG. 7.1). The first peak at 154°C can be attributed to reducible species of Ruthenium, the second at 451°C to the reduction of Cobalt and

Iron oxides and the third, at 813°C, to the reduction of aluminate species deriving from metal oxide-support interactions with formation of covalent bonds. The percentage of reduction of metal oxides is 16% that increases to 31% if the aluminate species are also considered.

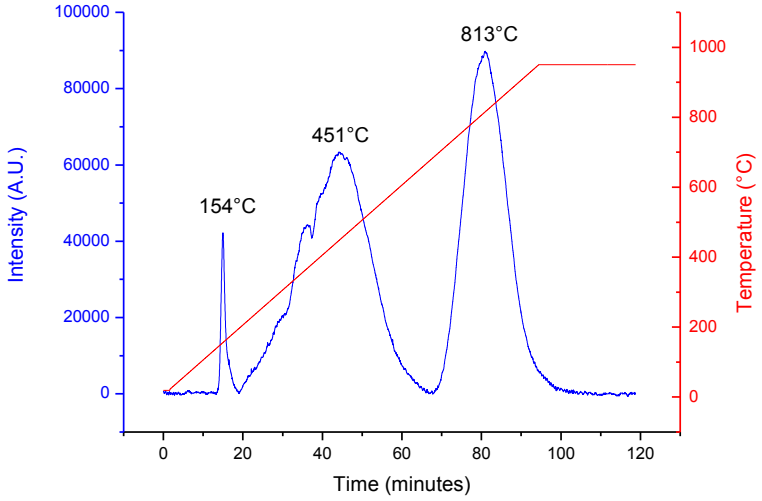

FIG. 7.1: TPR profile for FT05

The TPR profile for FT06 (FIG. 7.2) shows the presence of a peak of very low intensity at 170°C; this peak can be assigned to reducible species of Ruthenium deriving from the interaction with supporting alumina. Another broad peak of very high intensity starts at around 240°C, it is due to the reduction of metal oxides of Iron and Cobalt. Another peak is present at 800°C and it can be assigned to the species strongly bonded formed by the interaction between metal oxides and the support (spinels). The percentage of reduction of this catalyst is 56%. The reduction temperature of this sample is higher than expected. In fact, the presence of Ruthenium should lead to a decrease in the reduction temperature, but this fact is not observed in this case, probably because the preparation method is not favourable for a good dispersion.

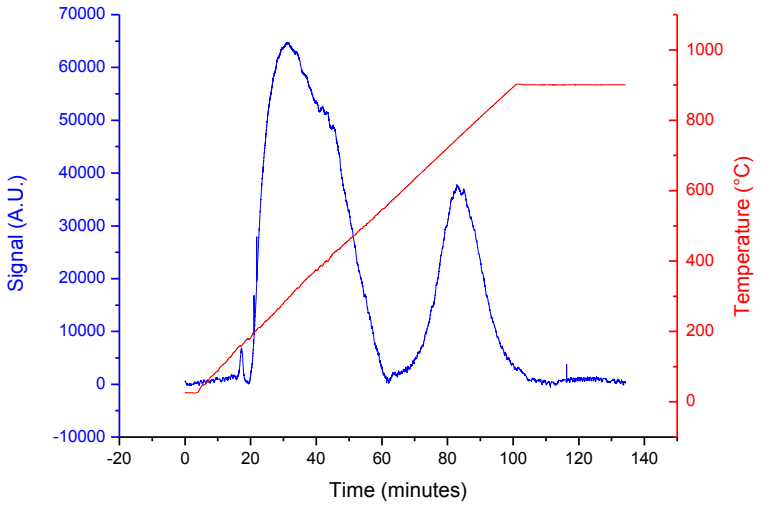

FIG. 7.2: TPR profile for FT06

The TPR analysis for FT07 shown in FIG. 7.3 evidences a negative peak centered at 225°C, probably due to the development of carbon monoxide coming from the cluster, that contains carbonyl groups as ligand. At the temperature of 250°C we can observe a peak that can be assigned to the reduction of metal particles partially oxidized by interaction with the support. In this case, however, the peak is not very significant for the calculations because the active phase is already at the metal state before the activation. The activation step is necessary to assure the chemical stabilization of the system.

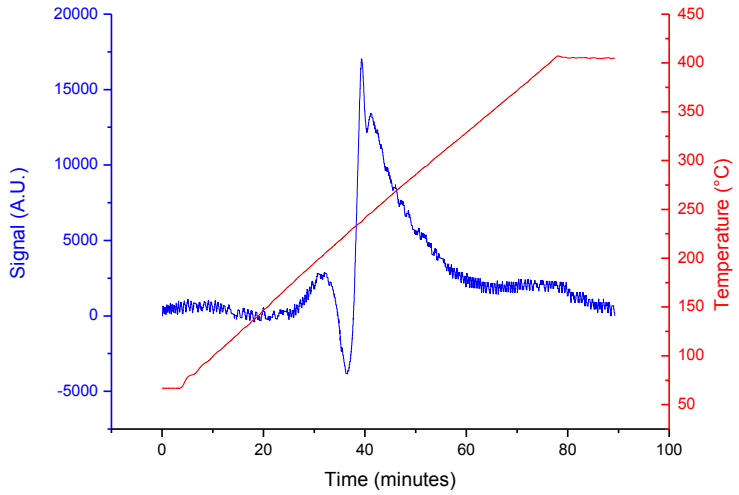

FIG. 7.3: TPR profile for FT06

7.3.2 – TPO

TPO analysis was done on the samples after a procedure of activation that simulates the activation treatment in the plant. For these catalysts, the activation treatment is carried out in a flow of hydrogen at 400°C for 4h.

The FT05 sample (FIG.7.4) shows two peaks at 200°C and 400°C, probably due to the formation of cobalt oxides and iron oxides. The total re-oxidation is 41%.

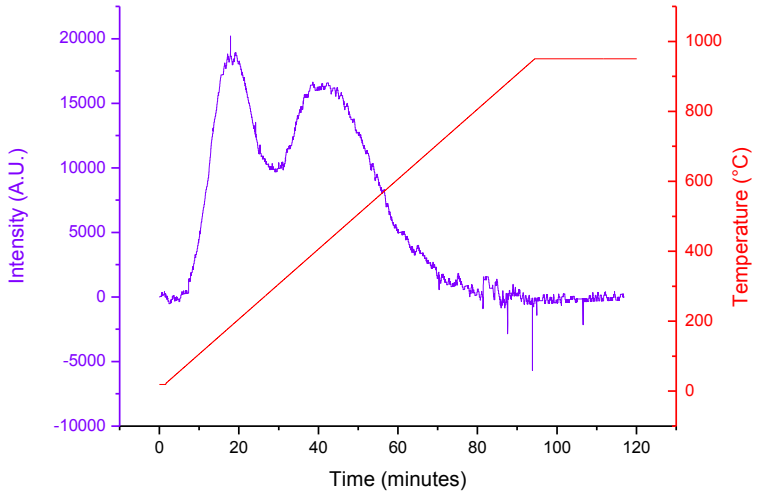

FIG. 7.4: TPO profile for FT05

Also the TPO analysis for FT06 (FIG. 7.5) was done after a pretreatment of activation for 4 h at 400°C. The profile shows a broad peak but of very low intensity, which starts at 100°C with a maximum at 300°C. Another small peak can be observed at the temperature of 700°C. Both these peaks are due to the reoxidation of Cobalt and Iron. This behaviour means that the amount of metal actually present at themetallic state is not very high and then there are not so much active phases for the Fischer-Tropsch synthesis. Calculation data show that the amount of metal re-oxidizable is only 19%.

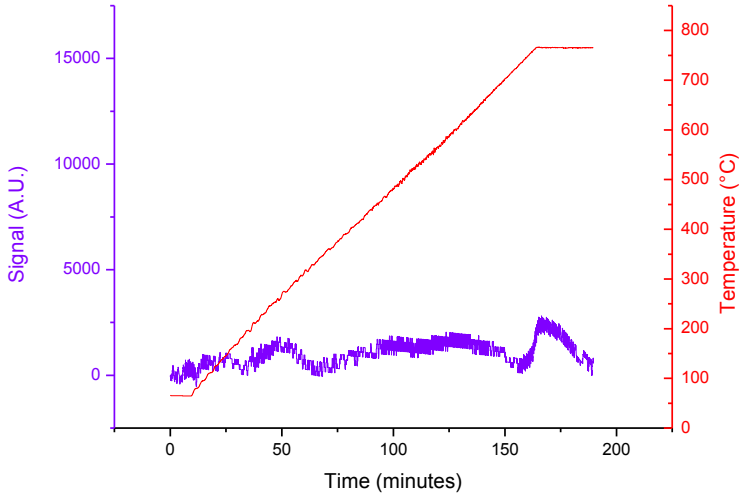

FIG. 7.5: TPO profile for FT06

The TPO profile for catalyst FT07 (FIG 7.6) shows two different peaks, due to the oxidation of Iron and Cobalt metals respectively. The percentage of re-oxidized metal calculated from the data of this analysis is 66%.

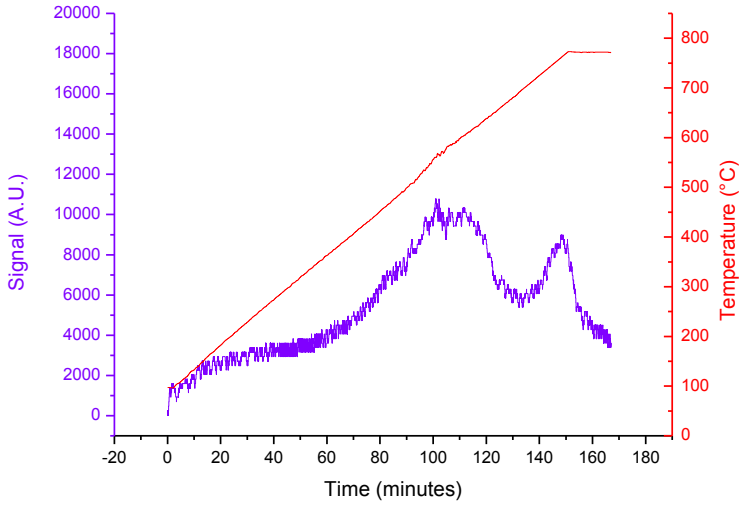

FIG. 7.6: TPO profile for FT07

7.3.3 H_2-TPD analysis

Also the TPD data were collected after a pre-treatment of hydrogen absorption at 400°C for 4h. From the analysis of the data for FT05, three peaks can be observed (FIG. 7.7) probably due to the three different metals (Ru, Co, Fe) present in the sample. The number of active sites totally resulted 2.0×10^{20} and the dispersion degree is 12.6%. The size of particles is 8 nm.

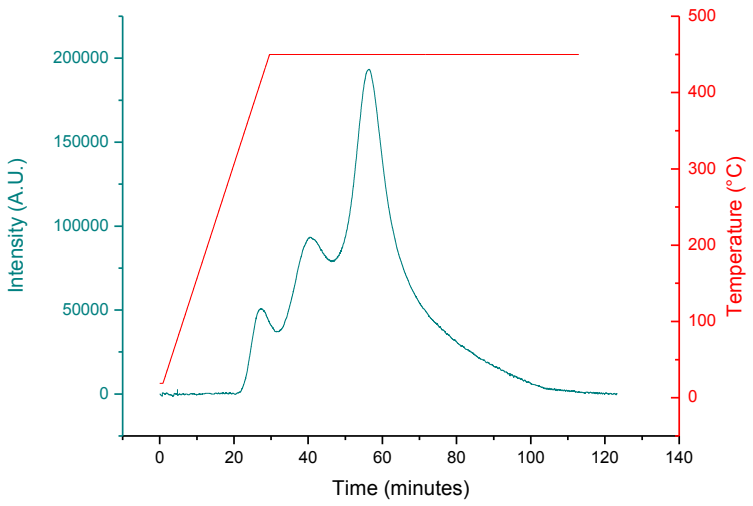

FIG. 7.7: H_2-TPD profile for FT05

The H_2-TPD profile for sample FT06 (FIG 7.8) shows a unique peak very intense at 400°C due to the desorption of hydrogen chemically absorbed on the surface of the catalyst. Data elaboration shows that the dispersion of metal is 8,3% and the number of active sites is $1.3x10^{20}$ per gram of catalyst. The estimated size of particles is around 12 nm.

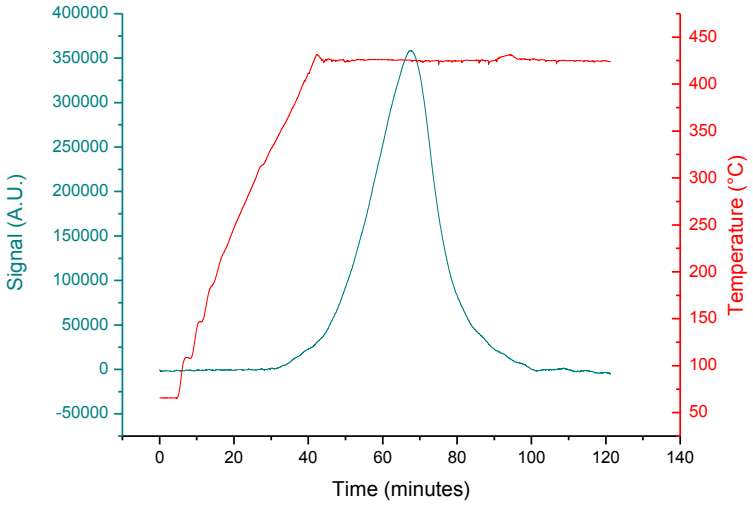

FIG. 7.8: H_2-TPD profile for FT06

The H_2-TPD profile acquired for FT07 (FIG. 7.9) shows two peaks at 150°C and 400°C respectively. These peaks are due to two different kinds of desorption, and consequentially two different types of active sites, one for Iron particles and the other for the Cobalt particles. However, the calculated data seem not so good if compared to the other analyses. The number of active sites is

$2.5x10^{19}$ per gram of catalyst; the dispersion degree is 1.6% and the estimated diameter of the particles resulted around 6 nm.

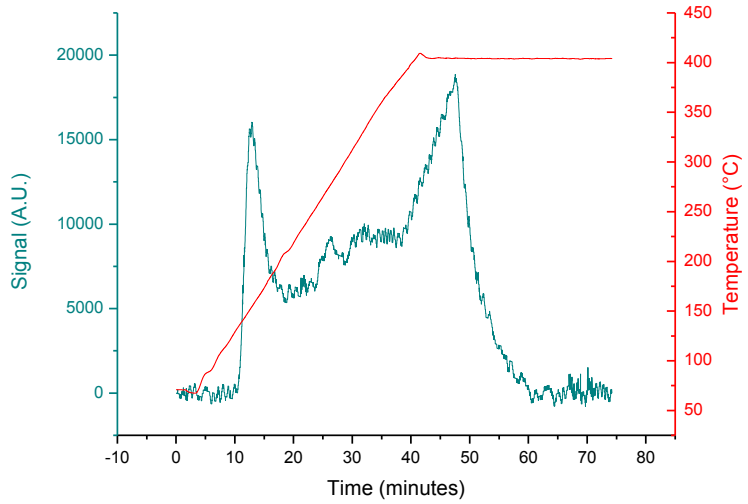

FIG. 7.9: H_2-TPD profile for FT07

7.3.4 Surface Area

In table 7.2 the measured values of surface area are reported.

SAMPLE	SURFACE AREA (m^2/g)
FT05	110
FT06	90
FT07	199

Table 7.2: surface area of the samples

The high difference observed for FT07 with respect to the other samples is probably due to the different precursors and thermal history of this sample.

7.3.5 XRD

The XRD spectra acquired for FT05 (FIG. 7.10) show that the catalyst is completely amorphous.

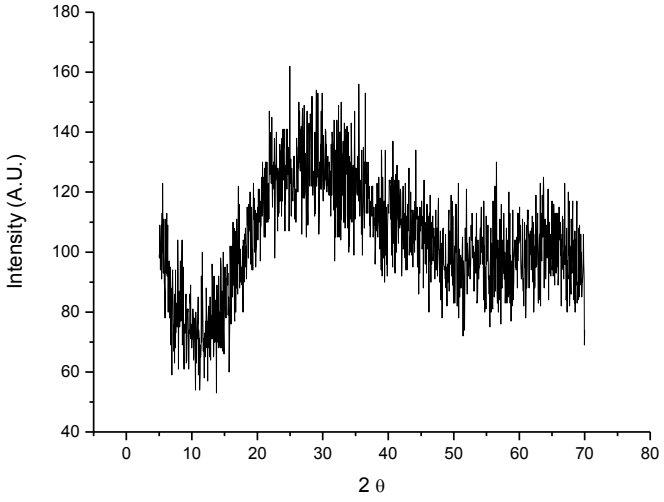

FIG. 7.10: XRD spectrum for FT05

The XRD spectra acquired for FT06 (FIG. 7.11) show again a completely amorphous structure, as expected for a catalyst prepared with the sol-gel technique.

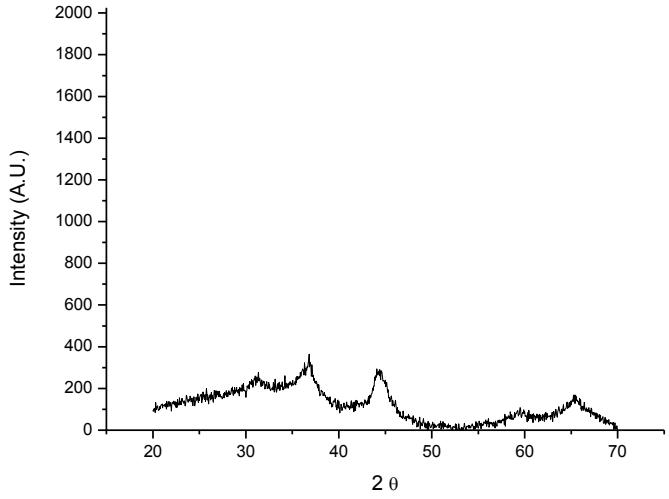

FIG. 7.11: XRD spectrum for FT06

Also in the case of FT07, the XRD (FIG. 7.12) spectrum shows a completely amorphous sample. The peaks at low angles are hardly to assign, but those could be due to the ligand groups present in the cluster structure.

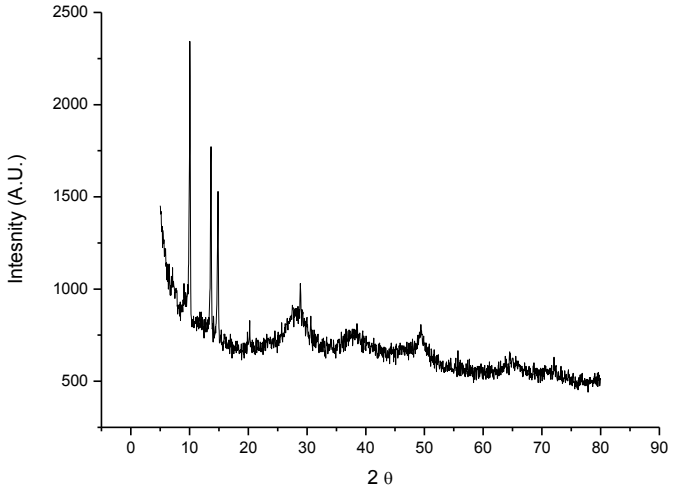

FIG. 7.12: XRD spectrum for FT07

7.3.6 IR analysis

The FT-IR spectra for FT05 (FIG. 7.13) were acquired before and after calcination. The signal of calcinated catalyst, reported in red line with respect to not-calcinated sample, reported in blue, shows the disappearance of the bands of nitrates at 1380 cm^{-1} and a big decreasing of presence of –OH groups (up to 3000 cm^{-1}).

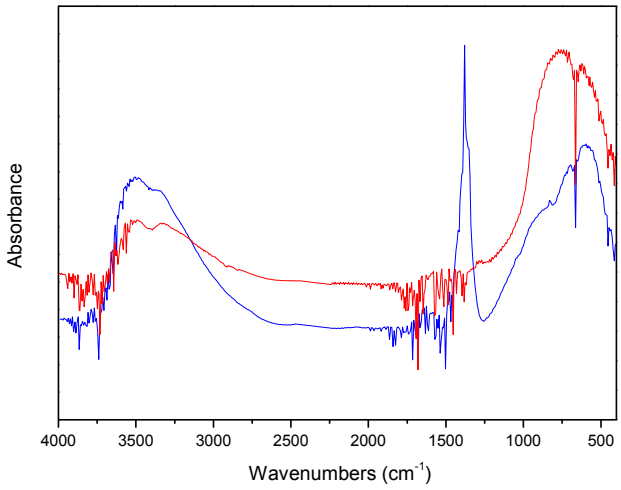

FIG. 7.13: IR spectra for FT05

Also in the case of FT06 (FIG.7.14) the IR spectra are acquired before (blue line) and after calcination (red line). The large band present at around 3500 cm^{-1}, due to the presence of hydroxide groups, and the double peak at 1300-1400 cm^{-1}, assignable to the nitrates, disappear after the calcination. It remains only the broad peak at low wavenumbers, due to the bonds between metal and oxygen.

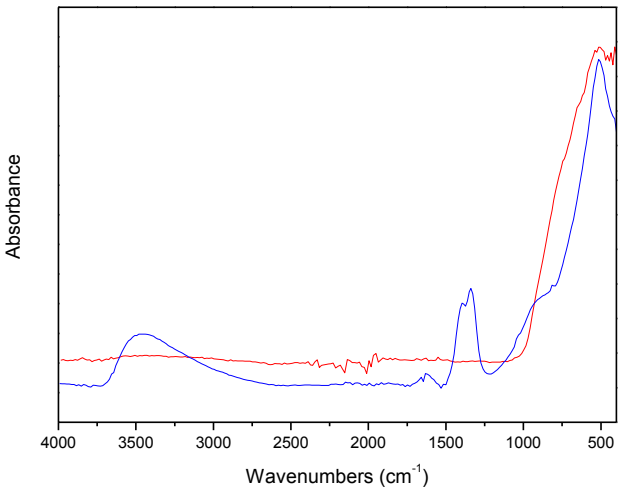

FIG. 7.14: IR spectra for FT06

The IR spectrum of the sample FT07 (FIG.7.15) was acquired before the activation, because the step of calcination for this sample is avoided. The spectrum shows several peaks between 2200 and 1600 cm^{-1}. These peaks are due to the presence of carbonyl groups as ligand inside the cluster. In the spectrum a peak at 550 cm^{-1} is also present , that means that there is the formation of a bond between the metal of the cluster and the support.

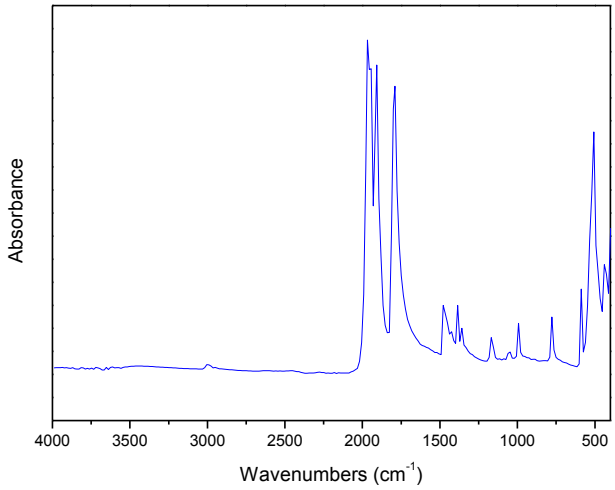

FIG. 7.15: IR spectrum for FT07

7.3.7 SEM images

The SEM image obtained with the FT05 sample (FIG 7.16 B) shows a good covering of the surface. Furthermore the EDX data (FIG 7.16 A) give different values than the expected ones: for Cobalt 11.76% and for Ruthenium 0.35%.

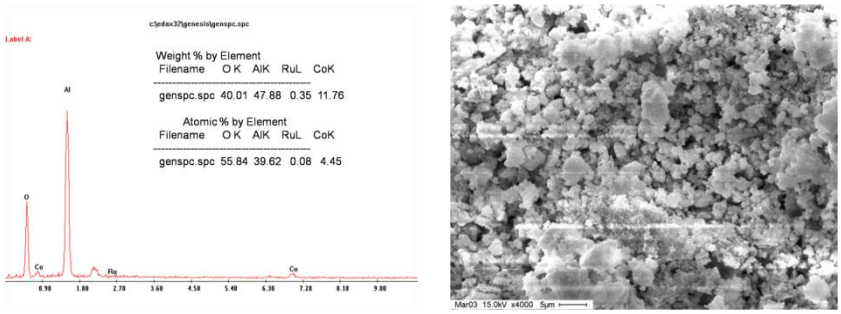

FIG. 7.16: A and B: EDX data and SEM image for FT05

Instead, SEM analysis of FT06 shows a catalyst not so much homogeneous, as can be observed in the figure 7.17 B. However, the EDX analysis (Fig 7.17 A) gives values of Iron of 5% and cobalt of 15%; these data are similar to the calculated ones.

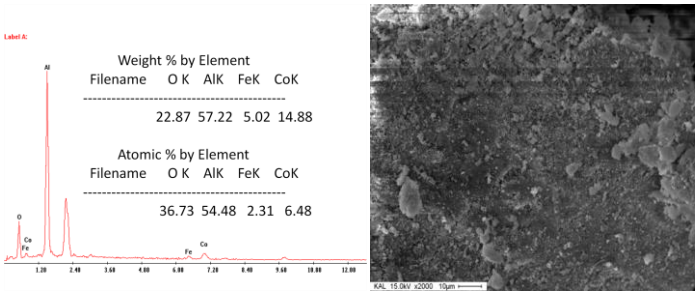

FIG. 7.17: A and B: EDX data and SEM image for FT06

7.3.8 TEM images

The TEM images of the sample FT06 (FIG 7.18 A and B) show a structure with a large dishomogeneity. Also the metal particles dispersed, that in the figure are the black points, seem to have a large range of dimensions. This is due to the sol-gel preparation that does not allow an high homogeneity of the structure.

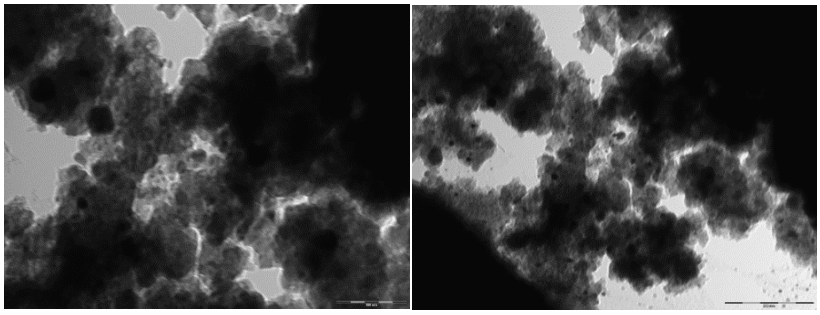

FIG. 7.18: A and B: TEM images for FT06

7.4 Catalytic tests

The catalytic tests were carried out in a fixed bed reactor. 5 gram of catalyst were charged into the reactor and activated under hydrogen flow at 400°C for 4h. After activation, a mixture of H_2 and CO, with molar ratio 2:1 was fed to the reactor. The catalyst was tested under pressure of 20 bar at different temperatures.

The data collected for FT05 (Graph 7.1) show that the conversion increases rapidly with temperature and the conversion is total at 250°C.

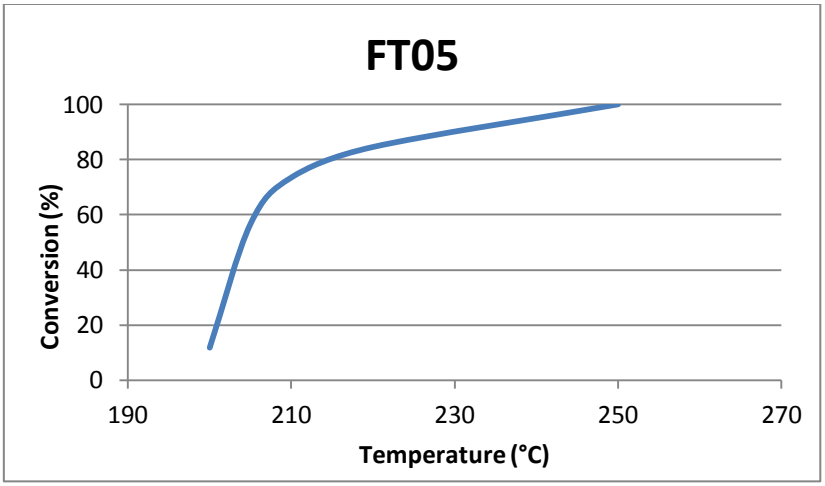

Graph 7.1: Conversion vs temperature for FT05

This catalyst was then tested at 205°C for 4 days. As shown in Graph 7.2, the conversion is stable at around 65%, without significant variations during the time.

The selectivity to methane is 40% and it decreases very slowly during the time. The selectivities to CO_2 and to lighter (C_2-C_4) hydrocarbons are overlapping and they decrease from 15% to 10% during the test.

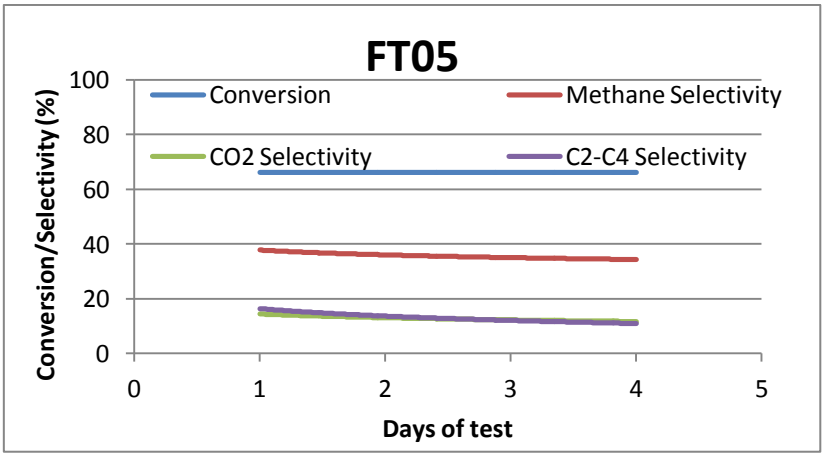

Graph 7.2: Conversion vs time for FT05

In this case, a large amount (35g) of condensed products was found after the test and 3 g of waxes were extracted from the catalyst. The analysis of condensed products (Graph 7.3) gives the α value of ASF distribution, that resulted as 0.81.

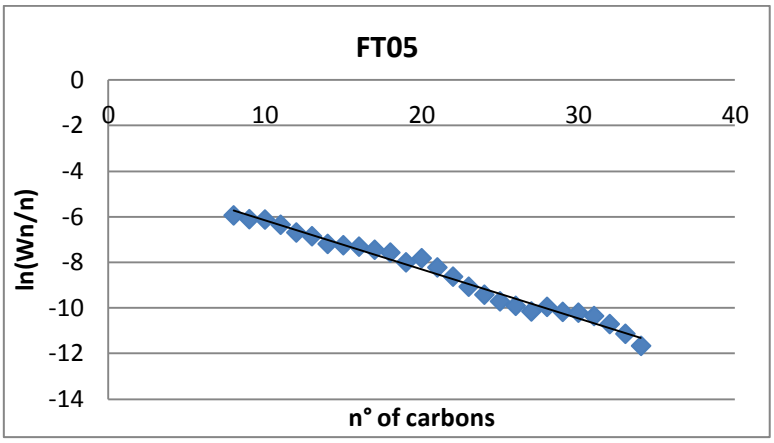

Graph 7.3: linearized production of condensed products for FT05

The results for FT06 are summarized in the following graph (Graph 7.4). It shows a constant increase of conversion at increasing temperatures, until a value around 70% is reached at 270°C.

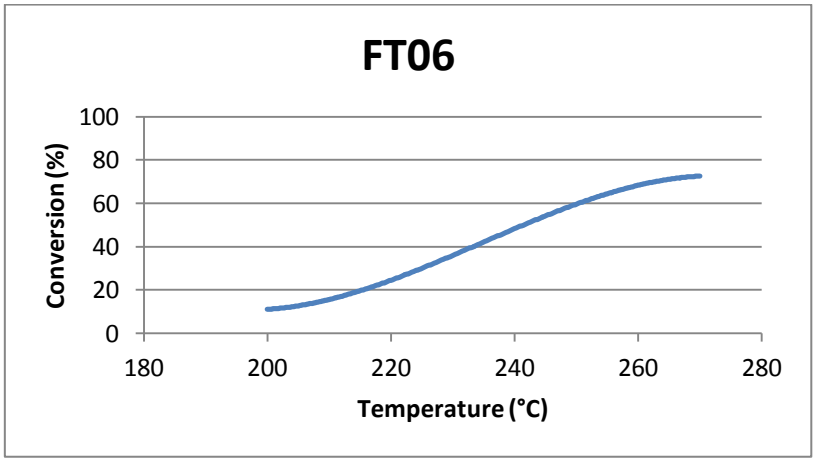

Graph 7.4: Conversion vs temperature for FT06

The productivity test was carried out for 4 days at 250°C.

Differently from the screening tests, when the conversion was around 60%, in the productivity test it was only 30%. This fact can be explained by the deactivation of catalyst during the screening test. The conversion during the time (Graph 7.5) decreases from 30% to around 20%. This confirms the deactivation of the catalyst during the use. Methane production is around 22% in all

days of test, as well as the CO_2 production and the C_2-C_4 production that are maintained at 3% and 11%, respectively.

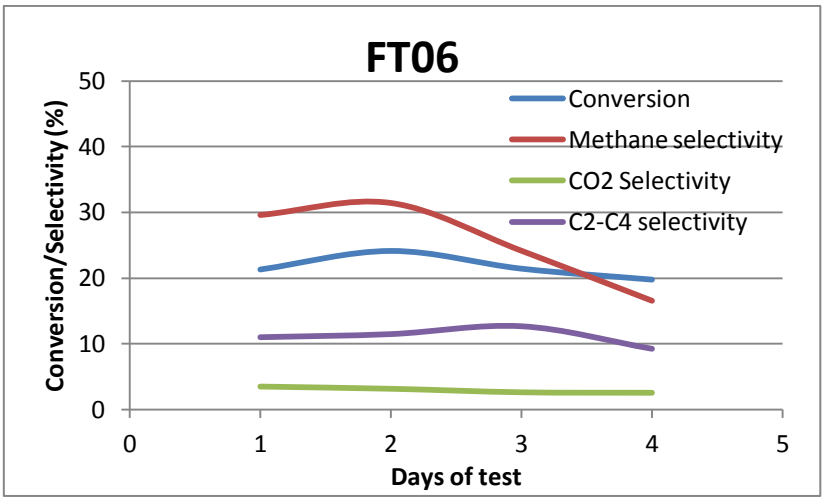

Graph 7.5: Conversion vs time for FT06

The analysis of condensed products collected, shown in the Graph 7.6 gives an α value for the ASF distribution of 0.72.

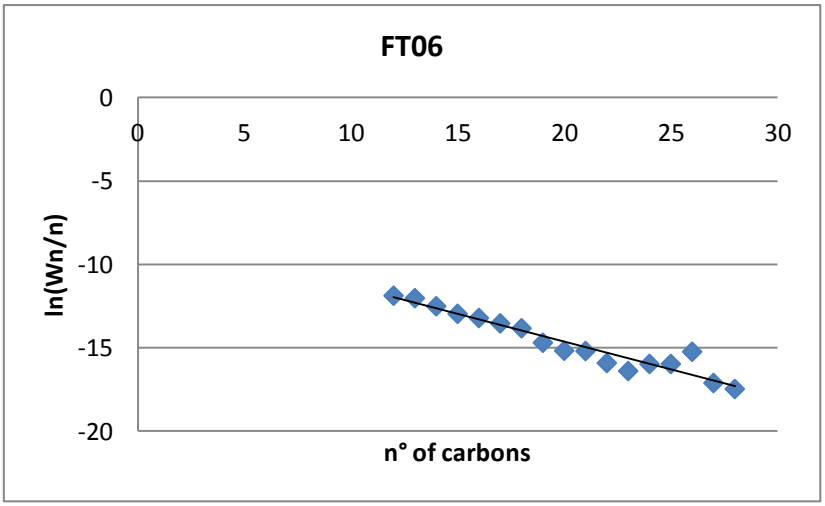

Graph 7.6: linearized production of condensed products for FT06

The catalyst FT07 was tested between 150°C and 270°C. The conversion is increased from 5% to 85% as it can be seen in the Graph 7.7.

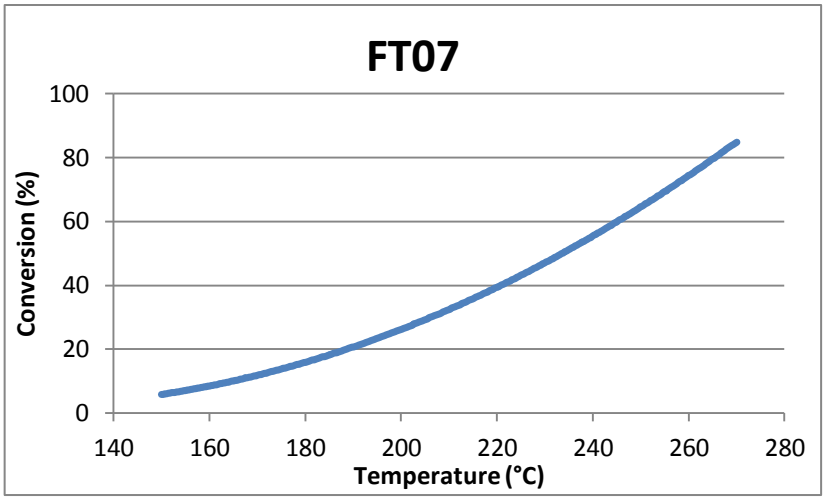

Graph 7.7: Conversion vs temperature for FT07

The productivity test at 250°C (Graph 7.8) initially shows a strange progress of the conversion. After it has a decrease from 60% to 45%, then it is stabilized. This trend can be due to an initial completion of the activation step following a modification of the cluster structure. Then the catalyst is subjected to a partial deactivation. Also in this case, the production of methane, CO_2 and C_2-C_4 remain quite constant; the selectivity to methane is 45%, while those to CO_2 and to C_2-C_4 hydrocarbons both are around 15%.

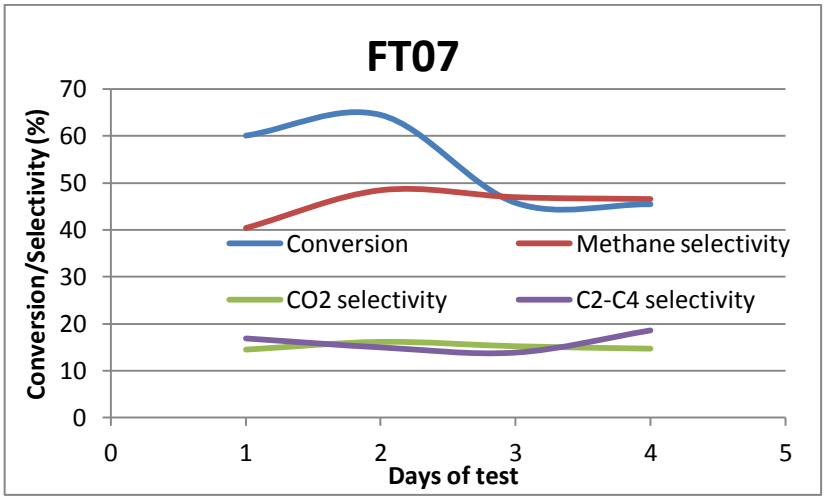

Graph 7.8: Conversion vs time for FT07

After discharging of liquid products, the analysis (Graph 7.9) shows that the ASF distribution of the products gives $\alpha = 0.79$

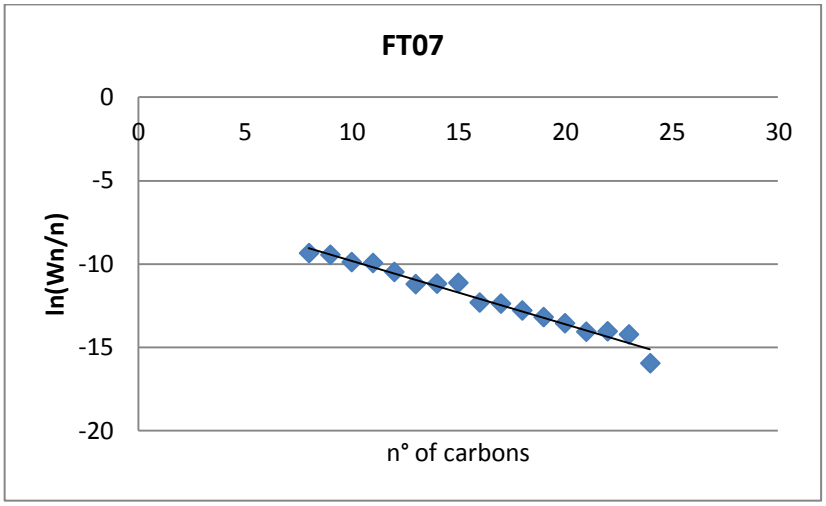

Graph 7.9: linearized production of condensed products for FT07

7.5 Conclusions

From the analysis of the data and of the catalytic tests for these catalysts, it results that an high rate of gelification for FT06 causes the agglomeration of metal particles observed by the characterization analyses. The inclusion of the active phase deeply inside the support is reflected in a very lower catalytic activity, also accompanied by a low selectivity to heavy products.

The use of clusters as precursors in the catalyst FT07 seems more interesting than the previous one. For example, according to the TPR profile, this catalyst is expected to be better than FT06. Catalytic tests show indeed an higher activity that corresponds at 250°C to a conversion of around 50%. Notwithstanding in this case the selectivity to lighter products seems higher, the ASF distribution seems better than the other one.

In any case, FT05 is the most interesting catalyst among all tested. Characterizations give very promising data, with respect to the other catalysts. The results of the activity tests show high conversions already at low temperatures. The conversion remains stable at 70% when the test is carried out for 4 days at 205°C. Also the selectivity to lower products is stable during the test. The α value of this sample is 0.81 and again it is the best value seen for all these catalysts.

Bibliography

[1] K. W. Jun, H. S. Roh, K. S. Kim, J. S. Ryu, K. W. Lee; *Applied Catalysis A: General* ***2004.*** *259, 221*

[2] A. Y. Khodakov, W. Chu, P. Fongarland; *Chem. Rev.* ***2007.*** *107, 1692*

[3] M. Reinikainen, M. K. Niemela, N. Kakuta, S. Suhonen; *Appl. Catal. A* ***1998.*** *174, 61*

[4] W. J. Wang, Y.W. Chen*; Appl. Catal.* ***1991.*** *77, 223*

[5] R. L. Chin, D. M. Hercules; *J. Phis. Chem.* ***1982.*** *86, 360*

[6] R. Bechara, D. Balloy, D. Vanhove; *Appl. Catal.* ***2001.*** *207, 343*

[7] H. Xiong, Y. Zhang, S. Wang, J. Li; *Catal. Commun.* ***2005.*** *6, 512*

[8] W. Ma, G. Jacobs, D. E. Sparks, M. K. Gnanamani, V. Ramana, R. Pendyala, C. H. Yen, J. L.S. Klettlinger, T. M. Tomsik, B. H. Davis; *Fuel* ***2011.*** *90, 756*

[9] P.Chini, L. Colli, M. Peraldo; *Gazz. Chim. Ital.* ***1960.*** *90, 1005*

Chapter 8 – Egg-shell catalysts.

8.1 Introduction

In this section, first of all, a reference catalyst, FT08, is prepared by the "to incipient wetness" impregnation technique[1,2], characterized and tested. Then, a procedure for the optimization of silica preparation to use as catalyst support is carried out, starting from a work of T. Lopez[3], by optimizing the synthesis procedure to control the surface area. The best support was then used to prepare three catalysts, with 13% by weight of cobalt as the active phase.

These three catalysts are prepared by a grafting method that permits to obtain a tiny layer of support including the active phase over another silica support[4,5,6] prepared before. This is the method defined as "egg-shell"[4]. The difference between these three catalysts is in the amount of support in the shell layer.

Another catalyst (FT10) is prepared with the egg-shell method, but using alumina as core for the egg-shell.

The prepared catalysts are summarized in Table 8.1

SAMPLE	ACTIVE PHASE	SUPPORT	METHOD OF PREPARATION
FT08	13% Co	silica	Incipient wetness
FT09-A	13% Co	silica/silica	Egg-shell
FT09-B	13% Co	silica/silica	Egg-shell
FT09-C	13% Co	silica/silica	Egg-shell
FT10	13% Co	silica/alumina	Egg-shell

Table 8.1: method of preparation and precursors for these catalysts.

8.2 Preparation

FT08

The reference catalyst was prepared by the incipient wetness method. The composition is 13% by weight of Co over a support of commercial silica with a particle size<80 mesh. The incipient wetness point with water over this support was found to be 1.9 ml/g silica. 10 g of this support were impregnated drop by drop with a solution of 7.4 g of $Co(NO_3)_2 \cdot 6H_2O$ dissolved in 19 ml of pure water. This catalyst was then dried at 110°C for one night and finally it was calcinated at 400 °C for 4 h.

As above indicated, this catalyst was used as reference one to compare with the others prepared by the "egg-shell" method.

8.2.1: Optimization of silica core

To optimize the preparation of the silica support, the work started following the procedure described by T. Lopez[3].

In order to obtain 6 g (0.1 moles) of silica support, 22.2 mL of TEOS and 41.5 mL of absolute ethanol were mixed in a flask, then they were refluxed under energetic stirring. When reflux condition has been attained, 27.1 mL of a saturated solution of oxalic acid (corresponding to 0.02564 moles) were added to the solution, then it was left under reflux again for 1h. After cooling the solution, 5 mL of water were added to complete the gelification. The solution was then left to evaporate under hood and the powder was dried in an oven for one night a 110°C. This support will be indicated as: Support 1. Ten supports were synthesized following this method, by varying the amount of oxalic acid in each sample. Table 8.2 shows the amount of oxalic acid used for 6 gram of each silica sample produced, and the molar ratio (R) between SiO_2 and oxalic acid.

	Oxalic Acid (moles)	Molar ratio (SiO_2/Oxalic acid)
Support 1	0.02564	3.9
Support 2	0.04167	2.4
Support 3	0.05000	2.0
Support 4	0.05882	1.7
Support 5	0.06667	1.5
Support 6	0.07692	1.3
Support 7	0.08333	1.2
Support 8	0.09091	1.1
Support 9	0.10000	1.0
Support10	0.01695	5.9

Table 8.2: moles of oxalic acid and molar ratio SiO_2/oxalic acid for each support prepared.

The B.E.T. surface area was used to evaluate the goodness of the prepared supports. Table 8.3 shows the surface area determined for each sample, as well as Graph 8.1 shows the surface area plotted versus the reverse of R.

Support 1	Support 2	Support 3	Support 4	Support 5
511 m^2/g	760 m^2/g	680 m^2/g	668 m^2/g	631 m^2/g
Support 6	Support 7	Support 8	Support 9	Support 10
600 m^2/g	643 m^2/g	600 m^2/g	612 m^2/g	398 m^2/g

Table 8.3: Surface area for all support prepared.

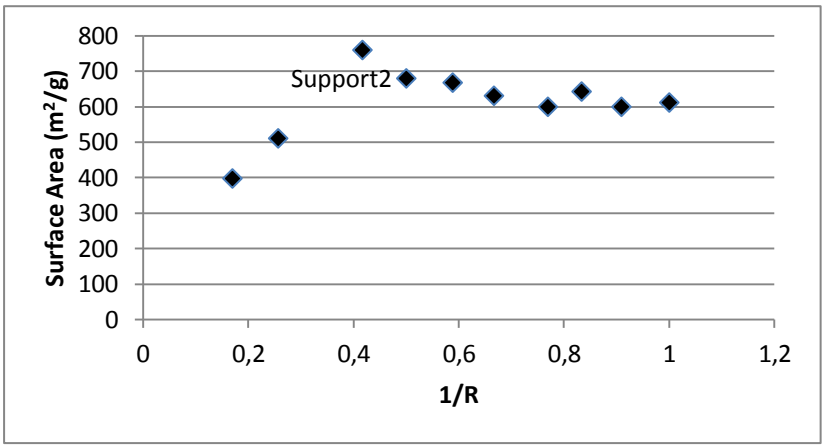

Graph 8.1: Surface area of samples vs 1/R.

Regarding the results of this characterization, Support 2 shows a very high surface area of 760 m^2/g, therefore it was chosen to prepare the core for the synthesis of egg-shell catalysts.

8.2.2: Preparation of silica-core catalysts

Three "Egg-shell" catalysts were prepared starting from Support 2 as core.

PREPARATION OF FT09-A

The composition of catalyst FT09-A is 13%$Co/SiO_2/SiO_2$. The technique of preparation was the egg-shell method. The core of the support was prepared following the procedure optimized for the Support 2. The shell containing Cobalt and again Silica was prepared from a solution of TMOS, ethanol and $Co(NO_3)_2{\cdot}6H_2O$. According to the incipient wetness point (in this case 0.65 ml per gram of core), in order to obtain this catalyst with 10 g of Silica-core, 7.83 g of $Co(NO_3)_2x{\cdot}6H_2O$ were dissolved in a solution composed by 5 ml of ethanol and 1.5 ml of TMOS, with a TMOS/ethanol molar ratio equal to 0.3. This solution was added drop by drop to 10 g of core silica. Then the catalyst was dried for 4 days at room temperature and 1 night a 110°C. Finally it was calcinated in an oven at 400°C for 4 h.

PREPARATION OF FT09-B

The composition of catalyst FT09-B, the technique of preparation and the core of catalyst are the same as for FT09-A. The shell containing Cobalt and again Silica was prepared from a solution of TMOS, ethanol and $Co(NO_3)_2 \cdot 6H_2O$. For the formation of the shell, the TMOS/Ethanol molar ratio was 0.5 and, in this case, the incipient wetness point was 0.87 ml per gram of core. For this catalyst 8.26 g of $Co(NO_3)_2 \cdot 6H_2O$ were dissolved in a solution of 5.8 ml of ethanol and 2.9 ml of TMOS. This solution was added drop by drop to 10 g of core silica. Then the catalyst was dried for 4 days at room temperature and 1 night a 110°C. Finally it was calcinated in an oven at 400°C for 4 h.

PREPARATION OF FT09-C

Sample FT09-C is completely analogue to FT09-A and B, but in this case the TMOS/Ethanol molar ratio was 0.6. The core is the same as for the other samples; the solution to the formation of shell shows an incipient wetness point of 0.89 ml per gram of core. Regarding that, the catalyst was prepared by gelification of a solution of 8.39 g of $Co(NO_3)_2 \cdot 6H_2O$, 5.5 ml of ethanol and 3.4 ml of TMOS over 10 gram of silica core. Also in this case, the catalyst was dried for 4 days at room temperature and 1 night a 110°C and finally it was calcinated in an oven at 400°C for 4 h.

FT10

The composition of this catalyst is analogue to FT9-A, but the core in this case is composed of alumina: $13\%Co/SiO_2/Al_2O_3$. In order to obtain 10 grams of alumina, 48.3 g of $Al(sec\text{-}OBu)_3$ were dissolved in 300 ml of isopropyl alcohol. The solution was left under vigorous stirring, then it was left to gelificate by the moistness present in the atmosphere. The gel was aged for a week, thenit was dried at 110°C for 1 night until a powder was obtained. A solution of TMOS and ethanol (molar ratio TMOS/ethanol = 0.3) was used to form the shell of silica around the particles of alumina. 10 g of alumina were impregnated drop by drop with a solution of 5 ml of ethanol, 1.5 ml of TMOS and 7.84 g of $Co(NO_3)_2 \cdot 6H_2O$ as performed for FT9-A. The TMOS including the Cobalt precursor gelified over the alumina core. The sample was left to age again for a week, then dried for 1 night at 110°C and, finally, calcinated for 4 h at 400°C.

8.3 Characterization

8.3.1 TPR

The TPR profile for the reference catalyst (FIG 8.1) shows two peaks partially overlapping at a temperature of about 400°C. These signals are due to the reduction from CoO and Co_2O_3 to the metallic status. Another peak of very low intensity is present at 700°C. This peak can be assigned to hardly reducible metal-support species. The metal reducibility of FT08 catalyst resulted 87%.

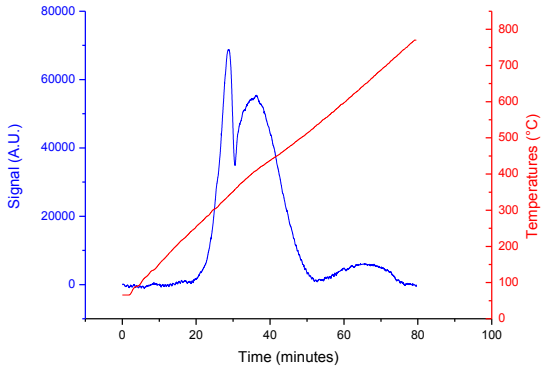

FIG. 8.1: TPR profile for FT08

The TPR analysis done on sample FT09-A (FIG. 8.2) shows a peak at around 400°C, that seems formed by the overlapping of two peaks. These two peaks are due to the reduction of Co^{3+} at Co^{2+} and of Co^{2+} to Co^{0} respectively. Another peak of very low intensity can be observed at temperatures of about 700°C. This peak can be assigned to the species formed by Cobalt-Silica interactions with very high bonding strength and then very hardly to reduce. Calculation made with the aid of calibration curve, shows that the total reduction of the sample was 87%, that decreases to a value of 78% if the last peak was excluded because the corresponding species is not activable in plant conditions.

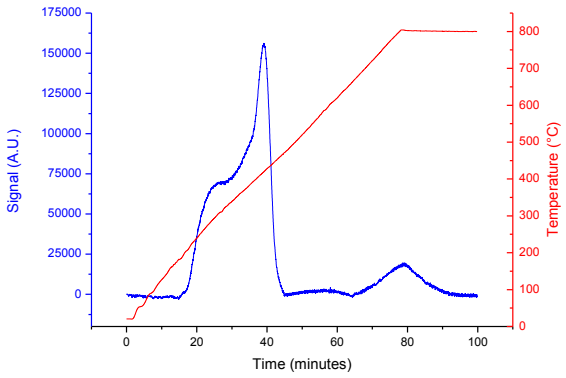

FIG. 8.2: TPR profile for FT09-A

The TPR profile for sample FT09-B (FIG. 8.3) is very similar to that of sample FT09-A. The two peaks at 400°C assigned to the reduction of cobalt oxides are a little more defined than for FT09-A; the peak at 700°C due to the cobalt silicate species is also present. The total percentage of reduction in this case is 63%, that decreases to 49% when the peak at 700°C is excluded from the calculation.

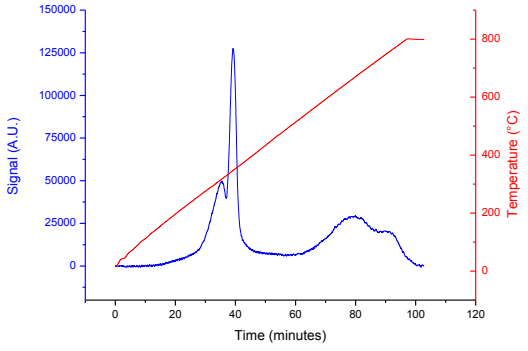

FIG. 8.3: TPR profile for FT09-B

Regarding the TPR profile for sample FT09-C (FIG. 8.4) we can observe that the peaks at 400°C are completely overlapping and it is not possible to distinguish between the reduction of CoO and of Co_2O_3. Also in this case it is present the peak at a temperature around 700°C due to the strong interaction between metal and support. In this case the amount of cobalt reduced is 56%, but without the peak at 700°C this value becomes 41%. A significative loss in the amount of reducible

metal can be observed going from FT09-A to FT09-C. This fact is not strange. In fact, if we consider that following the increasing of the value of the TMOS/Ethanol molar ratio it correspondingly increases the amount of the silica in the shell, then the system progressively becomes more similar to a bulk sol-gel catalyst, and the amount of active metal available decreases by the increased inclusion in the silica-support structure.

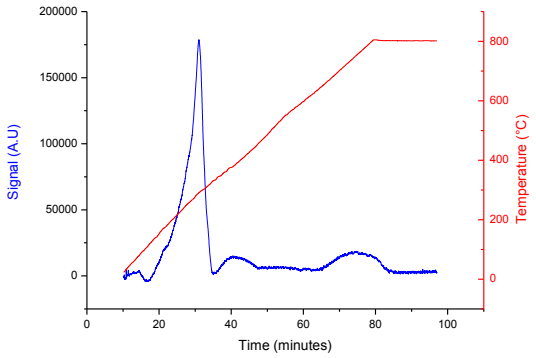

FIG. 8.4: TPR profile for FT09-C

The TPR profile for sample FT10 (FIG. 8.5) shows two intense peaks: the first, at 370°C, is due to the reduction of cobalt oxides to the metal state; the second, at 730°C, is assignable to species originated by the interaction cobalt-support very strongly bonded. The total reduction of the sample is 67%; this value decreases to 45% if only the first peak is considered. This sample hence shows a lower reducibility than the corresponding with a silica-core.

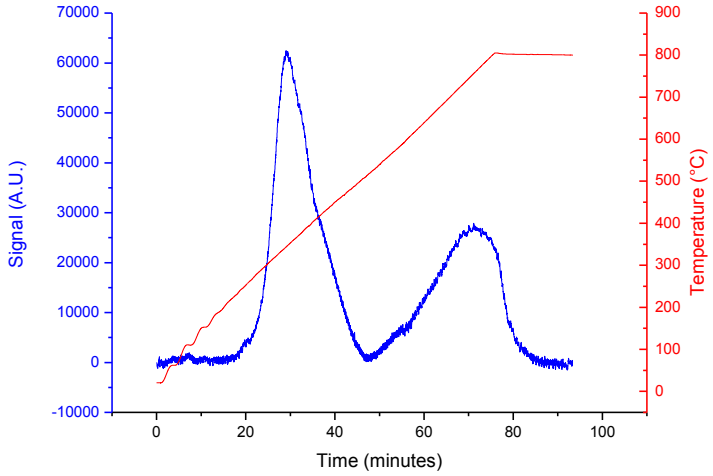

FIG. 8.5: TPR profile for FT10

8.3.2 TPO

The TPO data were collected after an activation treatment at 400°C for 4h under hydrogen flow.

The TPO profile registered on sample FT08 (FIG. 8.6), after the activation treatment, shows only a peak of re-oxidation of metallic cobalt, at a temperature of 200°C. The analysis shows that the reoxidation is complete at 400°C, with a maximum at 200°C. The reoxidation degree of metal is 17%.

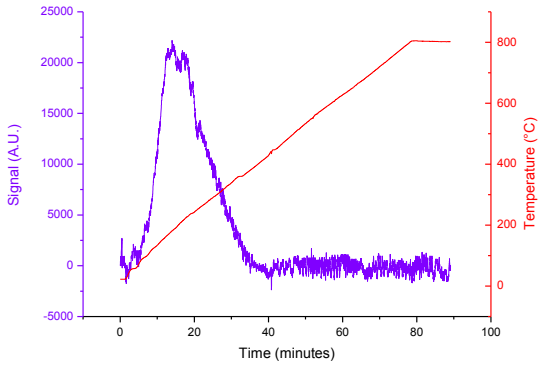

FIG. 8.6: TPO profile for FT08

The TPO analysis of sample FT09-A (FIG. 8.7) was done after the activation pretreatment. The graph shows only a peak centered around 200°C with a shoulder at temperatures slightly higher. The re-oxidation is complete at 400°C. The calculation based onthe calibration curve of the instrument for that analysis shows that the amount of cobalt re-oxidized is 33%; this is the amount of really active metal in the catalyst after activation in plant conditions.

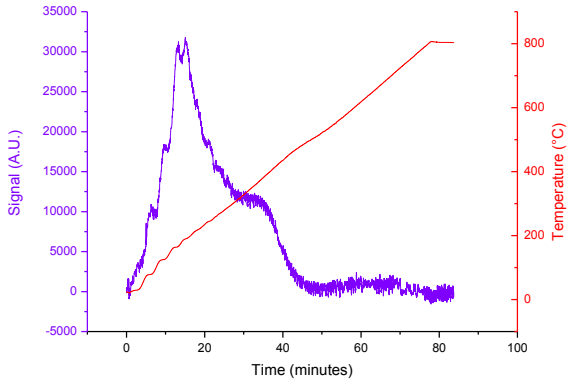

FIG. 8.7: TPO profile for FT09-A

The TPO profile of FT09-B was made after the same activation treatment as for FT09-A. The graph of the analysis (FIG. 8.8) is similar to that for FT09-A. There is the peak at 200°C, but it is not present the shoulder at a temperature slightly higher; perhaps the first peak has involved the second signal. Also in this case the re-oxidation process is complete at 400°C. In this case, the amount of cobalt re-oxidized is less than for FT09-A: it is only 19%.

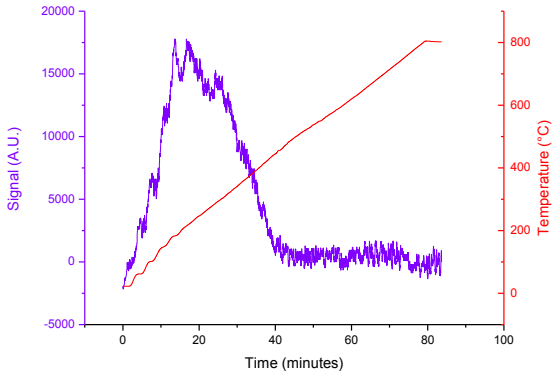

FIG. 8.8: TPO profile for FT09-B

The TPO analysis over sample FT09-C (FIG. 8.9) gives a graph very similar to the others, particularly to that for FT09-A. There were present the same peak and the shoulder at the same temperatures and, as for the other TPO profiles, the oxidation of the catalyst, done after the pretreatment of the sample, is complete at 400°C. This sample shows an amount of oxidizable metal of 17%.

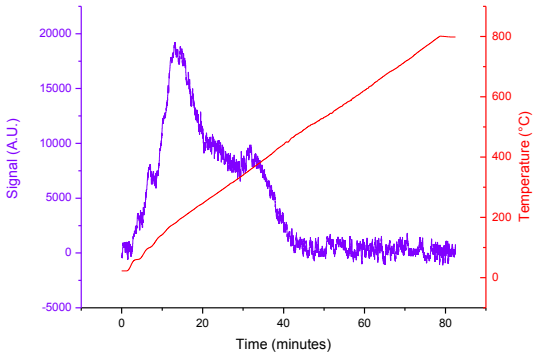

FIG. 8.9: TPO profile for FT09-C

The TPO profile of sample FT10 (FIG. 8.10) was done, as for the others, after a pretreatment of activation under hydrogen flow (50 ml/min) for 4 h at 400°C. There is only a peak centered at 200°C due to the re-oxidation of cobalt. The amount of metal estimated by this analysis resulted as 31%, very close to the analogue FT09-A.

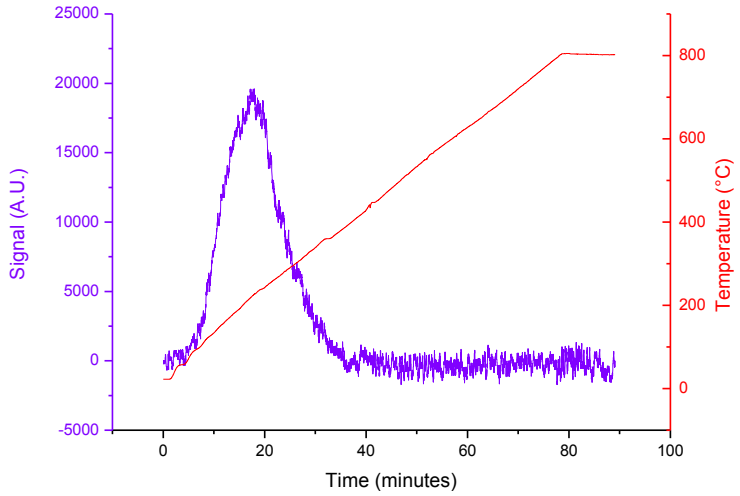

FIG. 8.10: TPO profile for FT10

8.3.3 H_2-TPD

The TPD profiles were acquired after a treatment of adsorbing hydrogen at 400°C for 4 hours. The H_2-TPD profile for catalyst FT08 (FIG. 8.11) shows the peak at room temperature due to desorption of hydrogen physisorbed on the surface. The second peak is a band between 50°C and 400°C due to the desorption of hydrogen chemically adsorbed. The calculation gives the number of active sites, that resulted $6*10^{19}$ per gram of catalyst, the dispersion degree of 9.6% and the average size of particles of 10 nm.

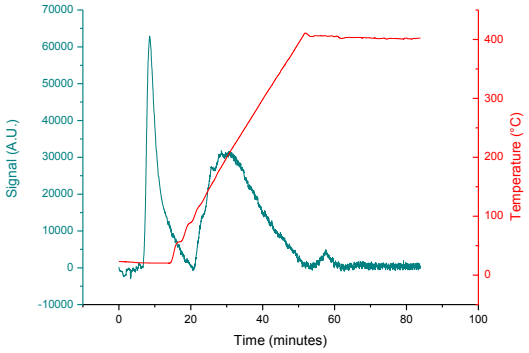

FIG. 8.11: H_2-TPD profile for FT08

From the H_2-TPD profile for FT09-A (FIG. 8.12) it can be observed a narrow and intense peak at room temperature. This peak is due to desorption of hydrogen physically adsorbed. It is not relevant for the characterization. The band of chemical desorption of hydrogen for the catalyst, between room temperature and 300°C, resulted by the overlapping of several peaks. Every peak is due to the interaction between hydrogen and different active sites of the catalyst. This sample shows 1.1 x 10^{20} active sites per gram of catalyst, a dispersion of metal of 7.8% and the average size of particles of 12 nm.

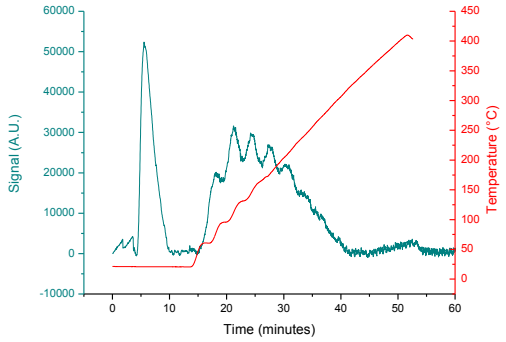

FIG. 8.12: H_2-TPD profile for FT09-A

The H_2-TPD profile for FT09-B (FIG. 8.13) is very similar to that of FT09-A. The data calculated are the following: 5.6 x 10^{19} active sites per gram of catalyst, a dispersion of metal of 7.9% and the average size of particles of 12 nm.

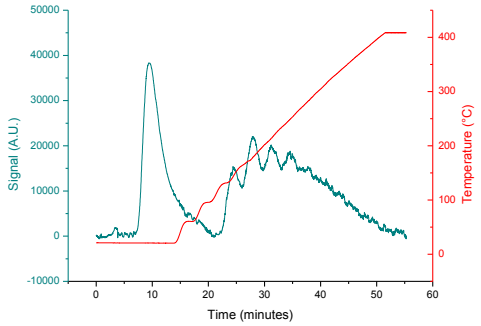

FIG. 8.13: H_2-TPD profile for FT09-B

Also the H_2-TPD profile for FT09-C (FIG. 8.14) is very similar to FT09-A and FT-09B, but in this case the data calculated are: 6.8 x 10^{19} active sites per gram of catalyst, a dispersion of metal of 10% and the average size of particles of 10 nm.

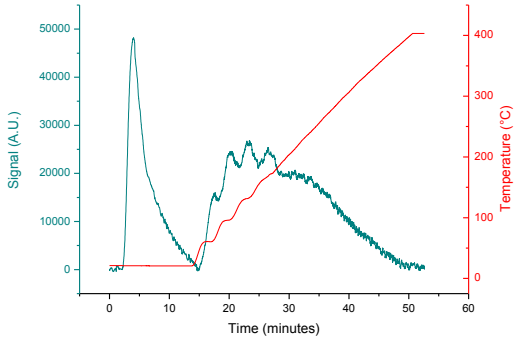

FIG. 8.14: H_2-TPD profile for FT09-C

The H_2-TPD profile for FT10 (FIG. 8.15) is very similar to those for the samplesFT09-A, B and C. Also in this case, there is the peak at room temperature associated with the physical desorption of hydrogen and also in this case the band due to the chemical desorption of hydrogen is formed by a several number of peaks each one associated to a different interaction between hydrogen and surface cobalt sites. The values calculated are similar to those for FT09-A: in fact the number of active sites is 1.2 x 10^{20}, the dispersion is 9% and the average size of particles is 11 nm.

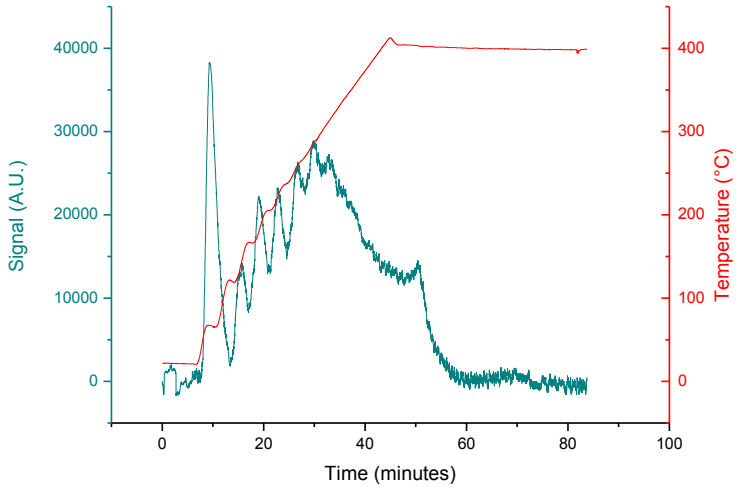

FIG. 8.15: H_2-TPD profile for FT10

8.3.4 Surface Area

By keeping in mind the area determined for the support of FT09, the surface area of catalysts are shown in Table 8.4

SAMPLE	SURFACE AREA (m^2/g)
FT08	386
FT09-A	640
FT09-B	620
FT09-C	597
FT10	256

Table 8.4: surface area of the samples

8.3.5 XRD

The X-Ray Diffraction analysis performed on the structure of FT08 (FIG. 8.16) shows as expected a generally amorphous sample. However, there are three peaks at 2θ = 37°, 59° and 65° assignable to the presence of Co_3O_4[7].

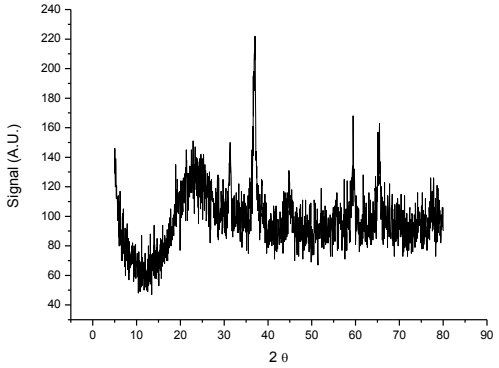

FIG. 8.16: XRD spectrum for FT08

By observing the XRD spectra for FT09-A, B and C, (FIG. 8.17, 8.18 and 8.19 respectively) we can evidence the same features for all the samples. The three catalysts show an amorphous structure, as expected when a sol-gel method is used for the synthesis. Also in this case however, the three catalysts show the typical peaks assignable to the crystalline structure of Co_3O_4[7].

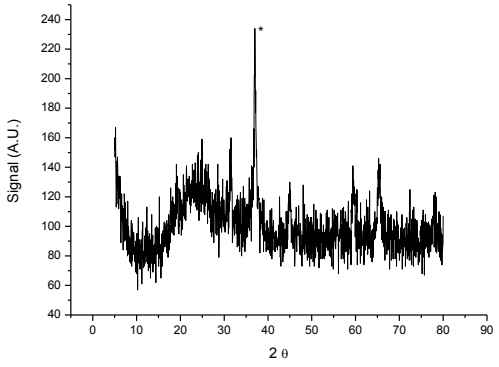

FIG. 8.17: XRD spectrum for FT09-A

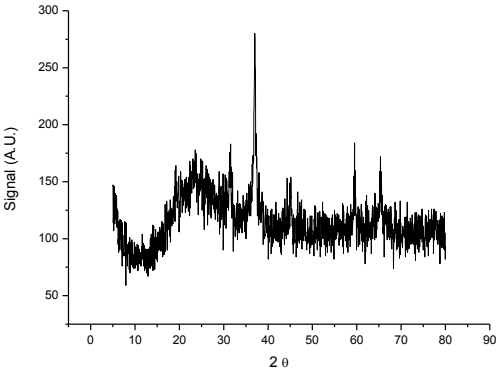

FIG. 8.18: XRD spectrum for FT09-B

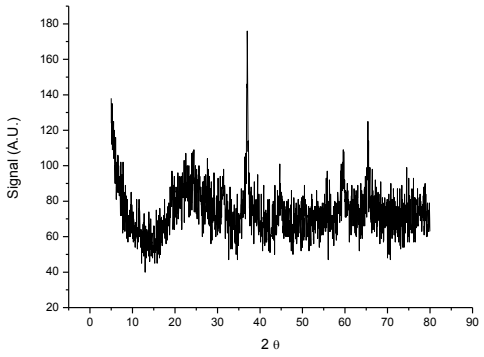

FIG. 8.19: XRD spectrum for FT09-C

The XRD analysis of the sample FT10 (FIG. 8.20) also shows an amorphous structure of the support. The only peak recognizable, very weak, at 37° is due to the presence of Cobalt as Co_3O_4 into the structure.

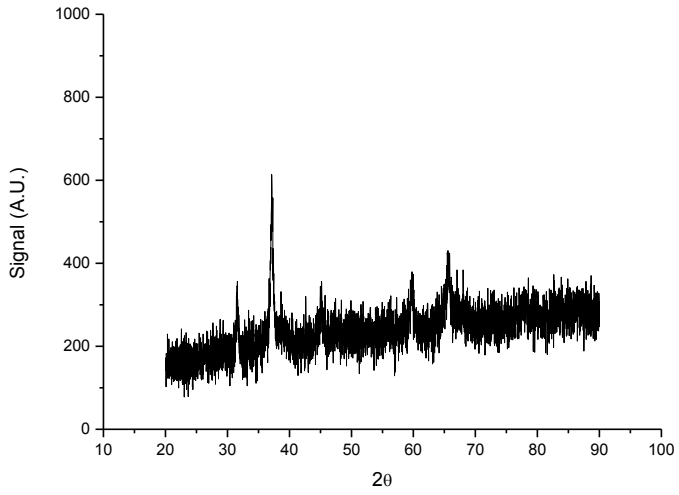

FIG. 8.20: XRD spectrum for FT10

8.3.6 FT-IR

The IR spectrum acquired before the calcination (blue line) for sample FT08 (FIG. 8.21) shows an intense band due to the hydroxide surface groups at wavenumbers around 3500 cm^{-1}. The peak at 1350 cm^{-1} is assigned to the nitrates coming from $Co(NO_3)_2 \cdot 6H_2O$. The other band at 1200 cm^{-1} is due to the silica bond with oxygen. In the calcinated sample (red line), the band of hydroxide groups is almost disappeared, as well as the band due to nitrates.

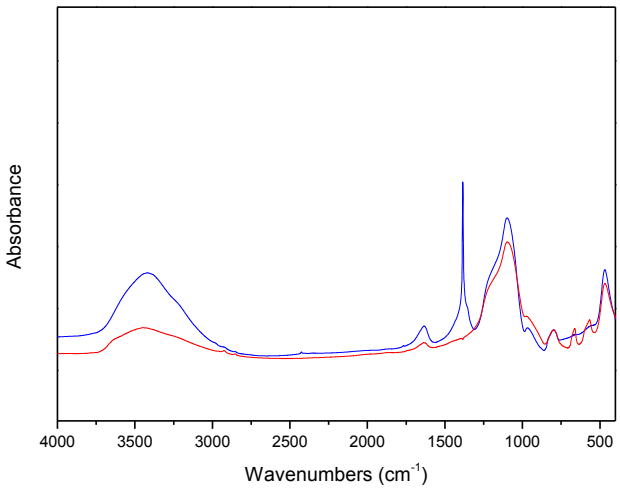

FIG. 8.21: IR spectra for FT08

The IR spectra acquired for samples FT09-A, B and C (FIG. 8.22, 8.23 and 8.24 respectively) are discussed together because they are very similar . The spectrum acquired before the calcination (blue line) shows the band of the hydroxide groups at wavenumbers up to 3000 cm^{-1}. This signal disappears after the calcination (red line). Also the signal assigned to nitrates, at 1300 cm^{-1}, disappears when the calcination is carried out. The signals due to the Si-O bond are very weak, because the high quantity of $Co(NO_3)_2$ on the surface covers the other signals.

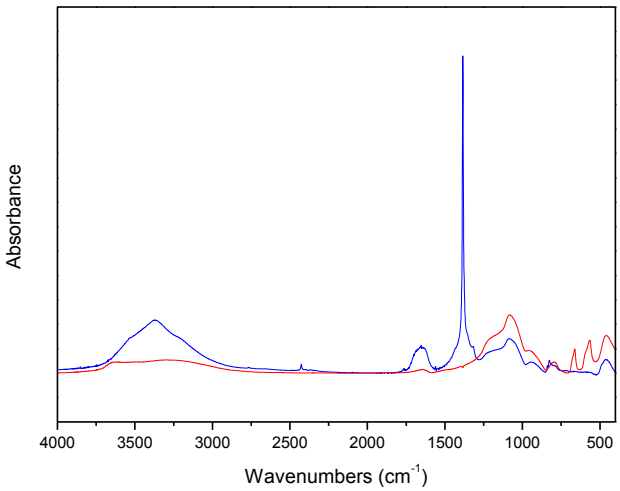

FIG. 8.22: IR spectra for FT9-A

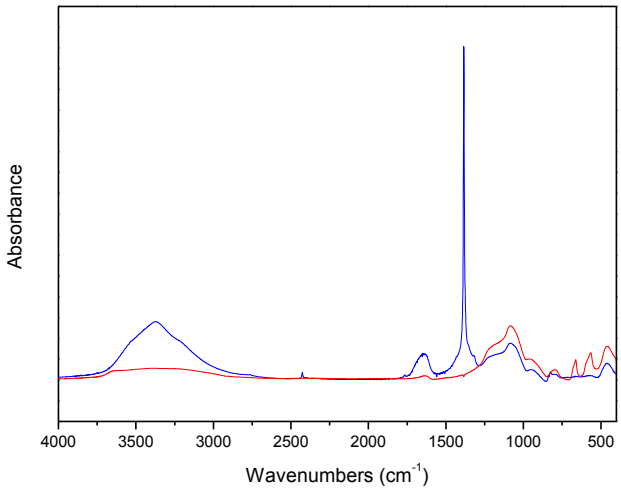

FIG. 8.23: IR spectra for FT9-B

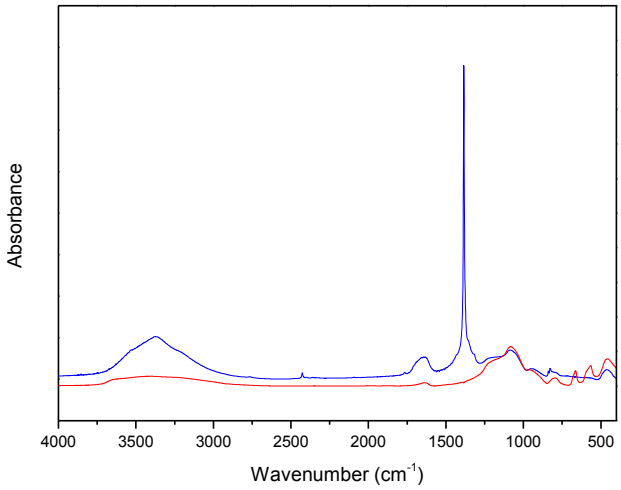

FIG. 8.24: IR spectra for FT9-C

The IR spectra acquired for sample FT10 are very similar to the previous ones. Also in this case, there is the band of the hydroxide groups and the peaks of nitrates in the uncalcinated sample (blue line), that disappear after the calcination (red line). It is not present the band due to the Si – O bond, but this is not strange because the layer of the shell is very tiny.

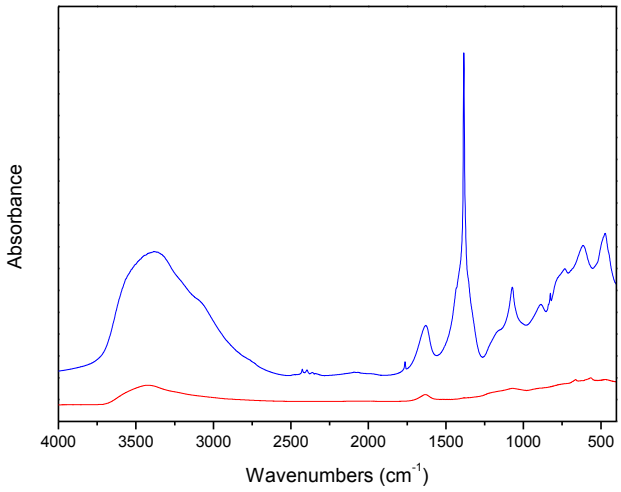

FIG. 8.25: IR spectra for FT10

8.3.7 TEM images

The TEM image of FT08 (FIG. 8.26)shows an amorphous catalyst where the cobalt, that is shown in black in the figure, is dispersed with low homogeneity.

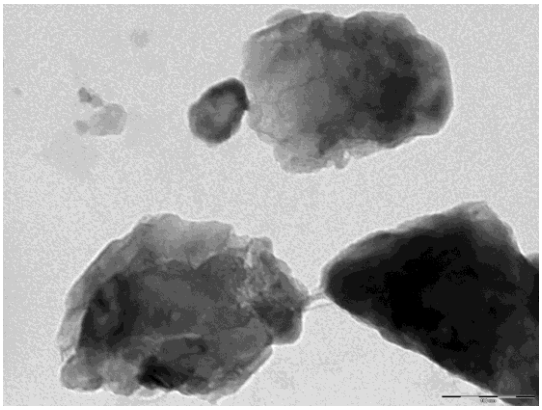

FIG. 8.26: TEM image for FT08

The TEM images obtained for the three catalysts FT09-A, B and C (FIG. 8.27) show in all cases a large dishomogeneity in the size of particles and in the deposition of metal. However it is possible to recognize the formation of the shell around the core.

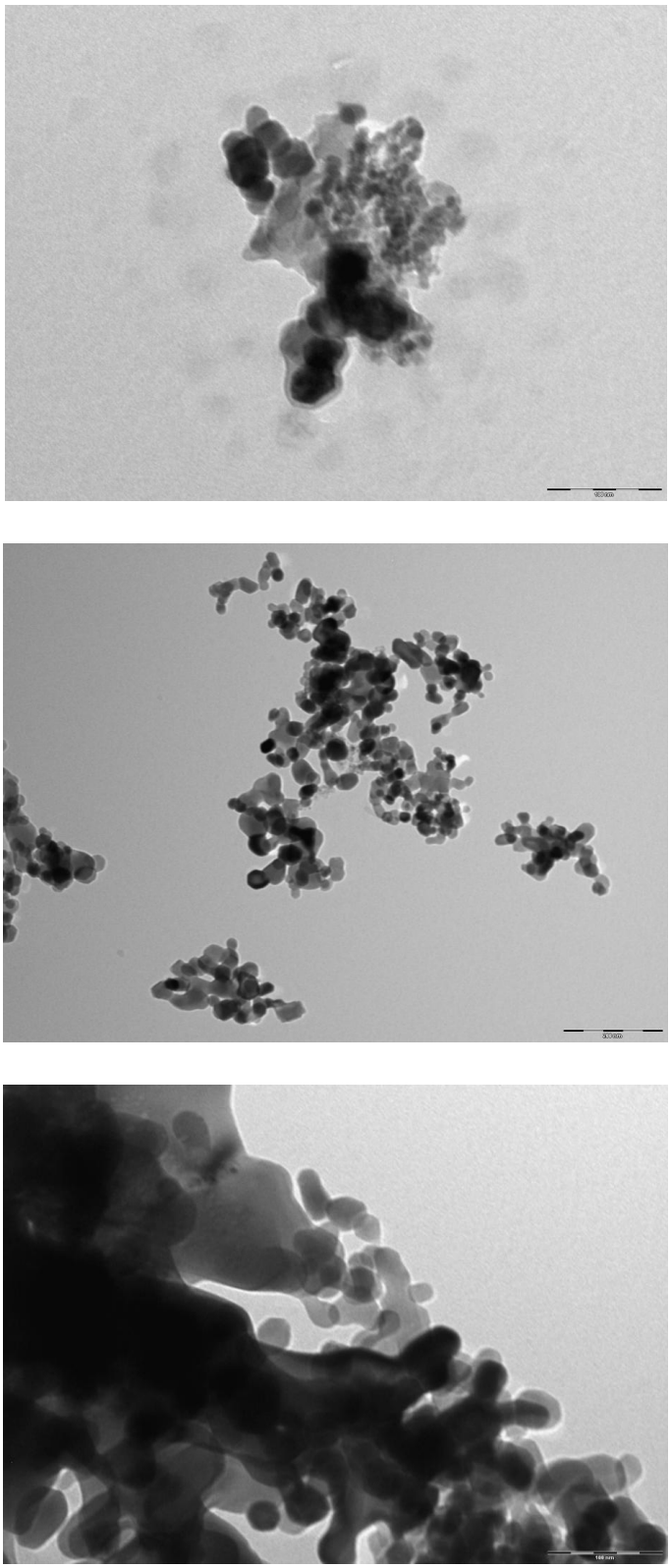

FIG. 8.27: TEM images for FT09-A, FT09-B, FT09-C

The TEM image of FT10 (FIG. 8.28) shows that the structure of the catalyst is very complex. However, for the bigger particles, it is possible to recognize also in this case a tiny layer of shell over the core of particle.

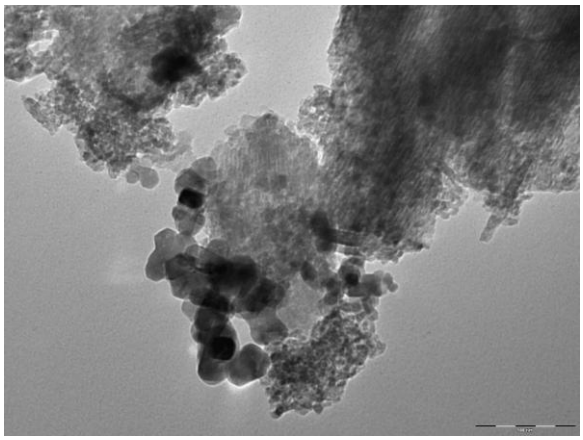

FIG. 8.28: TEM image for FT10

8.3.8 SEM images

The SEM image of FT08 (FIG. 8.29) shows a sample composed by particles with a size not much different between each other. Based on the EDX analysis, the amount of cobalt on the surface results 20%, a bit higher than the calculated value. This fact is probably due to a not homogeneous deposition of the metal on the surface sample. This not homogeneous deposition is also observed when the image is transformed and the cobalt particles are red pictured .

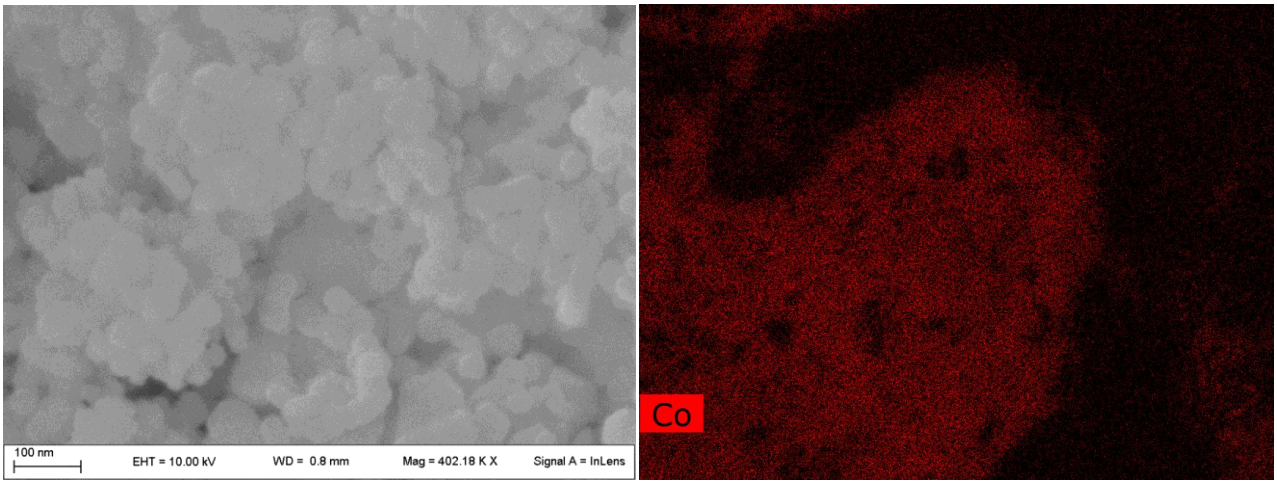

FIG. 8.28: SEM images for FT08

The SEM images collected for the three catalysts FT09 (FIG. 8.29) show that the sizes and the shapes of particles are very different. This is due to the use of the sol-gel method that is not able

to control these parameters. Also the EDX analyses show a percentage of cobalt of 21, 22 and 20% respectively, that is quite different from the theoretical 15%.

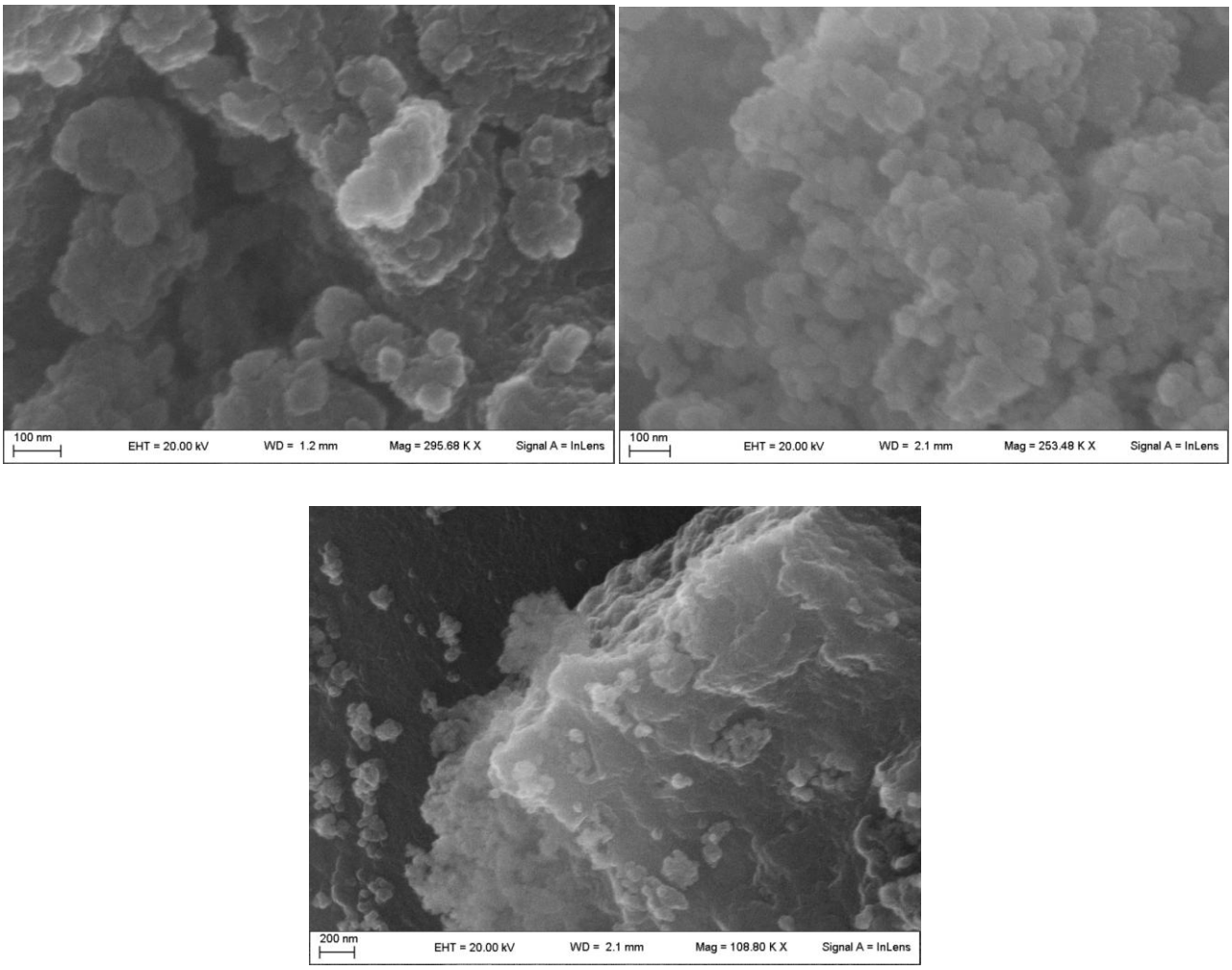

FIG. 8.29: SEM images for FT09-A, B and C

The SEM image of FT10 shows, as well as for TEM, a complex and unorganized structure of the catalyst. The size and the shape of the particles are very variable, and the particles seem to be aggregated between them. This effect is probably due to the gelification of silica layer that forms a bonded network that encapsulates the alumina core. Despite the amount of cobalt is 24%, rather than the theoretical 15%, the amount of silica determined by the EDX mapping is 4%, very similar to that calculated of 6%.

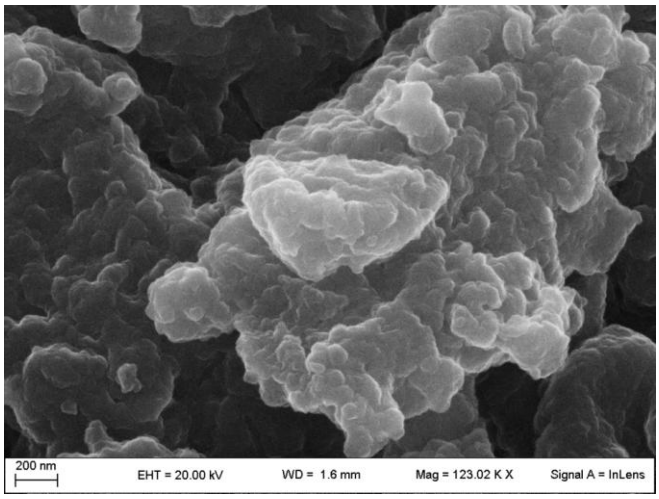

FIG. 8.30: SEM image for FT10

8.4 Catalytic Tests

Catalytic tests have been carried out in a fixed bed reactor. 4 g of each catalysts were charged into the reactor. Before starting the tests, the catalysts were activated for 4h at 400°C under hydrogen flow. For the tests, a mixture of H_2 and CO, with molar ratio 2:1, was fed to the reactor. The total feeding flow is 12 l/h: 8 l/h of hydrogen and 4 l/h of CO. The tests are carried out under a pressure of 20 bar.

The data of test of FT08 are collected between 180°C and 250°C. As it can be seen by observing the Graph 8.2, the conversion increases rapidly with temperature up to 100% at 240°C, then it begins to decrease.

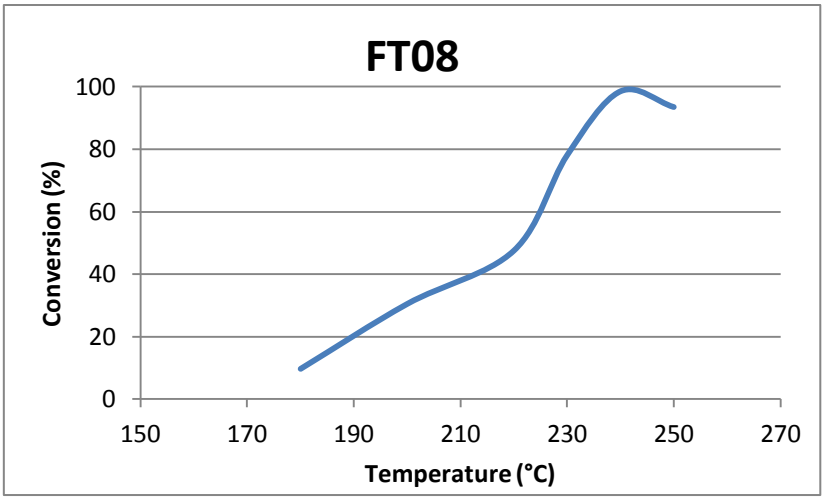

Graph 8.2: Conversion vs temperature for FT08

Another test with this catalysts was carried out at the same conditions, but by maintaining the temperature constant at 220°C, in order to evaluate the behaviour of the catalyst during the time (Graph. 8.3).

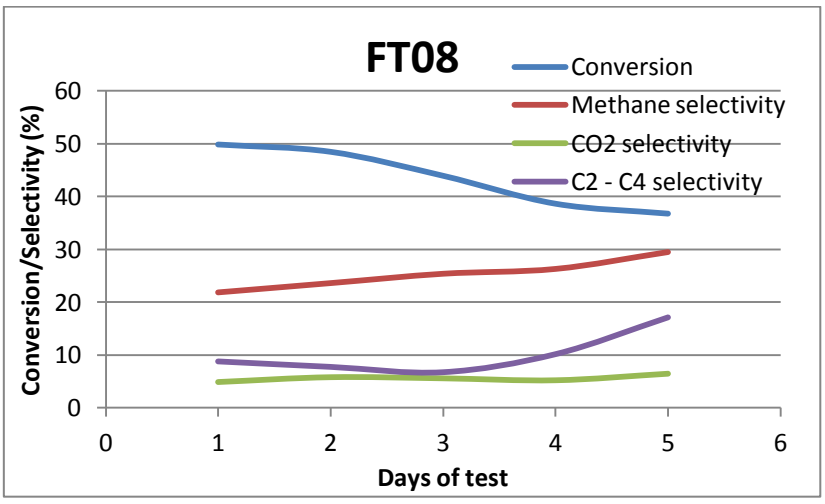

Graph 8.3: Conversion vs time for FT08

By regarding the data, a little decrease of the conversion is observed. It passes from around 50% to a little less than 40%. To this trend, due to an incipient deactivation, an increase is associated of the production of methane (from 20 to 30%) and of $C_2 - C_4$ hydrocarbons (from 10 to around 20%), while the CO_2 production remains unaltered. The liquid phase discharged at the end of the test shows a good agreement with the ASF theory (Graph 8.4), with an α value of 0.79.

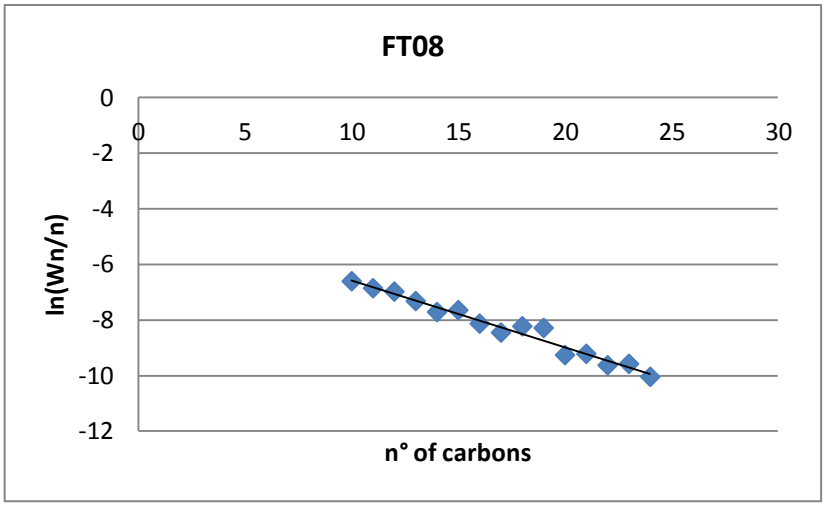

Graph 8.4: linearized production of condensed products for FT08

By regarding the results of the characterization of the FT09 catalysts, we decided to catalytically test the FT09-A which seems the better one. The condition of catalytic tests are those already seen for FT08.

The conversion at 190°C was 60% (Graph 8.5) and the catalyst reaches a total conversion at 220°C, before starting to decrease.

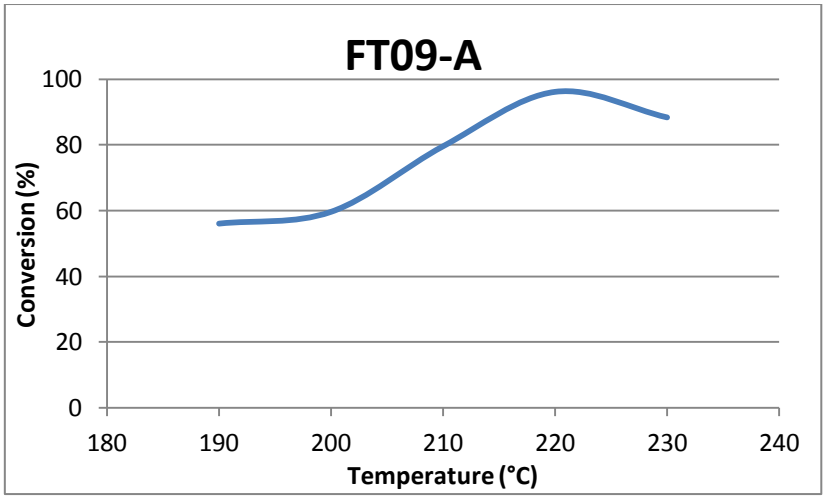

Graph 8.5: Conversion vs temperature for FT09-A

Also in this case, a test at constant temperature at 220°C was carried out (Graph 8.6). By regarding the graph of this test, a rapid deactivation of the catalyst is observed. The conversion

decreases from 100% to 40%. However, the selectivity to methane and to C_2-C_4 hydrocarbons remains almost unaltered at 20 and 10% respectively. The CO_2 production, instead, is present also in the first moments of the test, then it decreases rapidly until it disappears.

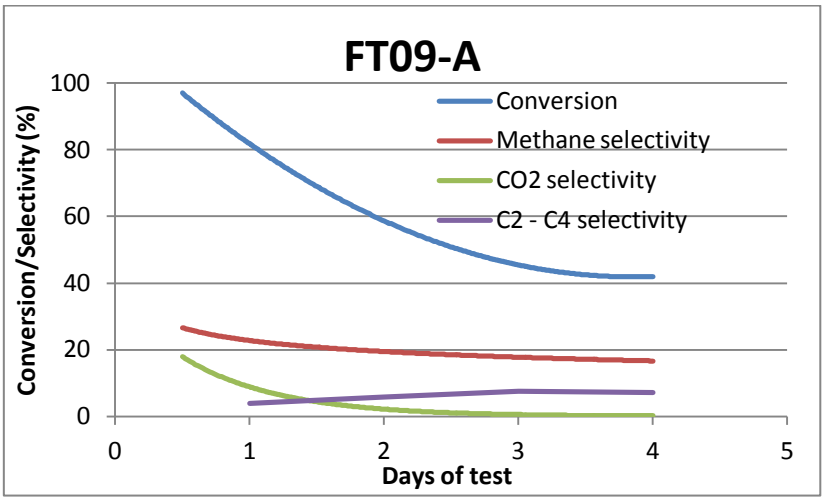

Graph 8.6: Conversion vs time for FT09-A

The hydrocarbon liquid phase collected at the end of the test was analyzed and the results are shown in the graph: this graph shows that it results an α value of 0.72. However, the decrease of conversion during the test let us think about a deactivation due to the formation of waxes. Then, a procedure of extraction was carried out over the discharged catalysts. More than 6 g of solid hydrocarbons were found on the catalysts. That means around 1.5 g of waxes for each gram of catalyst. The deposition of waxes on the catalyst surface causes an occlusion of the pores and the resulting decrease of the conversion. These waxes are not included in the calculation of ASF distribution, so the resulting α value is underestimated.

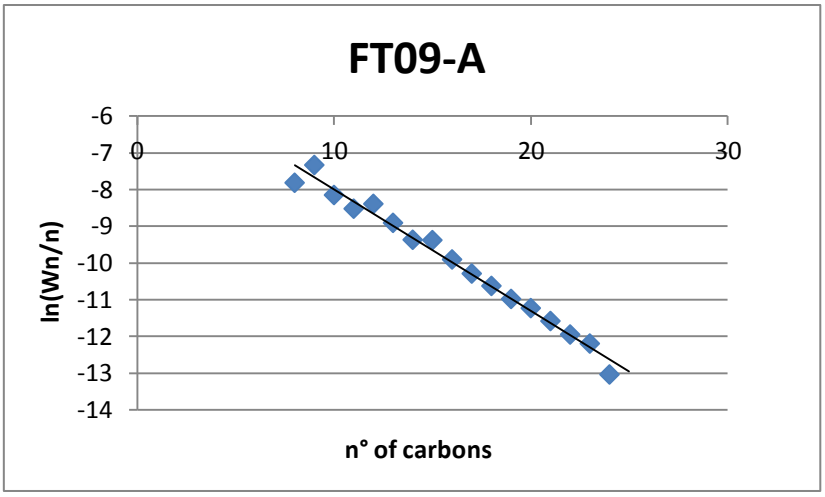

Graph 8.7: linearized production of condensed products for FT09-A

The catalyst FT10 was tested between 180°C and 220°C. It shows a small increase of conversion at increasing temperatures (Graph 8.8). The conversion increases from 45% to 65%.

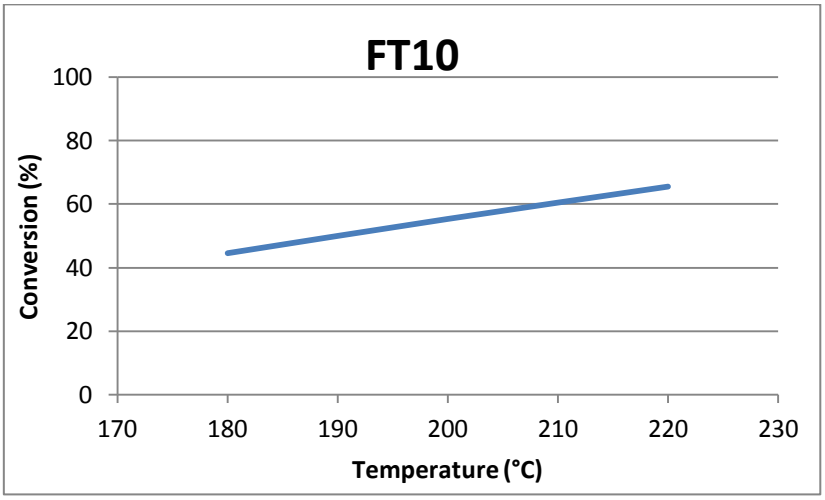

Graph 8.8: Conversion vs temperature for FT10

Also in this case the test at constant temperature was carried out at 220°C, to compare the results with the others obtained at the same temperature.

By regarding the graph, the conversion decreases rapidly and linearly during the test, from 65% to 35%. The selectivity to methane, and to lighter (C_2-C_4) hydrocarbons remain almost unaltered

during the test and always at low values. This means that, as already shown in the case of FT09-A, there is an high formation of solid products that deactivates the catalyst.

It is interesting to note that there is not production of CO_2.

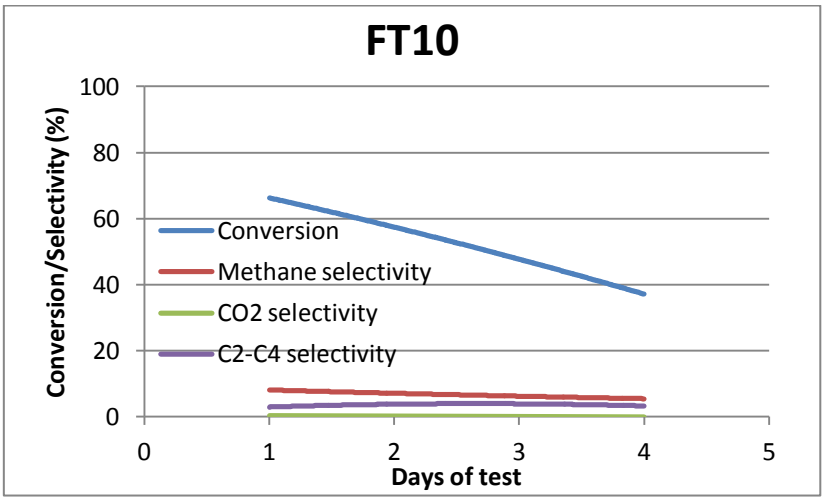

Graph 8.9: Conversion vs time for FT10

The results of the analysis of liquid phase collected are plotted in the graph, with an α value of 0.70, but also in this case this value is underestimated due to the exclusion of solid products.

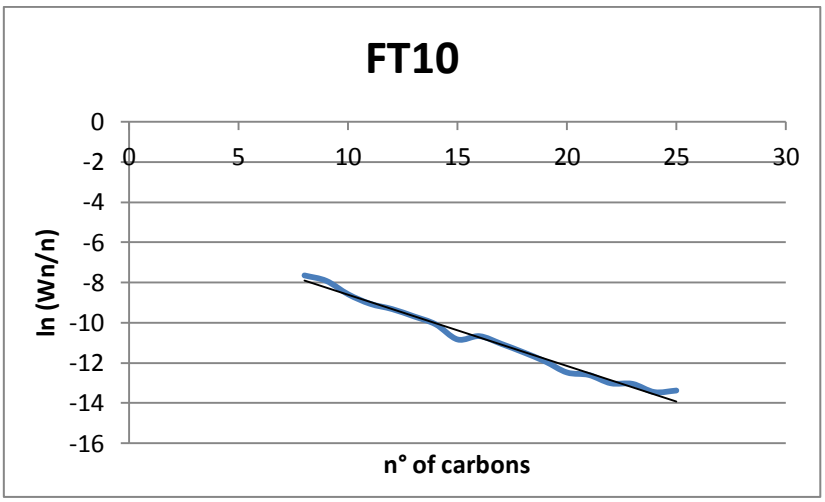

Graph 8.10: linearized production of condensed products for FT10

8.5 Conclusions

By this part of work, it was possible to optimize the parameters for the preparation of egg-shell catalysts supported over silica by using the sol-gel technique. The optimal amount of oxalic acid, used as precursor of CO_2 that gives an high porosity during the gelification, was determined by B.E.T. surface area.

The next step was to found the optimal ratio alkoxide/solvent in order to form the best upper layer in the "egg-shell" catalyst. The study was made with three different molar ratios of TMOS/ethanol: .,3, 0.5, and 0.6. From IR, XRD and electronic microscopy analyses, no differences between samples were observed. Otherwise, the TPR, TPO, H_2-TPD, and surface area analyses showed that, in the case of 0.3 molar ratio (FT09-A), the resulting catalyst with the smaller uplayer, was the best one between the three catalysts. This catalyst was tested in the plant and compared with a reference catalyst prepared by the incipient wetness impregnation method.

The results showed that the catalyst was highly active and selective to the desired products, but the formation of waxes during the test deactivated rapidly the catalyst itself. This deactivation was then due to the formation of desired products and, however, was reversibly; further procedures of reactivation gave back the catalyst newly active. Similar results were obtained for an analogue egg-shell catalyst, again with a shell of silica, supported over a core of alumina.

Bibliography

[1] A. Di Michele; PhD Thesis: **"Sonochemical synthesis of metal nanoclusters and their application in the Fischer-Tropsch process";** 2007

[2] C. Perego, P. Villa; *Catalysis Today.* ***1997.*** *34, 281*

[3] T. Lopez; *React. Kinet. Catal. Lett.* ***1992.*** *46, 42*

[4] A. Y. Khodakov, W. Chu, P. Fongarland; *Chem. Rev.* ***2007.*** *107, 1692*

[5] M. Voß, D. Borgmann, G.Wedler; *Journal of Catalysis* ***2002.*** *212, 10*

[6] A. M. Saib, M. Claeys, E.V. Steen*; Catal. Today* ***2002.*** *71,395*

[7] C. Chen, H. Yuuda, X. Li; *Appl. Catal. A* ***2011.*** *396, 116*

CHAPTER 9: Other egg-shell catalysts

9.1 Introduction

In this section we want to evaluate the effects of the increase of the amount of metal in the egg-shell cobalt catalysts. To this aim, four catalysts are prepared; two supported on silica[1,2,3] and other two supported on alumina[1,2,4,5]. The first catalyst (FT11) was prepared by the incipient wetness method, by depositing a 17% by weight of metal on a commercial silica as support[6,7]. Another catalyst (FT12), with the same amount of cobalt, was prepared by the egg-shell method, as described in the previous chapter, by using silica as core and also as shell layer. The two other catalysts FT13 and FT14 are analogues but prepared on alumina. In the case of FT14 the shell layer is always silica. Finally, two other catalysts were prepared using the egg-shell method, the first on a core of silica (FT15) and the second one on a core of alumina (FT16). In both catalysts, ethylene glycol[8] was added to analyze the effect of the presence of a template agent during the preparation.

In Table 9.1 all the catalysts were summarized.

SAMPLE	ACTIVE PHASE	SUPPORT	PREPARATION METHOD
FT11	17% Co	Silica	Incipient wetness
FT12	17% Co	Silica/Silica	Egg-shell
FT13	17% Co	Alumina	Incipient wetness
FT14	17% Co	Silica/Alumina	Egg-shell
FT15	17% Co	Silica/Silica	Egg-shell + Ethylene Glycol
FT16	17% Co	Silica/Alumina	Egg-shell + Ethylene Glycol

Table 9.1: method of preparation and precursors for alumina supported catalysts.

9.2 Preparation

FT11

The composition of this catalyst is 17% by weight of Co on a commercial silica as support. The method of preparation is that of impregnation “to incipient wetness” from a solution of metal salt. Before the preparation, the incipient wetness point for a solution of ethanol was calculated over the chosen support. The incipient wetness point resulted 1.9 ml of ethanol per gram of silica. 20 g of silica were then impregnated with a solution of 19.7g of $Co(NO_3)_2 \cdot 6H_2O$ dissolved in 19 mL of ethanol. The catalyst was aged for a week, then dried at 110°C for 1 night; finally, the sample was calcinated at 400°C for 4 h.

FT12

In order to obtain 40 g of silica support, 148 ml of tetramethoxysilane (TMOS) were dispersed in 277 ml of ethanol. The solution was refluxed, then 293 ml of a saturated solution of oxalic acid in water were added. After 1h under reflux, the solution was rapidly cooled in an ice bath. 33 ml of water were then added drop by drop to favour the gelification. The gel was then aged for a week, and finally dried in an oven at 110°C for 1 night. For this support the incipient wetness point was determined with a solution of ethanol and TMOS with TMOS/Ethanol molar ratio = 0,3. The incipient wetness point resulted 1.24 ml/g. To impregnate 10 g of support, 11g of $Co(NO_3)_2 \cdot 6H_2O$ were dissolved in 12.4 ml of the solution of TMOS/Ethanol and the solution was drop by drop added to the prepared alumina. The system was then left aging for a week, dried at 110°C for a night and finally calcinated at 400°C for 4h.

FT13

This catalyst was prepared by impregnation “to incipient wetness” on a commercial alumina (SNAMPROGETTI). The incipient wetness point with ethanol on this sample is 0.89 ml/g. Then, 10 g of alumina were impregnated drop by drop with a solution of 9.9 g of $Co(NO_3)_2 \cdot 6H_2O$ dissolved in 8.9 ml of ethanol. The sample was aged for 7 days, dried at 110°C for a night and finally calcinated at 400°C for 4 h.

FT14

Also in this case, as well as for FT12, the catalyst is constituted by a core and a shell. In this case, the core is composed by alumina. In order to obtain 10 g of alumina, 40 g of aluminium isopropoxide were dissolved in 90 ml of isopropyl alcohol. To obtain the gelification, 22 ml of water were added drop by drop. The gel was left to evaporate for 2 week, then it was dried at 110°C for 1 night. The incipient wetness point determined on this support for a solution of TMOS/Ethanol = 0.3:1, as molar ratio, was 2.23 ml per gram of support. According to this result, 11.84 g of $Co(NO_3)_2 \cdot 6H_2O$ were dissolved in a solution of 17.2 ml of ethanol and 5.1 of TMOS. After aging for two weeks , the catalyst was dried at 110°C for 1 night and finally calcinated at 400°C for 4h.

FT15

This catalyst was prepared by the same method as for FT12, but adding a little amount of ethylene glycol as template agent to the solution of TMOS, Ethanol and Cobalt nitrate before starting the synthesis. We verified that the addition of this component did not lead to change the incipient wetness point for this system. The amount of added glycol was 1:1 as molar ratio with regard to cobalt.

FT16

As well as for the preparation of FT15, the synthesis of FT16 catalyst followed the same procedure as for FT14, but with the addition of Ethylene Glycol in 1:1 molar ratio with cobalt to the formation of the shell.

9.3 Characterization

9.3.1 TPR analyses

The TPR profile for the catalyst FT11 (FIG. 9.11) shows two well defined peaks centered at 350°C and 440°C, respectively. The first one is the peak of reduction of cobalt oxides. The second one is

assignable to the formation of cobalt silicates. The total reduction is 50%, with a value of 33% if the reduction of only cobalt oxides is considered.

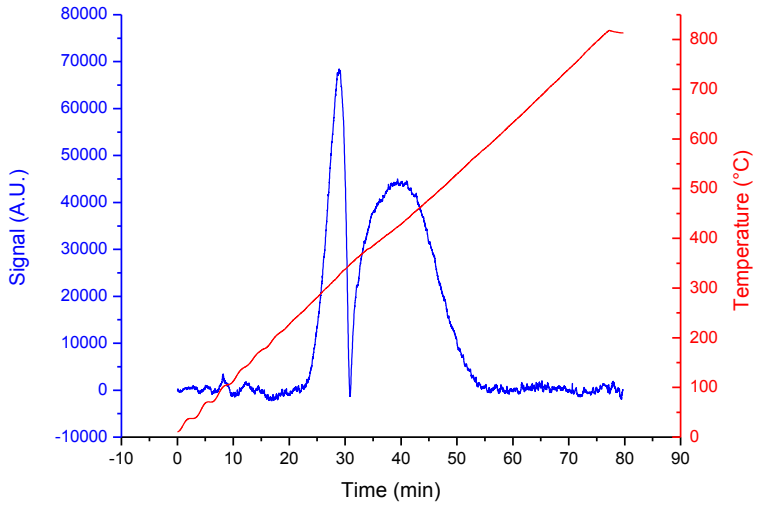

FIG. 9.1: TPR profile for FT11

Two peaks can be observed into the TPR profile for the FT12 catalyst (FIG. 9.12). The first one is at 385°C and it corresponds to the reduction of cobalt oxides. The second peak is at 740°C and is due to the formation of cobalt silicates. The total reducibility of this sample is 55%, but it decreases to 43% if only the first peak is considered.

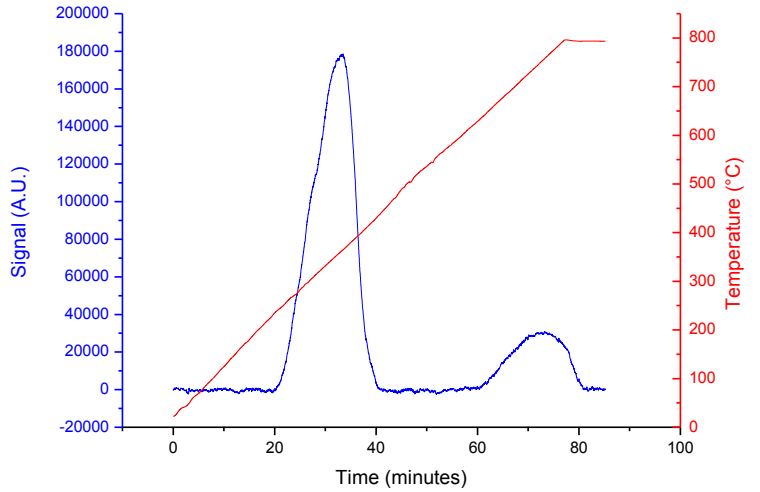

FIG. 9.2: TPR profile for FT12

The TPR profile for FT13 (FIG. 9.3) shows a little peak at low temperature (265°C), followed by a very intense peak at higher temperature (595°C). The first peak is assignable to the reduction of cobalt oxides, while the second peak is due to the reduction of cobalt aluminates species. The total reducibility is 81%.

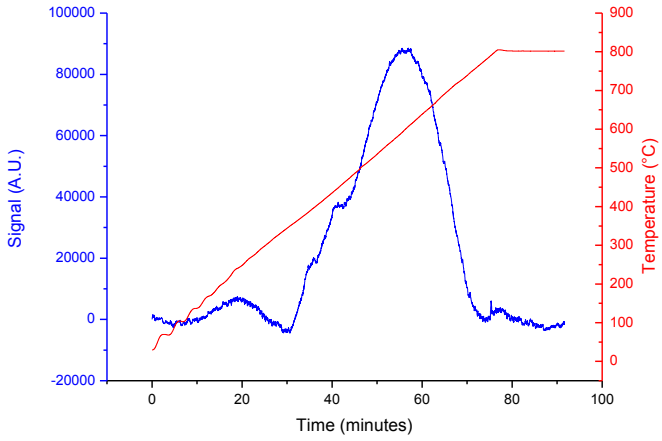

FIG. 9.3: TPR profile for FT13

The TPR profile for FT14 (FIG. 9.4) shows a double peak around 400°C formed by the overlapping of two signals due to the different species of cobalt oxides. The second peak, very large, centered at 675°C, is due to the formation of cobalt silicates and aluminates. The total reducibility is 79%, but by excluding the second peak, the reducibility decreases to 46%.

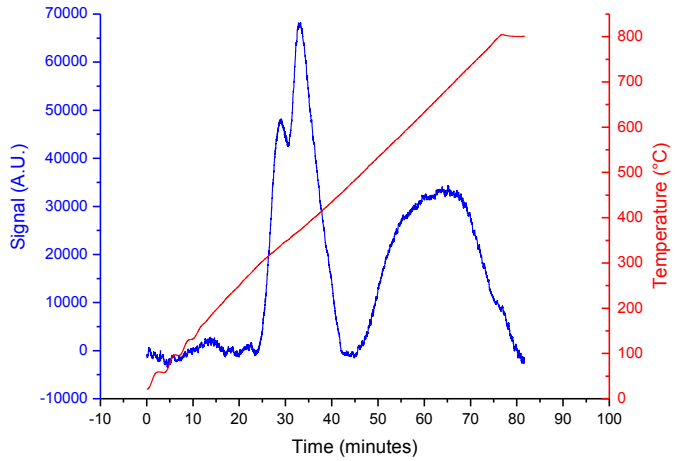

FIG. 9.4: TPR profile for FT14

The TPR profile registered for FT15 (FIG. 9.5) is very similar to those for the other preparations without ethylene glycol. The peak of reduction of cobalt oxides is at 350°C. The second peak, due to the cobalt silicates, shifts to 775°C. This shift is observed also from literature data. The total reducibility is 55%, that decreases to 50% if the second peak is excluded.

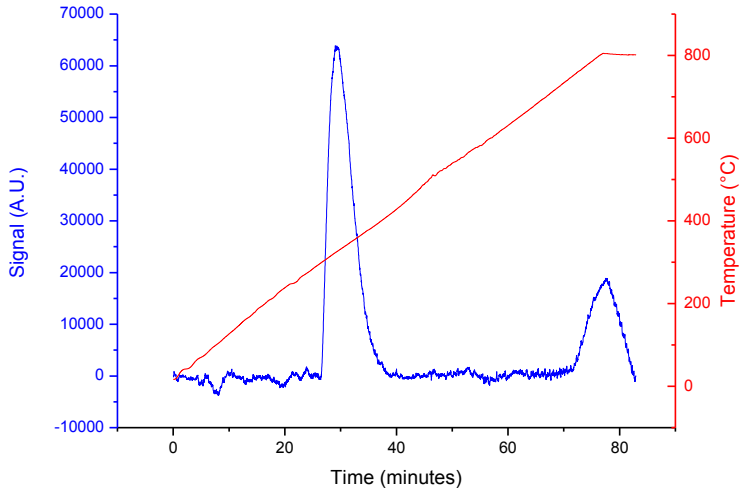

FIG. 9.5: TPR profile for FT15

For the sample FT16 (FIG. 9.6), as well as for FT15, we can observe the peak due to the reduction of cobalt oxides at 350°C and a peak due to the formation of cobalt-aluminates shifted at higher temperatures (770°C) with respect to the other samples prepared without ethylene glycol added. The reducibility of this sample is 89%, but it decreases to 73% if the second peak is not considered.

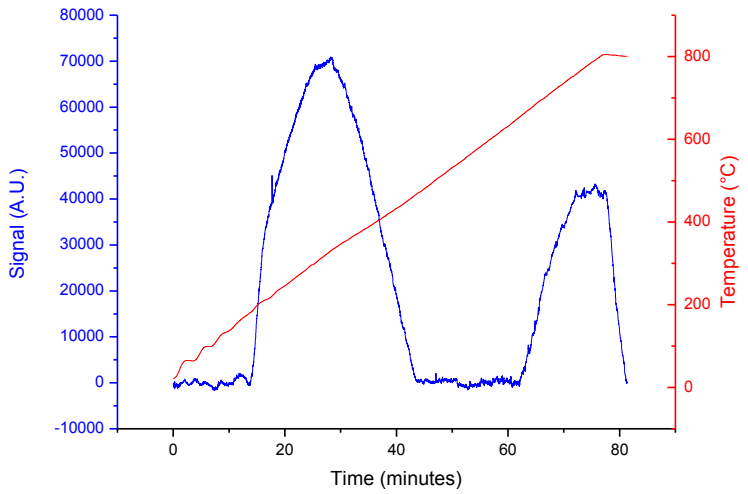

FIG. 9.6: TPR profile for FT16

TPO analyses

All TPO analyses were performed after an activation treatment under hydrogen at 400°C for 4h.

In the case of FT11 (FIG. 9.7), a peak followed by a little shoulder can be observed between 200°C and 300°C. This signals are ascribed to the oxidation of Co^0 to Co^{2+} and Co^{3+} respectively. The amount of total re-oxidizability of this catalyst is 31%.

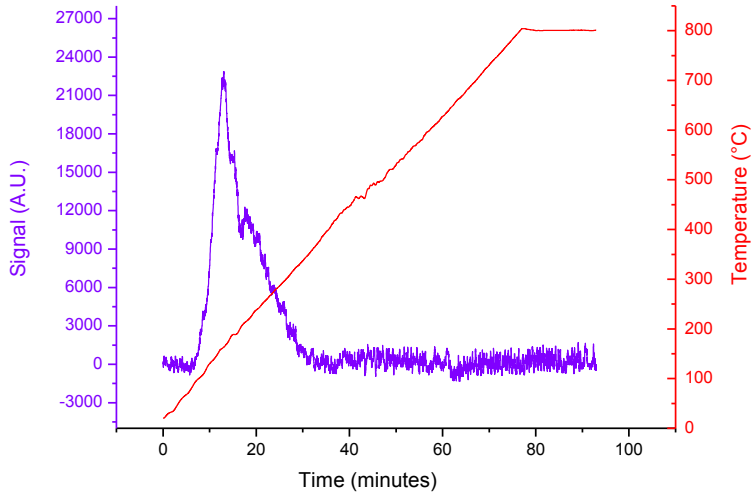

FIG. 9.7: TPO profile for FT11

In the case of FT12 (FIG. 9.8), a only peak, probably resulting from the overlapping of the two peaks due to the oxidation of Co^0 to Co^{2+} and Co^{3+}, can be observed between 150 and 400°C. The metal re-oxidized is 14%.

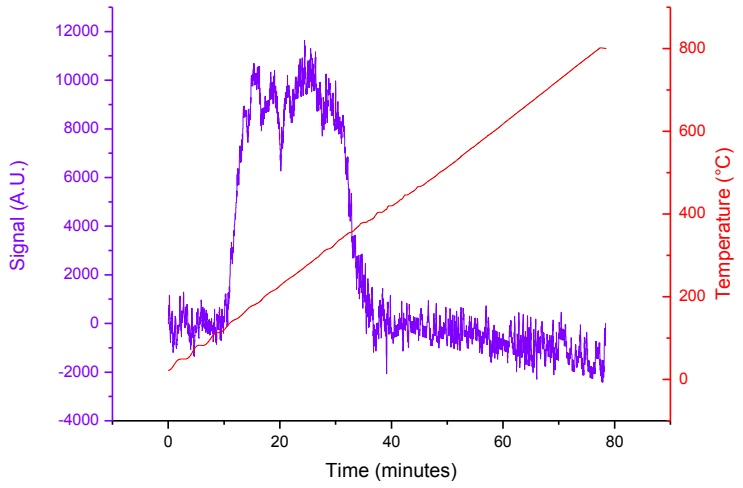

FIG. 9.8: TPO profile for FT12

The TPO profile for FT13 (FIG. 9.9) is similar to that for FT11. The only peak is between 150°C and 300°C with a tail until 400°C. The amount of metal oxidized is 67%.

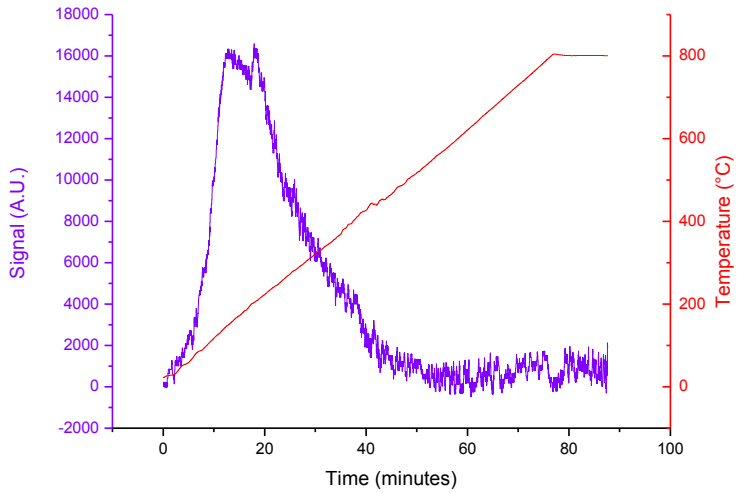

FIG. 9.9: TPO profile for FT13

In the TPO profile registered for FT14 (FIG. 9.10), a only peak can be observed, around 200°C, but a weak shoulder is present before almost totally hidden under the principal signal, that can be due to the overlapping of the two oxidation steps of cobalt to give cobalt oxides. The amount of reduced metal resulting by the calculation for this sample is 50%.

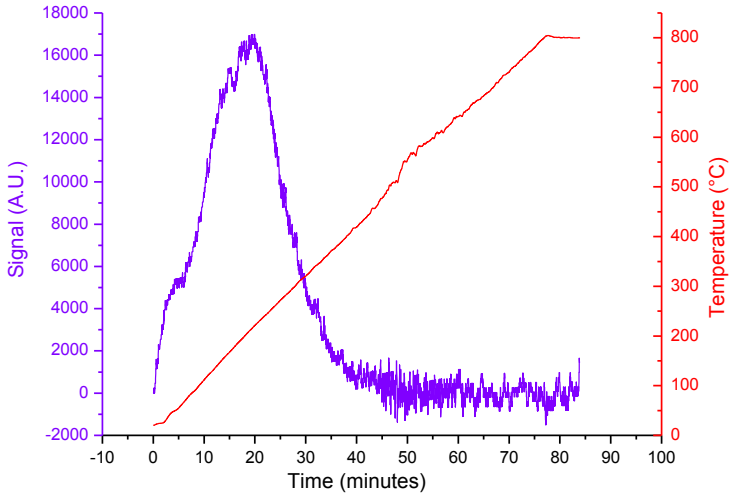

FIG. 9.10: TPO profile for FT14

Before the acquisition of the TPO profile, the FT15 catalyst was activated as previously done for the other catalysts. The signal (FIG. 9.11) is very noisy, but two different peaks can be recognized from this analysis. As well as for the other samples, the oxidation treatment brings to the formation of two oxidized species of cobalt: CoO and Co_2O_3. The re-oxidizability of this sample is 19%.

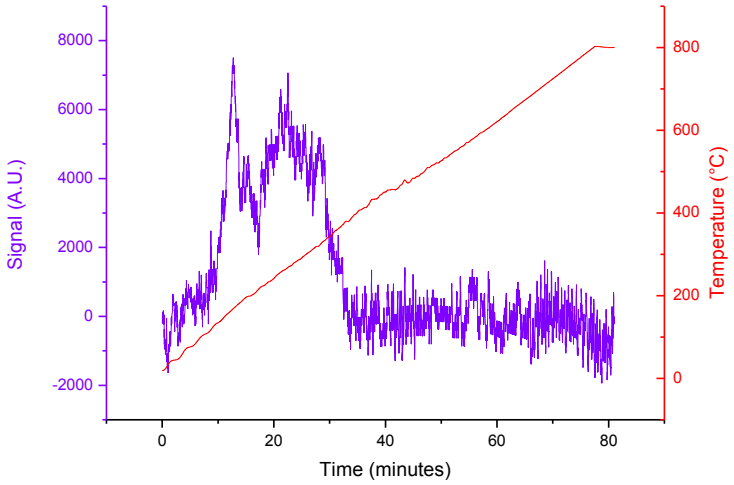

FIG. 9.11: TPO profile for FT15

The TPO analysis performed for the FT16 catalyst (FIG. 9.12), as well as for the other TPO profiles collected, shows an only peak at a temperature lower than 300°C, affected by an higher noise, as already seen for FT15. The metal oxidized in this case is 12%.

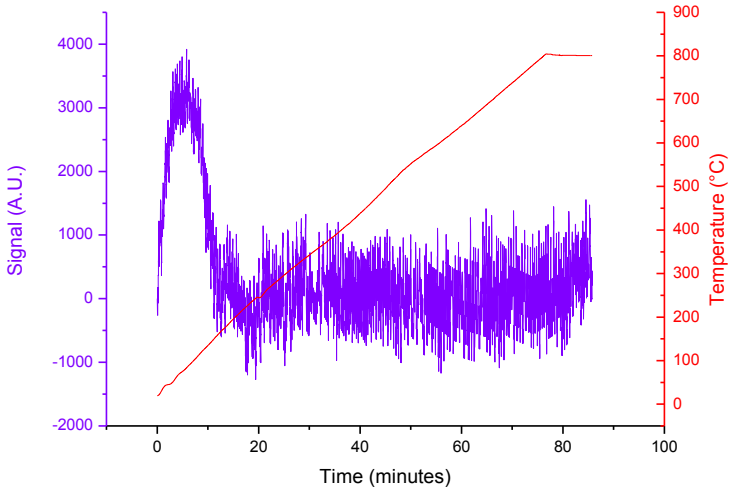

FIG. 9.12: TPO profile for FT16

9.3.3 H_2-TPD analyses

The H_2-TPD analysis was carried out after the treatment of chemiadsorption of hydrogen, already shown for the other catalysts.

In the profile of FT11 (FIG. 9.13), it can be observed two peaks due to the physidesorption of Hydrogen up to room temperature and a band at higher temperature due to the desorption of chemically adsorbed hydrogen. The data from this analysis give as result that the number of active sites is 4.88 x 10^{19}, the dispersion degree is very low: 3%, and the average size of particles is 34 nm.

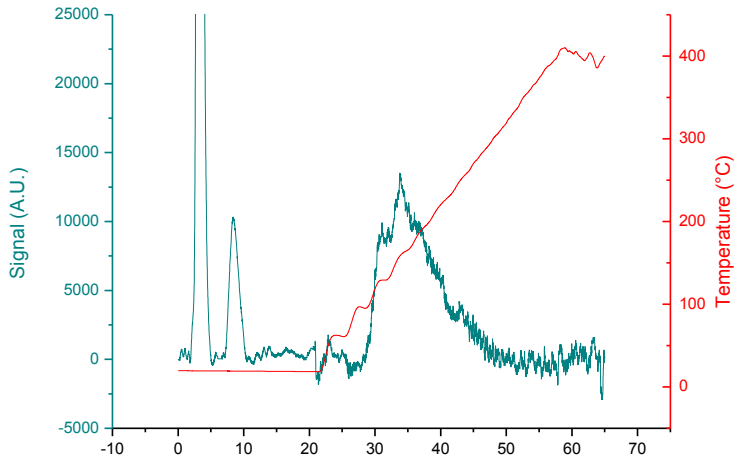

FIG. 9.13: H_2-TPO profile for FT11

The H_2-TPD analysis for the catalyst FT12 (FIG. 9.14) shows the usual peak for the desorption of hydrogen physically adsorbed up to room temperature and the peak of desorption of chemically adsorbed hydrogen between 150°C and 250°C. The number of active sites for this catalyst is 2.58x10^{19} per gram of catalyst, the dispersion degree is very low: 2%, and the diameter of particles results higher than the others: 64%.

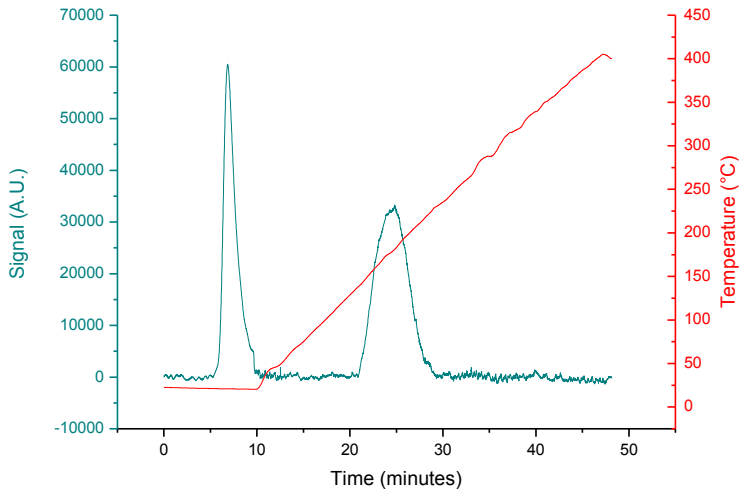

FIG. 9.14: H_2-TPO profile for FT12

The H_2-TPD profile for FT13 (FIG. 9.15) shows, as usual, the peak of physidesorption and a large band between 100°C and 400°C for the chemidesorption. By this graph, the number of active sites per gram of catalyst resulted 1.2 x 10^{20}, together with a dispersion of 7% and an average size of particles of 13 nm.

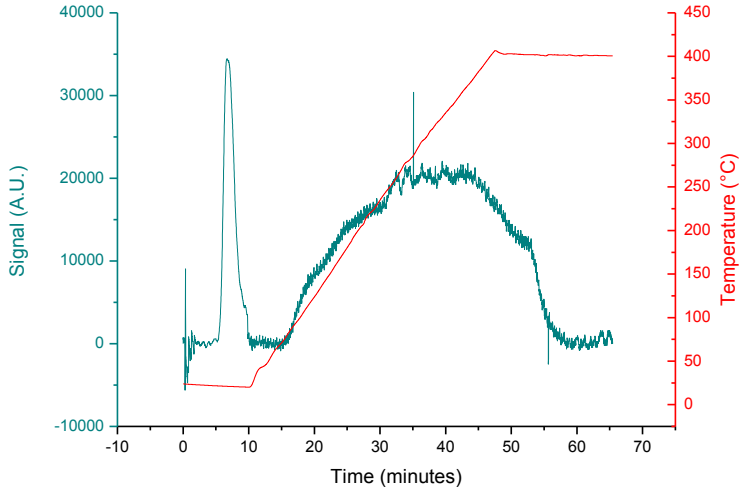

FIG. 9.15: H_2-TPO profile for FT13

The H_2-TPD profile for FT14 (FIG. 9.16) shows the peak of desorption of hydrogen physically adsorbed up to room temperature. The signal of the chemically adsorbed hydrogen is a large band between 100°C and

400°C. The data give a number of actives sites of 1.4 x 10^{20}, a dispersion degree of 8% and a diameter of particles of 12 nm.

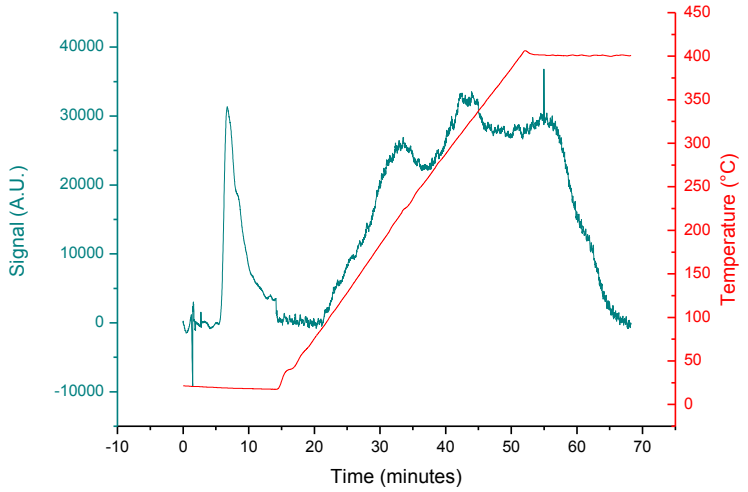

FIG. 9.16: H_2-TPO profile for FT14

The H_2-TPD analysis of sample FT15 (FIG. 9.17) shows two peaks for the desorption of physically adsorbed hydrogen. From the band due to the chemically adsorbed hydrogen, centered at 200°C, a value of 1.59 x 10^{19} is calculated for the active sites, together with a dispersion degree of 1% and an average size of particles of 103 nm. These values are the worst between all values seen until this catalyst.

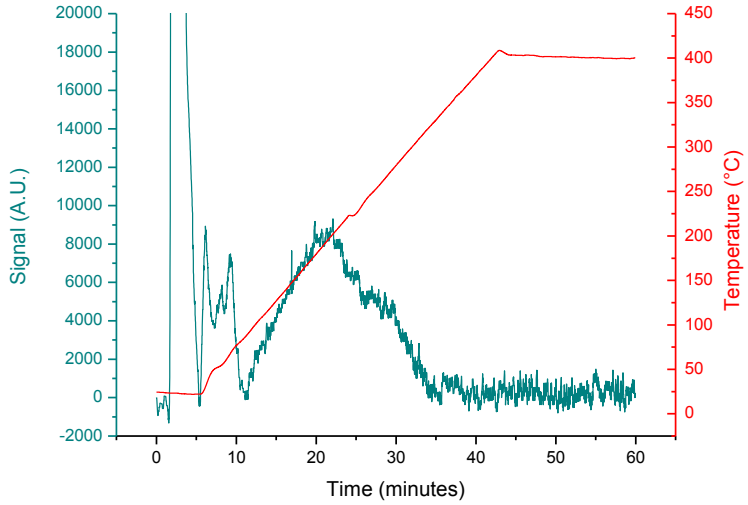

FIG. 9.17: H_2-TPO profile for FT15

From the H_2-TPD analysis made on FT16 (FIG. 9.18), the peak due to physidesorption of hydrogen is not present. The desorption of chemically adsorbed hydrogen is centered at 375°C. The number of active sites for this sample is 4.60 x 10^{19} per gram of catalyst. The dispersion of metal is 3% and the diameter of the particles is around 35 nm.

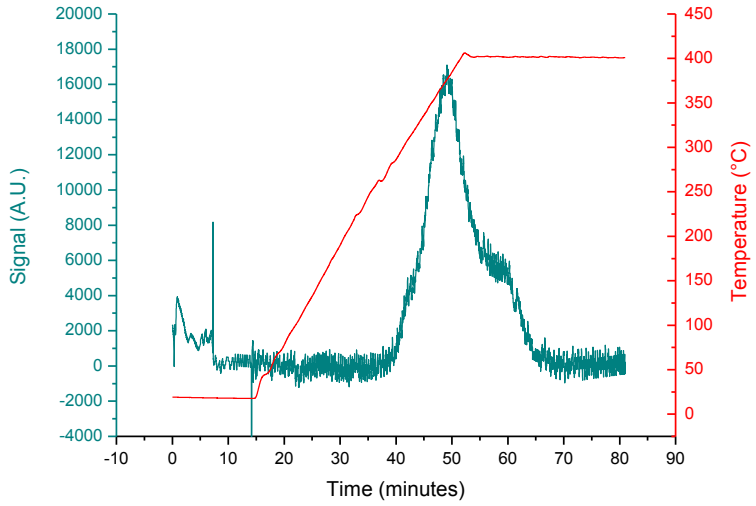

FIG. 9.18: H_2-TPO profile for FT16

9.3.4 Surface Area

The surface area of catalysts are reported in Table 9.2

SAMPLE	SURFACE AREA (m^2/g)
FT11	338
FT12	723
FT13	164
FT14	365
FT15	527
FT16	362

Table 9.2: surface area of the samples

9.3.5 XRD analyses

The XRD spectra for the catalysts FT11, FT12, FT13 and FT14 are shown below (FIG. 9.19, 9.20, 9.21 and 9.22 respectively).

All the samples result completely amorphous but some peaks can be evidenced at 2θ = 31.3°; 36.8°; 38.5°; 44.8°; 59.3° and 65.2°, that are due to Co_3O_4[10].

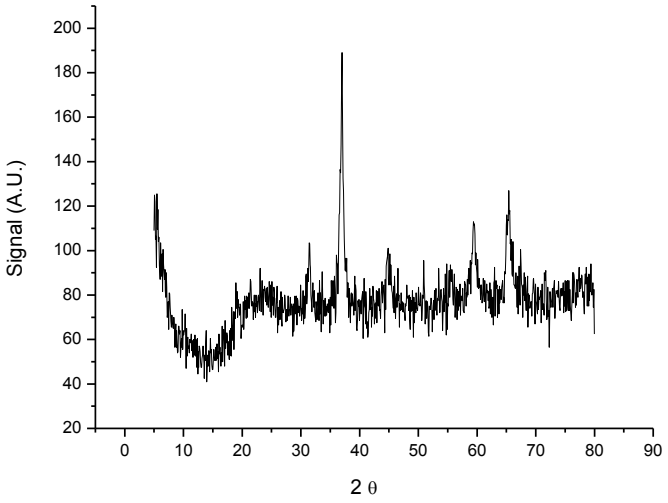

FIG. 9.19: XRD spectrum for FT11

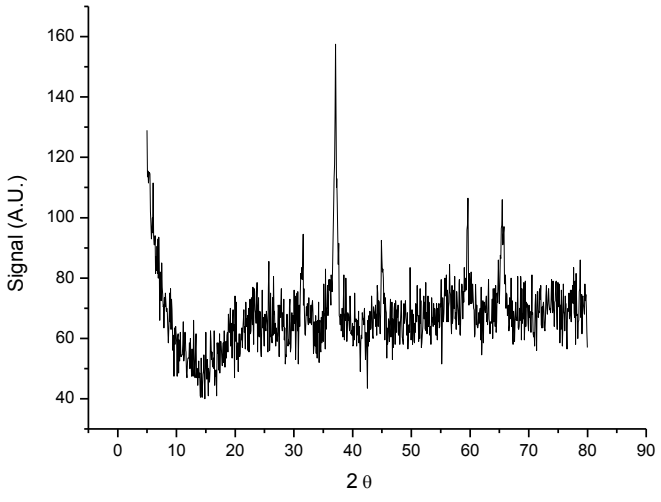

FIG. 9.20: XRD spectrum for FT12

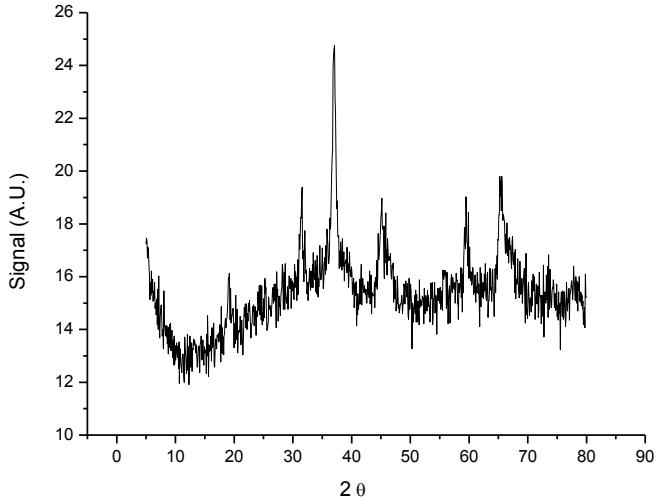

FIG. 9.21: XRD spectrum for FT13

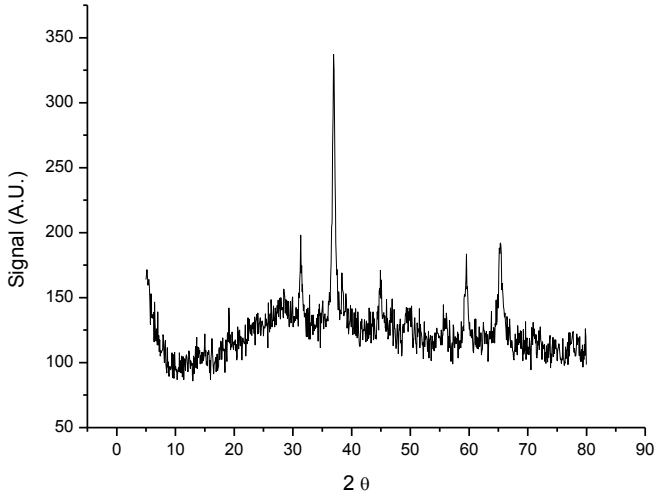

FIG. 9.22: XRD spectrum for FT14

The XRD spectra of samples FT15 and FT16 (FIG. 9.23 and 9.24) show again amorphous structures, but in this case the addition of the template agent also causes the disappearance of signals due to the cobalt oxides[9].

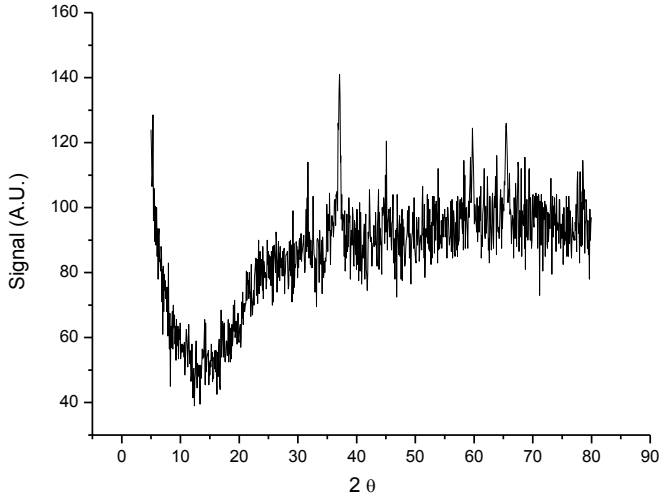

FIG. 9.23: XRD spectrum for FT15

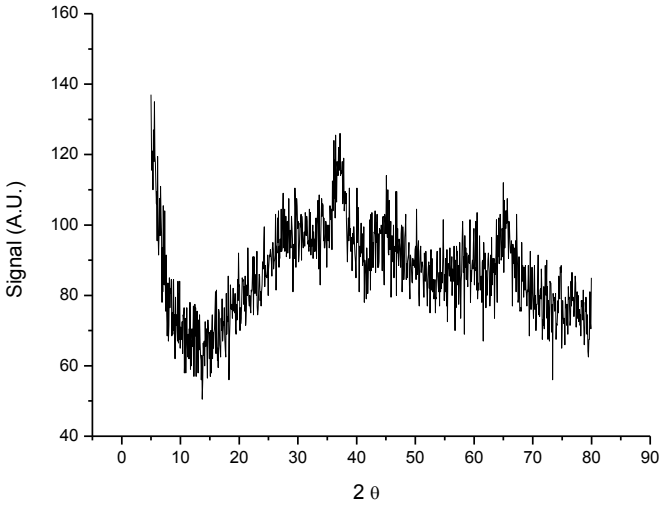

FIG. 9.24: XRD spectrum for FT16

9.3.6 FT-IR

The IR spectra acquired for FT11 and FT12 (FIG. 9.25 and 9.26) are very similar. The blue lines are the spectra acquired before the calcination treatment, while the red lines are the spectra collected after the thermal treatments. In both cases, the disappearance of the bands associated to water and to the hydroxide groups on the surface can be observed, as well as the disappearance of the

band due to nitrates around 1500 cm^{-1}. These bands resulted much more intense for the egg shell catalyst (FT12) with respect to the impregnated catalyst (FT11). In both cases, the signal at around 1000 cm^{-1} remains present after the calcination step. This peak is associated to the Si-O bond.

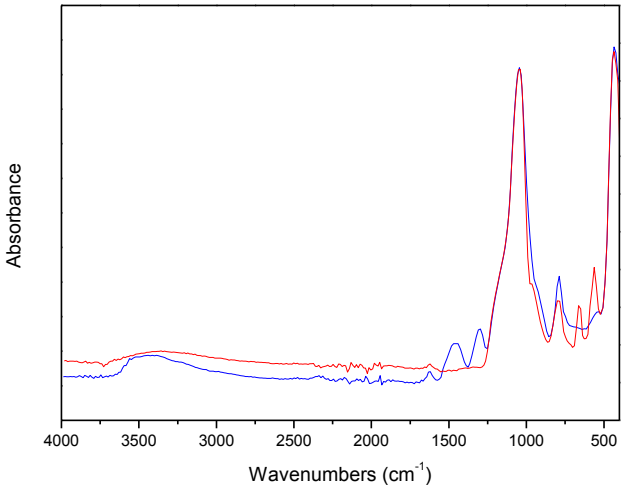

FIG. 9.25: IR spectra for FT11

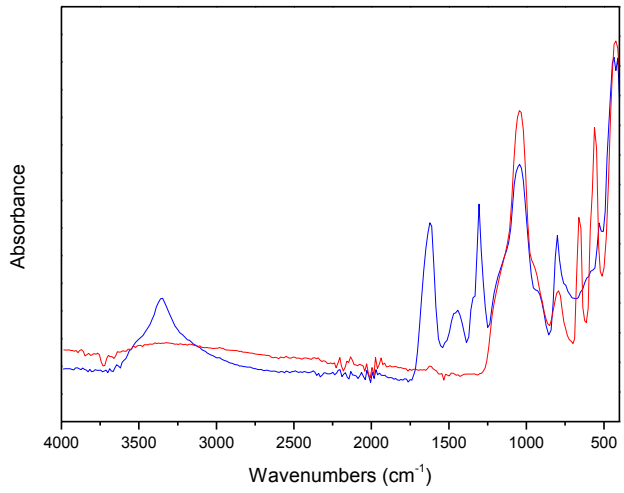

FIG. 9.26: IR spectra for FT12

The same considerations can be made for FT13 and FT14 catalysts, that are supported over alumina (FIG. 9.27 and 9.28). In the case of FT13, the peak due to the Si-O bond is absent, while it is present in the FT14 sample, due to the shell of silica.

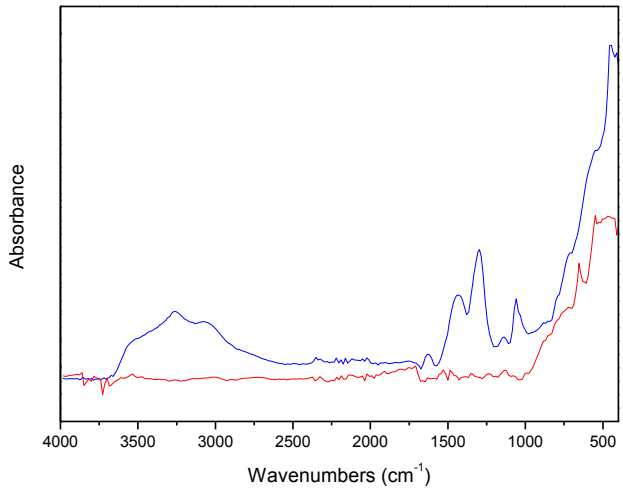

FIG. 9.27: IR spectra for FT13

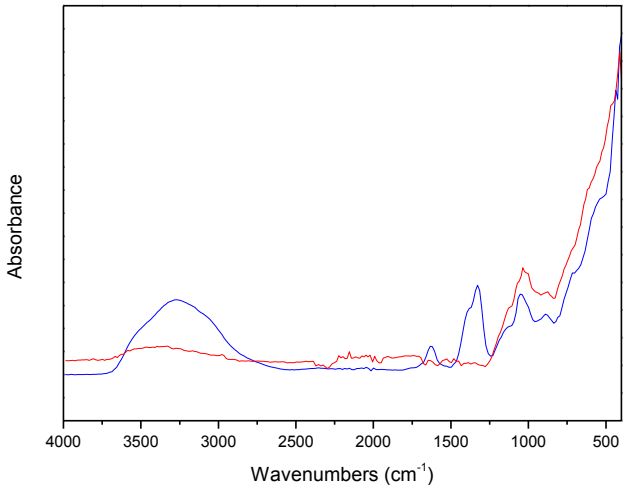

FIG. 9.28: IR spectra for FT14

The IR spectra acquired for FT15 (FIG. 9.29) show the same peaks before observed for FT12, with the signals of –OH groups and NO_3^- groups that disappear after the calcination treatments, while the signal due to the silicates remains present after the thermal treatment. The IR spectra of FT16 (FIG. 9.30) shows instead the peaks already seen for FT14, with the disappearance of the signals of hydroxide and nitrate groups. The amount of ethylene glycol added is too low, then it is not possible to see the associated signals in the spectra.

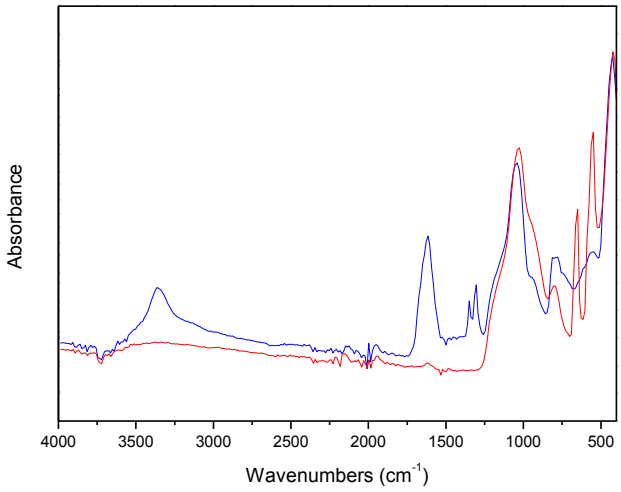

FIG. 9.29: IR spectra for FT15

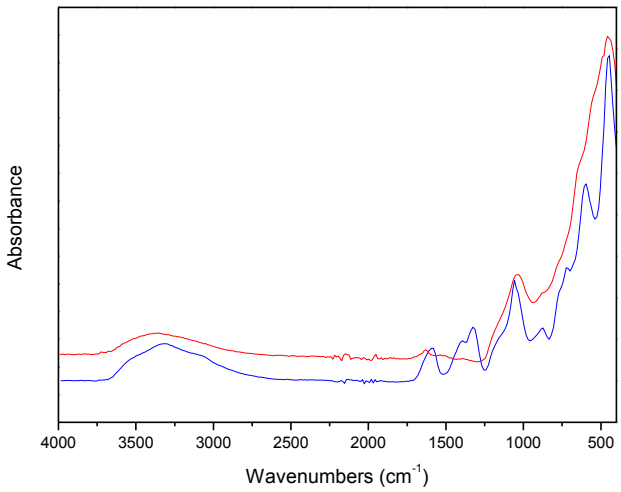

FIG. 9.30: IR spectra for FT16

9.3.7 TEM images

The TEM image of the sample FT11 (FIG. 9.31) shows the usual structure of commercial silica, that seems composed.

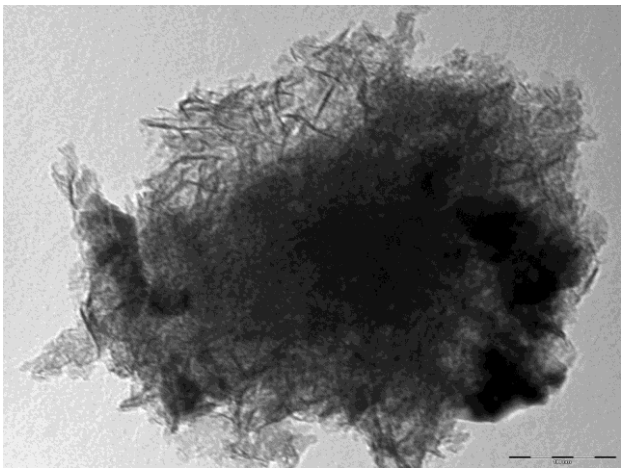

FIG. 9.31: TEM images for FT11

In the next image (FIG. 9.32 and 9.33), instead, the structure of egg-shell catalyst FT12 is shown. This structure is formed by the assembly of different particles and the shell around the particles can be observed.

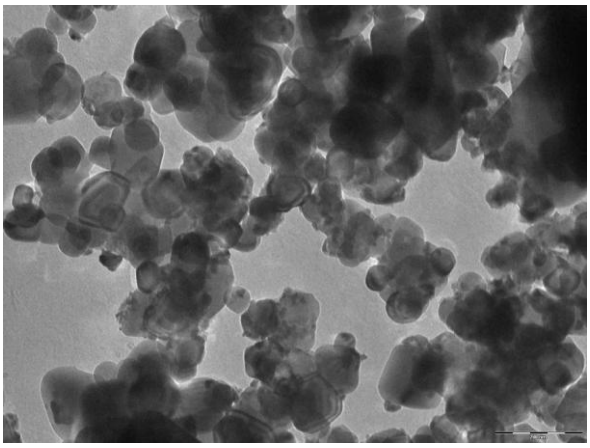

FIG. 9.32: TEM images for FT12

In the following figure, the egg-shell structure of the particle is well evidenced.

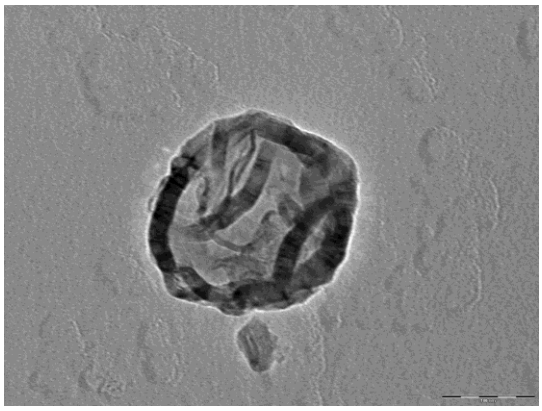

FIG. 9.33: TEM images for FT12

As expected, the TEM image of sample FT13 (FIG 9.34) shows the assembled structure typical of commercial alumina.

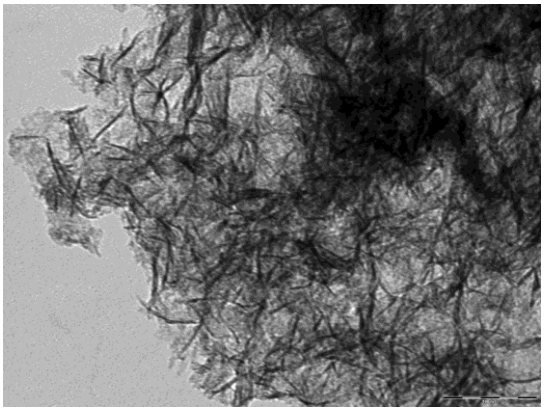

FIG. 9.34: TEM images for FT13

Also in the case of sample FT14, such as above seen for FT12, the egg-shell structure can be recognized from the TEM images (FIG. 9.35 and 9.36).

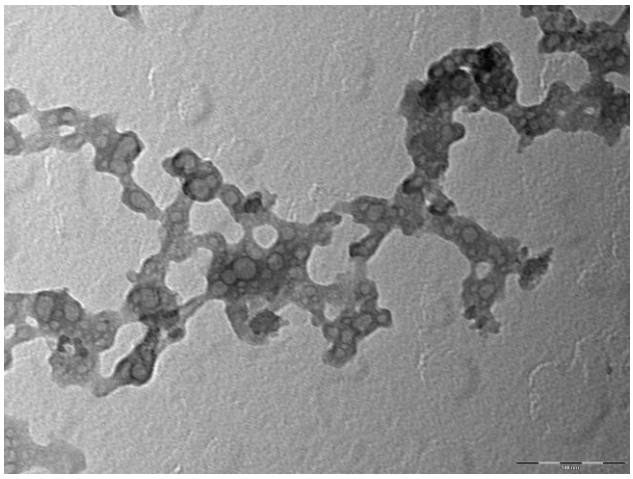

FIG. 9.35: TEM images for FT14

The following image for FT14 very well shows the structure as expected for an egg shell.

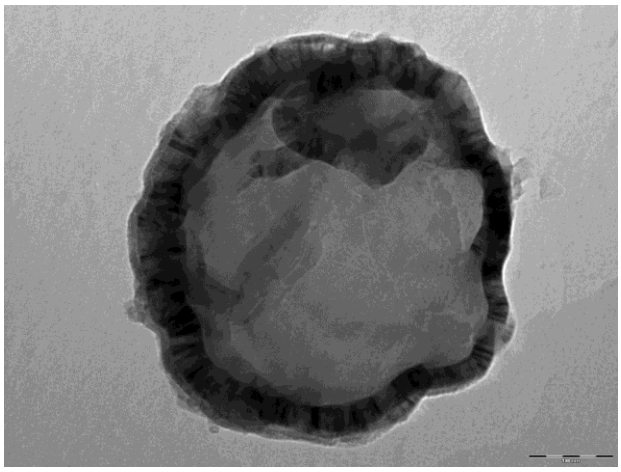

FIG. 9.36: TEM images for FT14

The TEM images collected for the catalysts FT15 and FT16 (FIG. 9.37 and 9.38 respectively), show an increase of the disorder and in this case the egg-shell structure is not clear as that seen for the other catalysts.

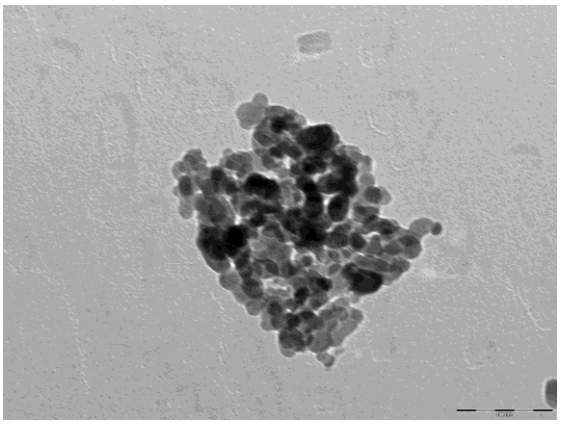

FIG. 9.37: TEM images for FT15

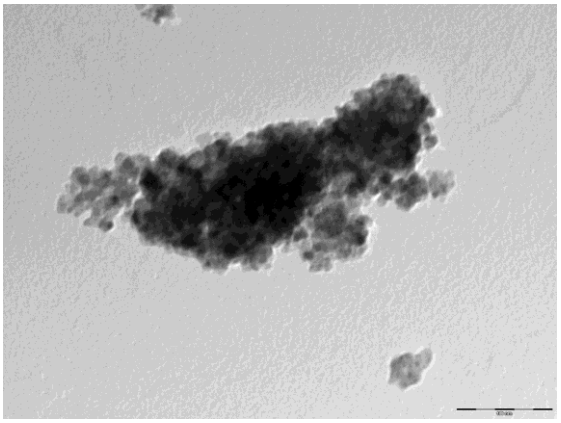

FIG. 9.38: TEM images for FT16

9.3.8 SEM images

The SEM images show that the dispersion of metal is better in the case of FT12 sample (FIG. 9.40) than for the impregnated catalyst FT11 (FIG. 9.39).

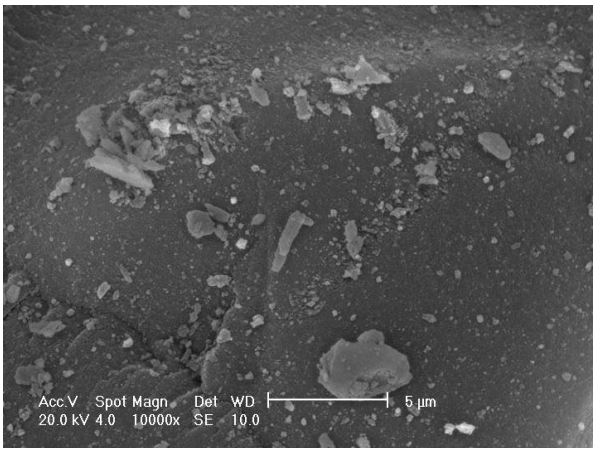

FIG. 9.39: SEM images for FT11

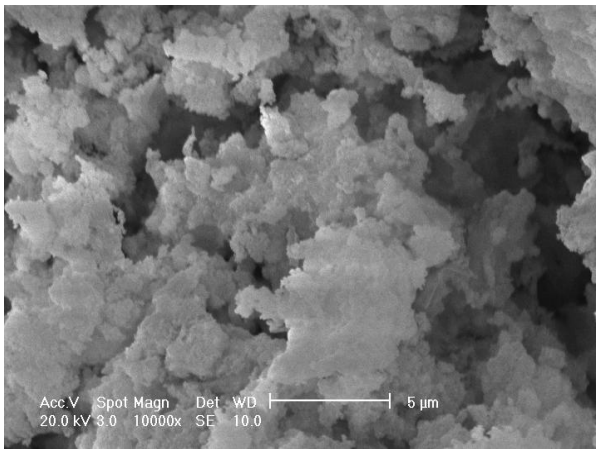

FIG. 9.40: SEM images for FT12

Also in the case of the alumina supported catalysts, the impregnated catalyst FT13 (FIG. 9.41) results to show a lower dispersion than the corresponding egg-shell catalyst FT14 (FIG. 9.42).

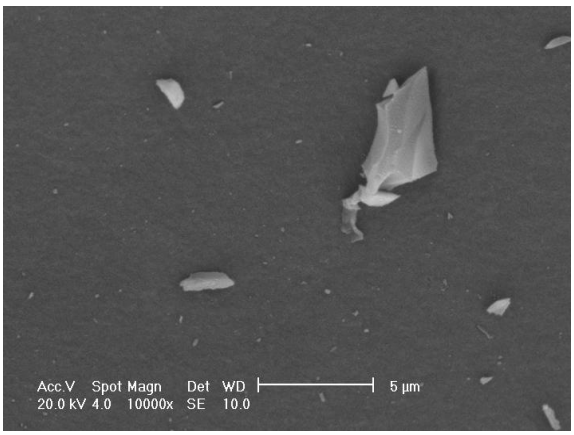

FIG. 9.41: SEM images for FT13

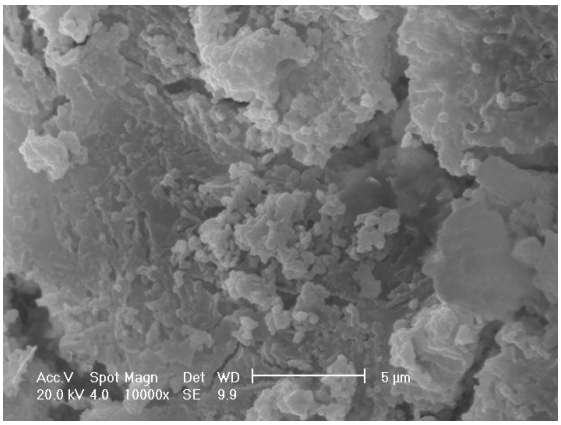

FIG. 9.42: SEM images for FT14

In the case of the catalysts prepared with the addition of ethylene glycol, FT15 and FT16, the SEM images (FIG. 9.43 and 9.44) show that the structure is largely inhomogeneous and the metal is not well dispersed over the surface.

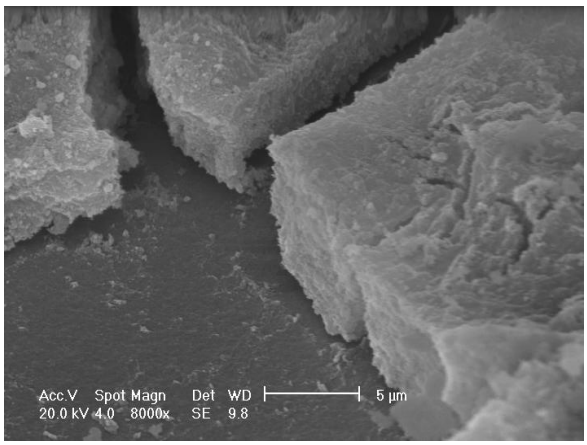

FIG. 9.43: SEM images for FT15

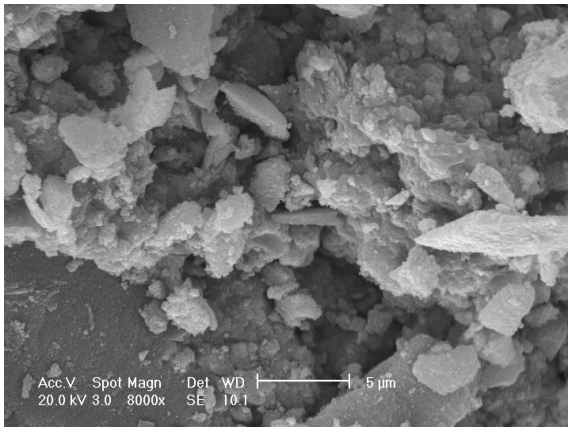

FIG. 9.44: SEM images for FT16

Catalytic tests

Catalysts FT11, FT12, FT13 and FT 14 were tested in a fixed bed reactor under pressure. 4 gram of each catalyst were charged into the reactor and pre-activated under hydrogen flow at 400°C. After the activation treatment, a mixture of H_2 and CO, with the molar ratio of 2:1 was fed to the reactor. The catalysts were tested at a pressure of 20 bar.

The conversion for catalyst FT11 (Graph 9.1) shows a quick and linear increase of activity at increasing temperatures, but the conversion does not start until 230°C and at 320°C the half of total conversion must be yet reached.

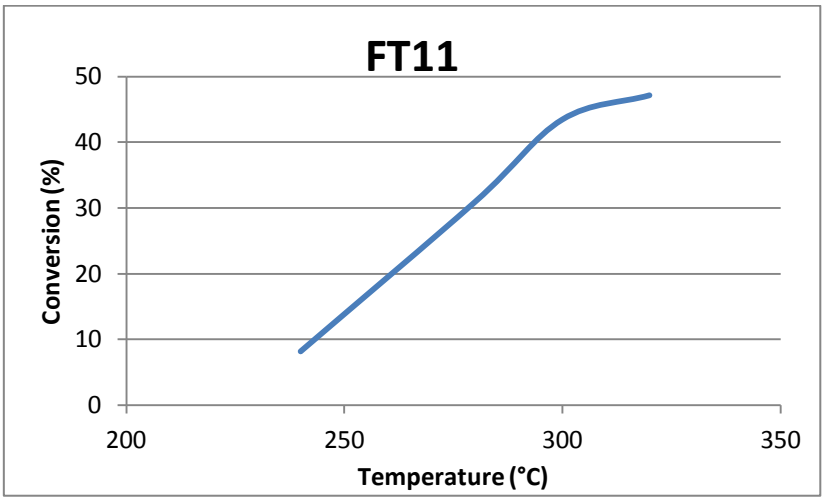

Graph 9.1: Conversion vs temperature for FT11

The productivity test, however, shows a slightly higher conversion, with values around 60% (Graph 9.2). These values decrease slowly during the test. The amounts of methane, CO_2 and lighter hydrocarbon products remain almost unaltered during this catalytic test.

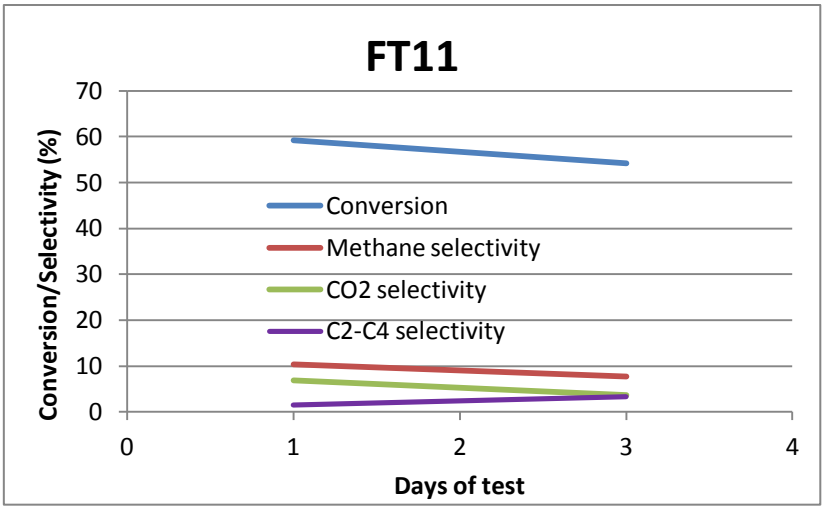

Graph 9.2: Conversion vs time for FT11

The ASF distribution resulting from the analysis done on the discharged organic liquid phase is reported as follows (Graph 9.3) and from the calculations show the alpha value results 0.71. This low value is as expected for an impregnated catalyst.

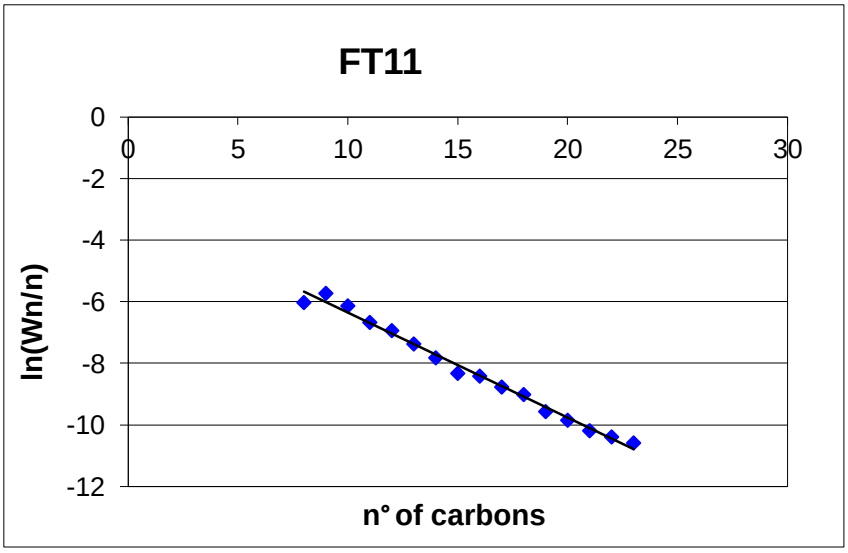

Graph 9.3: linearized production of condensed products for FT11

The catalyst FT12 shows a regular increase of conversion at increasing temperatures between 200°C and 300°C, then it tend to stabilize at around 70% of conversion (Graph 9.4).

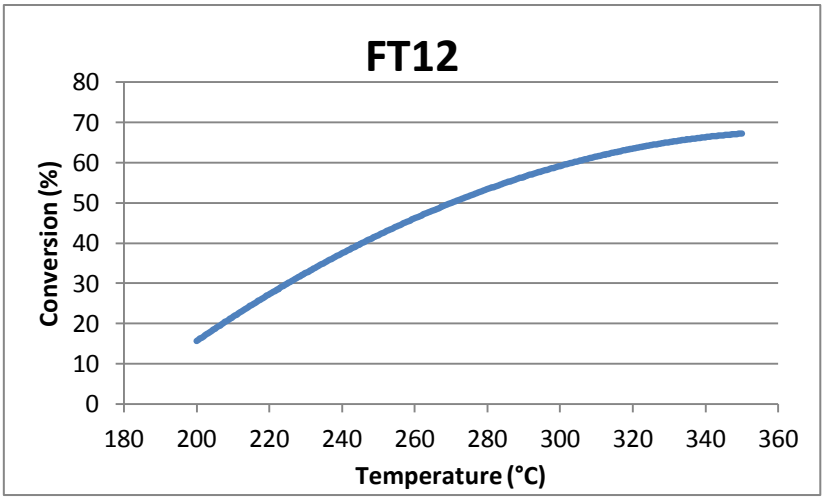

Graph 9.4: Conversion vs temperature for FT12

The productivity test was performed at 275°C. The conversion rapidly decreases from 75% to 35% during 4 days, while the methane selectivity and C_2-C_4 selectivity remain at the same values, at around 30% and 8% respectively. The CO_2 selectivity indeed seems to decrease from 18% to values lower than 10% during the test.

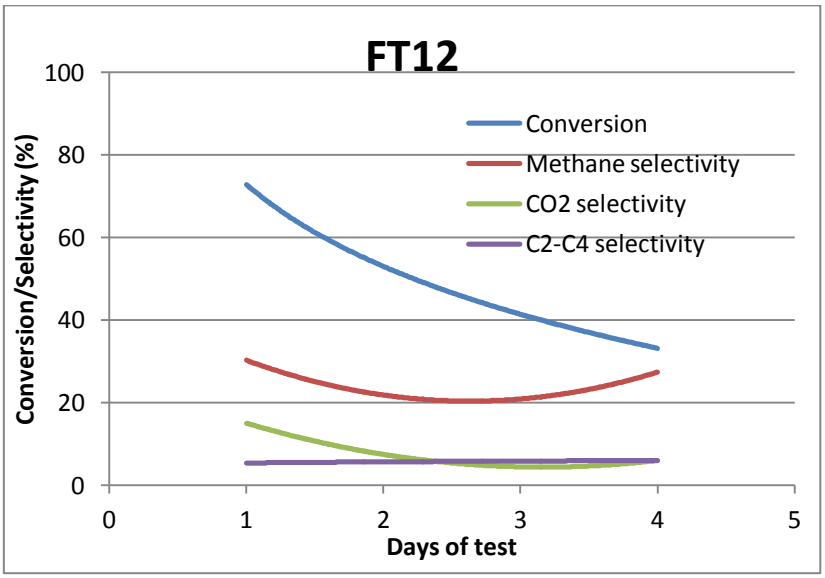

Graph 9.5: Conversion vs time for FT12

The analysis of organic condensed phase shows an alpha value of 0.75. As expected, this data is higher than that for FT11. The deactivation of the catalyst is due to an high production of solid

waxes that remain on the surface of catalyst itself; as a matter of fact, around the 8% of selectivity is assignable to the waxes.

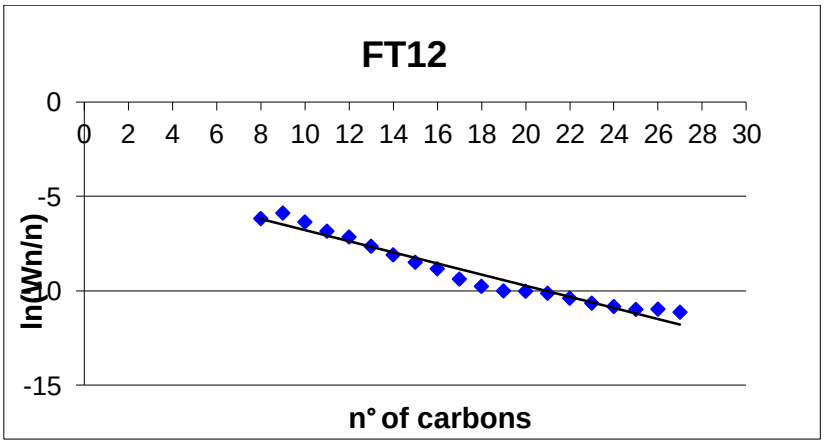

Graph 9.6: linearized production of condensed products for FT12

The catalyst prepared by impregnation of commercial alumina FT13 shows a conversion not so high, (Graph. 9.7) that reaches a value of 55% at 300°C.

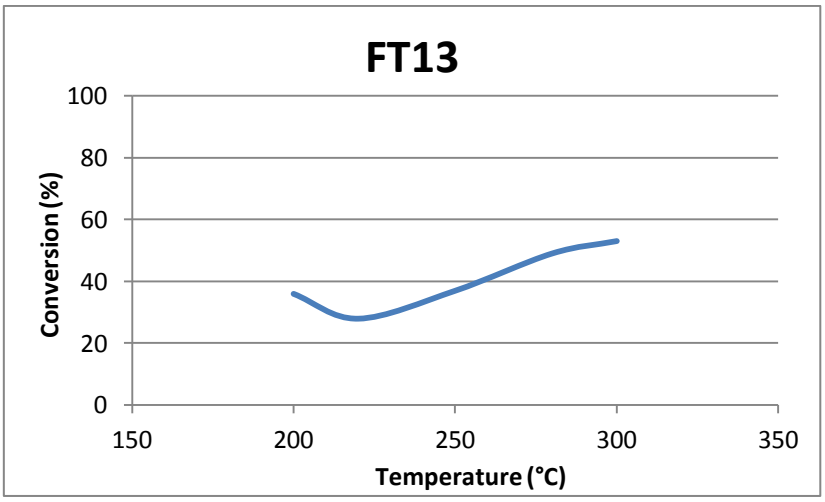

Graph 9.7: Conversion vs temperature for FT13

The productivity test was performed at 280°C (Graph 9.8). The activity decreases rapidly during he last days of the test, probably due to the deactivation in the presence of water. The selectivity to methane seems to tend to decrease slowly, while the C_2-C_4 selectivity and the CO_2 selectivity both remain unaltered during the test.

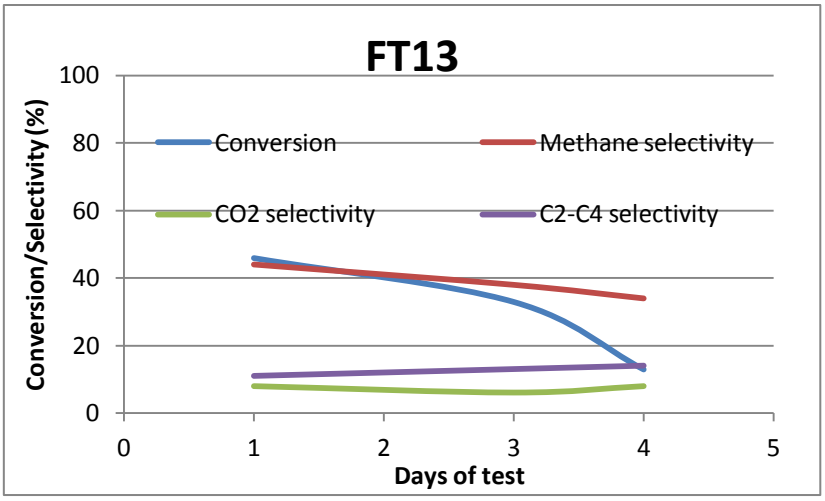

Graph 9.8: Conversion vs time for FT13

The alpha value of this catalyst, calculated by the organic phase analysis, results 0.74.

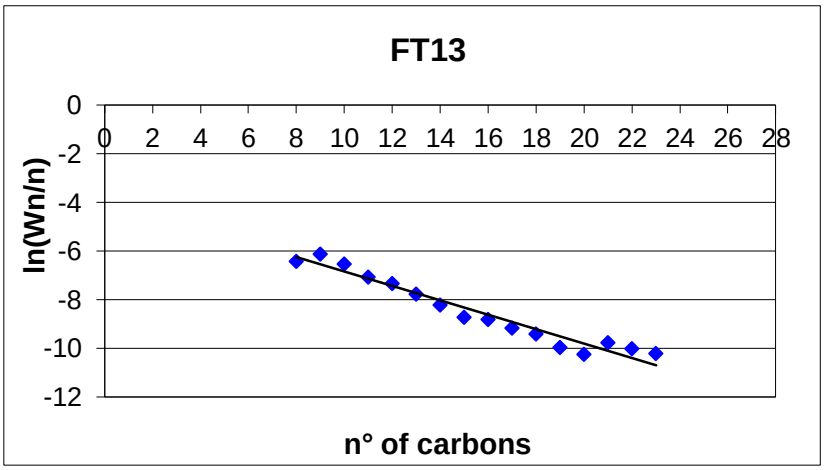

Graph 9.9: linearized production of condensed products for FT13

The conversion shown for the catalyst FT14 (Graph 9.10) is higher than for FT13, but at higher temperatures. In fact, at 350°C the 80% of CO is converted by the reaction.

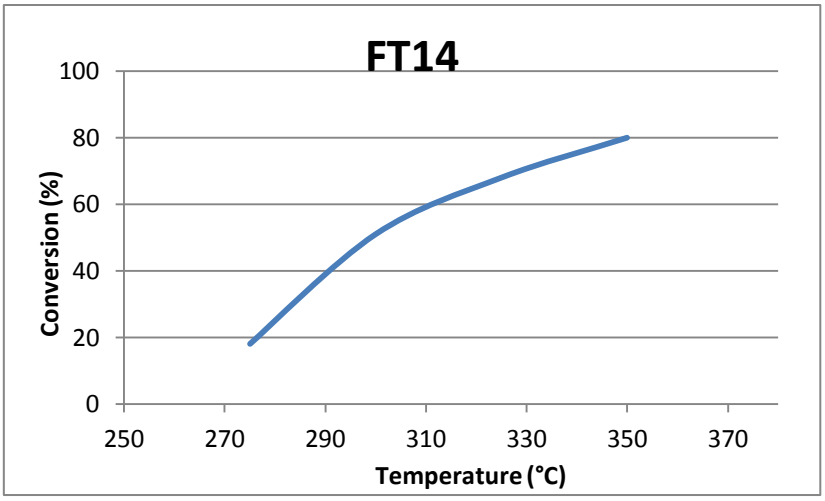

Graph 9.10: Conversion vs temperature for FT14

The catalytic test of productivity during the time was carried out at 300°C (Graph 9.11). As already observed for the catalyst FT13, also in this case the conversion remains unaltered during the test until the last days, when it decreases rapidly. The selectivity to methane, CO2 and C2-C4 products remains unaltered during the test.

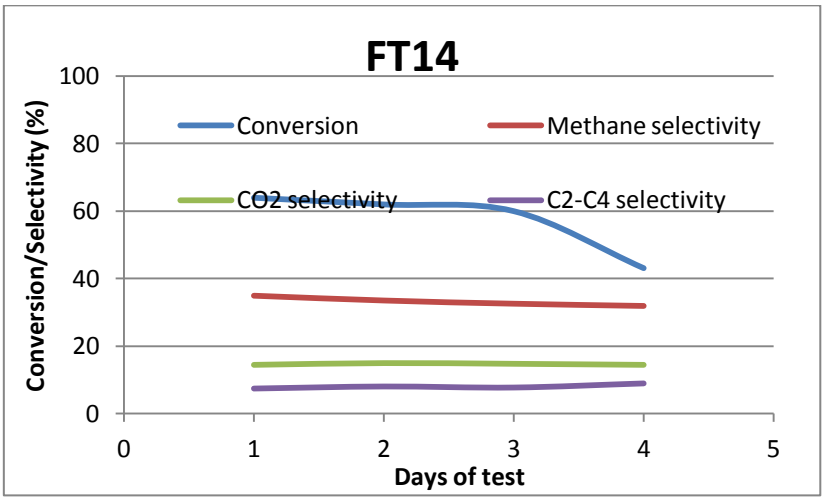

Graph 9.11: Conversion vs time for FT14

In this case, a lower amount of condensed product is collected and it is not possible to calculate the ASF distribution. This fact is probably due to an higher production of oxygenated by-products, that were found in the collected aqueous phase.

Following the poor characteristics observed during the analyses, the catalysts FT15 and FT16 were tested in the lab plant only at atmospheric pressure. In Table 9.3, the conversion of the catalyst FT15 as a function of the temperature is reported.

T (°C)	**Conversion (%)**
250	20
275	28
300	31
325	26
350	98

Table 9.3: conversion of catalyst FT15.

The catalyst shows a very low activity, that until 325°C is too low to give interesting results. Only at temperatures higher than 325°C the conversion shows a rapid increase and becomes almost complete.

The results of activity tests for FT16 are shown in the Table 9.4

T (°C)	Conversion
200	7
230	6
250	12
275	20
300	21
325	46
350	72

Table 9.4: conversion of catalyst FT15.

The behaviour of this catalyst is similar to the corresponding FT15 over silica; in this case the activity is also very low up to 325°C, then it tends to increase, while at 350°C it is not complete, but it is limited at around 70%.

9.5 Conclusions

The catalytic tests show that the anchoring method is better than the impregnation one for the catalysts supported on silica. As a matter of fact, the activity of the egg-shell catalyst FT12 produces higher hydrocarbons than FT11 at the same temperature. Also, the production of waxes results higher than for the other catalyst, as well as the alpha value of the ASF distribution. These results are also expected after observing the data collected from the surface area and the TPR analyses.

The results are more difficult to compare for the catalysts FT13 and FT14, supported over alumina. The main difference between them is in the fact that a very low amount of organic phase was collected for the egg-shell catalyst. This fact is connected with an higher production of oxygenated by-products, collected in the aqueous phase. The characterization tests, however, seem to give different results: the egg-shell catalyst, as a matter of fact, shows an higher reducibility, an higher

surface area, an higher dispersion and an higher amount of active sites than the impregnated catalyst.

The difference between the characterization data and the results of the catalytic tests could be partially due to the formation of CO2. In fact, in the case of the egg-shell catalyst the formation of CO2 is two times than for FT13. This higher selectivity to CO2 production is probably connected with the formation of carbon tars by the Boudouard reaction. This kind of carbon is deposited over the surface of the catalyst, then preventing the formation of longer hydrocarbon chains on the active sites.

By observing the characterization and the catalytic tests of the catalysts prepared in the presence of ethylene glycol, they show poor results; the presence of ethylene glycol seems not to have positive effects on the formation of smaller particles on the surface of the catalyst. Probably the addition of the template agent only during the formation of the shell is not sufficient to assure the high dispersion of the active phase.

Bibliography

[1] A. Y. Khodakov, W. Chu, P. Fongarland; *Chem. Rev.* ***2007.*** *107, 1692*

[2] M. Voß, D. Borgmann and G.Wedler; *Journal of Catalysis* ***2002.*** *212, 10 (2002)*

[3] A. M. Saib, M. Claeys, E. V. Steen*; Catal. Today* ***2002.*** *71 ,395*

[4] R. Bechara, D. Balloy, D. Vanhove; *Appl. Catal.* ***2001.*** *207, 343*

[5] H. Xiong, Y. Zhang, S. Wang, J. Li; *Catal. Commun.* ***2005.*** *6, 512*

[6] A. Di Michele; PhD Thesis: **"Sonochemical synthesis of metal nanoclusters and their application in the Fischer-Tropsch process"**; 2007

[7] C. Perego, P. Villa; *Catalysis Today.* ***1997.*** *34, 281*

[8] N. Koizumi, S. Suzuki, S. Niiyama, Y. Ibi, T. Shindo, M. Yamada; *Applied Catalysis A: General* ***2011.*** *395, 138*

[9] T. Mochizuki, T. Hara, N. Koizumi, M. Yamada; *Applied Catalysis A: General* ***2007.*** *317, 97*

[10] C. Chen, H. Yuuda, X. Li; *Appl. Catal. A* ***2011.*** *396, 116*

CHAPTER 10: Titania as support

10.1 Introduction

In this section, five catalysts are prepared in order to have informations about the role of titania when it is used as support for Fischer-Tropsch synthesis[1,2]. Five catalysts are prepared all with 17% by weight of Co as active phase. FT17 is prepared by impregnation of a commercial titania[3,4] with a cobalt nitrate solution. FT18 is prepared by the bulk sol-gel method[3,4]. The preparation way used for FT19 is the same as for FT18, but as last step a solution containing triruthenium dodecacarbonyl[5,6] is added to the catalyst. FT20 has the same composition as FT19, but the addition of the ruthenium precursor is performed before the gelification step. FT21 is prepared with the egg-shell method, with a core of titania prepared by the sol-gel method and a shell of silica that contains the cobalt.

In table 10.1 are summarized the composition of the catalysts.

SAMPLE	ACTIVE PHASE	SUPPORT	PREPARATION METHOD
FT17	17%Co	Titania	Incipient wetness
FT18	17%Co	Titania	Bulk sol-gel
FT19	17%Co – 0,5% Ru	Titania	Bulk sol-gel
FT20	17%Co – 0,5% Ru	Titania	Bulk sol-gel
FT21	17%Co	Silica/Titania	Egg-shell

Table 10.1: method of preparation and precursors for these catalysts.

10.2 Preparation

FT17

The preparation of this catalyst followed the “to incipient wetness” impregnation technique. The used support was a commercial titania. The amount of cobalt deposited over the support was 17% by weight. The incipient wetness point of ethanol resulted 1.4 ml per gram of titania.

10.00 g of support were impregnated with a solution of 9.87 g of $Co(NO_3)_2 \cdot 6H_2O$ dissolved in 14 ml of ethanol. The sample was left aging for 4 days, then it was dried in an oven for 1 night at 110°C and finally calcinated at 450°C for 5 hours.

FT18

This preparation was carried out by using the bulk sol-gel method. In order to obtain 10 g of support, 35.5 g of $Ti(iPrO)_4$ were dissolved in 175 ml of isopropyl alcohol. A solution of 9.86 g of $Co(NO_3)_2 \cdot 6H_2O$ in 14 ml of ethanol was prepared. The solution was mixed and 22 ml of water were added to induce the gelification. The catalyst was aged for a week, then dried at 110°C for 1 night and finally calcinated at 450°C for 5h.

FT19

3 gram of this catalyst were prepared by the same method as FT18, but, after the aging step, a solution of 0.0318 g of $Ru_3(CO)_{12}$ dissolved in 15 ml of ethanol was added to impregnate the sample. The catalyst was also dried at 110°C for 1 night.

FT20

The solution of the support precursor was prepared by dissolution of 35 ml of $Ti(iPrO)_4$ in 175 ml of isopropyl alcohol. Apart 9.86 g of $Co(NO_3)_2 \cdot 6H_2O$ were dissolved in 14 ml of ethanol and 0.106 g of $Ru_3(CO)_{12}$ were dissolved in 50 ml of THF. The solutions were then mixed together and 12 ml of water were added drop by drop to favour the gelification. Also in this case the gel, after the aging step, was dried in an oven at 110°C for 1 night and finally calcinated at 450°C for 5 h.

FT21

12 g of TiO_2 were prepared by the sol-gel technique, by dissolving 45 ml of $Ti(iPrO)_4$ in 225 ml of isopropyl alcohol and then adding drop by drop 22 ml of water to induce the gelification. After aging for 4 days and drying at 110°C for 1 night, the support was impregnated with a solution prepared from 12.55 g of $Co(NO_3)_2 \cdot 6H_2O$, 15 ml of ethanol and 4.5 ml of TMOS. The catalyst was then left to gelificate until a complete evaporation of the solvent (4 days), dried in an oven for 1 night at 110°C and finally calcinated for 5h at 450 °C.

10.3 Characterization

10.3.1 TPR

The TPR profile for the catalyst FT17 (FIG.10.1) shows only a peak of reduction of cobalt oxides. This peak is centered at 400°C. The reducibility of this sample resulted low, around 9%. This fact is probably due to the low surface area of the support, that causes a low dispersion of the metal connected to the agglomeration of metal particles.

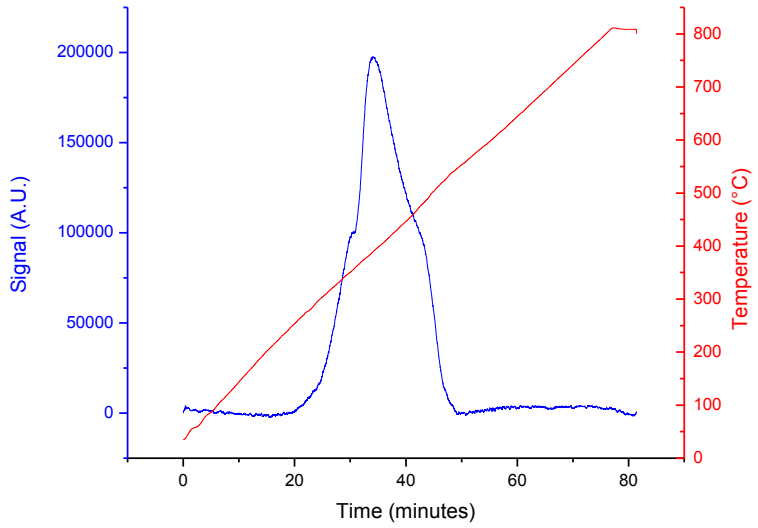

FIG. 10.1: TPR profile for FT17

From the TPR analysis for FT18 (FIG. 10.2) we can observe two peaks at 450°C and 640°C respectively. The first one is due to the reduction of cobalt oxides. The second is assigned to the reduction of cobalt strongly bonded to the titania support . In this case, the calculation of the separated peaks is not easy. However the amount of cobalt reduced corresponding to the first peak seems to be 7%, that increases to 17% if the second peak is considered too in the calculation.

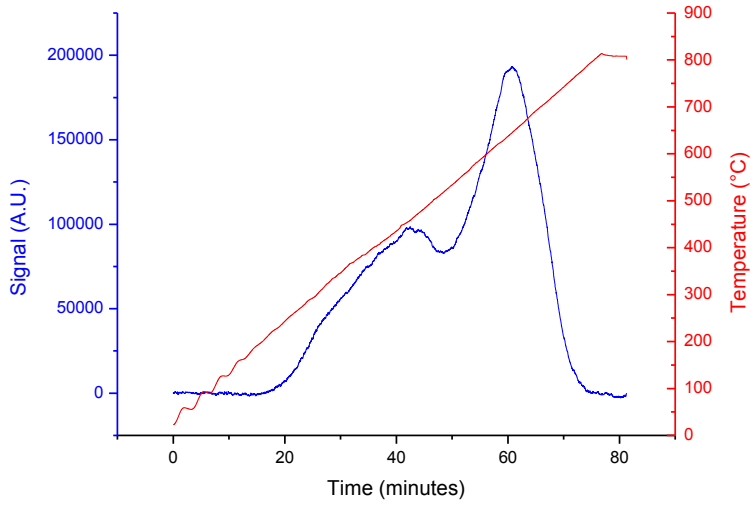

FIG. 10.2: TPR profile for FT18

Three signals are present in the TPR profile of FT19 (FIG. 10.3). The first one at 320°C is probably due to the reduction of a ruthenium oxidized species originated by the preliminary interaction with the support; the second peak at 460°C and the third one at 550°C are probably due to the two species of cobalt oxides. The reducibility of this catalyst is 9%.

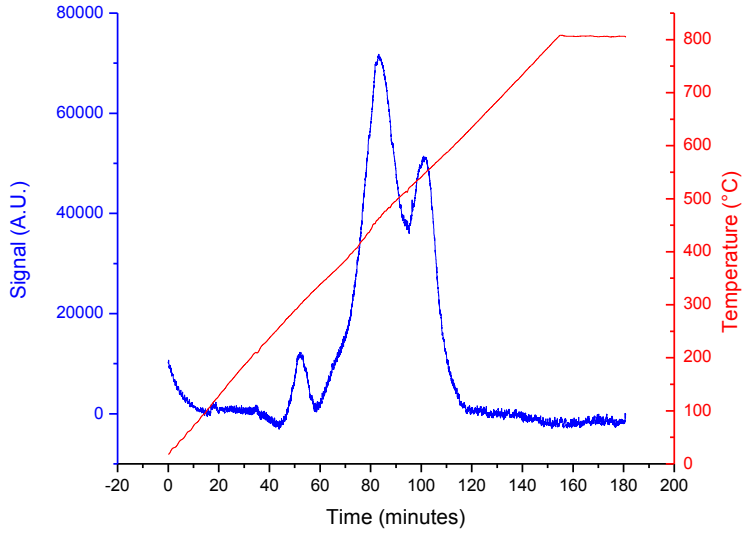

FIG. 10.3: TPR profile for FT19

Three peaks can be also observed in the TPR profile of FT20 (FIG. 10.4). The first one, at 160°C, due as above indicated to the oxidized ruthenium, is not significant. The peaks at 280°C and 460°C are due to the reduction of cobalt oxides. The addition of Ruthenium causes a decrease of the temperature of reduction of Cobalt oxide. Notwithstanding, the reducibility of the catalyst remains very low: about 10%.

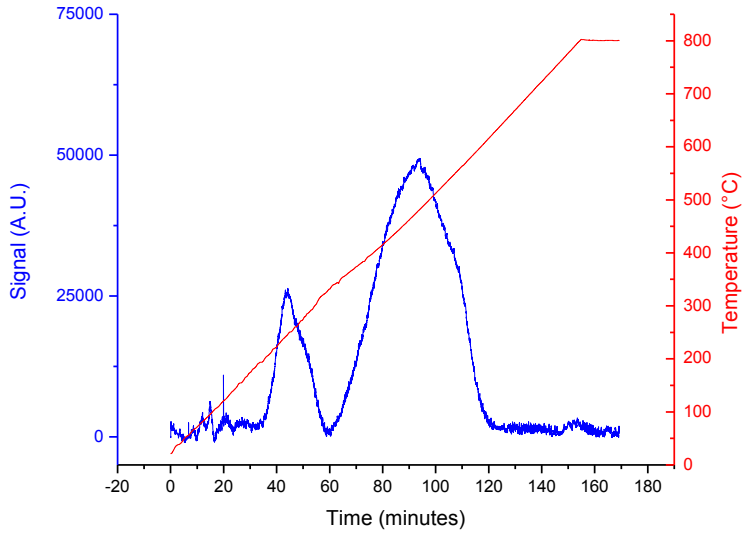

FIG. 10.4: TPR profile for FT20

In the TPR profile of sample FT21 (FIG. 10.5), two peaks can be observed: the first one at 355°C is due to the reduction of Cobalt oxides and the second, at 645°C, is due to the reduction of silico-titanate species. The total reducibility is 10%; the reducibility of Cobalt Oxide is 6.5%.

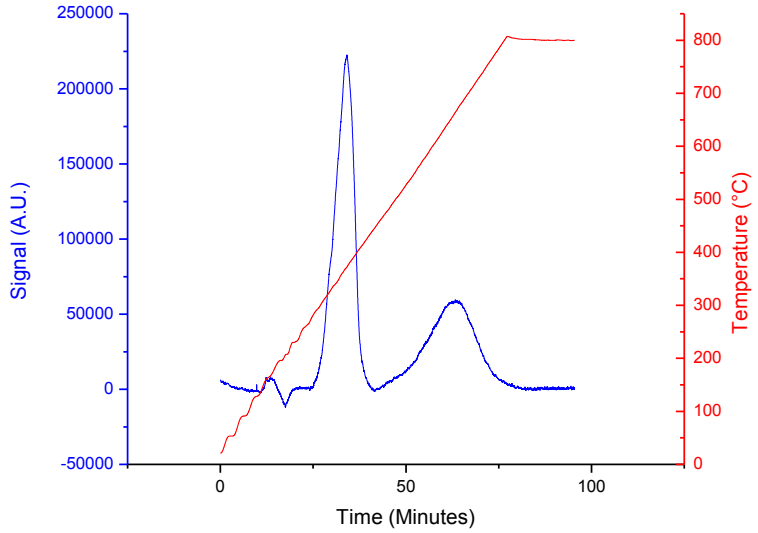

FIG. 10.5: TPR profile for FT21

10.3.2 TPO

The TPO analysis for FT17 (FIG. 10.6) gives a graph in which we can observe a band formed by the overlapping of two peaks at 190°C and 290°C. The oxidation of the sample starts at temperatures under 200°C. The amount of reoxidized metal is 14%.

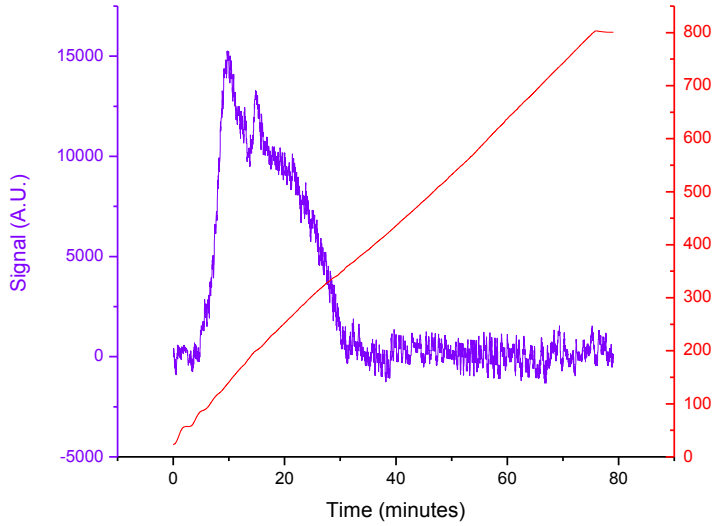

FIG. 10.6: TPO profile for FT17

The TPO profile for FT18 catalyst (FIG 10.7) is similar to that for FT17; in fact it is present a band formed by the overlapping of two peaks at around 200°C and 300°C. Also in this case the reoxidation starts at low temperatures. The percentage of reoxidation of metal is 21%.

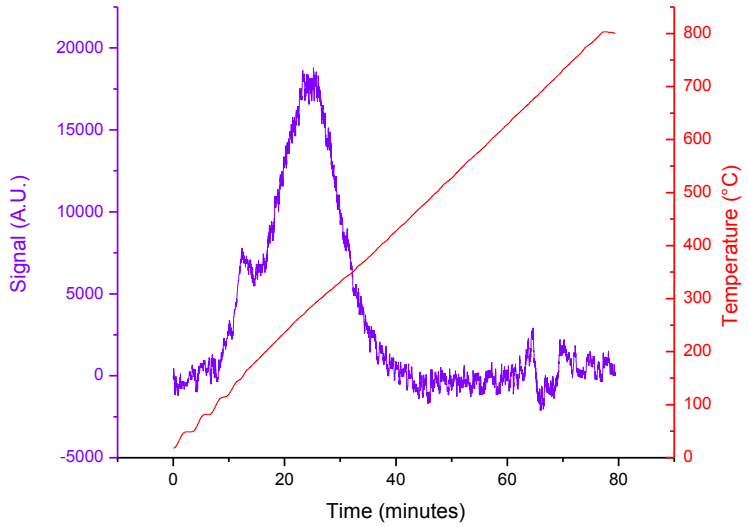

FIG. 10.7: TPO profile for FT18

The TPO profile of the catalyst FT19 (FIG. 10.8) shows a peak slightly shifted with respect to that of the unpromoted catalyst. However, the addition of Ruthenium seems to not have effect on the formation of the active phase; in fact the re-oxidizability is the same as for FT18.

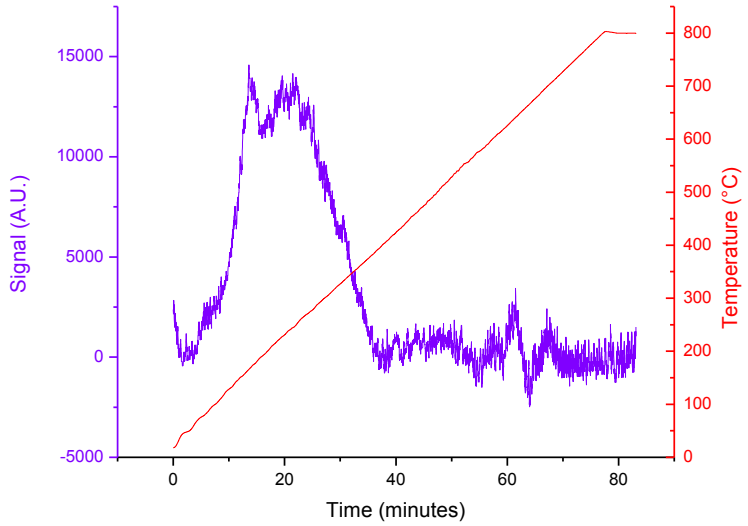

FIG. 10.8: TPO profile for FT19

The TPO profile of FT20 (FIG. 10.9) shows a band constituted by two peaks between 100°C and 300°C. These two peaks are assignable to the oxidation of cobalt to CoO and Co_2O_3. The amount of re-oxidized metal is 12%.

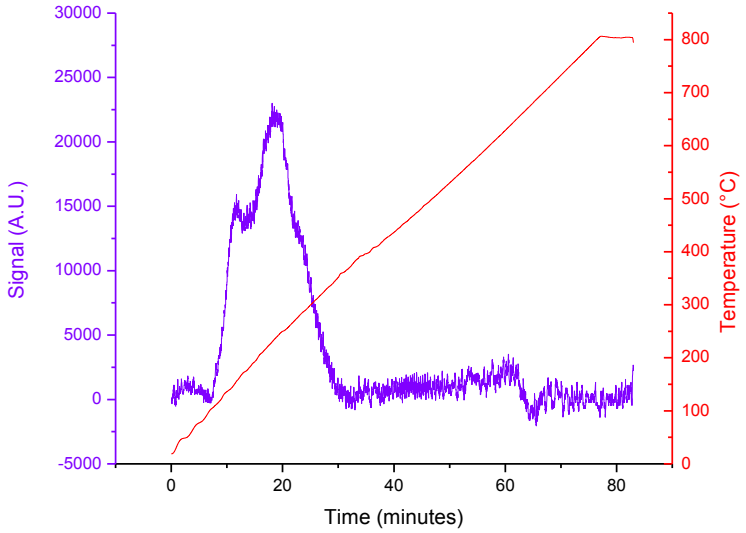

FIG. 10.9: TPO profile for FT20

The TPO profile for the sample FT21 (FIG. 10.10) shows a large band between 100°C and 400°C. The calculation from this analysis gives that a re-oxidation degree of metal of 14%.

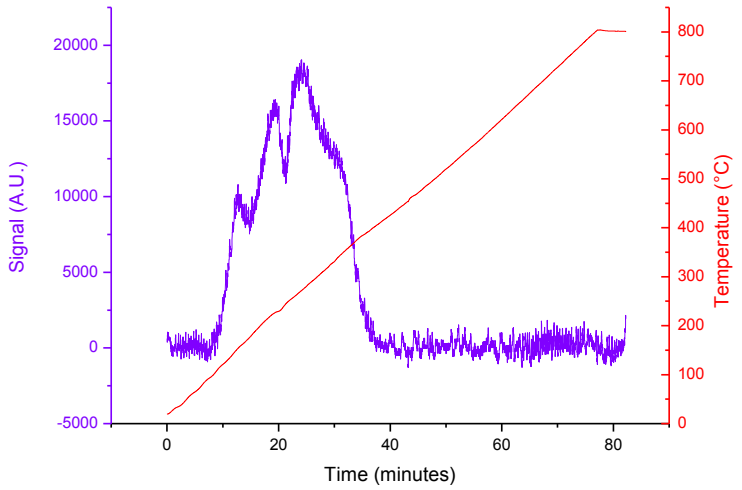

FIG. 10.10: TPO profile for FT21

10.3.3 Surface Area

The surface area of the catalysts, determined by the B.E.T. method at single point, are shown in the table 10.2.

SAMPLE	SURFACE AREA (m^2/g)
FT17	16
FT18	61
FT19	37
FT20	51
FT21	178

Table 10.2: surface area of the samples

The addition of Ruthenium in FT19 causes a significant decrease of the surface area value. Indeed, the increase of the surface area for the catalyst FT21 is due to the use of silica as shell superimposed on the titania support.

10.3.4 XRD analyses

The XRD spectrum of the sample FT17 (FIG. 10.11) shows peaks at 2θ = 26°, 38°, 48°, 55°, 63°, 70° and 75°. These peaks are assignable to TiO_2 in the anatase form.

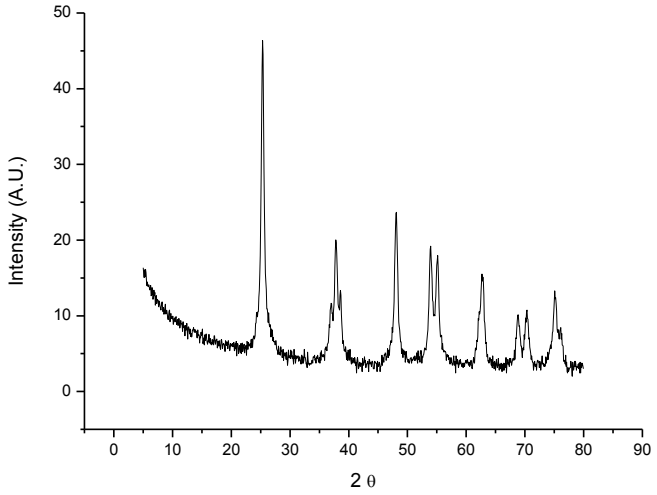

FIG. 10.11: XRD spectrum for FT17

The analysis of FT18 (FIG. 10.12) gives an XRD spectrum typical of an amorphous material; in fact the signal is very low with respect to the noise. However, into the spectra some signals can be recognized associated with the anatase form of TiO_2.

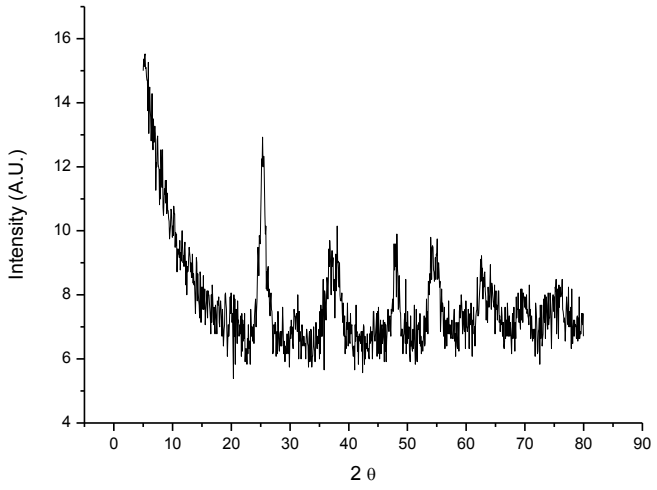

FIG. 10.12: XRD spectrum for FT18

In the XRD spectrum for FT20 (FIG. 10.13) the signals are very hard to recognize. It means that the material is in this case completely amorphous.

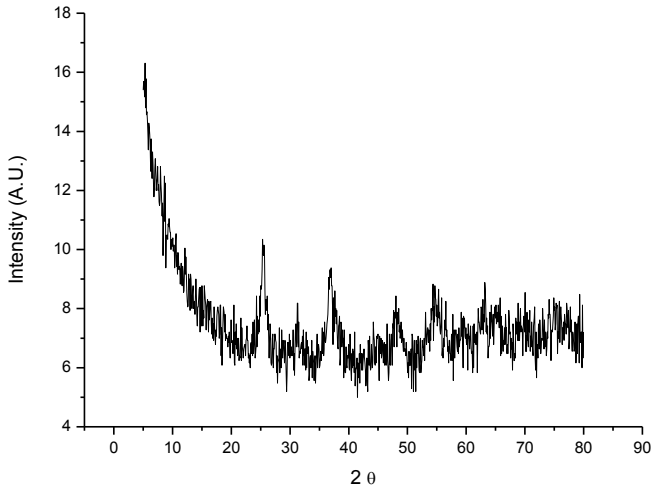

FIG. 10.13: XRD spectrum for FT20

Also in the case of FT21, as for FT20, the structure is completely amorphous (FIG. 10.14). Only a very small peak can be observed at 2θ = 37°, that can be assigned to the presence of Co as Co_3O_4.

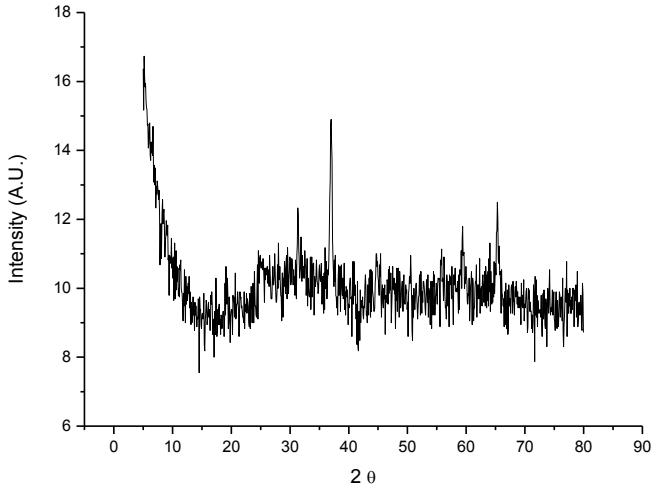

FIG. 10.14: XRD spectrum for FT21

10.3.5 FT-IR

For all catalysts, the IR spectra were acquired before (blue line) and after the calcination treatment (red line) (FIG 10.15, 10.16, 10.17 and 10.18). In all cases, the blue spectra show two

peaks at 1290 and 1460 cm^{-1}. These signals are due to the presence of NO_3^- groups. In some cases the band of water is also present. These signals disappear after the calcination is carried out.

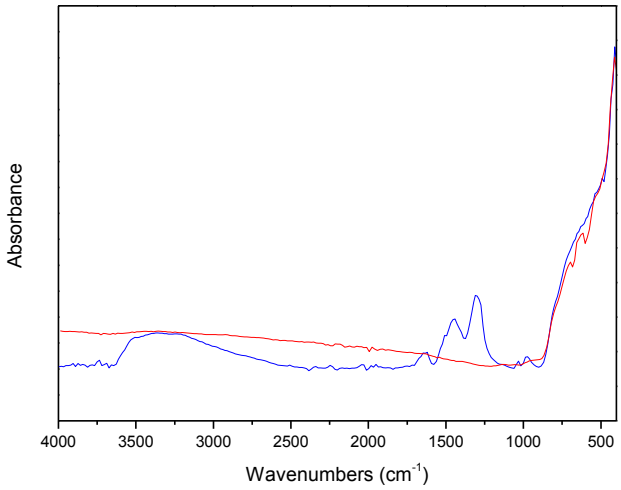

FIG. 10.15: IR spectra for FT17

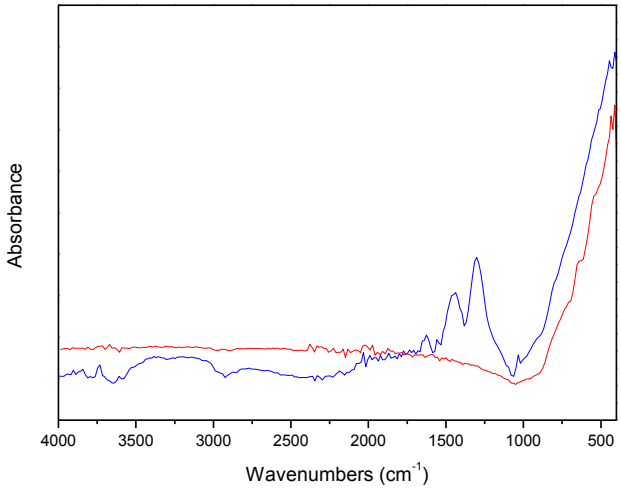

FIG. 10.16: IR spectra for FT18

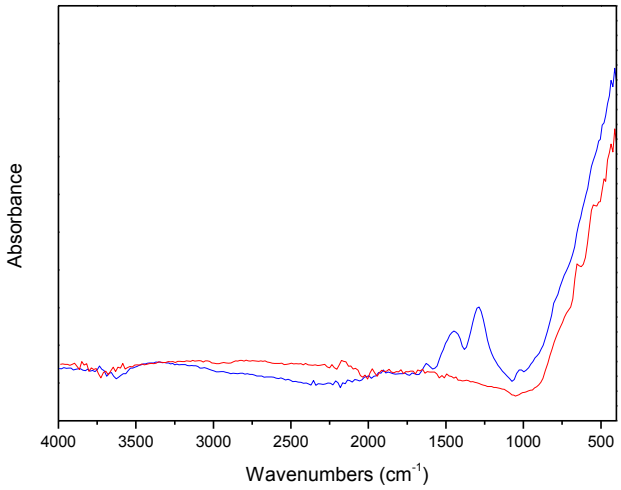

FIG. 10.17: IR spectra for FT20

The IR analysis for FT21 catalyst (FIG. 10.18) also shows a peak at 1030 cm^{-1}. This peak, that remains present also after the calcination step, is due to the silicium-oxygen bond.

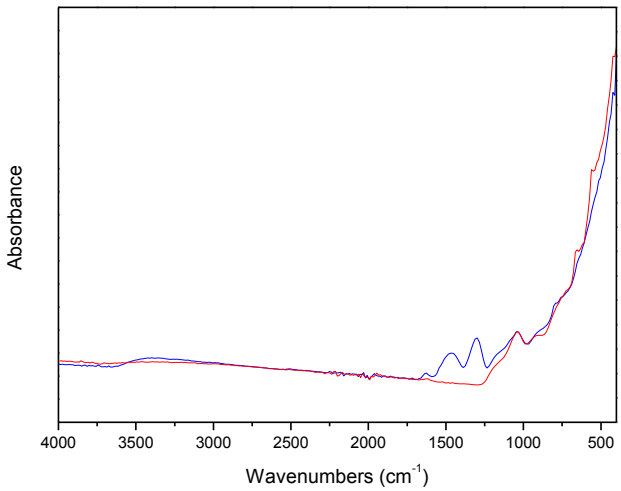

FIG. 10.18: IR spectra for FT21

10.3.6 SEM and TEM images

The electron microscopy images were collected for FT17 and FT21.

The SEM image of FT17 (FIG. 10.19) shows a relevante dishomogeneity of the surface but a good dispersion of the metal particles over the surface itself.

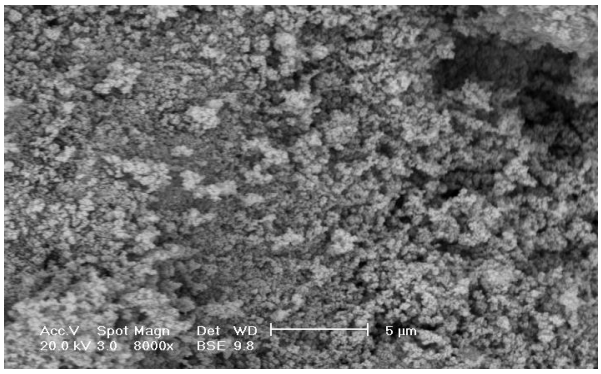

FIG. 10.19: SEM image for FT17

The SEM image collected for the sample FT21 (FIG. 10.20) shows indeed a structure that seems a conglomerate. This conglomeration is surely due to the agglomeration of silica when it gelificates during the formation of the shell.

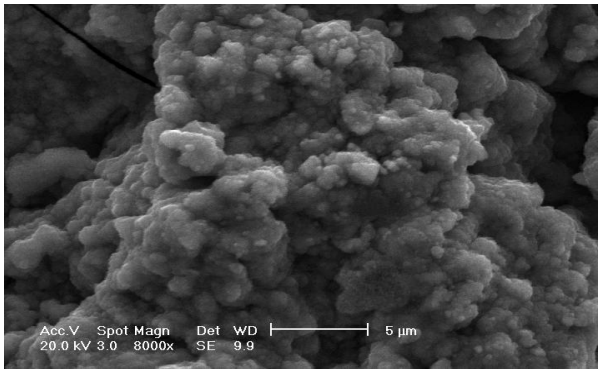

FIG. 10.20: SEM image for FT21

The TEM image collected for the catalyst FT17 (FIG. 10.21) shows very similar and ordered metal particles. This fact is probably due to the use of a commercial material as support.

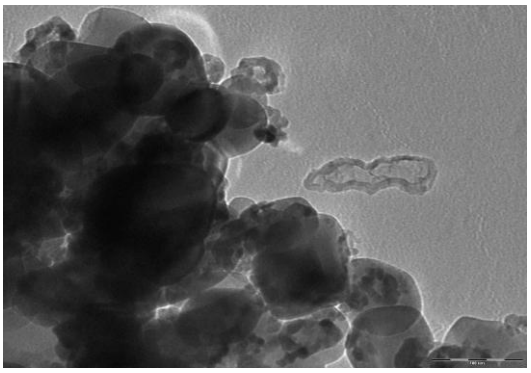

FIG. 10.21: TEM image for FT17

The TEM image of FT21 for a single grain (FIG. 10.22) shows indeed the typical egg-shell structure with the core of titania and the shell of silica including the metal particles.

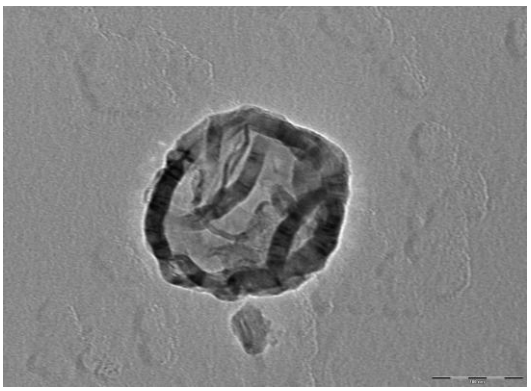

FIG. 10.22: TEM image for FT21

10.4 Catalytic tests

The catalytic tests are carried out in the lab plant at room pressure; for all catalysts the conversion as a function of temperature is shown in the Table 10.3

	TEMPERATURE (°C)				
CATALYST	**200**	**250**	**300**	**350**	**400**
FT17	0	0	10	12	37
FT18	0	0	5	6	26
FT19	0	3	9	23	-
FT20	6	16	19	18	-
FT21	14	16	17	16	-

Table 10.3: conversion for catalyst FT17, FT18, FT19, FT20, FT21

The results show that these catalysts are not very active for the Fischer-Tropsch synthesis[7]. In particular, the impregnated catalyst, the bulk sol-gel catalyst and the bulk sol-gel catalyst with ruthenium added by impregnation show some activity only over 300°C. The catalyst FT20, that contains ruthenium inside the bulk of the structure starts to convert the reagents at lower temperatures. The catalyst FT21, formed by an egg-shell of silica over the titania support seems the best between these catalysts. However, these catalysts show a light decrease of the conversion when higher temperatures are reached.

In order to better understand the behaviour of titania when it is used as support, the catalyst FT17, taken as a reference for the entire set of titania supported catalysts, and FT21, the egg-shell catalyst, are tested under 20 bar of pressure.

4 gram of catalyst were charged into the reactor and the catalysts were activated at 400°C under hydrogen flow.

FT17 shows a low activity up to 325°C, then the CO conversion rapidly increased until a total conversion is reached (Graph 10.1).

The selectivity to methane follows a strange behaviour: it is initially around 40%, then it decreases to less than 20% and then it increases again to 30%. The amount of CO_2 production is very high, and it increases at increasing temperatures until a more than 20% value at 350°C. The selectivity to lighter hydrocarbons (ethane, propane and butane) decreases from 10% to 5% between 325°C and 350°C.

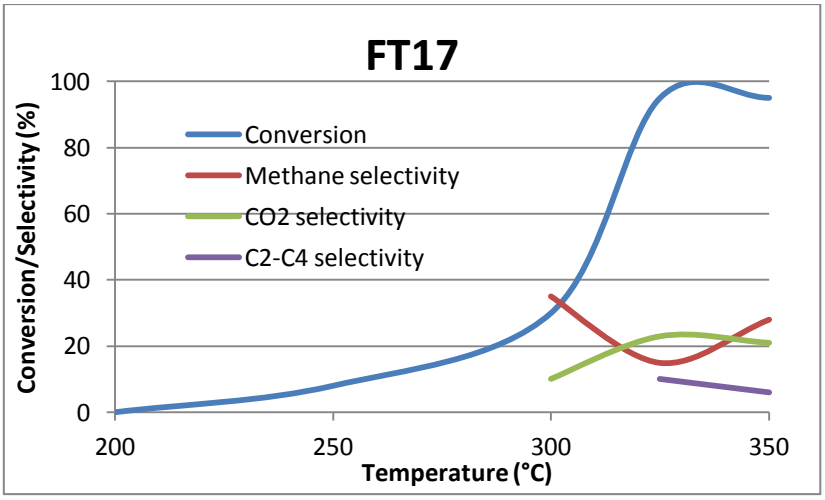

Graph 10.1: Conversion vs temperature for FT17

Instead the FT21 catalyst shows a relevant increasing of activity already at 220°C and it reaches the total conversion at 250°C, then it decreases rapidly at higher temperatures, probably because of a deactivation of the catalyst (Graph 10.2).

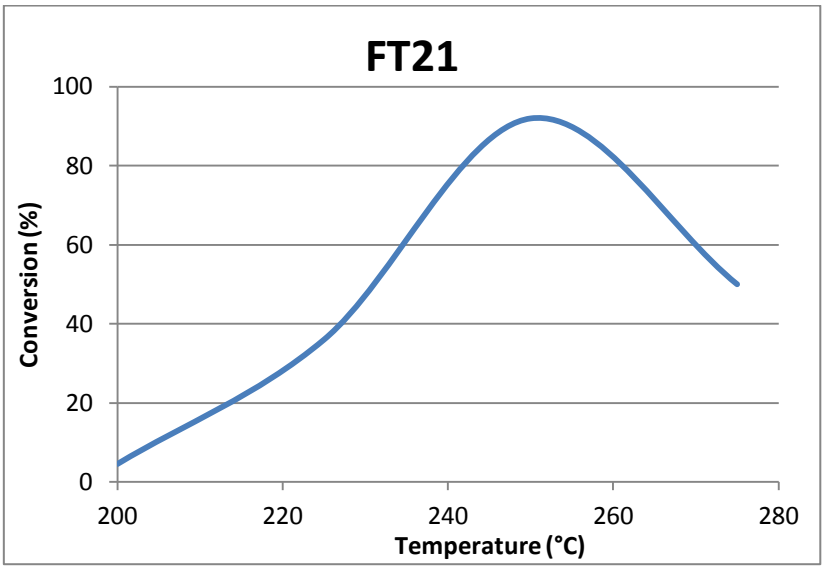

Graph 10.2: Conversion vs temperature for FT21

A life time test was carried out at 250°C (Graph 10.3). The conversion, strangely, seems to increase from around 80% to 95%. Also the methane selectivity shows a strange tendency: it seems to decrease during the time. This behaviour is accompanied by an increase of the CO_2 production. Probably, during the test, the ability of titania to oxidize CO[8,9] plays an important role beside the Fischer-Tropsch synthesis, and it could explain this strange behaviour observed.

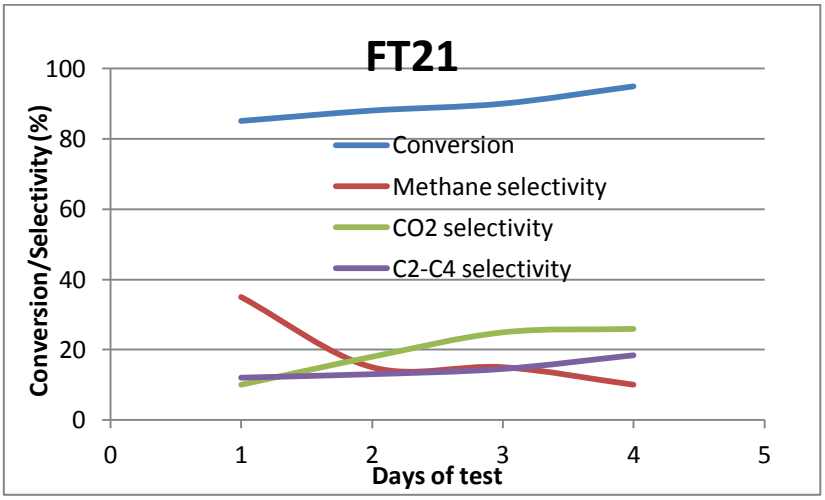

Graph 10.3: Conversion vs time for FT21

The alfa value calculated for this catalyst is not high, as expected: 0.66.

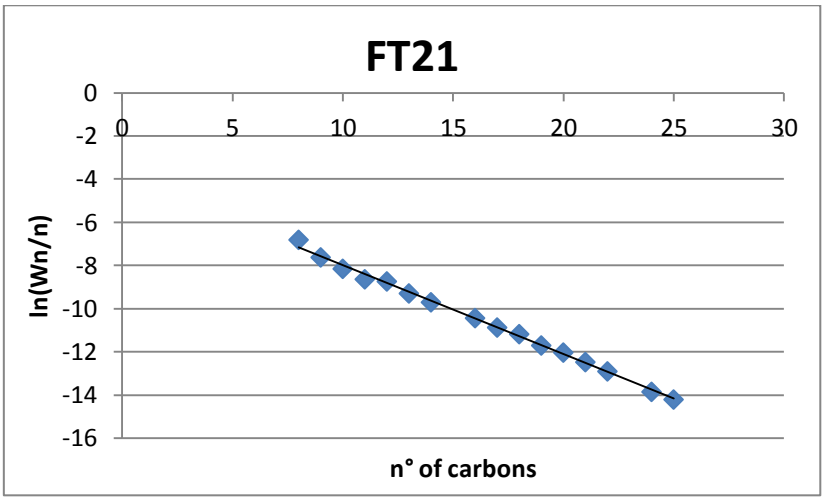

Graph 10.4: linearized production of condensed products for FT21

10.5 Conclusions

The characterizations and activity tests for titania-supported catalysts show that this support is not convenient for the Fischer-Tropsch synthesis. In particular, the surface area results very low if compared with the other supports usually indicated for this synthesis. However, despite the capability of TiO_2 to give oxidation of CO becomes prevalent during the test, the egg-shell catalyst results more active than the others, that still demonstrating the goodness of this technique of preparation.

Bibliography

[1] Y. Yao, D. Hildebrandt, D. Glasser, X. Liu; *Ind. Eng. Chem. Res.* ***2010.*** *49, 11061*

[2] M. Voß, D. Borgmann, G. Wedler; *Journal of Catalysis* ***2002.*** *212, 10*

[3] A. Di Michele; PhD Thesis: **"Sonochemical synthesis of metal nanoclusters and their application in the Fischer-Tropsch process"**; 2007

[4] C. Perego, P. Villa; *Catalysis Today.* ***1997.*** *34, 281*

[5] B. Jongsomjit, C. Sakdamnuson, J. Panpranot, P. Praserthdam*; React. Kinet. Catal. Lett.* ***2006.*** *88, 65*

[6] N. Escalona, C. Medina, R. Garcıa, P. Reyes; *Catalysis Today* ***2009.*** *143, 76*

[7] B. Jongsomjit, T. Wongsalee, P. Praserthdam; *Materials Chemistry and Physics* ***2006.*** *97, 343*

[8] Y. Tay; J. Murakami, K. Tajiri, F. Ohashi, M. Data, S. Tsubota; Applied Catalysis A: General **2004.** 268, 183

[9] W. S. Epling, P. K. Cheekatamarla, A. M. Lan*; Chemical engineering journal* ***2003.*** *93, 61*

Chapter 11 – Clusters as active phase precursors

11.1 - Introduction

In this chapter, 4 catalysts are prepared by the egg-shell method. In all cases, the support is the same and it is composed by a core of silica and a shell of silica as well[1,2]. The amount of active phase is 17% by weight for all catalysts and it is obtained starting from different kinds of cluster. The active phase of catalyst FT22 is prepared by a cluster of Cobalt and Iron with 3:1 molar ratio. This composition is obtained by using the cluster $(N(C_2H_5)_4)[FeCo_3(CO)_{12}]$. The active phase of catalyst FT23 is composed by the same amount of metals but with the reversed molar ratio and this composition is obtained by using the cluster $[(Ph_3P)_2N][Fe_3Co(CO)_{13}]$. The active phase of catalyst FT24 is composed only by cobalt, added to the system as $Co_2(CO)_8$. Catalyst FT25 is prepared like as FT22, but by the addition of 0.4% of platinum as promoter[1,3]. Table 11.1 summarizes all these catalysts.

SAMPLE	SUPPORT	ACTIVE PHASE	RAW MATERIAL
FT22	silica/silica	12.75% Co – 4.25% Fe	$N(C_2H_5)_4)[FeCo_3(CO)_{12}]$
FT23	silica/silica	4.25% Co – 12.75% Fe	$[(Ph_3P)_2N][Fe_3Co(CO)_{13}]$
FT24	silica/silica	17% Co	$Co_2(CO)_8$
FT25	silica/silica	12.75% Co – 4.25% Fe – 0.5% Pt	$(C_2H_5)_4N$ $[FeCo_3(CO)_{12}]$ + H_2PtCl_6

Table 11.1: method of preparation and precursors for these catalysts.

11.2 Preparation

FT22

The core of catalyst FT22 is prepared as described in the chapter 8, by following the optimized method previously discussed. The active phase is synthesized by a procedure from the literature[4]. The steps of this procedure are the following described. 510 mg of $Co_2(CO)_8$ and 0.11 ml of $Fe(CO)_5$ were mixed under argon atmosphere with 20 ml of acetone "air free" (AF). The solution was heated at 40°C for 4h and then at 60°C for 10h. After cooling, the solvent is removed under vacuum and the intermediate product $[Co(CH_3COCH_3)_6][FeCo_3(CO)_{12}]_2$ is obtained. This product is dried at 50°C for 1h. The viscous residue is dissolved in 20 ml of water AF. The mixture is filtered and a red solid based on the anionic cluster $[FeCo_3(CO)_{12}]^-$ is obtained. The anionic phase is balanced by the addition of 230 mg of NEt_4Br. The precipitate obtained after 10 minutes of stirring is the desired product: $(N(C_2H_5)_4)[FeCo_3(CO)_{12}]$. The product is then purified by filtration and washing with 30 ml of distilled water AF and finally dried under vacuum. By this method, 0.583 g of the product are obtained. The procedure is repeated until the required amount of cluster is obtained. The quality of the obtained cluster is confirmed by the IR analysis between 2200 and 1600 cm^{-1} of the product dissolved in acetone.

The comparison of the band obtained (FIG. 11.1) with the literature data, confirmed that the synthesis is successful.

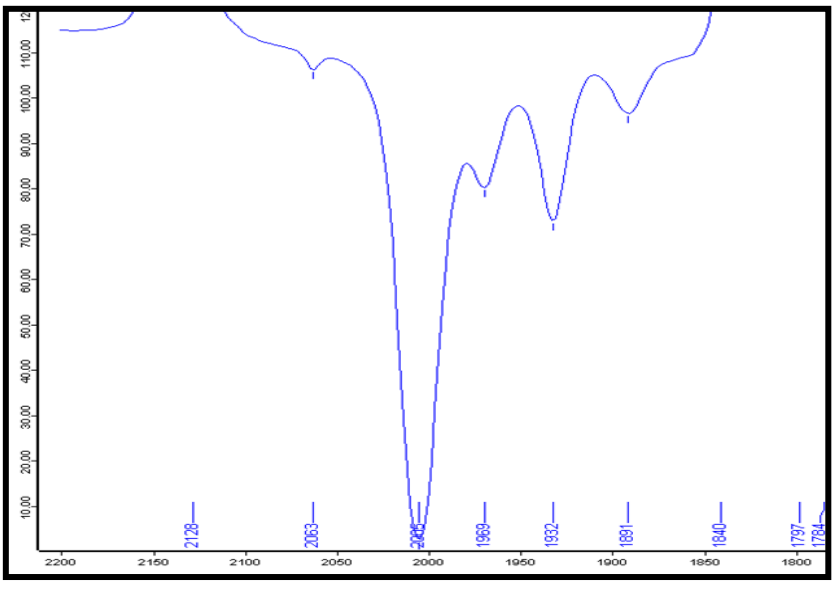

FIG. 11.1: experimental IR spectrum of cluster $(C_2H_5)_4N$ $[FeCo_3(CO)_{12}]$

The cluster is dissolved in acetone. A sol of 0.72 ml of TMOS in 2.4 ml of ethanol is added and the mixture is used to impregnate 4.72 g of silica as core. The system gelifies and the catalyst is then dried at 60°C.

FT23

Catalyst FT23 is constituted by a core of silica, a shell of silica as well and it is prepared by including the cluster $[(Ph_3P)_2N][Fe_3Co(CO)_{13}]$ as precursor of the active phase. The core is produced by the same method as FT22. The active phase is produced starting from the cluster $((Ph_3P)_2N)_2[Fe_4(CO)_{13}]$. The procedure known from the literature is described as follows[5].

5 ml of $Fe(CO)_5$ were added to 8.7 ml of pyridine and the system was refluxed at 120°C for 1h. The red-brune solid obtained was filtered and purified by washing with diethyl ether. The obtained product is the cluster $[Fe(C_5H_5N)_6][Fe_4(CO)_{13}]$; it was dried under vacuum for 10 minutes.

500 mg of the obtained product were dissolved in 10 ml of CH_3OH and a solution of 594 mg of $(Ph_3P)_2NCl$ (PPNCl) dissolved in 6 ml of methanol was added to the first solution. After 15 min of stirring, the formation of a solid phase was observed. This solid was filtered by washing with methanol, then it was dried under vacuum for 1 night. The solid was redissolved in 10 ml of CH_3CN, then the product was filtered. The clean solution obtained was added very slowly to 10 ml of methanol, then it was put to cool in a fridge for 10 days, in order to obtain the desired product by the method of slow diffusion. The solid $((Ph_3P)_2N)_2[Fe_4(CO)_{13}]$ obtained was filtered and washed with 10 ml of methanol.

The synthesis of the final precursor of the active phase $(Ph_3P)_2N)[Fe_3Co(CO)_{13}]$ follows by applying another procedure well known from the literature[6].
202.6 g of $((Ph_3P)_2N)_2[Fe_4(CO)_{13}]$ and 41.2 mg of $Co_2(CO)_8$ were dissolved in 10 ml of CH_2Cl_2. The solution was dried to remove some byproducts. The addition of 15 ml of diethyl ether dissolved the desired product, while another byproduct remained solid. After filtration, the product $[(Ph_3P)_2N][Fe_3Co(CO)_{13}]$ was recovered and purified by slow diffusion in 36 ml of pentane for 3 days in the fridge.

0.398 g of the final product were obtained by this method. The procedure was repeated until the total required amount of the active phase precursor was obtained. The evaluation of the quality of the synthesis was based on the IR spectrum (FIG. 11.2) obtained between 2200 and 1600 cm^{-1}, after dissolution of the cluster in CH_2Cl_2.

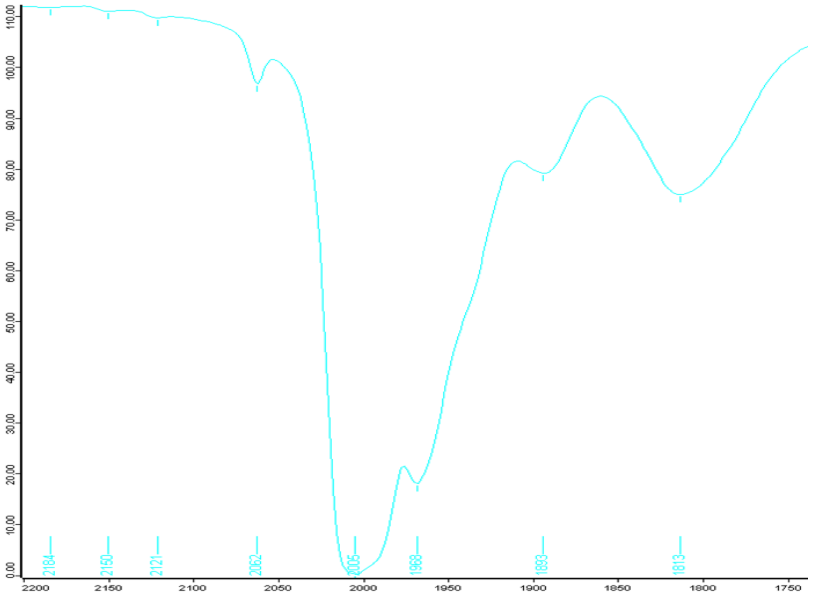

FIG. 11.2: experimental IR spectrum of cluster $[(Ph_3P)_2N][Fe_3Co(CO)_{13}]$

The comparison between the obtained bands and the literature data, confirmed that the synthesis was successful.

The formation of the shell follows the path yet described for FT22.

FT24

The synthesis of core of FT24, as well as the synthesis of its shell, follows the procedure yet described for FT22. In this case the active phase is only constituted by Co. It was added as $Co_2(CO)_8$ dissolved in acetone.

FT25

Catalyst FT25 was synthesized by the same method used for FT22. At the end of the synthesis, H_2PtCl6 was added in the calculated amount to obtain the 0.4% by weight of Pt relating to the support.

11.3 Characterization

11.3.1 TPR profiles

The TPR profile of FT22 (FIG. 11.3) shows a negative peak at 250°C due to the release of carbonyl groups from the cluster. The positive shoulder after the negative peak is due to the methanation of these species by the hydrogen.

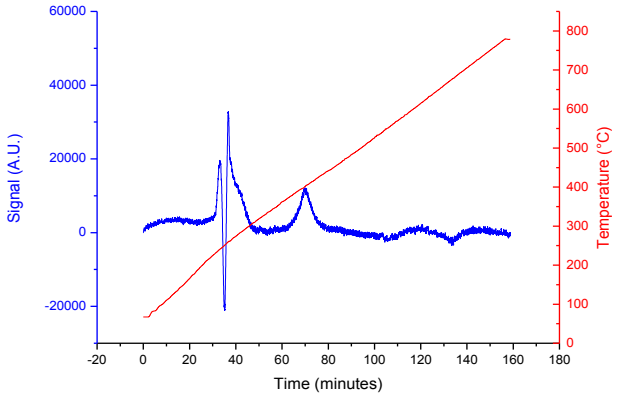

FIG. 11.3: TPR profile for FT22

The TPR profile for the catalyst FT23 (FIG. 11.4) shows again a negative peak at temperatures around 250°C. The following positive peak, in this case, is very intense. The high intensity of this peak is due to the combination of two contributes. The first one, as previously observed, is assignable to the consumption of hydrogen by the CO released from the clusters. The second one is due to an high presence of iron. The iron present in the cluster strongly interacts with the support during the gelification step and it is oxidized by the support. This oxidized iron is then reduced by the hydrogen and this consumption contributes to the high intensity of the signal.

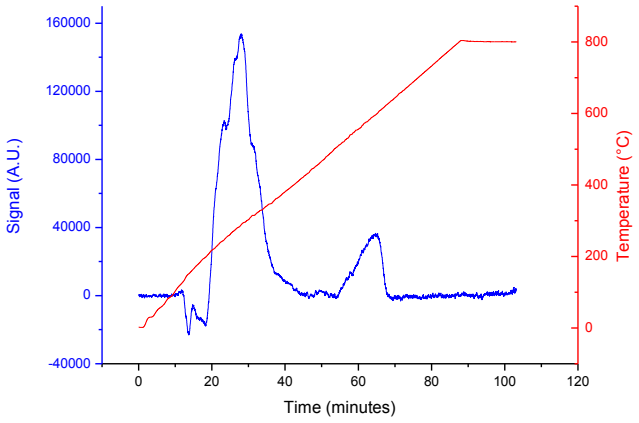

FIG. 11.4: TPR profile for FT23

The TPR profile for FT24 (FIG. 11.5) shows two peaks at 250°C and 400°C, respectively. The peak at 250°C is probably due to the interaction of hydrogen with the carbonyl groups released by the cluster. The second peak is due to the reduction of cobalt oxides to metallic cobalt. These oxides are formed during the gelification process from the interaction between silica and cobalt carbonyl.

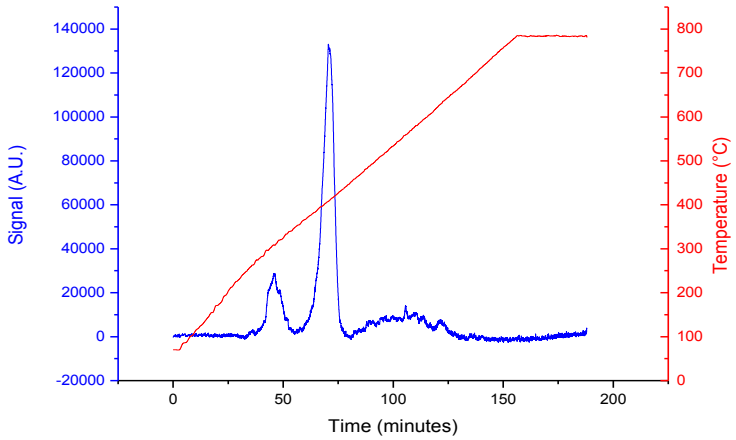

FIG. 11.5: TPR profile for FT24

The TPR analysis of the sample FT25 (FIG. 11.6), as expected, gives a graph identical to that for FT22.

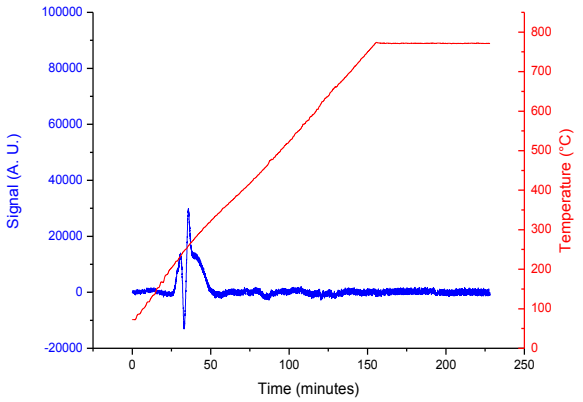

FIG. 11.6: TPR profile for FT25

11.3.2 TPO profiles

The TPO profiles for catalysts FT22, FT24 and FT25, strangely, do not show any signal (FIG. 11.7, 11.8 and 11.9 respectively). Probably, the amount of metal re-oxidized is so low that it is not revealed by the instrument.

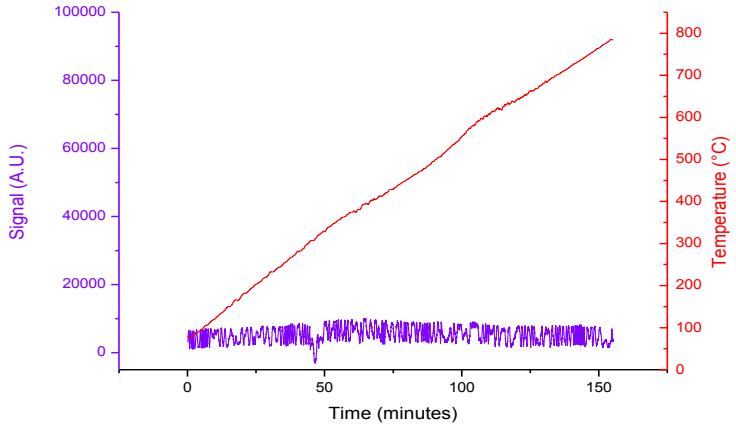

FIG. 11.7: TPR profile for FT22

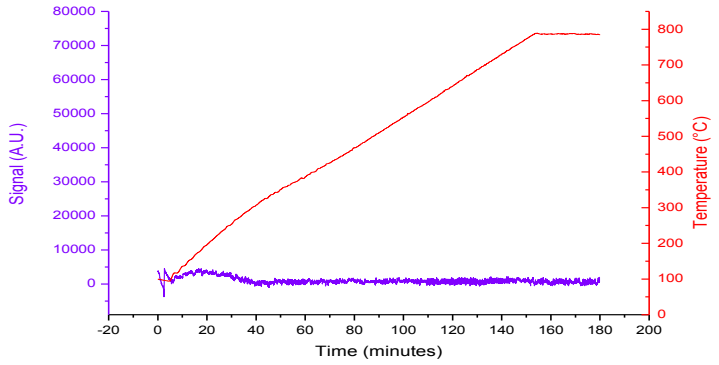

FIG. 11.8: TPR profile for FT24

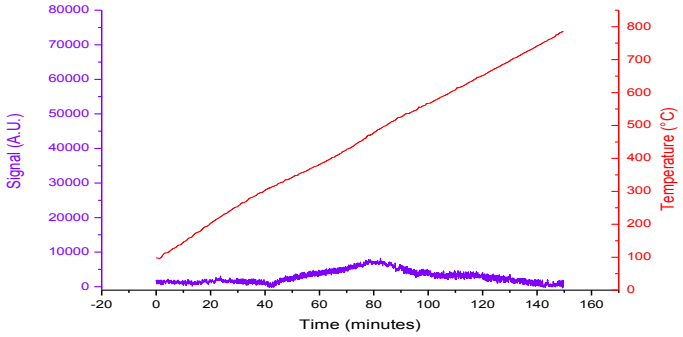

FIG. 11.9: TPR profile for FT25

11.3.3 Surface Area

The surface area of the samples are reported in the table 11.2

SAMPLE	SURFACE AREA (m2/g)
FT22	299
FT24	336
FT25	180

Table 11.2: surface area of the samples

11.3.4 XRD

The XRD spectra of all samples (FIG. 11.10, 11.11 and 11.12) show that the structures of these catalysts are completely amorphous.

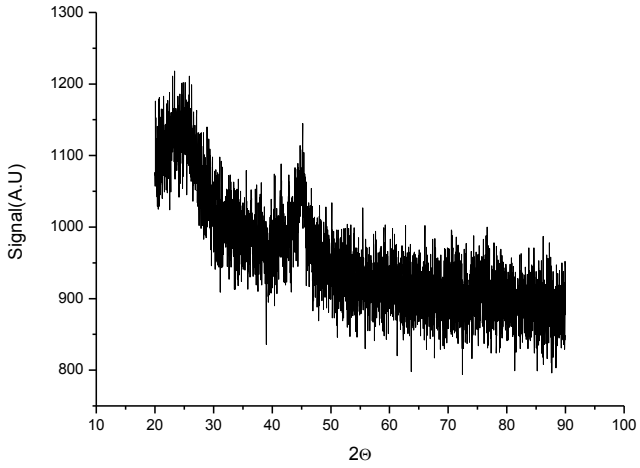

FIG. 11.10: XRD spectrum for FT22

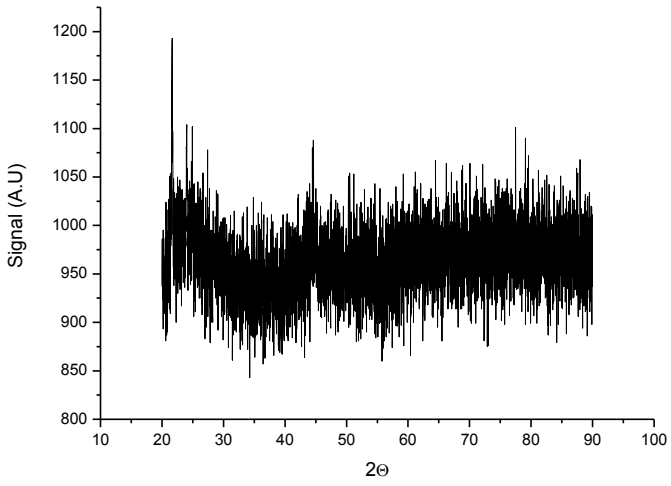

FIG. 11.11: XRD spectrum for FT24

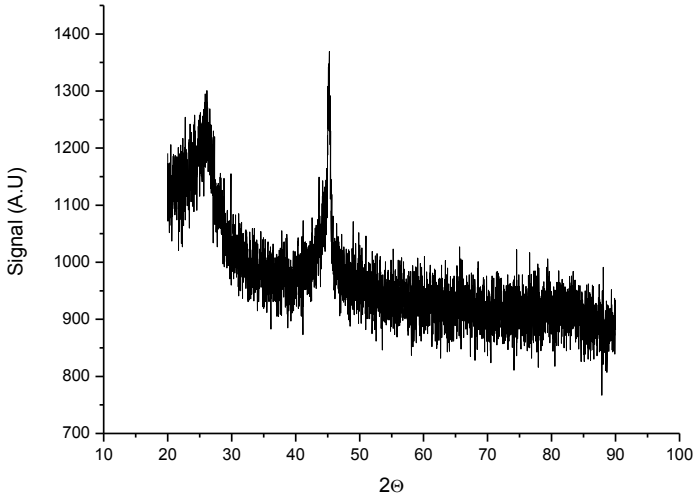

FIG. 11.12: XRD spectrum for FT24

11.3.5 FT-IR

The IR spectra of this series of samples have been collected before the activation treatment and after the catalytic test, since the catalysts are not calcinated. The blue spectra correspond to the fresh catalysts, while the red spectra are those collected for the tested samples.

For all catalysts, it can be observed (FIG. 11.13, 11.14 and 11,15) that the band of –OH groups at 3500 cm^{-1} and the bands present between 2200 cm^{-1} and 1600 cm^{-1} disappear after the thermal treatments. Instead, the band at 1000 cm^{-1} due to the silicates remains still present after the tests.

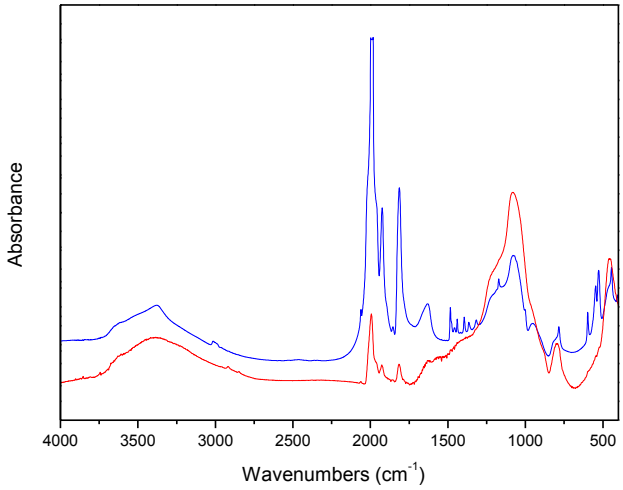

FIG. 11.13: IR spectra for FT22

It is noteworthy that in the IR spectrum collected for the discharged catalyst FT24 (FIG. 11.14) some peaks at wavenumbers just below 3000 cm^{-1} due to the C-H bonds appear after the tests. These signals are probably due to hydrocarbon waxes retained by the catalyst surface.

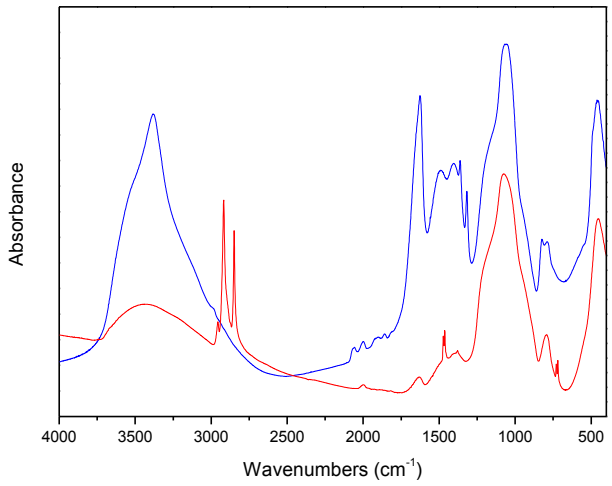

FIG. 11.14: IR spectra for FT24

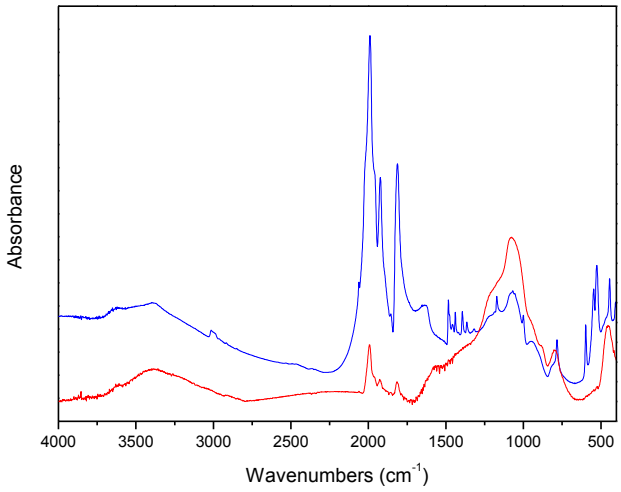

FIG. 11.15: IR spectra for FT25

11.3.6 SEM images

The SEM images for catalysts FT22, FT24 and FT25 (FIG 11.16, 11.17 and 11.18) are reported below. These images generally show a good dispersion of the metallic particles on the surface of the catalysts. Furthermore, the sample seems to be not too much disordered. Also the EDX analysis gives values very similar to the theoretical ones for cobalt. In the case of Iron,

nevertheless, the values are quite different. This fact can be due to a stronger interaction of iron with the support, that bringing to the inclusion of this metal inside the bulk of the support.

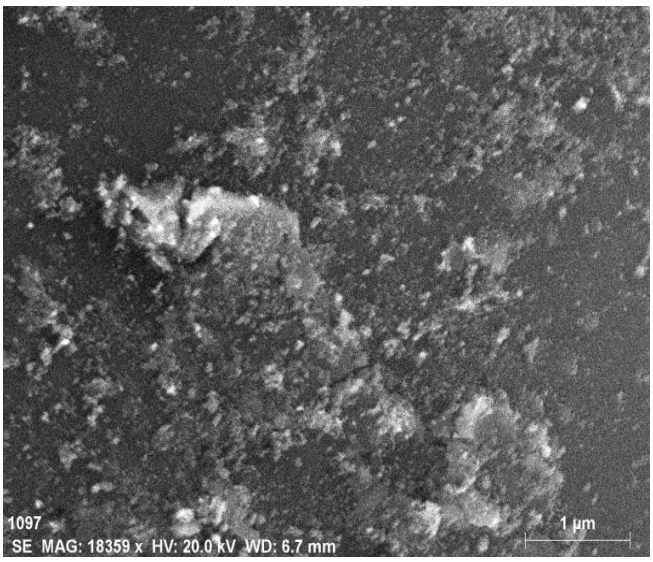

FIG. 11.16: SEM image for FT22

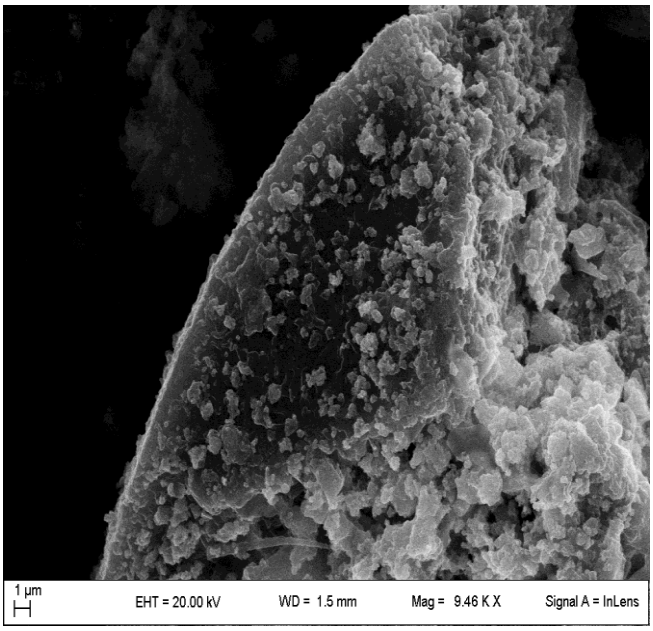

FIG. 11.17: SEM image for FT24

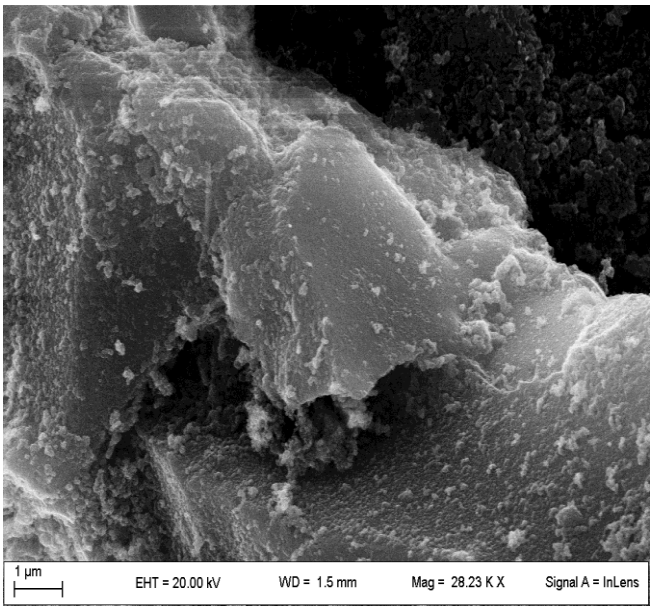

FIG. 11.18: SEM image for FT25

11.4 Catalytic tests

The tests catalytic were performed in the lab plant at atmospheric pressure. 1 g of each catalyst was charged into the reactor. The catalysts were activated at 400°C under hydrogen for 4 h, before starting the test.

The CO conversions as a function of temperature for FT22 are shown in the Table 11.3

Temperature (°C)	**Conversion (%)**
175	7
200	10
225	19
250	28
275	40
300	55
325	71
350	85

Table 11.3: conversion of catalyst FT22.

The sample FT24 (Table 11.4) shows higher values of CO conversion at the increase of temperature. Already at 250°C, the CO is totally converted to products. Furthermore, this catalyst is the only one that shows some selectivity to carbon containing products higher than methane and CO_2 at atmospheric pressure.

Temperature (°C)	Conversion (%)
175	38
200	52
225	75
250	98

Table 11.4: conversion of catalyst FT24.

The results of the catalytic test for FT25 are shown in the table 11.5

Temperature (°C)	Conversion (%)
175	5
200	7
225	17
250	25
275	28
300	37
325	43
350	62
375	83

Table 11.4: conversion of catalyst FT25.

Catalyst FT24 shows very interesting results. In order to obtain more informations, it was tested also in the plant by operating at a pressure of 20 bar. 4 g of catalyst were charged and activated under hydrogen at 400°C, then a mixture of H_2 and CO with molar ratio 2/1 was fed to the reactor, with a total flow of 12 l/h. As already seen in previously described tests, the activity increases very rapidly at increasing temperatures: very good values of conversion were shown by this sample at 250°C (Graph 11.1).

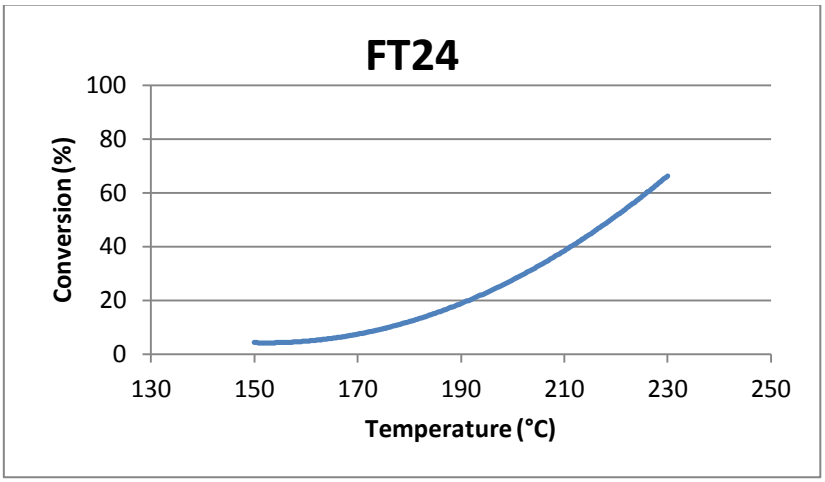

Graph 11.1: conversion vs temperature for FT24.

A life time test with this catalyst was done at 220°C (Graph 11.2). In this case the conversion decreases from 80% to the half after only three days; the selectivity to methane also decreases by decreasing the activity, while the productions of CO_2 and C_2-C_4 hydrocarbons remain unaltered.

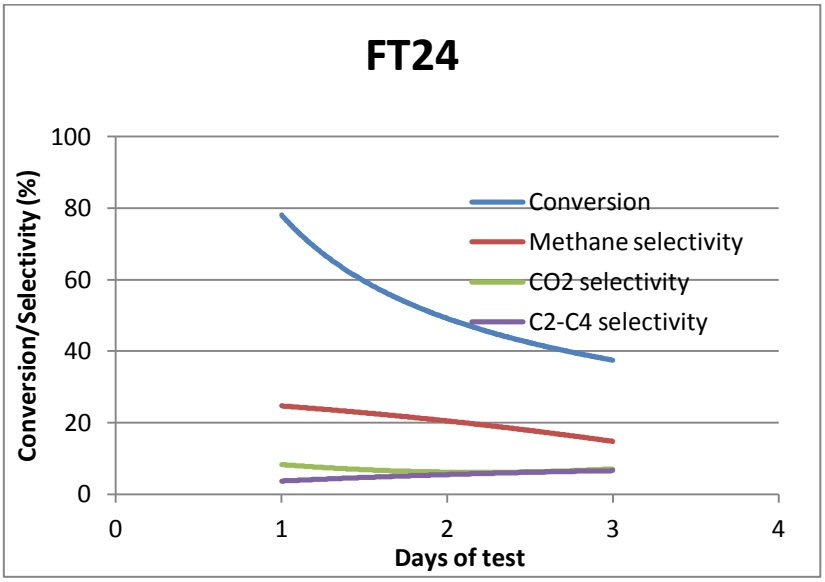

Graph 11.2: conversion vs temperature for FT24.

The deactivation of the catalyst is surely due to the high formation of waxes, that remain on the surface of the catalyst and bring to the lowering of the activity. In fact, after the test an high amount of liquid hydrocarbons is collected, but also an high amount of solid products are founded in the traps used to collect the condensed phases. 3.5 g of waxes were collected into the traps and more than 4 g of solid are discharged from the catalyst after the extraction treatment. The analysis of condensed products (Grashows an alpha value of 0.77. However, this value is lower than the real one because the solid waxes are not included in the calculations.

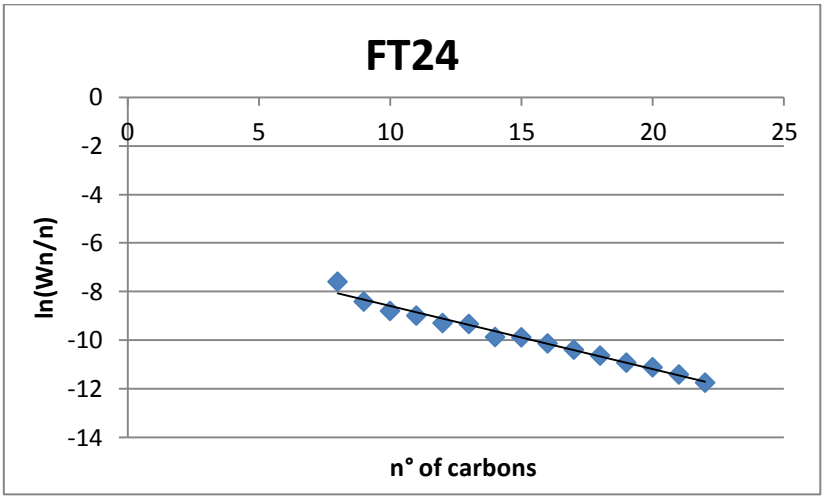

Graph 11.2: conversion vs temperature for FT24.

11.5 Conclusions

In this section, four catalysts have been prepared by the egg-shell method, starting from clusters as raw materials for the active phases. The catalyst FT23 has not been tested because the phosphinic ligands were released during the activation treatment and they condensed at the exit of the reactor, by causing an occlusion of the system that hindering the flow of gases. The catalyst FT21, with an active phase composed by Fe and Co at a 3/1 molar ratio, shows a moderate activity. The catalyst FT25, with the same composition, but promoted with Pt, shows instead an activity slightly lower. This is due to the presence into the structure of traces of chloride ions, deriving from the precursor of the promoter. It is known that the presence of chlorides can causes an irreversible deactivation of many catalysts.

The more interesting results were shown by the catalyst FT24, with only Cobalt as active phase. Its high activity brings to high formation of waxes. This kind of products remains held up on the surface of the catalyst and that makes worst the catalytic behaviour. However, it was

demonstrated that this deactivation effect is reversible, in fact further procedures of reactivation made the catalyst totally active again. This deactivation problem can be avoided by the use of other reaction systems, such as the use of a slurry reactor.

Bibliography

[1] A. Y. Khodakov, W. Chu, P. Fongarland; *Chem. Rev.* ***2007.*** *107, 1692*

[2] M. Voß, D. Borgmann, G. Wedler; *Journal of Catalysis* ***2002.*** *212, 10*

[3] G. E. Batley, A. Ekstrom, D. A. Johnson; *J. Catal.* ***1975.*** *34, 368*

[4] P.Chini, L. Colli, M. Peraldo*; Gazz. Chim. Ital.* ***1960.*** *90, 1005*

[5] K. Whitmire, J. Ross, C. B. III Cooper, D. F. Shriver; Inorg. Synth.; **1982.** 21, 66

[6] C. P. Hordwitz, E. M. Holt, D. F . Shriver; *Organometallics* ***1985.*** *4, 11117*

Section 3: Ammonia

Chapter 12: Ammonia synthesis: General

12.1 History

Ammonia synthesis starting from molecular nitrogen and hydrogen is one of the most studied heterogeneous catalyzed processes, because ammonia is one of the most important raw materials for chemical industries. Up to 70% of produced ammonia is used as a raw material in the production of fertilizers [NH_4NO_3, $(NH_4)_2SO_4$, $(NH_4)_3PO_4$, etc]; the rest is used in the polymers production, in the nitric acid production and also in the explosives production field.

Since 1800, scientists tried to produce ammonia by hydrogenation of nitrogen but only in 1908 Fritz Haber reached the goal to find an iron based catalyst useful in the synthesis. In the 1910, Carl Bosch provided the industrial process nowadays called as “Haber-Bosch” (FIG. 12.1).

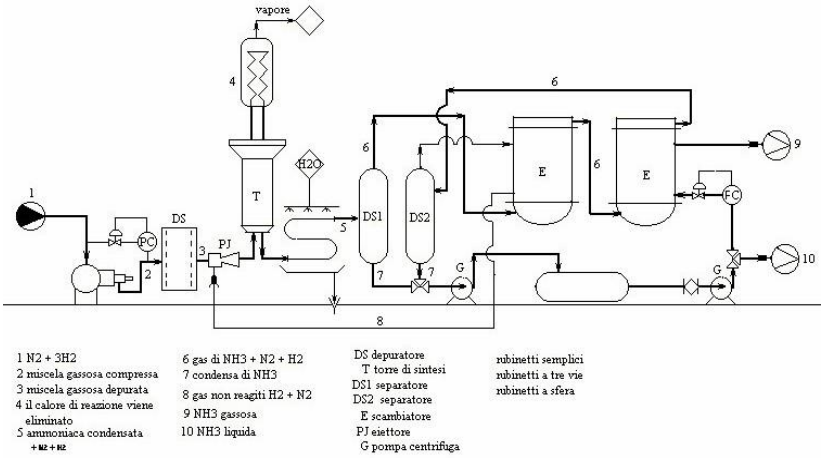

FIG 12.1 - Haber-Bosch Process

This process uses an iron catalyst, obtained from the reduction of magnetite ($FeO{\cdot}Fe_2O_3$) and promoted with alkaline oxides[1,2] (K_2O and CaO).

The range of operating conditions is between 140 and 320 atm of pressure and between 350°C and 550°C of temperature.

During the years many processes were developed with a large range of operating conditions. (table 12.1)

Process	Pressure (atm)	Temperature (°C)	Catalyst	Conversion (%)
Haber-Bosch	250	550	Iron activated	15 - 20
N.E.C.	250	500	Iron activated	18 - 20
Kellogg	300	500	Iron activated	20 - 30
Uhde	300	500	Iron activated	18 - 22
Claude	1000	600	Iron activated	40 - 85
Casale	600	600	Iron activated	20 - 21
Fauser	300	530	Iron activated	18 - 20
Mont Cenis	100	400	$Fe(CN_3)$	10-20

Table 12.1:Operating conditions for different ammonia production plants

The iron–based catalysts used in the ammonia production were the same until the end of ’80, when Kellogg begins to use a different catalytic system, based on Ruthenium as active phase, promoted with Cesium and Barium and supported over carbon.

Those new catalysts allowed more soft conditions, at lower temperature (350°C) and lower pressure[3].

12.2 Thermodynamical considerations

The formation of ammonia from elements follows the reaction:

$$N_{2\,(g)} + H_{2\,(g)} \rightleftharpoons 2NH_{3\,(g)}$$

Keq for this reaction at 25°C is 5.47*10^5; it was obtained from the equation:

$$\ln \mathrm{Keq} = -\frac{\Delta G^{\circ}}{RT} = -\frac{\Delta H^{\circ}}{RT} + \frac{\Delta S^{\circ}}{R} \qquad (21)$$

where ΔH° and ΔS° are -91.8 KJ/mol and –198.5 J/mol·K, respectively.

This high value of the equilibrium constant means that the formation of ammonia is highly thermodynamically favoured, but the kinetic barrier is so high that in fact the reaction does not start.

The reaction mechanism is the following:

$$N_{2\,(g)} + * \rightleftharpoons N_{2,ads} *$$

$$N_{2,ads} * + * \rightleftharpoons 2N_{ads} *$$

$$H_{2\,(g)} + 2* \rightleftharpoons 2H_{ads} *$$

$$N_{ads} * + H_{ads} * \rightleftharpoons NH_{ads} * + *$$

$$NH_{ads} * + H_{ads} * \rightleftharpoons NH_{2,ads} * + *$$

$$NH_{2,ads} * + H_{ads} * \rightleftharpoons NH_{3,ads} * + *$$

$$NH_{3,ads} * \rightleftharpoons NH_{3\,(g)} + *$$

The rate determining step is the breaking of the triple bond NΞN of the N_2 molecule. The energy required for this breaking is 941.7 kJ/mol.

In order to increase the reaction rate it is necessary an increase of temperature but the reaction is exothermic and, by applying the Van't Hoff equation:

$$\frac{d(\ln K)}{dT} = \frac{\Delta H_r^{\circ}}{RT^2} \qquad (22)$$

it is clear that the equilibrium constant decreases at increasing temperatures. As an example, at the temperature of 350°C the equilibrium constant value decreases to $4.7*10^{-3}$. A compromise is required in order to push the reaction. From Le Chatelier principle, since the number of moles decreases during the reaction, high pressures favour the process (FIG. 12.2)

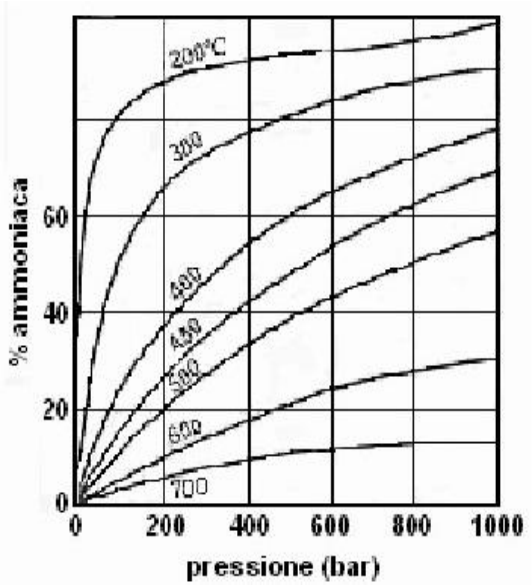

FIG. 12.2: Ammonia production in function of pressure at different temperatures

The following graph (FIG. 12.3) shows indeed the change of the equilibrium curve as a function of temperature and pressure.

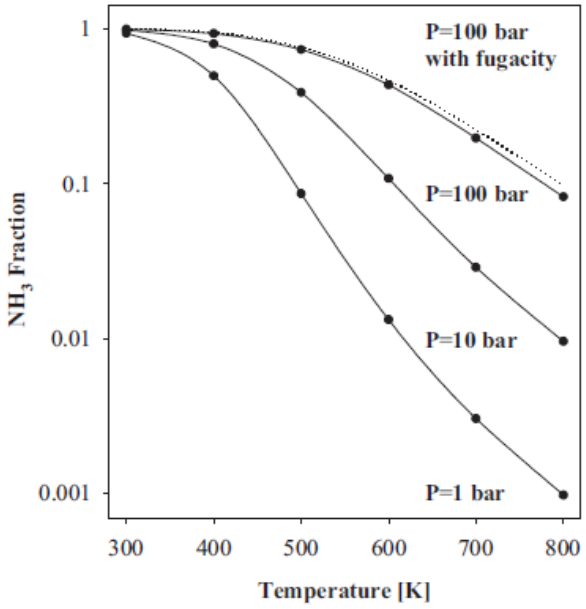

FIG. 12.2: Changing of equilibrium in function of temperature at different pressures

By considering these observations, a specific catalyst is necessary to push the reaction rate at low temperatures and pressures, in order to lower the operating conditions in the plants.

12.3 Catalysts

The choice of the catalyst for the ammonia synthesis is driven by some aspects:

- the ability of the catalyst to absorb N_2 and then break the triple bond;
- the ability to favour the reaction of atomic nitrogen with hydrogen;
- the ability to form a weak bond with NH_3, in order to easily release the product;
- the ability to operate at low temperatures;
- the stability along the time.

Several transition metals can be used as catalysts in the ammonia synthesis. The volcano curve[4] (FIG. 12.3) shows the activity of metals for the ammonia production.

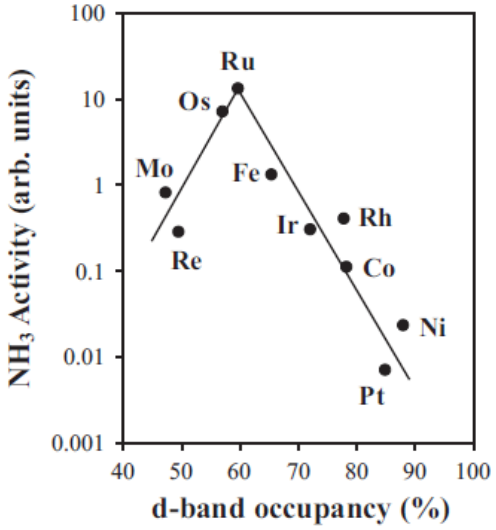

FIG. 12.3: Volcano curve for the metals

As already said, the most used metal is the iron coming from magnetite. The impurities present inside the structure (MgO, ZrO_2, TiO_2, SiO_2, Al_2O_3, Cr_2O_3) are the activators of the catalyst itself and it can be more promoted by the addition of alkaline oxides.

The mechanism of adsorption of nitrogen by iron is the following:

$$nFe + N \text{ —> } Fe_nN + H \text{ —> } Fe_nNH + H_2 \text{ —> } nFe + NH_3$$

In the last years, new catalysts based on Ruthenium were introduced in the industrial field. Kellogg was the first, with KAAP process in the 1992, followed in 1999 by Farmland-Misschem Ltd. and PCS Nitrogen Trinitad Ltd. The catalysts used for those processes were obtained by impregnation of carbon.

Despite the high cost of Ruthenium, the advantage is in the high activity that allows to operate at lower temperatures and pressures, with high TOF (Turn Over Frequency) values.

Many studies[5] show that the activity of Rruthenium is highly dependent on the raw materials, according to the following scheme:

$$Ru_3(Co)_{12} > Ru(NO)(NO_3)_3 > K_2RuO_4 > Ru(acac)_3 > RuCl_3 \cdot 3H_2O$$

Also with this catalyst the reaction path is the same, with the dissociative adsorption of N_2 as the rate determining step. An inconvenient of the use of ruthenium is its ability to absorb hydrogen. In order to avoid this event, the feed gas is usually composed by an excess of nitrogen with respect to the stoichiometric 3:1 ratio. Other solutions are to increase the availability of electrons by the active phase, by using a basic support, such as magnesium oxide[6,7], and the promotion with alkaline and/or earth-alkaline metals (typically Cs, Ba, K, Na) or La[8,9]. The problem connected with the use of magnesia as support is its poor mechanical strength. For this reason, other inorganic oxides are used as substitutes or are combined with MgO, for example Al_2O_3[7]. Nowadays, other kinds of carbon, as carbon nanotubes or nanofibers, are commonly used as catalyst supports. One of the most important factor to keep under control is the purity of raw materials, because impurities as sulphur or halides can irreversibly poison the catalysts.

Bibliography

[1] en.wikipedia.org/wiki/Haber-Bosch_process

[2] I. Chorkendorff, J.W. Niemantsverdriet; **"Concept of modern catalysis and kinetics"** Chapter 8: Heterogeneous catalysis in practice: hydrogen; Ed. Wiley, 2003

[3] I. Chorkendorff, J.W. Niemantsverdriet; **"Concept of modern catalysis and kinetics"** Chapter 6: Surface reactivity; Ed. Wiley, 2003

[4] D. Szmigiel, W. Raròg-Pilecka, E. Miśkiewicz, M. Gliński, M. Kielak, Z. Kaszkur, Z. Kowalczyk; *Applied Catalysis A: General* ***2004.*** *273, 105*

[5] P. Seetharamulu, V. S. Kumar, A.H. Padmasri, B. D. Raju, K.S. Rama Rao; *Journal of Molecular Catalysis A: Chemical* ***2007.*** *263. 253*

[6] O. Hinrichsen, F. Rosowki, A. Hornung, M. Muhler, G. Ertl; *Journal of Catalysis* ***1997.*** *165, 33*

[7] S. E. Siporin, R. J. Davis; *Journal of Catalysis* ***2004.*** *225, 359*

[8] P. Moggi, G. Albanesi, G. Predieri, G. Spoto; *Applied Catalysis A: General* ***1995.*** *123, 145*

Chapter 13: Ruthenium and Platinum-Ruthenium catalysts for ammonia synthesis

13.1 - Introduction

In this chapter four catalysts are compared. Two of these catalysts are supported over MgO[1,2,3,4]. The others are supported over carbon nanofibers functionalized with phosphine groups. The active phases for the catalysts supported on magnesia are Ru and Ru-Pt. The catalysts are promoted with cesium, added as Cesium oxalate. The catalysts supported over carbon nanofibers[5,6,7,8] have the same active phases than the others. Due to the low amount of available catalysts, AP03 and AP04 have been characterized only by TPR.

Table 13.1 summarizes the active phases and the support for these catalysts.

SAMPLE	SUPPORT	ACTIVE PHASE	PROMOTER	METHOD OF PREPARATION
AP01	MgO	5% Ru	Cesium	Bulk sol-gel
AP02	MgO	5% Ru – 1% Pt	Cesium	Bulk sol-gel
AP03	Carbon nanofibers	2% Ru	Cesium	-
AP04	Carbon nanofibers	2% Ru – 0.4% Pt	Cesium	-

Table 13.1: method of preparation and precursors for these catalysts.

13.2 Preparation

AP01

This sample was prepared by the sol-gel technique. The composition is 5% Ru (weight) over Magnesia promoted with Cs_2O, at Cs:Ru=1:1 (moles). 0.211 g of $Ru_3(CO)_{12}$ were weighed and dissolved in dry THF in order to obtain 5% Ru (weight) on the support. 0.175 g of $Cs_2(COO)_2$ were then dissolved in 4.5 ml of water and 80 ml of ethanol.

5.66 g of Magnesium ethoxide were added in a flask to 9 ml of water and 49 mL of ethanol. The system was heated and left under reflux for 3 h. After that, the Ruthenium solution was added to the magnesium ethoxide solution and it was cooled. After 1 h of stirring, also the Cesium solution was added to the system. The stirring was maintained for one night. The solution was transferred in a container and the solvent was left to evaporate during some days. Then the solid obtained was dried at 60°-70°C under nitrogen atmosphere for 6 h.

AP02

Also this sample was prepared by the sol-gel technique. The composition is Ru_5Pt promoted with Cs_2O (molar ratio 1:1 with Ruthenium). The support is magnesia and the weight of Ruthenium in the active phase is 5%. In order to obtain this composition, 0.211 g of $Ru_3(CO)_{12}$ and 0.0779 g of Pt^{II}acetylacetonate were dissolved in dry THF. 0.175 g of Cs oxalate were then dissolved in 4.5 ml of water and 80 ml of ethanol.
5.66 g of Magnesium ethoxide were dissolved under reflux in 9 ml of water and 49 ml of ethanol. The system was left under reflux for 3 h. After that the Ruthenium and Platinum precursors were added to the solution. After 1 h of stirring, also the Cesium solution was added to the system. The stirring was maintained for one night. The solution was transferred in a container and the solvent was left to evaporate during some days. The solid was finally dried at 60°-70°C under nitrogen atmosphere for 6 h.

AP03

This sample is composed by 2% (weight) of Ruthenium deposited over carbon nanofibres functionalized with phenyl-phosphines and promoted with Cesium oxide. This catalyst was prepared by Dott. Deborah Viddick at the Université Catholique of Louvain-La-Neuve(Belgium).

AP04

This sample is composed by 2% (weight) of Ruthenium and 0.4% (weight) of Platinum deposited over carbon nanofibres functionalized with phenyl-phosphines and promoted with Cesium oxide. Also this catalyst, as well as AP03, was prepared by Dott. Deborah Viddick at the Université Catholique of Louvain-La-Neuve (Belgium).

13.3 Characterization

13.3.1 TPR

The TPR analysis effected for AP01 (FIG. 13.1) shows two peaks at 426°C and 495°C respectively. The first peak can be assigned to the reduction of a little amount of Ruthenium that is oxidized by the interaction between the carbonyl cluster and the support. The other peak is probably due to the formation of –OH groups on the surface of the promoter after the decomposition of the precursor of Cesium to cesium oxide.

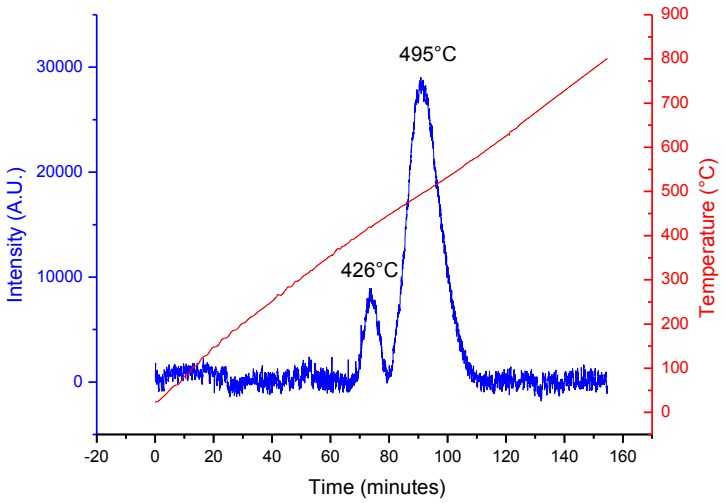

FIG. 13.1: TPR profile for AP01

The TPR profile for AP02 (FIG. 13.2) shows a shift of the peaks. The reduction of ruthenium occurs at lower temperatures (209°C). Indeed, the peak of decomposition and reduction of the cesium promoter is shifted to 582°C. This increase of temperature can be due to the presence of Platinum that keeps hydrogen and does not release it easily to the system for the reduction of the decomposition products.

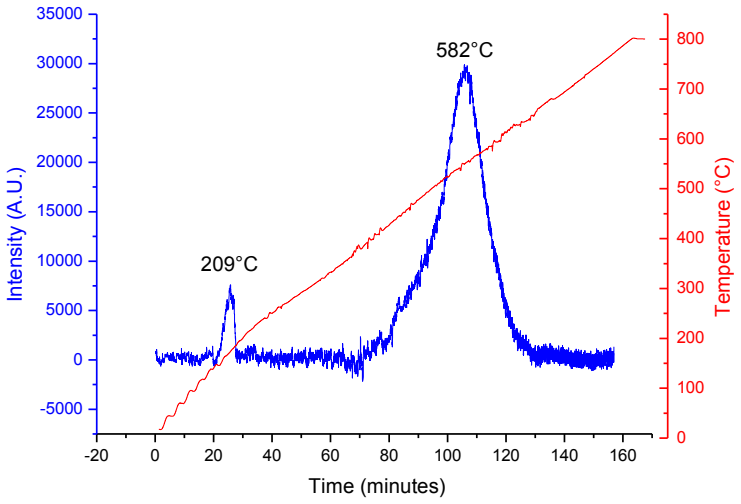

FIG.13.2 : TPR profile for AP02

The TPR profile for AP03 (FIG. 13.3) is composed by only a peak that can be assigned to a general reaction of the system with hydrogen, by formation of methane from the carbon of nanofibres and phosphine from the coordination compounds of the metal.

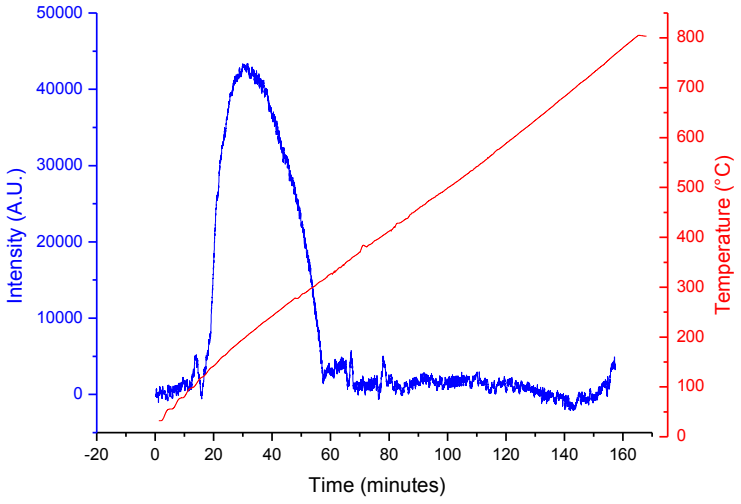

FIG. 13.3: TPR profile for AP03

The TPR profile for AP04 (FIG. 13.4), as already seen for AP03, is composed by a single peak that can be assigned to the general interaction of the system with hydrogen, by formation of methane

from the carbon of nanofibres and phosphine from the coordination compounds of the metal. This decomposition occurs at higher temperatures than for AP03. This observation is according to the hypothesis above proposed by comparing the TPR analyses for the samples AP01 and AP02: the Platinum keeps hydrogen that is not more available for the reduction of the decomposition products of the system.

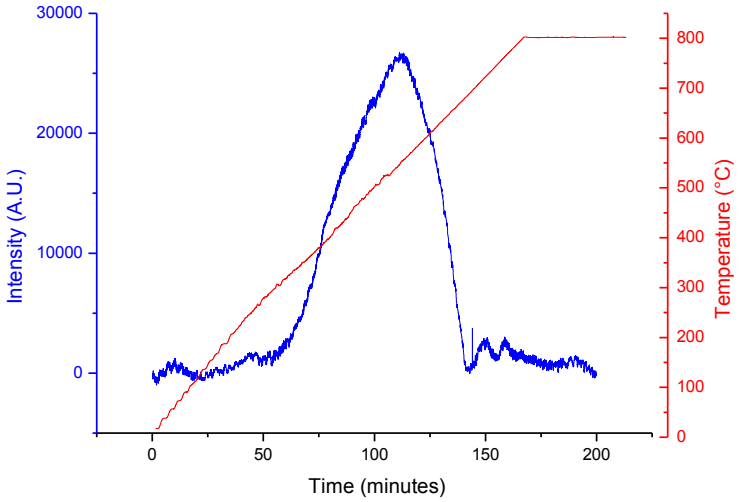

FIG. 13.4: TPR profile for AP04

6.3.2 Surface Area

The surface area was determined for AP01 and AP02. It results 53 m^2/g and 52 m^2/g, respectively. These values are not high and are typical of MgO obtained by a sol-gel method.

6.3.3 XRD

The XRD spectra were acquired before and after activation of the catalyst for AP01 and AP02. The spectrum of the notactivated catalyst for AP01 (FIG 13.5 A) seems to be very amorphous but we can found some broad little peaks at 2θ = 18°, 28°, 50°, 58°. These peaks are due to the formation of a few little crystals of brucite-type structures. After activation (FIG 13.5 B), the heating treatment transforms the structure and the resulted spectrum shows well defined intense peaks at 2θ = 37°, 43°, 62°, 78°. These peaks were assigned by a comparison with the literature data to the structure of MgO periclase[9].

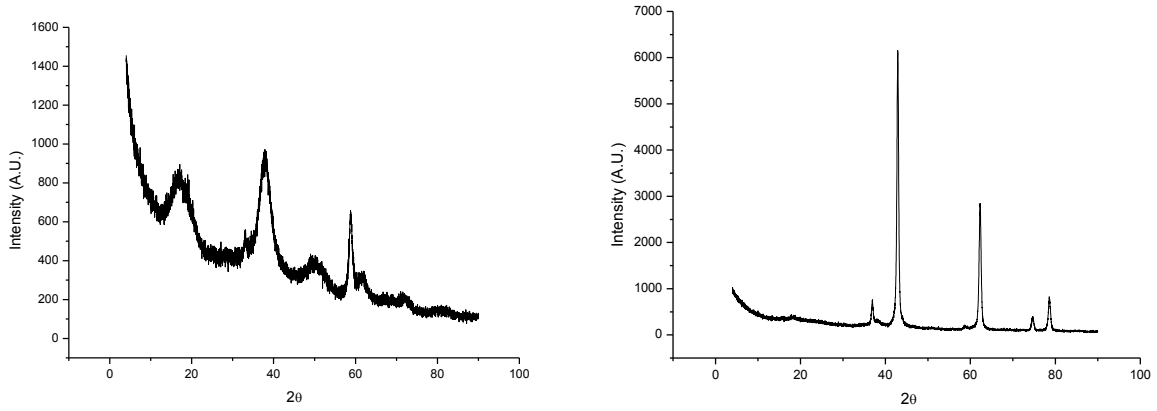

FIG. 13.5 A and B: XRD spectra for AP01

The XRD spectra of AP02 shows the same behaviour before (FIG. 13.6 A) and after activation (FIG. 13.6 B).

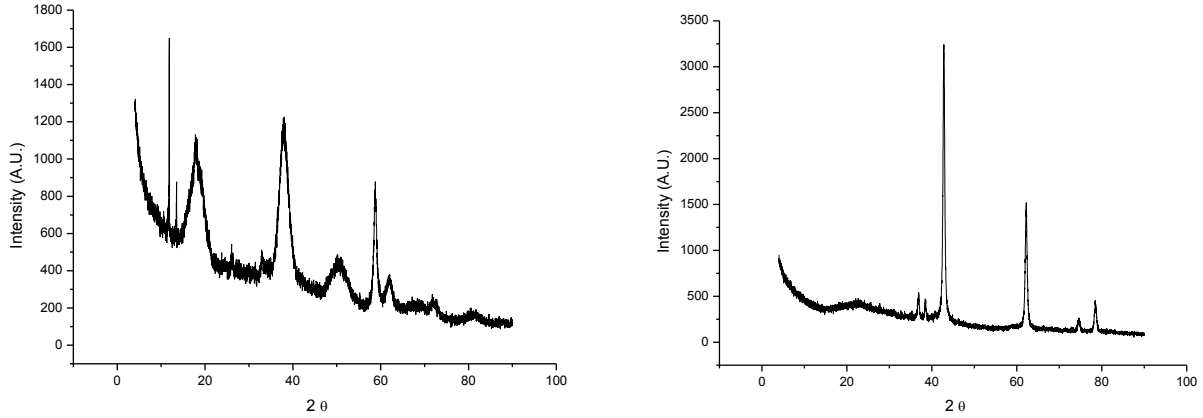

FIG. 13.6 A and B: XRD spectra for AP02

13.3.4 FT-IR

The IR spectra were acquired for AP01 and AP02 before and after activation. The spectrum acquired before activation (blue line) for AP01 (FIG 13.7) shows a broad band around 3000 cm^{-1} imputable to –OH groups associated present on the support and a narrow peak at 3700 cm^{-1} due to –OH groups unassociated. An intense peak is present at 1400 cm^{-1}. This peak is associated with the presence of Cesium Oxalate. In the spectrum acquired after activation (red line) the peaks of –OH groups associated and unassociated and the peak of the oxalate compound disappear. This means that the precursor is decomposed to Cs_2O, that is the expected promoter.

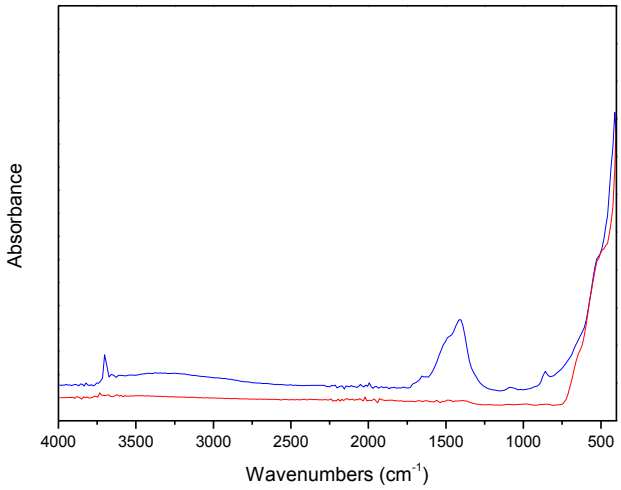

FIG 13.7 IR spectra for AP01

The IR spectra (FIG 13.8) acquired for AP02 are identical to those for AP01.

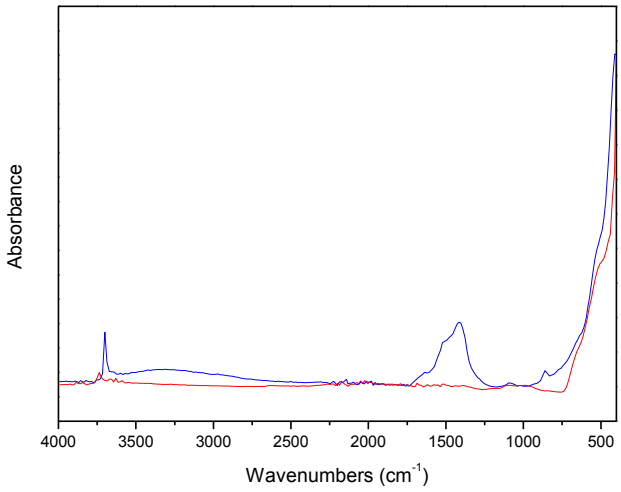

FIG 13.8: IR spectra for AP02

13.3.5 SEM images

The SEM images of AP01 sample were taken before and after activation (Fig. 13.9 A and B respectively). These images show an high dishomogeneity before the activation; this dishomogeneity was reduced after the heating treatment.

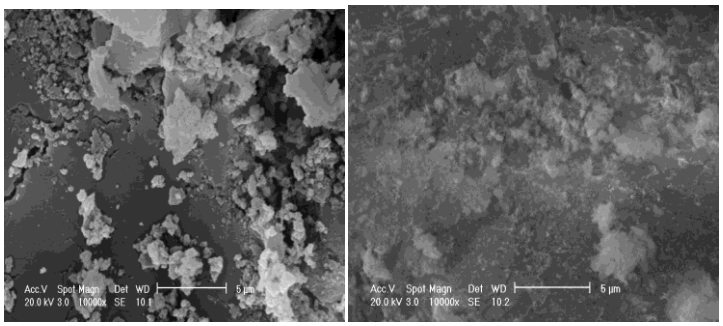

FIG. 13.9: SEM images for AP01 before (A) and after (B) activation treatment.

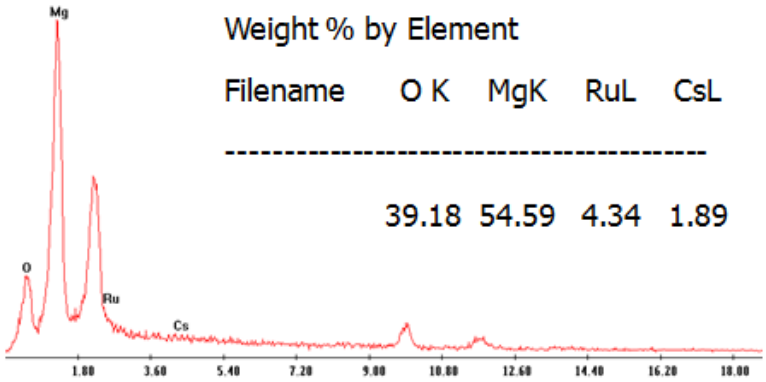

FIG. 13.10: EDX data for AP01.

The EDX data show how the real composition is similar to the theoretical one, indeed the amount of ruthenium is around 5%.

Also in the case of AP02, the SEM images were taken before and after activation (Fig. 13.11 A and B respectively). As above seen for AP02, also these images show an high dishomogeneity before the activation that decreases after the heating treatment.

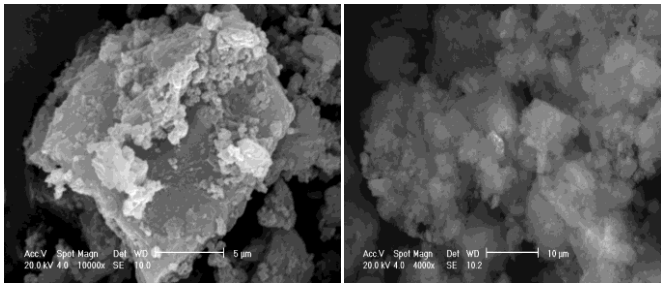

FIG. 13.11: SEM images for AP02 before (A) and after (B) activation treatment.

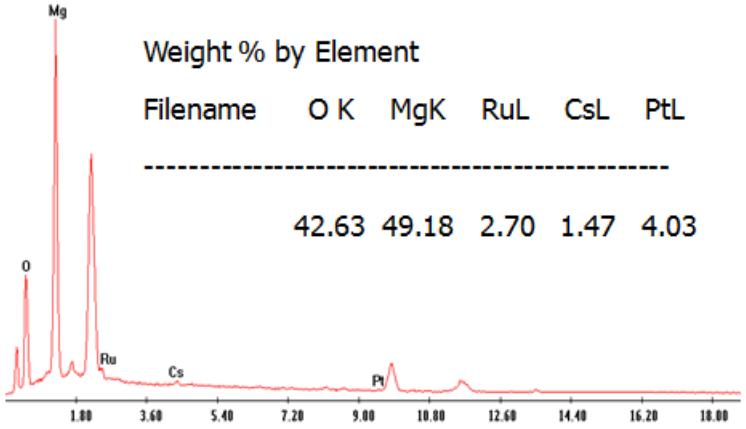

FIG. 13.12: EDX data for AP02.

In this case, the EDX data show that the real composition is different from the theoretical one but this fact can be explained with the dishomogeneity of the sample and not with a real loss of active phase.

13.3.6 TEM images

As already seen for the SEM images, also the TEM images were taken before and after activation.

In the case of AP01 (FIG 13.13 A and B) they show an increase of crystallinity after the thermal treatment. This is in agreement with the XRD data that showed the passage from an amorphous structure to a well defined structure of periclase after the activation treatment.

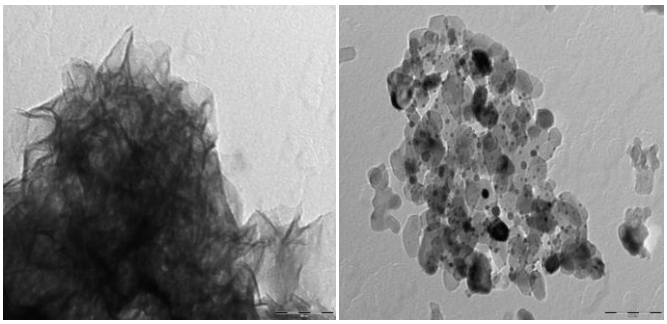

FIG. 13.13: TEM images for AP01 before (A) and after (B) activation

The TEM images collected for AP02 (FIG. 13.14 A and B) show the same features above seen for AP01: an increase in the presence of crystalline phases after the activation step.

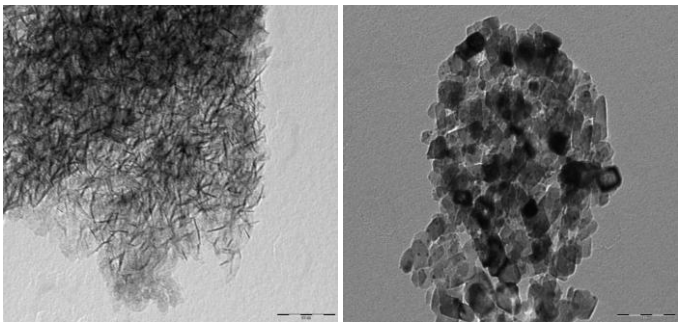

FIG. 13.14: TEM images for AP02 before (A) and after (B) activation

13.4: Catalytic activity

To make catalytic tests, the catalysts was charged into a fixed bed microreactor. The catalysts were activated under an inert atmosphere at 400°C for 6 h. The gas feed to the reactor has a flow rate of 40 ml/min, with 10 ml/min of nitrogen and 30 ml/min of hydrogen, to obtain a H_2/N_2 molar ratio of 3/1. The ammonia produced was collected in a solution of hydrochloric acid of known molarity. The ammonia is captured as NH_4Cl. The determination of the amount of ammonia produced was made by retro-titration of the acid excess. For AP01 and AP02 1 g of catalyst was charged into the reactor. Instead, AP03 and AP04 samples were very bulky, then only 0.5 g can be charged inside the microreactor.

AP01

Graph 13.1 shows the percentage of ammonia produced, compared with the equilibrium curve as a function of temperature. By the analysis of these data, we can observe the maximum of ammonia production at 325°C. The blue curve in the graph is the equilibrium curve calculated from data by Gillespie and Beattie.

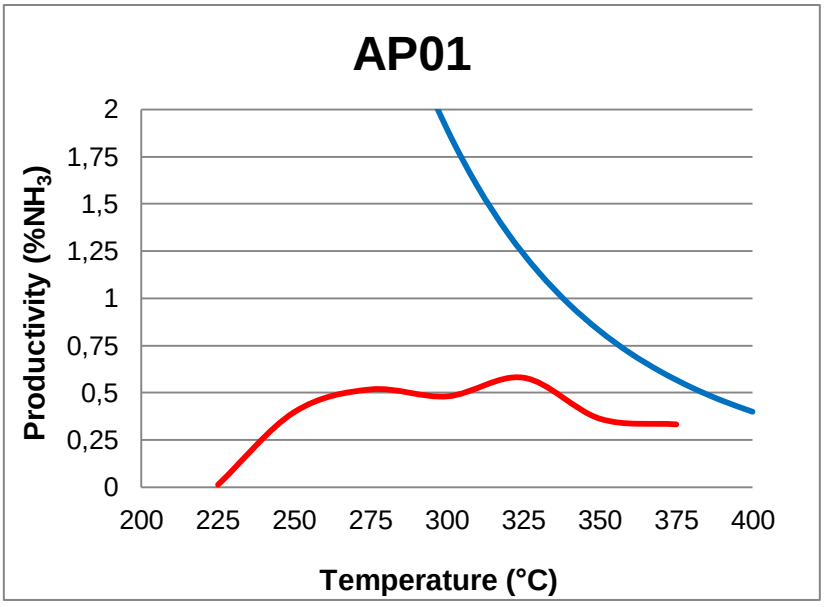

Graph 13.1: productivity of ammonia for AP01

Graph 13.2 shows the absolute production of ammonia for this catalyst. The maximum value is 0.75 mmol/h per gram of catalyst.

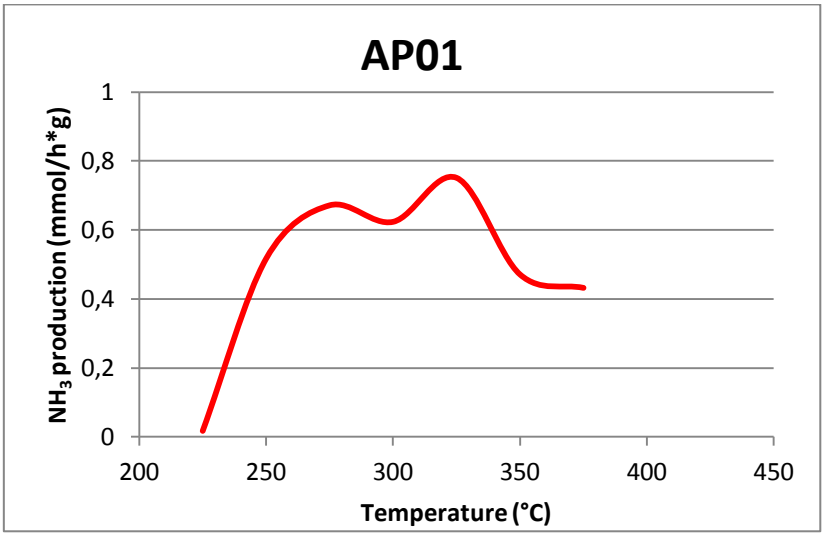

Graph 13.2: absolute production of ammonia for AP01

AP02

Also AP02 shows the maximum production of ammonia at 325°C (Graph 13.3).

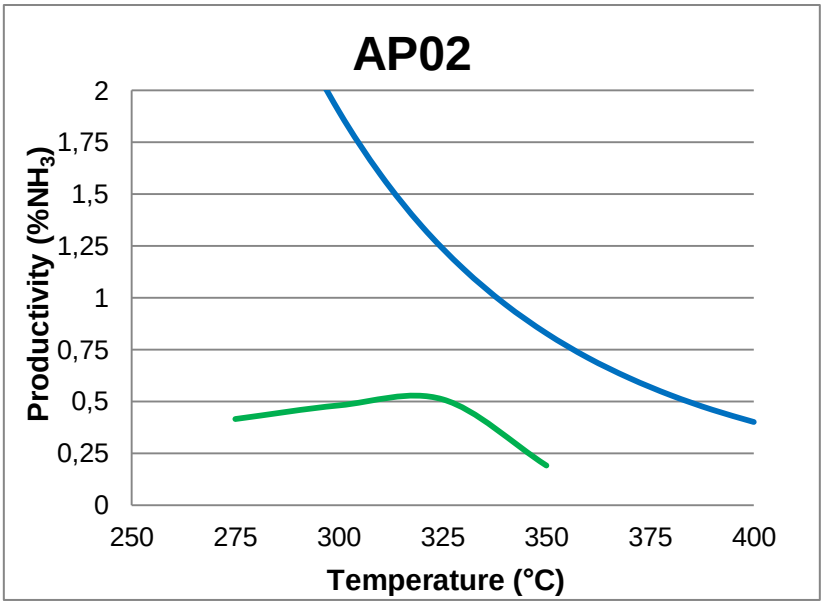

Graph 13.2: productivity of ammonia for AP02

By analysing the absolute ammonia production of this catalyst (graph 13.4), it can be observed that the behaviour is similar to AP01, with an absolute ammonia production of 0.7 mmol/h per gram of catalyst. This value is lower thanto the maximum one for AP01. The presence of platinum seems not to have positive effects for the catalytic activity.

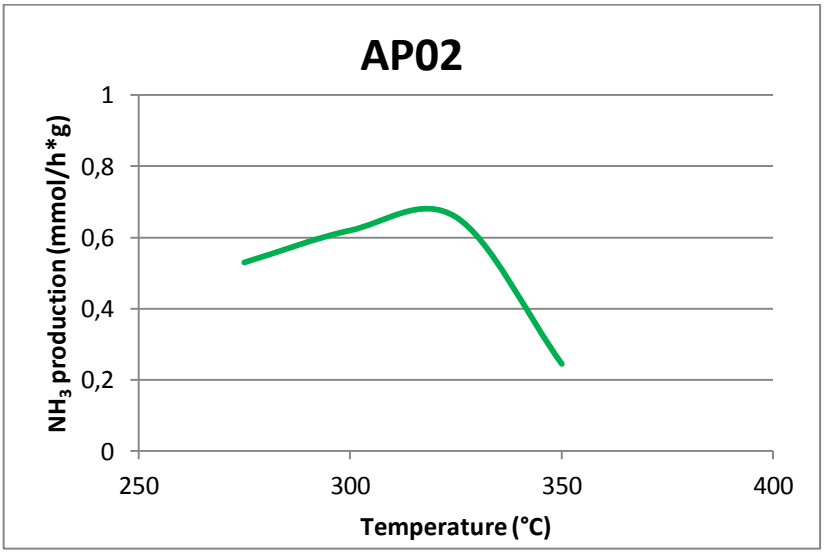

Graph 13.4: absolute production of ammonia for AP02

AP03

The catalyst AP03 (Graph 13.5) shows an evident decrease of the temperature corresponding to the maximum value of the ammonia production. It is reached at 250°C.

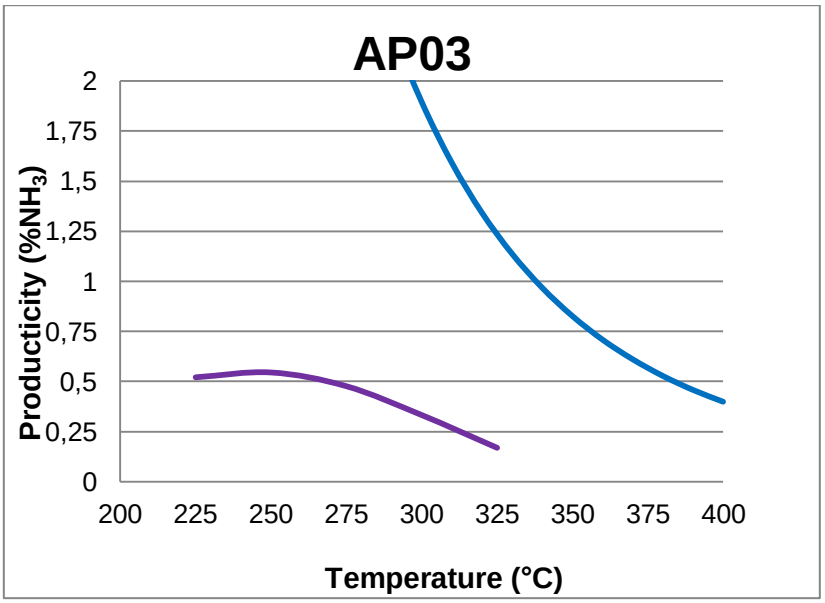

Graph 13.5: productivity of ammonia for AP03

It appears very interesting the Graph. 13.6, which shows the absolute ammonia production of the catalyst. By the data analyses, it results that the catalyst AP03 produces more than 1 mmol/h per gram of ammonia, the higher value observed for these catalysts. The productivity compared with the equilibrium curve in the Graph 13.5 results lower because the catalyst is more bulky and it was charged an amount only the half with respect to AP01 and AP02, then the effective contact time with the reagent gases was halved too.

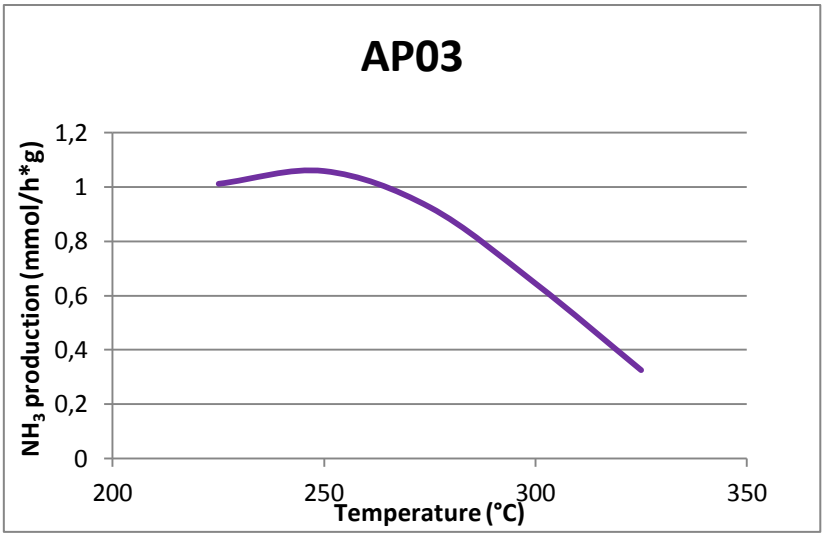

Graph 13.6: absolute production of ammonia for AP03

AP04

AP04 shows a conversion that seems not highly dependent on the temperature. The maximum, at 350°C, does not well distinguish itself from the curve in the graph 13.7.

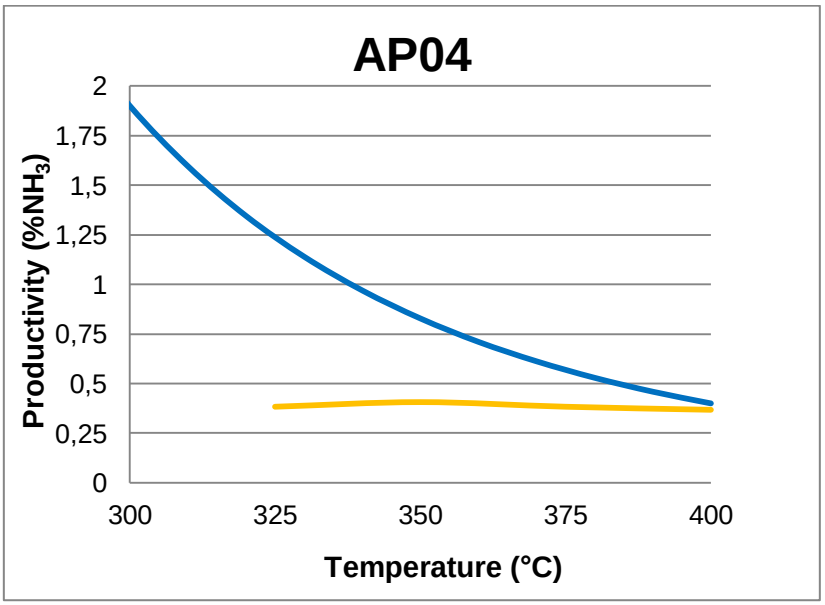

Graph 13.7: productivity of ammonia for AP04

As already seen for AP01 and AP02, also in this case the addition of platinum seems not to have a positive effect on the catalytic activity, indeed the absolute productivity (Graph 13.8) decreases from 1 mmol/h to 0.8 mmol/h per gram of catalyst.

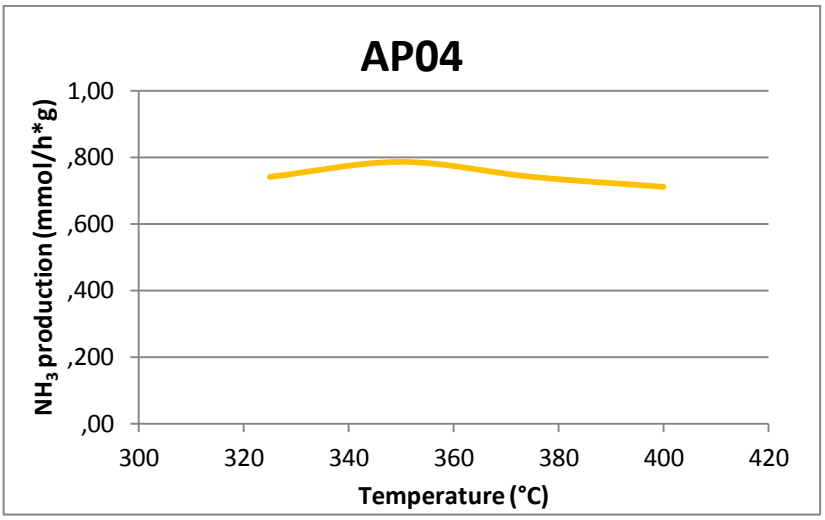

Graph 13.8: absolute production of ammonia for AP04

13.5: Conclusions

The characterization of catalysts AP01 and AP02 shows that they are very similar. From XRD spectra, a passage from an amorphous structure to a more ordinate structure can be observed after activation of the systems. The increase of order inside the structure is confirmed also by TEM and SEM images. Productivity tests show a similar catalytic behaviour for AP01 and AP02, with a little preference for the catalyst without Pt.

On the contrary, AP03 and AP04 show a different behaviour.

AP03 is highly dependent on temperature, while AP04 seems not dependent. Furthermore, the maximum of productivity is shifted of 100°C between them. AP03, the catalyst supported over carbon nanofibers with only Ru as active phase, shows the maximum absolute ammonia production, with more than 1 mmol/h of ammonia produced for each gram of catalyst.

Bibliography

[1] J. Iwamoto, M. Itoh, Y. Kajita, M. Saito, K. Machida; *Catalysis Communications* ***2007.*** *8, 941*

[2] R. Portillo, T. Lopez, R. Gomez, B. A. Morales, O. Novaro*; Langmuir* ***1996.*** *12, 40*

[3] J. A. Wang, X. Bokhimi, O. Novaro, T. Lopez, R. Gomez; *J. Mol. Catal. A* ***1999.*** *145, 291*

[4] P. Moggi, G. Predieri, A. Maione*; Catal. Lett.* ***2002.*** *79, 2*

[5] H. B. Chen, J. D. Lin, Y. Cai, X. Y. Whang, J. Yi, J. Whang, G. Wei, Y. Z. Lin, D. W. Liao*; Appl. Surf. Sci.* ***2001.*** *180, 328*

[6] H. Bielawa, O. Hinrichsen, A. Birkener, M. Muhler; *Angew. Chem. Int. Ed.* ***2001.*** *40, 1061*

[7] K. Aika, K. Shimazaki, Y. Hattori, A. Ohya, S. Ohshima, K. Shirota, A. Ozaki; *J. Catal.* ***1985.*** *92, 296*

[8] K. Aika, T. Takano, S. Murata; *J. Catal.* ***1992.*** *136, 126*

[9] M. A. Aramendia, J. A. Benitez, V. Borau, C. Jiménez, J. M. Marinas, J. R. Ruiz, F. Urbano; *Langmuir* ***1999.*** *15*

Chapter 14: Carbon nanofibers-supported catalysts

14.1 - Introduction

By regarding the results reported in the previous chapter, and particularly those for AP03, it is interesting to observe the behaviour of catalysts supported on carbon nanofibers[1,2,3,4]. In this section, 3 catalysts were compared. All catalysts are supported on carbon nanofibers functionalized with phosphine groups. The active phases contain ruthenium and their total weight is the 2% with respect to the support. Catalyst AP05 contains a cluster of Ruthenium and Gold. Catalyst AP06 contains a cluster of Ruthenium, Gold and Platinum. Catalyst AP07 contains a cluster of Ruthenium and Cobalt, with a 3:1 molar ratio. All clusters have been prepared by Dott. Deborah Vidick at the UCL (Universitè Catholique de Louvain-la-Neuve, Belgium). For the characterization, due to the little amount of samples, only TPR was carried out.

14.2 – TPR Characterization

The TPR profile for AP05 (FIG. 14.1) shows a series of peaks at 100°C, 350°C and 600°C probably due first of all to the interactions between hydrogen and carbon nanofibers and otherwise to the interactions of hydrogen with the decomposition products of the initial clusters.

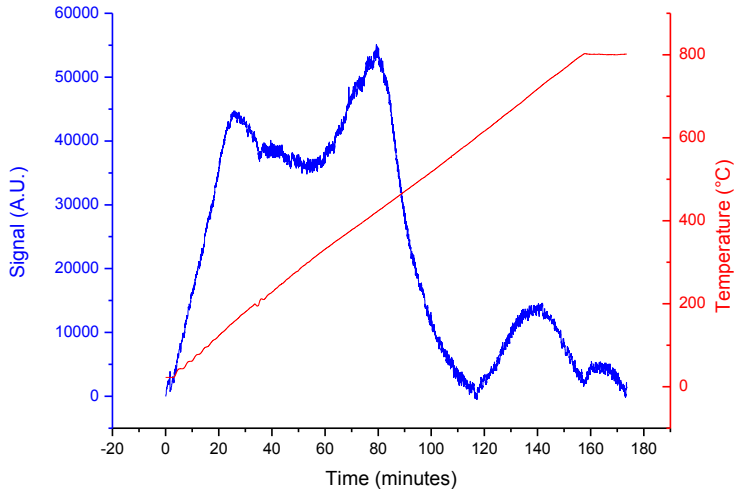

FIG. 14.1: TPR profile for AP05

Also in the case of AP06 (FIG. 14.2) several peaks are present, but the temperatures are very different because the metallic clusters used as precursors establish different interactions with the support.

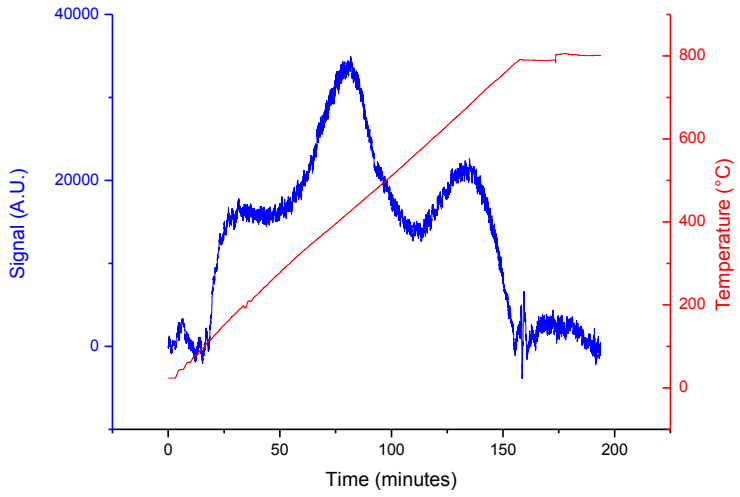

FIG. 14.2: TPR profile for AP06

The TPR analysis of the sample AP07 (FIG. 14.3) shows only a large peak that starts at 100°C, reaches the maximum intensity at 300°C, then it decreases slowly. This peak can be due to the superimposing of several peaks due to the decomposition of the precursor cluster.

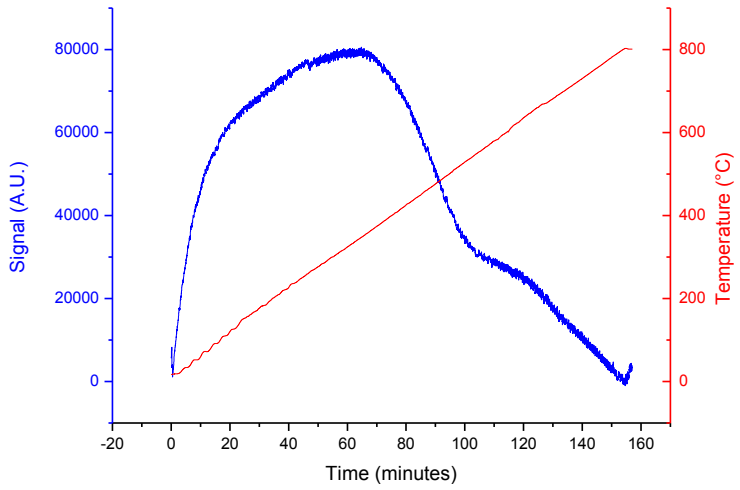

FIG. 14.3: TPR profile for AP07

14.3 – Catalytic tests

The catalytic tests were carried out in a fixed-bed microreactor, in the plant described in Chapter 4. 0.5 g of each catalyst were charged into the reactor and a flow of 10 ml/min of nitrogen and 30 ml of hydrogen was fed. The produced ammonia was collected as NH_4Cl in a solution by hydrochloric acid at known title.

The determination of the amount of ammonia produced was made by retrotitolation of the acid excess with a NaOH standard solution. The catalysts were previously activated at 400°C.

Graph 14.1 shows the production of ammonia for AP05 with respect to the equilibrium curve (blue line). We can observe that the maximum of productivity is around 375°C, but the temperature does not influence too much the activity. The ammonia concentration (Graph 14.2) in the effluent gases is around 0.2 %, a very low value. This catalyst is not promising to use for ammonia synthesis.

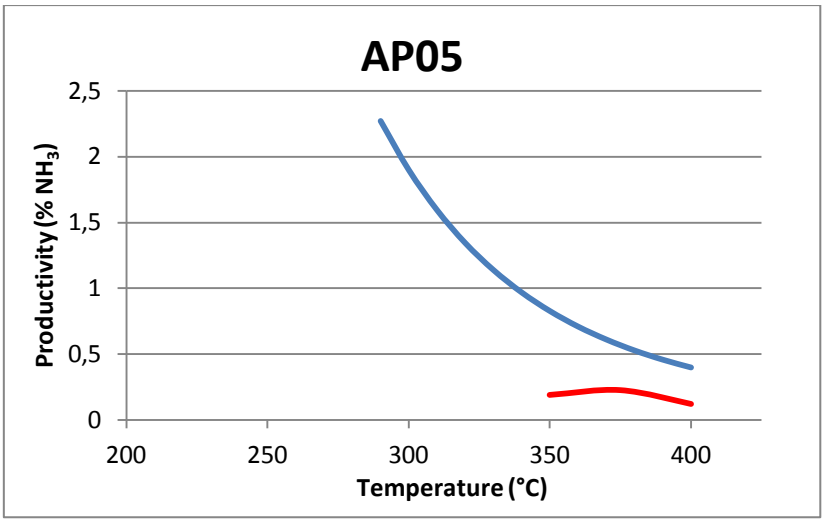

Graph 14.1: productivity of ammonia for AP05

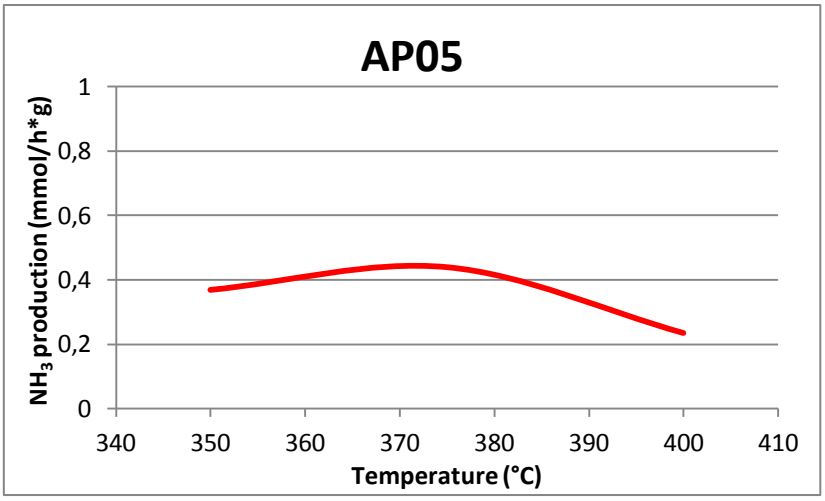

Graph 14.2: absolute production of ammonia for AP05

The activity in the ammonia synthesis of the catalyst AP06 (Graph 14.3) seems not be dependent on the temperature. The values of concentration of produced ammonia between 300°C and 400°C are always around 0.1%. The absolute hourly productivity per gram of catalyst is constantly of about 0.2 mmol/h*g (Graph 14.4). Also this catalyst, as already seen for AP05, is not promising to use for the ammonia synthesis.

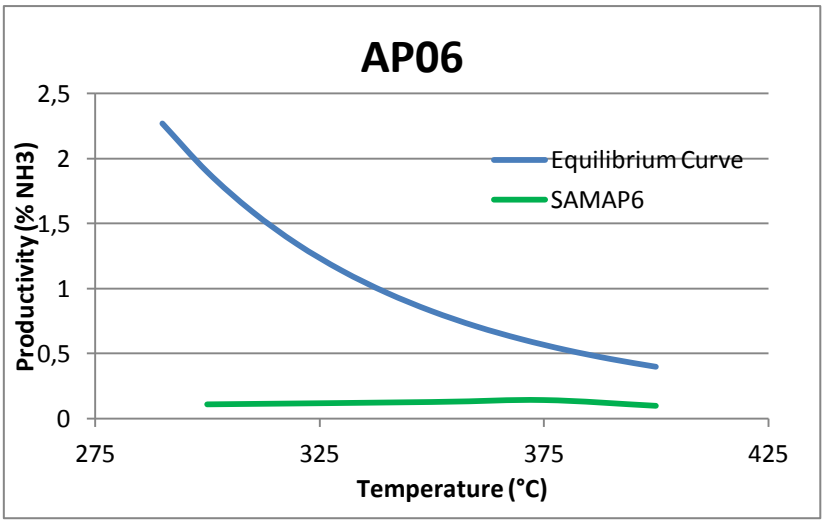

Graph 14.3: productivity of ammonia for AP06

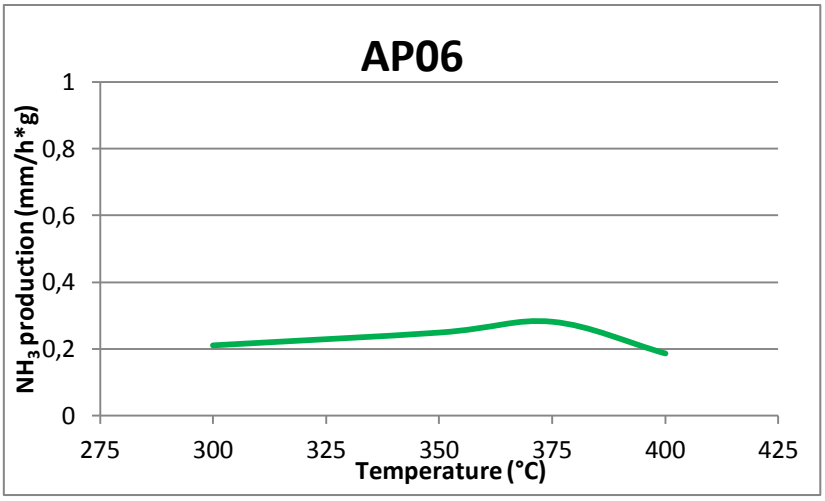

Graph 14.4: absolute production of ammonia for AP06

The activity range of temperatures for AP07 is limited between 275°C and 350°C. The maximum of productivity is attained at 325°C (Graph 14.5), with the 0.8% of ammonia concentration in the effluent gas (Graph. 14.6). By considering the absolute ammonia production, the best value for these tests of ammonia synthesis is observed. Indeed this catalyst shows the highest production between all tested catalysts, with a value of 1.6 mmol/h per gram of catalyst.

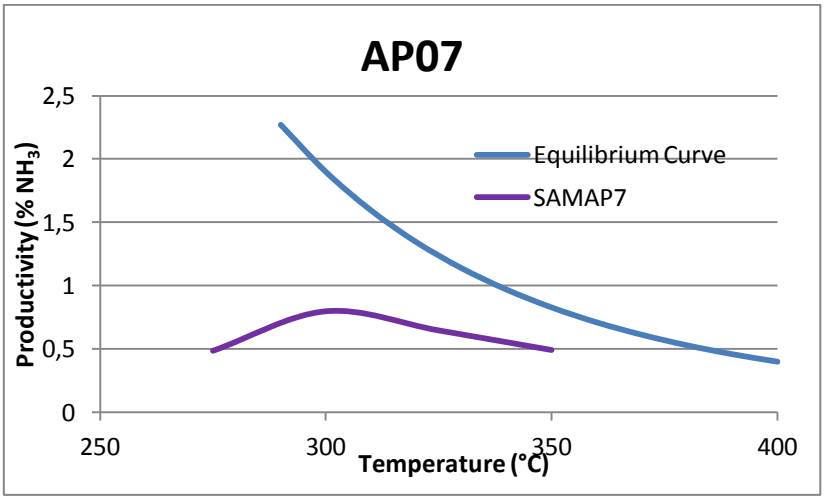

Graph 14.5: productivity of ammonia for AP07

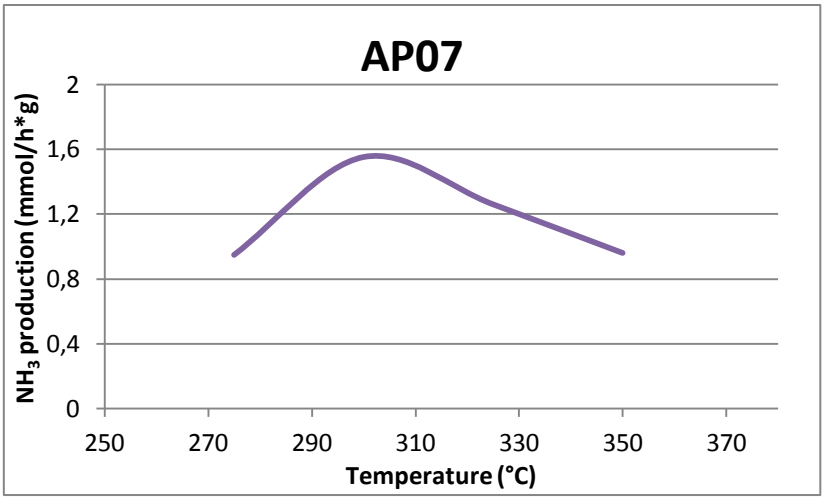

Graph 14.6: absolute production of ammonia for AP07

14.4 – Conclusions

By considering the results of these tests, clusters of Ru-Au and Ru-Au-Pt supported on carbon nanofibers do not seem interesting to prepare catalysts to be employed for the ammonia production. Indeed, the use as precursor of a cluster based on Ruthenium and Cobalt, with a molar ratio of 3:1, supported on carbon nanofibers, seems very interesting to continue its study for a possible application in industrial plants.

Bibliography

[1] H. B. Chen, J. D. Lin, Y. Cai, X. Y. Whang, J. Yi, J. Whang, G. Wei, Y. Z. Lin, D. W. Liao; *Appl. Surf. Sci.* ***2001.*** *180, 328*

[2] H. Bielawa, O. Hinrichsen, A. Birkener, M. Muhler; *Angew. Chem. Int. Ed.* ***2001.*** *40, 1061*

[3] K. Aika, K. Shimazaki, Y. Hattori, A. Ohya, S. Ohshima, K. Shirota, A. Ozaki; *J. Catal.* ***1985.*** *92, 296*

[4] K. Aika, T. Takano, S. Murata; *J. Catal.* ***1992.*** *136, 126*

Chapter 15 – Magnesia – Titania supports.

15.1 – Introduction

The purpose of this section is to compare the catalytic behaviour of Ruthenium catalysts when titania is used as co-support. In order to have reference data, a reference catalyst (AP08) was prepared by the sol-gel method: 5% (weight) of Ru[1] promoted with Cs_2O at 1:1 molar ratio are gelified in bulk with magnesia[2,3,4,5]. Two others catalysts, AP09 and AP10, are prepared with the same active phase and the same precursor by the bulk sol-gel method as well. In this case, the support is a mixture of MgO and TiO2 obtained by co-gelification from the respective precursors. The amount of titania in these catalysts is 50% (weight) and 20% (weight), respectively. Two other supports with the same amount of titania and magnesia are prepared. In this case, the precursors of the active phase and of the promoter are added by a classical impregnation method. These catalysts are called AP11 and AP12, respectively. The addition of titania is important for the mechanical stabilization of the system, since magnesia does not show good mechanical properties[6]. Table 15.1 summarizes the preparation of catalysts.

SAMPLE	SUPPORT	ACTIVE PHASE	PROMOTER	METHOD OF PREPARATION
AP08	MgO	5% Ru	Cs	Bulk sol-gel
AP09	50% MgO - 50% TiO_2	5% Ru	Cs	Bulk sol-gel
AP10	80% MgO - 20% TiO_2	5% Ru	Cs	Impregnation
AP11	50% MgO - 50% TiO_2	5% Ru	Cs	Bulk sol-gel
AP12	80% MgO - 20% TiO_2	5% Ru	Cs	Impregnation

Table 15.1: method of preparation and precursors for these catalysts.

15.2 – Preparation

AP08

The catalyst used as reference was prepared by the same procedure as for AP01, but adding the ruthenium precursor solution after a cooling treatment of the solution. The final composition is 5% by weight of Ruthenium on magnesium oxide as support and it is promoted by an equal amount in moles of cesium oxide. In order to obtain 3 g of magnesium oxide, a solution of 8.5 g of $Mg(OEt)_2$, 74 ml of ethanol and 6.75 ml of water was refluxed. After 3 h the solution was cooled and 0.315 g of triruthenium dodecacarbonyl, dissolved in THF, were added to this solution. The mixture was left under stirring for 1 h, then another solution of 0.26 g of $Cs_2(COO)_2$ dissolved in 120 ml of EtOH and 13.5 ml of water was added. The solution was left under stirring again for 1 h, then aged for a week and finally dried at 110°C under nitrogen flow at 60°C for 6 h.

AP09

4.25 g of $Mg(OEt)_2$ were dissolved in 35 ml of ethanol. The system was refluxed under vigorous stirring and a solution of 5.56 ml of $Ti(OiPr)_4$ dissolved in 7.1 ml isopropyl alcohol was then added. The system was left under reflux for 3h, then it was cooled and a solution of 0.32 g of $Ru_3(CO)_{12}$ dissolved in THF was mixed with the solution. The system was left under stirring again for 1h. A solution of 0.265 g of $Cs_2(COO)_2$ dissolved in 120 ml of ethanol and 13.5 ml of water was successively added to the solution, then the system was left to gelify during a week. The powder obtained was finally dried at 60°C under nitrogen flow.

AP10

The procedure of preparation is the same as for AP09, but changing the relative amounts of magnesium ethoxide and titania isopropoxide. 6.84 g of $Mg(OEt)_2$ were dissolved in 55 ml of ethanol. The system was refluxed under vigorous stirring and a solution of 2.22 ml of $Ti(OiPr)_4$ dissolved in 3 ml of isopropyl alcohol was added. The system was left under reflux for 3h, then it was cooled and a solution of 0.32 g of $Ru_3(CO)_{12}$ dissolved in THF was successively mixed to the solution. The system was left under stirring again for 1h. A solution of 0.265 g of $Cs_2(COO)_2$

dissolved in 120 ml of ethanol and 13.5 ml of water was then added to the solution and the resulting system was left to gelify during a week. After that, the drying step was performed as usually.

AP11

Catalyst AP11 was prepared by impregnation on a support obtained by the sol-gel method. In this case, the composition of the support is the same as for AP09. 4.25 g of $Mg(OEt)_2$ were dissolved in 35 ml of ethanol. The system was refluxed under vigorous stirring and a solution of 5.56 ml of $Ti(OiPr)_4$ dissolved in 7.1 ml of isopropyl alcohol was added. The system was left under reflux for 3h, then it was cooled, left to gelify during a week and finally calcinated at 450°C for 1 night. The support obtained was transferred into a solution of 0.32 g of $Ru_3(CO)_{12}$ dissolved in THF. After, another solution of 0.265 g of $Cs_2(COO)_2$, 120 ml of ethanol and 13.5 ml of water was added. Then the solvent was removed under vacuum in a rotating system. The solid was finally dried at 60°C under nitrogen flow.

AP12

Also this catalyst was prepared by the impregnation method. In this case, the support was the same as for AP10. 6.84 g of $Mg(OEt)_2$ were dissolved in 55 ml of ethanol. The system was refluxed under vigorous stirring and a solution of 2.22 ml of $Ti(OiPr)_4$ dissolved in 3 ml of isopropyl alcohol was added. The system was left under reflux for 3h, then it was cooled, left to gelify during a week and finally calcinated at 450°C for 1 night. The obtained support was transferred into a solution of 0.32 g of $Ru_3(CO)_{12}$ dissolved in THF. After, another solution of 0.265 g of $Cs_2(COO)_2$, 120 ml of ethanol and 13.5 ml of water was added. Then the solvents were removed under vacuum in a rotating system. The solid was finally dried at 60°C under nitrogen flow.

15.3 – Characterization

15.3.1 TPR profiles

The TPR profile for AP08 (FIG. 15.1) shows two peaks: the first one is a small peak centered at

about 200°C; the second is more intense than the first one and it is centered at 400°C. The first peak can be assigned to the reduction of Ruthenium oxidized. It is noteworthy that the Ruthenium is previously inserted at the metallic state. The appearance of this peak seems not justifiable, but the instauration of interactions between the precursor of the active phase and supporting magnesia can partially oxidize the metal. The second peak is probably due to the interaction between hydrogen and the decomposition products of the precursors.

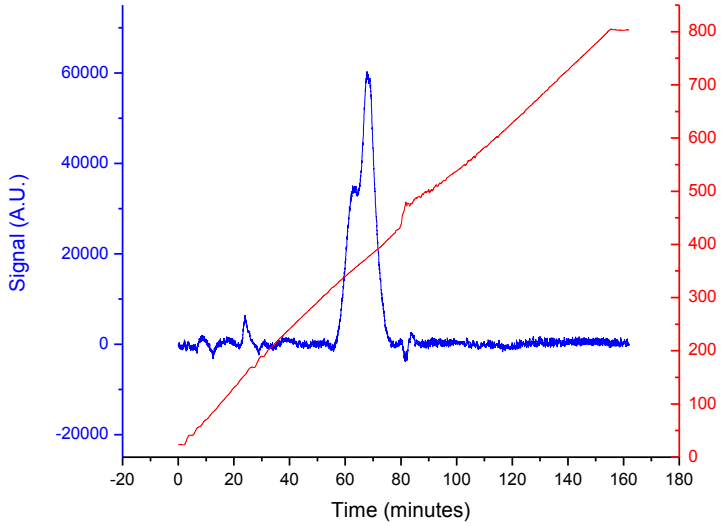

FIG. 15.1: TPR profiles for AP08

The TPR profile of AP09 (FIG. 15.2) shows only a large peak, centered at 300°C, probably due to the products of decomposition of the precursors. This very intense peak can cover other peaks eventually present.

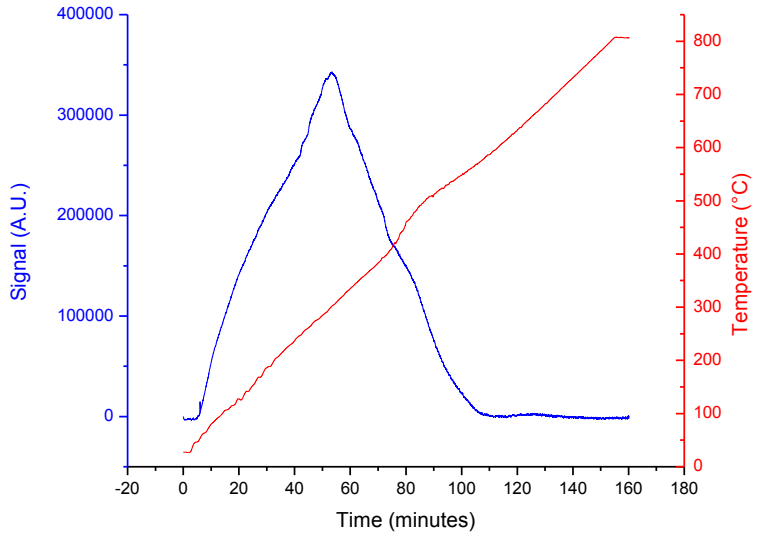

FIG. 15.2: TPR profiles for AP09

The TPR profile for AP10 (FIG. 15.3) is identical to that for AP08: also in this case it can be observed the weak peak at low temperatures due to the reduction of Ruthenium which has interacted with the support and the peak at 400°C due to the products of decomposition of the precursors.

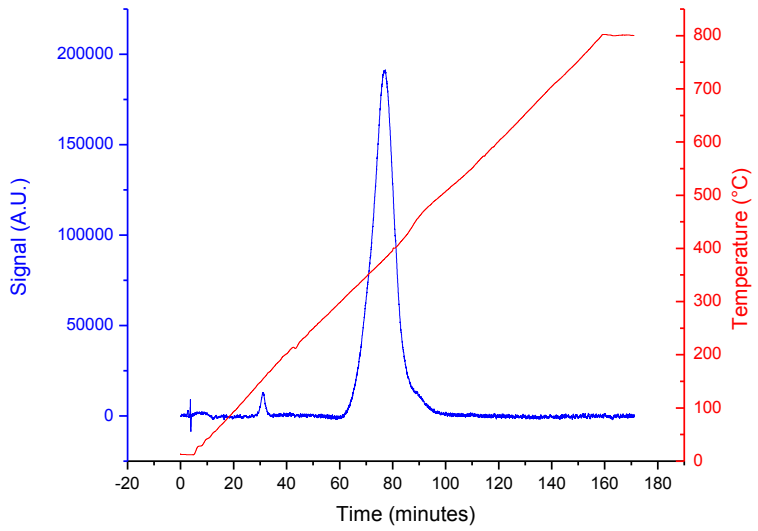

FIG. 15.3: TPR profiles for AP10

The TPR profile for AP11 (FIG. 15.4) shows the usual peak due to the reduction of partially oxidized Ruthenium at 200°C, while the peak due to the products of decomposition of the precursors is shifted to 350°C.

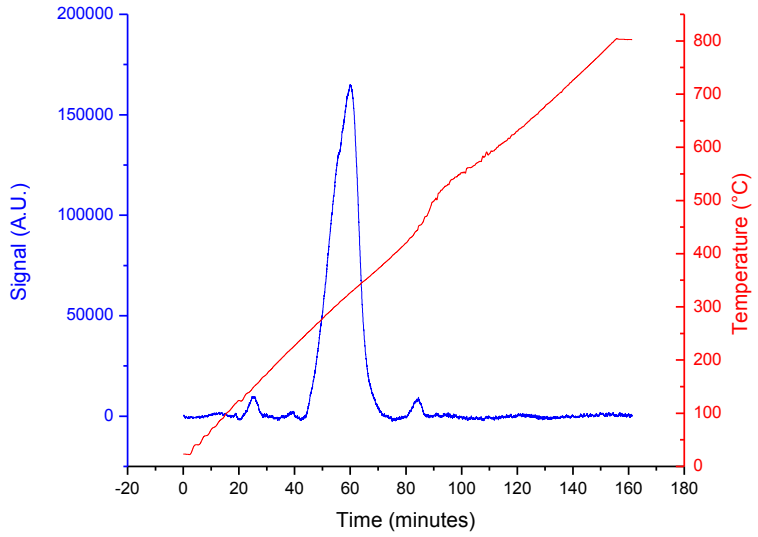

FIG. 15.4: TPR profiles for AP11

The TPR profile for AP12 (FIG. 15.5) is identical to TPR profile for AP10.

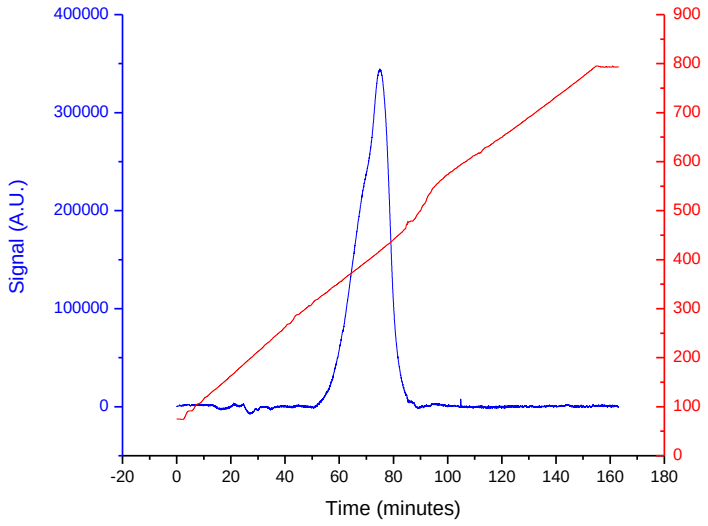

FIG. 15.5: TPR profiles for AP12

15.3.2 Surface Area

Table 15.2 reported the surface area values measured by B.E.T. for this set of catalysts.

SAMPLE	SURFACE AREA (m_2/g)
AP08	35
AO09	55
AP10	97
AP11	146
AP12	157

Table 15.2: surface area of the samples

The surface area of the impregnated catalysts results relatively high and similar between each other. The other catalysts show different values. Indeed, the area expected for AP08 is around 50-60 m^2/g, but it results quite lower than this value. The area of AP09 is in the expected range, because titania shows very low surface area values. The area of AP10 is also quite unexpected; it results 97 m^2/g. Probably, the presence of $Ti0_2$ influenced the distribution of MgO inside the structure.

15.3.3 XRD

The XRD spectrum acquired for AP08 (FIG. 15.6) after an activation treatment of 4h at 400°C, shows three main peaks at 2θ = 43°, 62° and 78° that are assignable to magnesium oxide in the form of periclase[7].

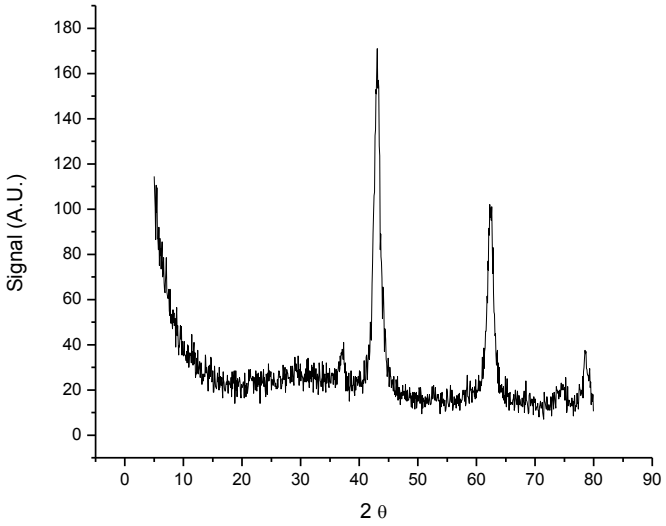

FIG. 15.6: XRD spectrum for AP08

The XRD spectrum acquired for AP9 after an activation treatment of 4h at 400°C (FIG.15.7) is prevalently amorphous, but two small peaks can be observed at 2θ = 43° and 62°, that are also assignable again to the periclase structure[7].

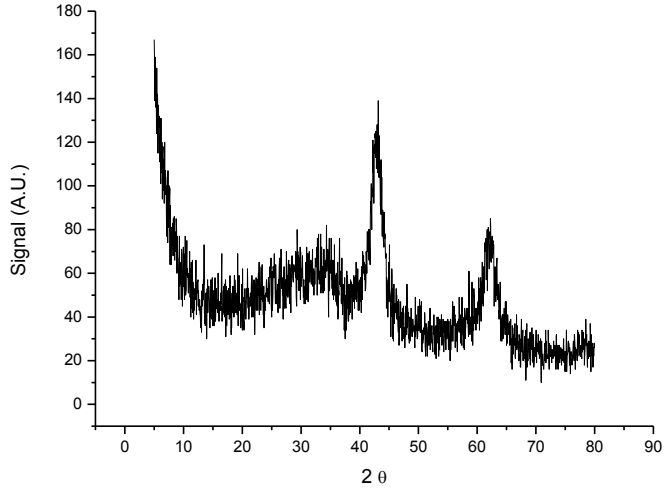

FIG. 15.7: XRD spectrum for AP09

The XRD spectrum acquired for AP10 after the activation treatment of 4h at 400°C (FIG. 15.8) shows two peaks at 2θ = 43° and 62°, that are assignable to magnesium oxide in the form of periclase[7]; in this case the structure seems more crystalline than that observed for AP09.

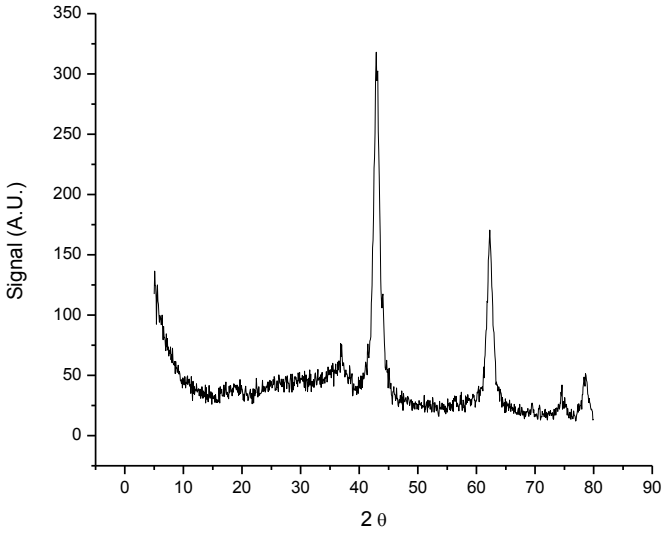

FIG. 15.8: XRD spectrum for AP10

The XRD spectrum of AP11 (FIG. 15.9) shows the same peaks as for AP10. Also in this case, only the structure of periclase[7] can be evidenced from the analysis.

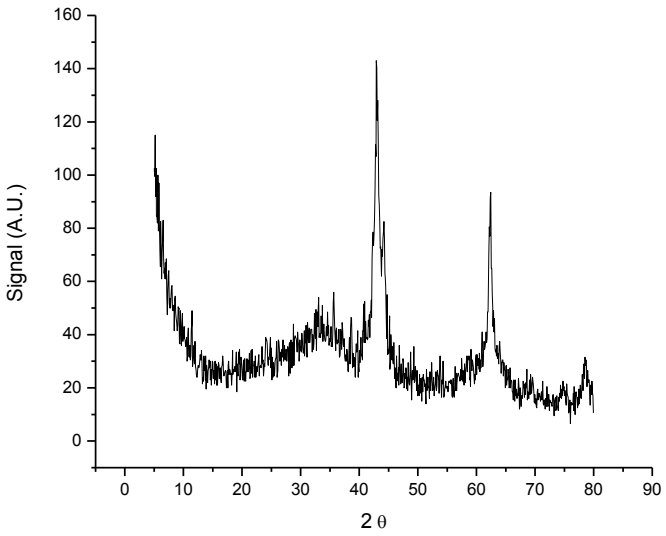

FIG. 15.9: XRD spectrum for AP11

The XRD spectrum of AP12 (FIG. 15.10) shows again, as well as for the other samples, the peaks associated to magnesium oxide with the structure of periclase[7].

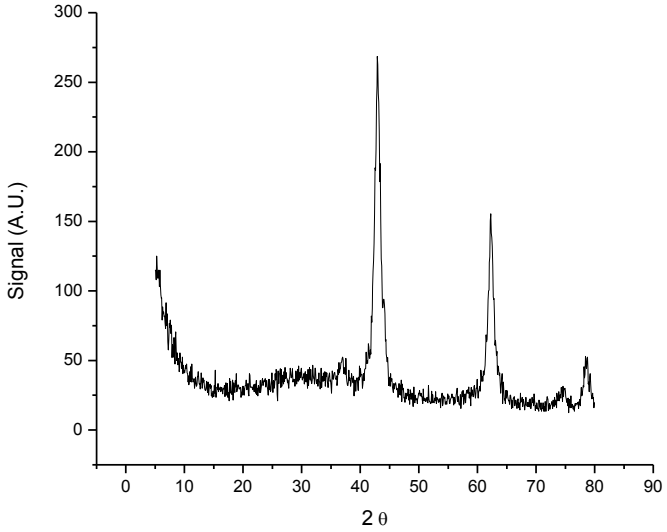

FIG. 15.10: XRD spectrum for AP12

15.3.4 FT-IR

The IR spectrum of AP08 (FIG. 15.11) acquired before activation (blue line) shows a narrow peak at high wavenumbers (up to 3500 cm^{-1}) that is due to the free -OH groups. A small band can be observed between 1250 cm^{-1} and 1750 cm^{-1}; this band is due to the overlapping of peaks due to the presence of oxalate as precursor of cesium. Both this signals disappear when the catalyst is activated (red line). After activation it remains only the peak at lower wavenumbers due to the presence of metal oxides.

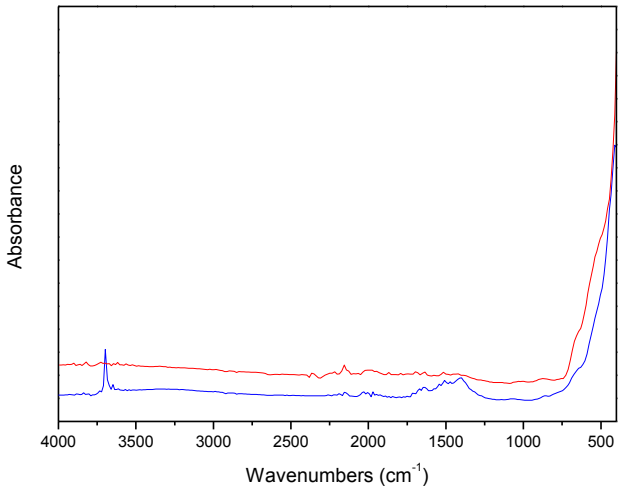

FIG. 15.11: IR spectra for AP08

The IR spectra acquired for samples AP09, AP10, AP11 and AP12 (FIG. 15.12, 15.13, 15.14 and 15.15 respectively) are totally similar to that for AP08. The only difference is that in their spectra, the bands of the hydroxide groups result more broadened. This fact means that the hydroxide groups are involved in the formation of hydrogen-bond.

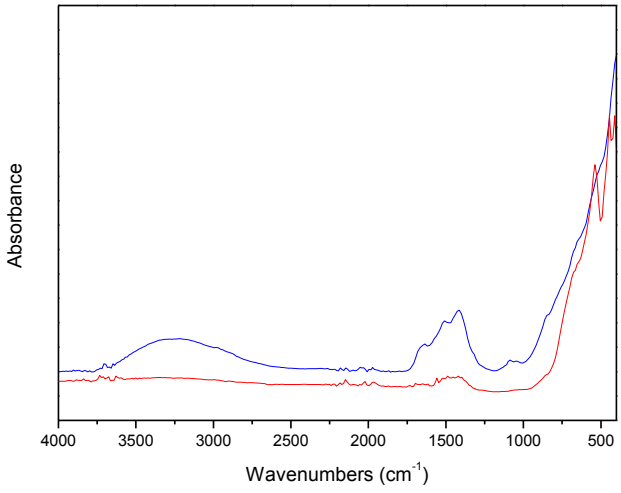

FIG. 15.12: IR spectra for AP09

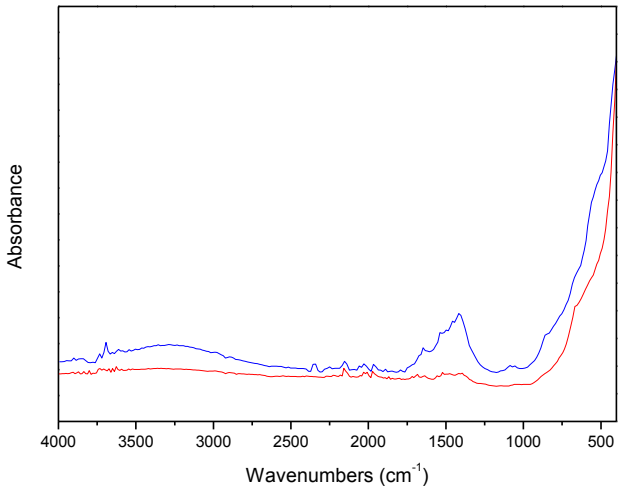

FIG. 15.13: IR spectra for AP10

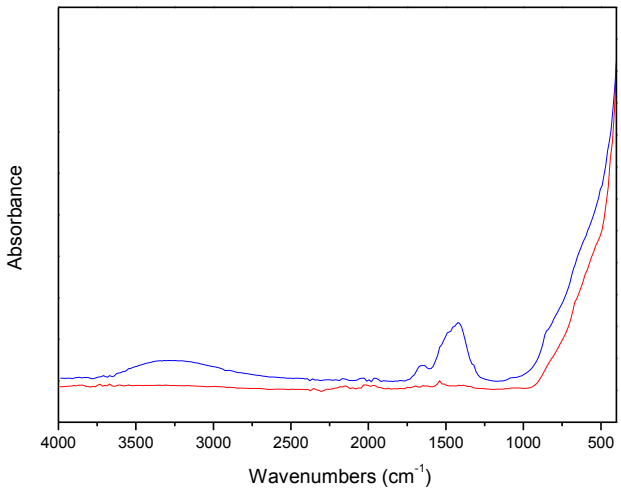

FIG. 15.14: IR spectra for AP11

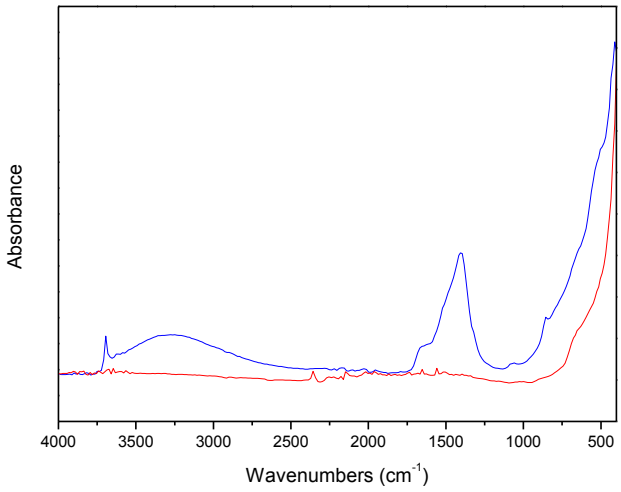

FIG. 15.15: IR spectra for AP12

15.4 Catalytic tests

The catalytic tests were performed in the plant yet described in Chapter 4. The operating conditions of the ammonia synthesis tests were the same previously described for the other catalysts and also the method of determination was the same. In this case, 1 g of catalyst weas charged for each test and it was activated under helium for 4h at 400°C.

The production of ammonia of catalyst AP08 shows a maximum at 275°C (Graph 15.1). The absolute productivity (Graph 15.2) of this reference catalyst is around 0.75 mmol/h per gram of catalyst. This value is the same as for AP01, but the maximum is shifted. Indeed, the previous obtained graph for AP01 showed a broad curve, with a maximum at 325°C. Furthermore, in this case the addition of ruthenium at a cold solution during the preparation can also play an important role for the availability of the active phase at the surface of the catalyst.

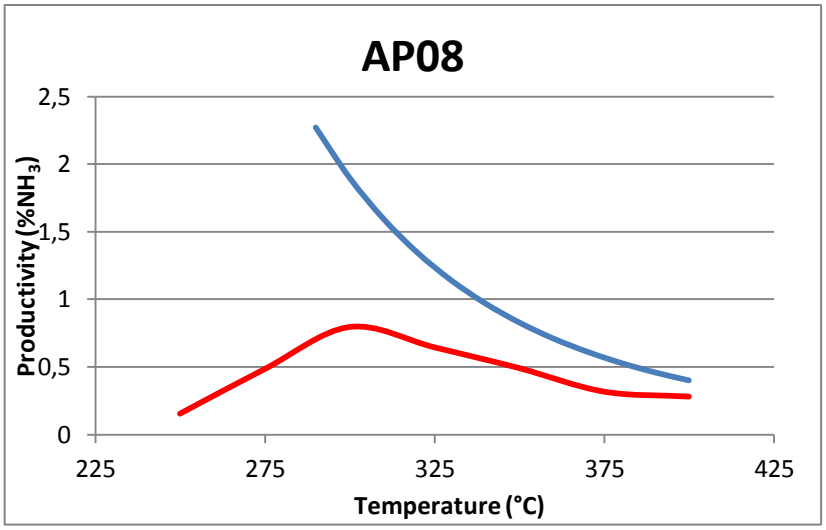

Graph 15.1: productivity of ammonia for AP08

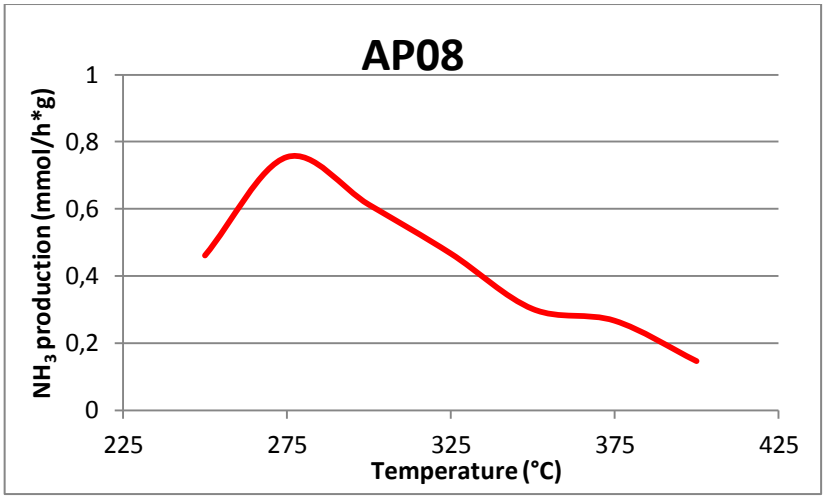

Graph 15.2: absolute production of ammonia for AP08

A marked decrease of the ammonia production was expected for AP09 (Graph 15.3), because the higher addition of TiO_2 enhances the mechanical characteristics but can diminish the catalytic activity. However, the decrease was not expected so highly. The absolute production was less than a third part than the reference catalyst AP08 (Graph 15.4).

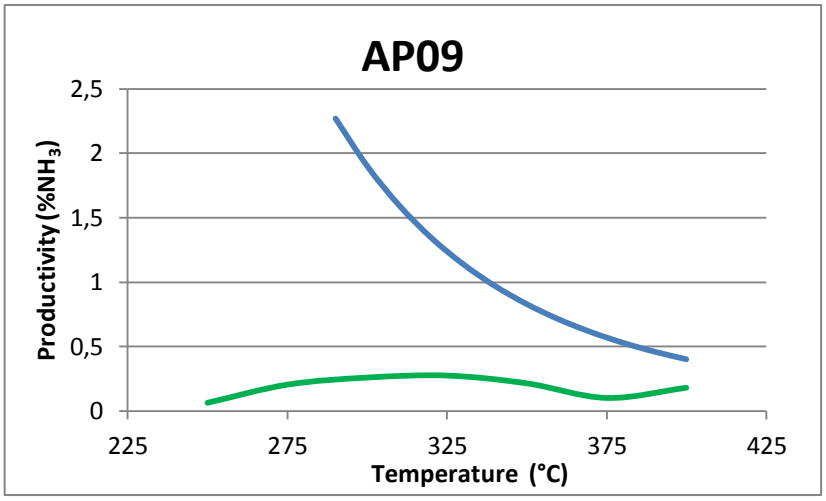

Graph 15.3: productivity of ammonia for AP09

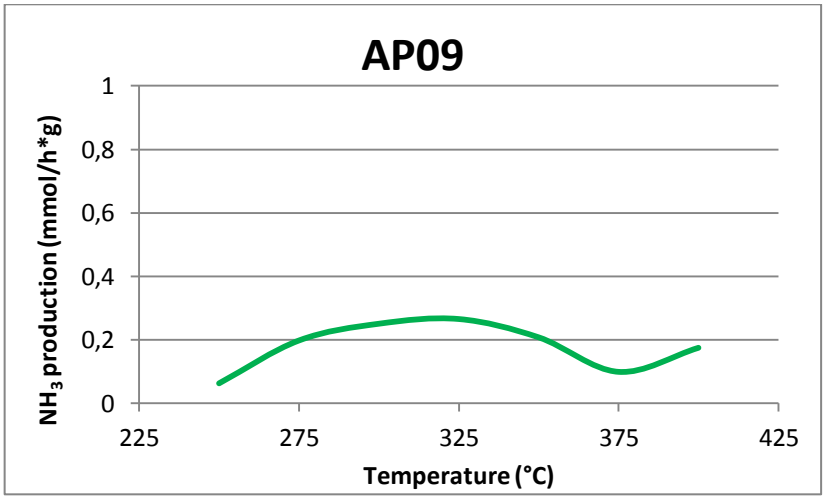

Graph 15.4: absolute production of ammonia for AP09

Catalyst AP10 (Graph 15.5) shows again the expected decrease of the catalytic activity. However, in this case, the decrease is lower than that occurred for AP09, because the amount of TiO_2 is 20%, other than 50% of the previous one.

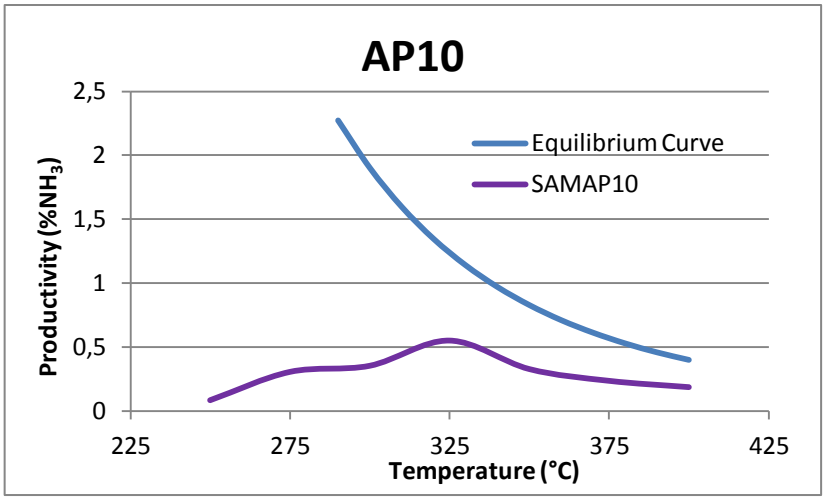

Graph 15.5: productivity of ammonia for AP10

By observing the following graph (Graph 15.6), the maximum of absolute productivity results 0.5 mmol/h*g, that is a value not so bad with respect to the 0.75 obtained with the reference catalyst.

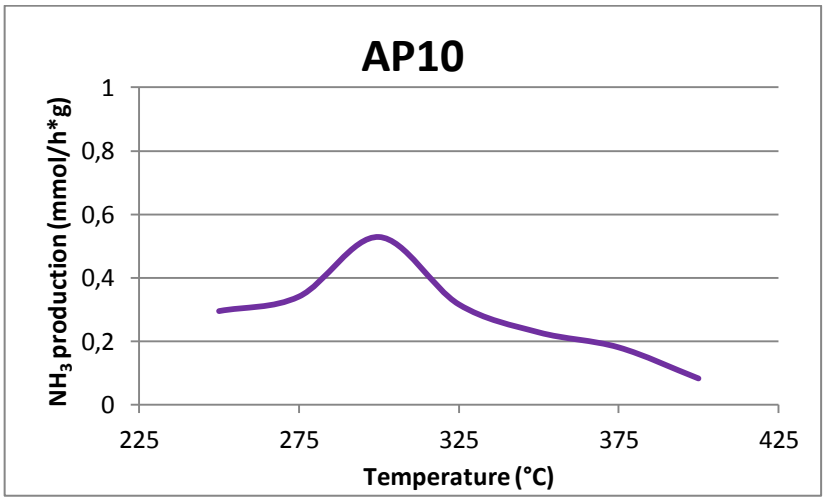

Graph 15.6: absolute production of ammonia for AP10

The productivity test for AP11 (Graph 15.7) shows the peak of productivity at 350°C. Also in this case, the productivity remains very low, also by comparing with the equilibrium curve. In particular, at the maximum the productivity is the half than the equilibrium value. Also by comparing with the homologous catalyst AP09, the absolute productivity (Graph 15.8) is lower: less than 0.4 mmol/h per gram of catalyst against a 0.5 value.

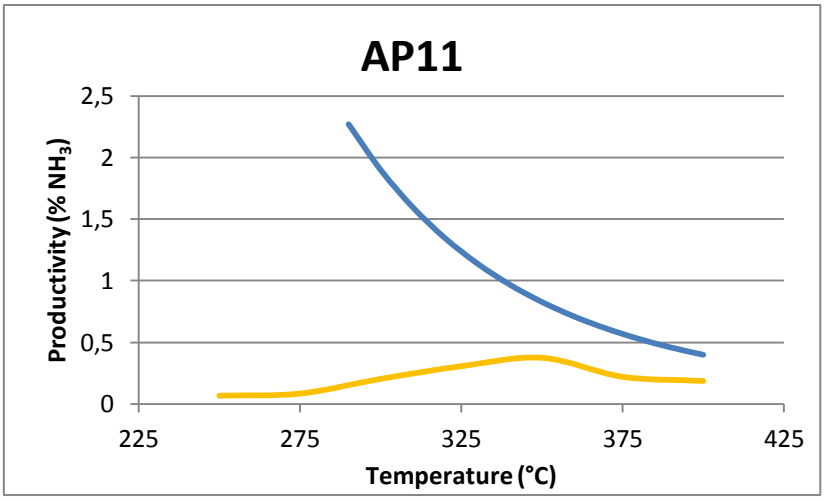

Graph 15.7: productivity of ammonia for AP11

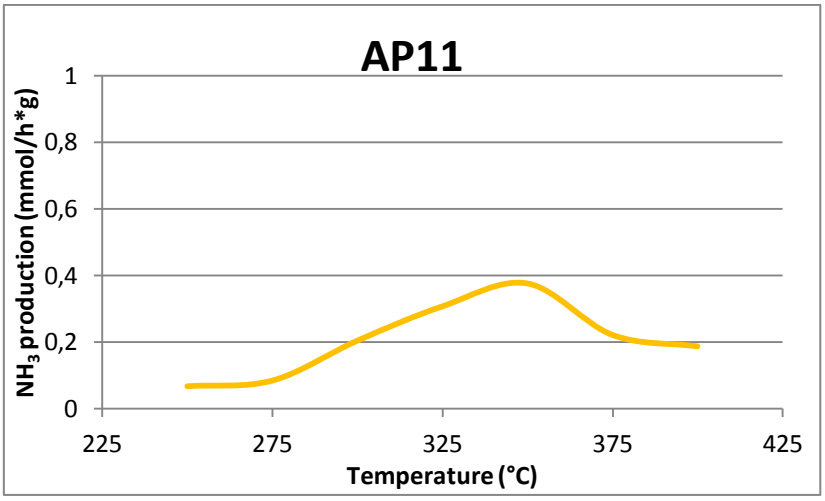

Graph 15.8: absolute production of ammonia for AP11

The graph for AP12 (Graph 15.9) shows that the dependence of the catalytic activity on the temperature is similar to those verified for the other catalysts. The peak is at 325°C and its value is a third than the maximum theoretical corresponding to the equilibrium value.

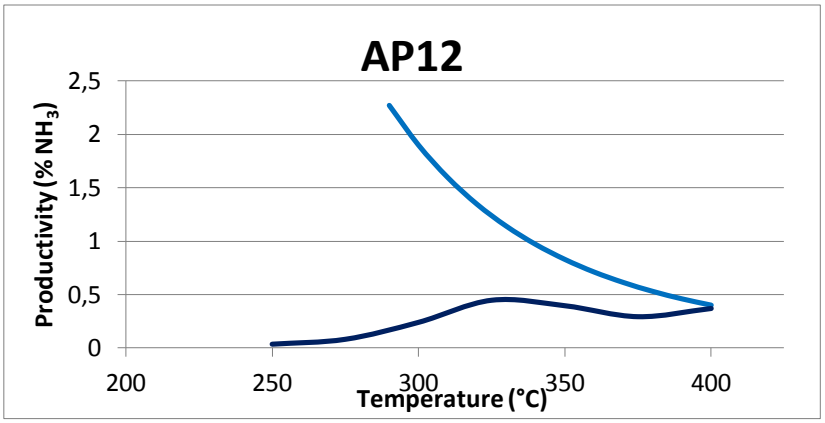

Graph 15.9: productivity of ammonia for AP12

The productivity reaches the equilibrium curve at 400°C. The absolute productivity (Graph 15.10) results similar to that for AP11, about 0.4 mmol/h*g, but in this case it is less lower with respect to the analogue catalyst AP10. This observed behaviour is probably due to the impregnation method. From this preparation method the resulting dispersion of the metal on the surface is not good, with a lower catalytic activity as a consequence.

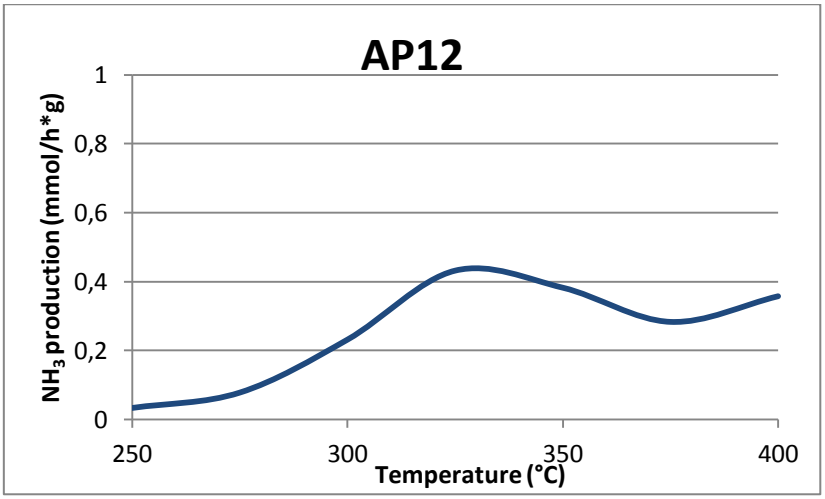

Graph 15.10: absolute production of ammonia for AP12

15.5 Conclusions

The TPR profiles obtained with the fresh samples show that the temperature of decomposition for all samples is lower than 400°C. The other analyses for fresh samples and activated samples

showed the decomposition of the precursors and the formation of the crystalline phase periclase (MgO) during the thermal treatment.

By considering the results of the catalytic activity tests for the impregnated catalysts, the addition of titania caused a marked decrease in the ammonia production, by comparing with a reference catalyst supported on magnesia. However, this decrease seems not so much dependant on the amount of added titania; indeed the absolute ammonia production results around 0.4 mmol/h*g for both impregnated catalysts (AP11 and AP12) with respect to 0.75 mmol/h*g value for the reference catalyst AP08. Also in the case of the bulk sol-gel prepared catalyst a decrease of activity is observed, but in this case that decrease is highly dependent on the amount of titania of the support. The catalyst with the lower amount of titania as support shows an absolute productivity of ammonia of 0.5 mmol/h*g.

Bibliography

[1] J. Iwamoto, M. Itoh, Y. Kajita, M. Saito, K. Machida; *Catalysis Communications* ***2007.*** *8, 941*

[2] R. Portillo, T. Lopez, R. Gomez, B. A. Morales, O. Novaro; *Langmuir* ***1996.*** *12, 40*

[3] J. A. Wang, X. Bokhimi, O. Novaro, T. Lopez, R. Gomez*; J. Mol. Catal. A* ***1999.*** *145, 291*

[4] P. Moggi, G. Predieri, A. Maione; *Catal. Lett.* ***2002.*** *79, 2*

[5] C. Zupanc, A. Hornung, O. Hinrichsen, M. Muhler, *Journal of Catalysis* ***2002.*** *209, 501*

[6] T. Lòpez, J. Hernàndez, R. Gòmez, X. Bokhimi, J.L. Boldù, E. Munoz, O. Novaro, A. Garcìa-Ruiz; *Langmuir* ***1999.*** *15, 5689*

[7] M. A. Aramendia, J. A. Benitez, V. Borau, C. Jiménez, J. M. Marinas, J. R. Ruiz, F. Urbano; *Langmuir* ***1999.*** *15, 1192*

Chapter 16: Influence of promoters

16.1 Introduction

The purpose of this section is to evaluate the influence of alkaline and earth-alkaline metals as promoters of ruthenium in the ammonia synthesis[1,2,3]. Therefore, 3 catalysts are prepared, with the same composition, but with different promoters.

The active phase for these catalysts is 5% by weight of ruthenium. The metal is supported on MgO/Al_2O_3[4,5], at a molar ratio 2/1. Catalyst AP13 is promoted with Cesium, at a molar ratio 1:1 with ruthenium. The two other catalysts, AP14 and AP15, are promoted with lithium and barium respectively, both at a molar ratio 1:1 with respect to ruthenium. These compositions are summarized in Table 16.1

SAMPLE	ACTIVE PHASE	SUPPORT	PROMOTER	PREPARATION
AP13	5% Ru	MgO/Al_2O_3	Cs	Bulk sol-gel
AP14	5% Ru	MgO/Al_2O_3	Li	Bulk sol-gel
AP15	5% Ru	MgO/Al_2O_3	Ba	Bulk sol-gel

Table 16.1: method of preparation and precursors for these catalysts.

16.2 Preparation

AP13

The composition of catalyst AP13 is 5% Ru (weight) on a support of MgO/Al_2O_3 promoted with cesium at a 1:1 molar ratio with respect to Ruthenium. For the synthesis of 2 g of support (Mg/Al molar ratio=2/1), 3.49 g of $Mg(OEt)_2$ were dissolved in 21 ml of ethanol and 3.125 of $Al(i\text{-}PrO)_3$ were dissolved in 62 ml of isopropanol. These solutions were mixed and refluxed until complete dissolution. After 3h of reflux, the solution was cooled, and another solution of 0.21g $Ru_3(CO)_{12}$ dissolved in THF was added to the first one. The mixture was left under vigorous stirring for 1h, then a solution of 0.175 g of $Cs_2(COO)_2$ dissolved in 80 ml of ethanol and 5 ml of H_2O was added to the system. The resulting solution was left under vigorous stirring again for 1 h, then it was left to gelify and aged during 7 days. Finally, the powder was dried at 60° under nitrogen flow.

AP14

The preparation of AP14 exactly follows the procedure described for AP13, but instead of cesium, lithium was used as promoter. After the addition of ruthenium precursor and the stirring steps, a solution of 0.1 g $CH_3COOLi \cdot 2H_2O$ dissolved in 4.5 ml of ethanol replaced the Cesium solution. As for the other catalyst, the system was left to gelify and to age during a week, then the sample was dried at 60°C under nitrogen flow.

AP15

Also in the case of AP16, the preparation procedure follows the same steps as for the previous samples, but in this case the promoter is Barium. The barium is added by a solution of 0.252 g of $Ba(CH_3COO)_2$, dissolved in 2 ml of water. Also in this case, after the stirring step, the system was left to gelify, then aged and finally dried at 60°C under nitrogen flow.

16.3 Characterization

16.3.1 TGA

The TGA analysis was done on sample AP13 (FIG. 16.1) between room temperature and 900°C under nitrogen atmosphere. By analyzing the graph, a decrease of the weight can be observed around 100°C when the water is loss from the sample. Another slow decrease of weight occurs at temperatures between 350°C and 400°C. This loss of weight is due to the decomposition of the oxalate that is the precursor of the promoter.

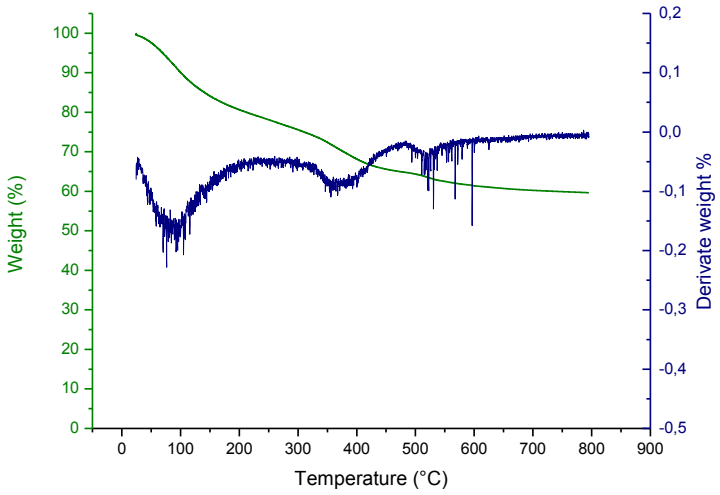

FIG. 16.1: TGA analysis of AP13

Also in the case of AP14, the TGA analysis (FIG. 16.2) was done for the sample between room temperature and 900°C under nitrogen atmosphere. The weight loss of water is present also in this case. Two other peaks can be observed in this case, one at 230°C and the other at 325°C. This peaks are probably due to the decomposition of the precursor, CH_3COOLi that, in this case, occurs in two steps.

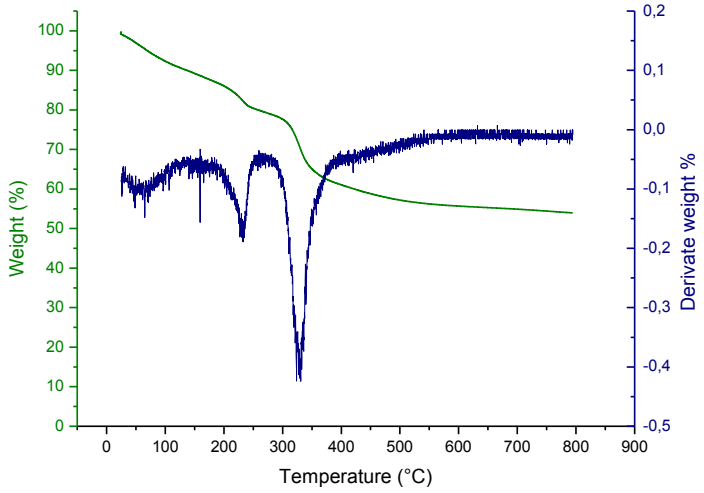

FIG. 16.2: TGA analysis of AP14

As for the previous samples, the TGA analysis is done for the catalyst AP15 between room temperature and 900°C under nitrogen atmosphere (FIG. 16.3). The weight loss at 100°C is again due to the loss of water. The weight loss at higher temperatures is due to the decomposition of the precursor of the promoter, $(CH_3COO)_2Ba$ and, in this case, it takes place in a single step at 320°C.

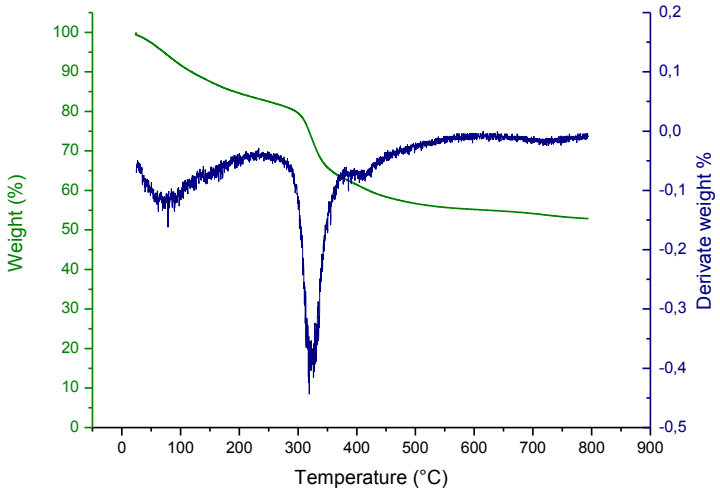

FIG. 16.3: TGA analysis of AP15

16.3.2 TPR profiles

The TPR profile for AP13 (FIG. 16.4) shows a band composed by the overlapping of two peaks centered at 320°C and 420°C, respectively. Probably, these peaks are the result of the decomposition of $Cs_2(COO)_2$, the precursor of the promoter, that releases CO_2 and this product can consume hydrogen by a methanation reaction.

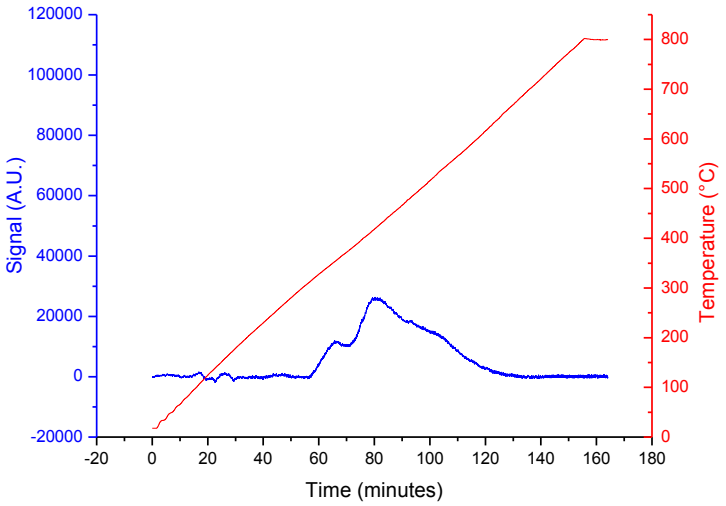

FIG. 16.4: TPR profile for AP13

In the following graph the TPR profile for AP14 is reported (FIG. 16.5). The first little peak at 100°C is assignable to the reduction of Ru^{2+} to metallic Ru. The system contains Ruthenium already at the metal state but some interactions between the support and the precursor of the active phase can occur, in particular with the surface –OH groups of the magnesium hydroxide. These interactions cause the oxidation of metal, which is after reduced by hydrogen during TPR. The peak centered at 300°C can be assigned to the hydrogen consumed by the interaction with CO coming from the carbonyl precursor of ruthenium, while the peak at 500°C can be due to the interaction of hydrogen with the decomposition products of the promoter precursor at increasing temperatures.

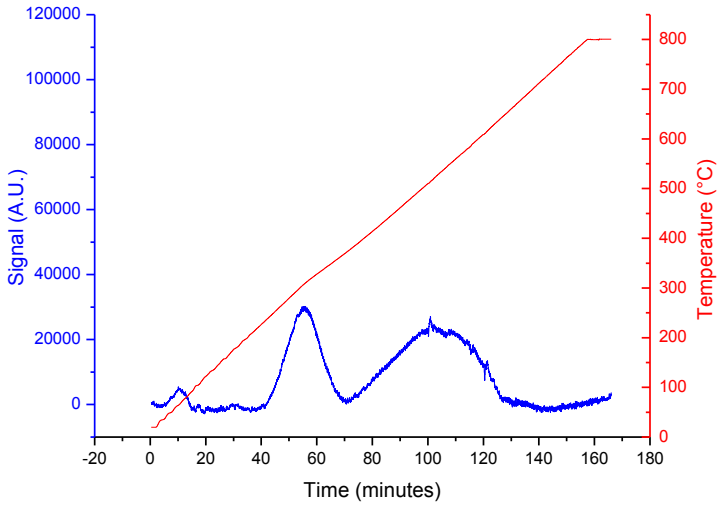

FIG. 16.5: TPR profile for AP14

Into the TPR profile for AP15 (FIG. 16.6) it can be seen only the peak with the maximum at 350°C, that can be assigned to the interaction of hydrogen with CO coming from the decomposition of $Ru_3(CO)_{12}$.

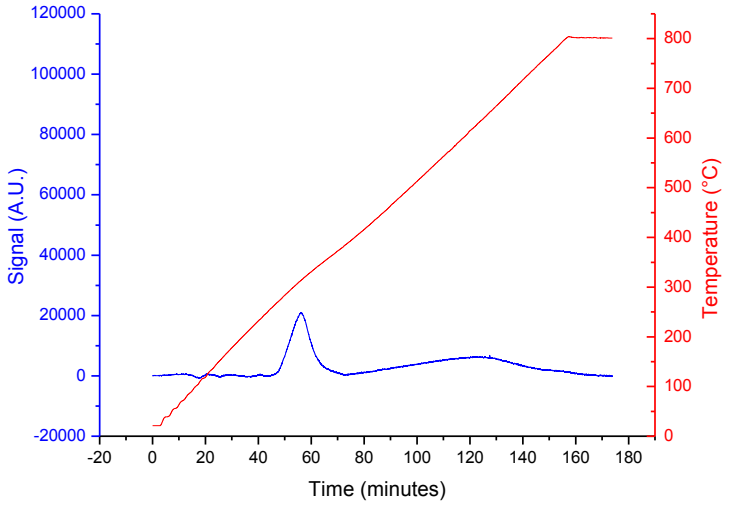

FIG. 16.6: TPR profile for AP15

16.3.3 Surface Area

The surface areas of the catalysts are reported in Table 16.2

SAMPLE	SURFACE AREA (m^2/g)
AP13	83
AP14	304
AP15	47

Table 16.2: surface area of the samples

The catalyst AP14 shows an high value of surface area, probably due to the use of a little amount of water. This fact can be reflected, during the gelification, into the formation of a network with an high number of alkoxide groups which releases volatile compounds during the thermal treatment of activation accompanied by the development of a large porosity of the sample.

Instead, in the case of the catalyst AP15, the low value of surface area is probably due to a larger amount of water used for the dissolution of $Ba(CH_3COO)_2$, that prevalently favours the hydrolysis reaction instead of condensation during the gelification process.

16.3.4 XRD

The XRD spectra of these catalysts (FIG. 16.7, 16.8 and 16.9) show a prevalently amorphous structure. However, some peaks, at $2\theta = 42.9°$ and $62.3°$ can be observed into the graphs. These peaks are due to the magnesium oxide that is present with the structure of periclase.

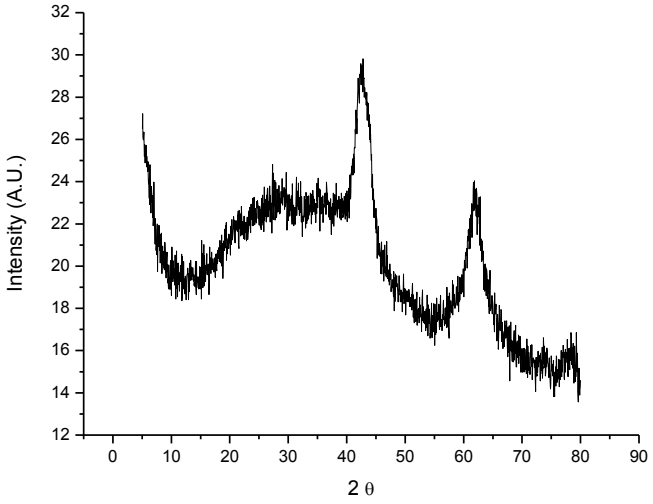

FIG. 16.7: XRD spectrum for AP13

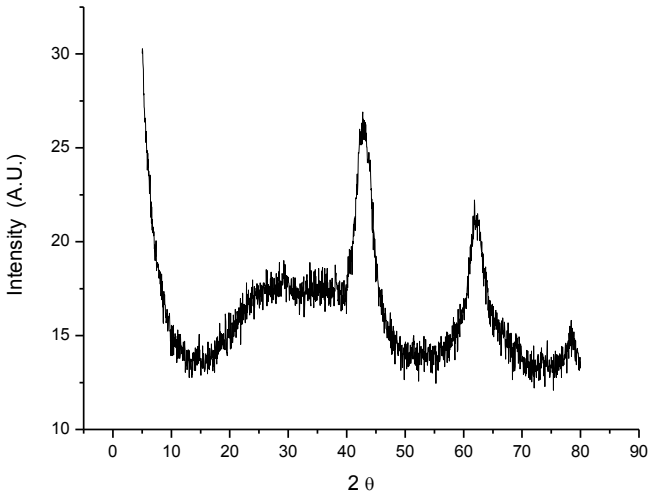

FIG. 16.8: XRD spectrum for AP14

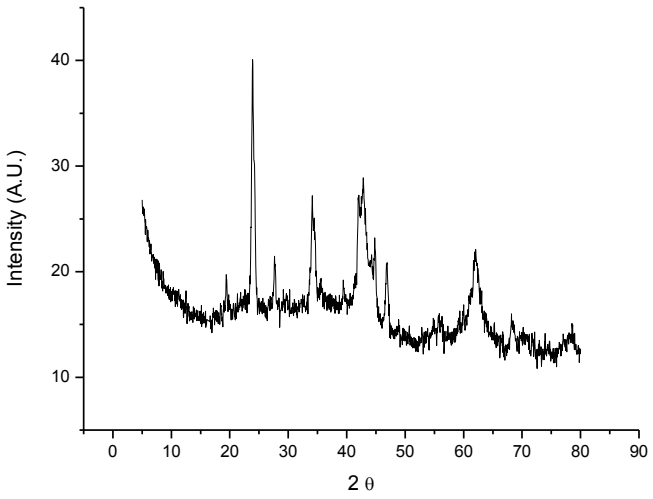

FIG. 16.9: XRD spectrum for AP15

16.3.5 FT-IR

The IR spectra of the three catalysts were collected (FIG. 16.10, 16.11, 16.12), as usual, before and after the activation step. The blue lines represent the spectra before the activation, while the red lines are those of the catalyst activated.

In all three cases, it can be observed the disappearance of the –OH band centered at 3500cm^{-1} and the disappearance of the bands due to the precursors of promoters, centered in all cases at 1500 cm^{-1}.

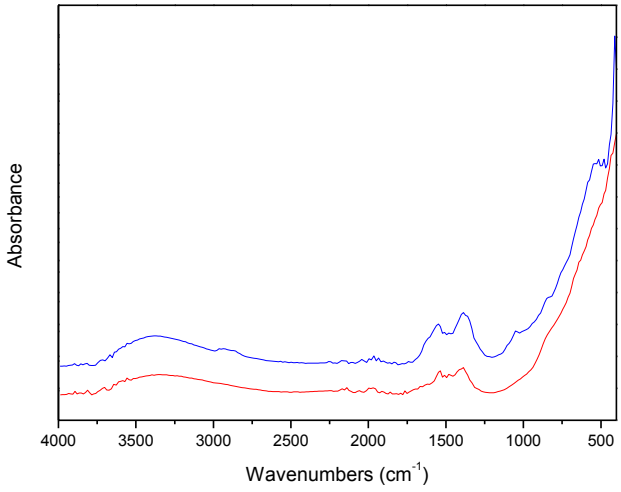

FIG. 16.10: XRD spectra for AP13

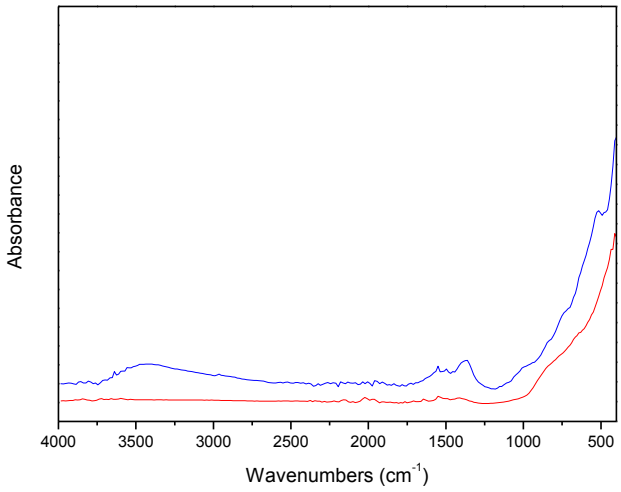

FIG. 16.11: XRD spectra for AP14

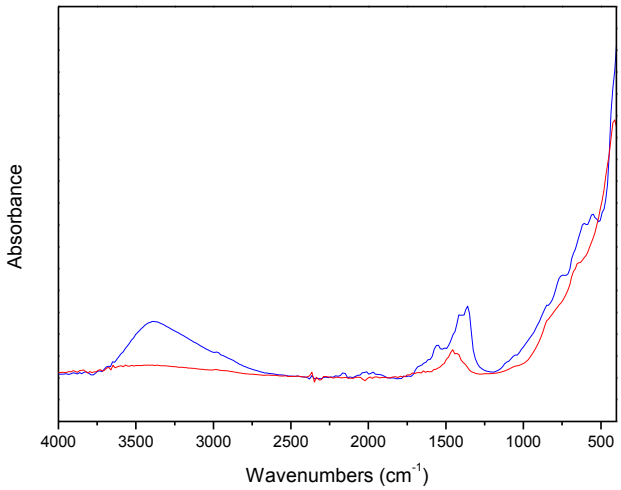

FIG. 16.12: XRD spectra for AP15

16.4 Catalytic tests

The catalytic tests are carried out in the plant previously described (Chapter 4). For each catalyst, 1 g of sample was charged into the reactor and subjected to the test.

The produced ammonia is captured as NH_4Cl and determined by the usual method of retrotitration of a solution initially containing a known amount of HCl.

The production of ammonia of catalyst AP13 (Graph 16.1) reaches the maximum at 325°C but it seems not so much affected by the increase of temperature between 300°C and 400°C.

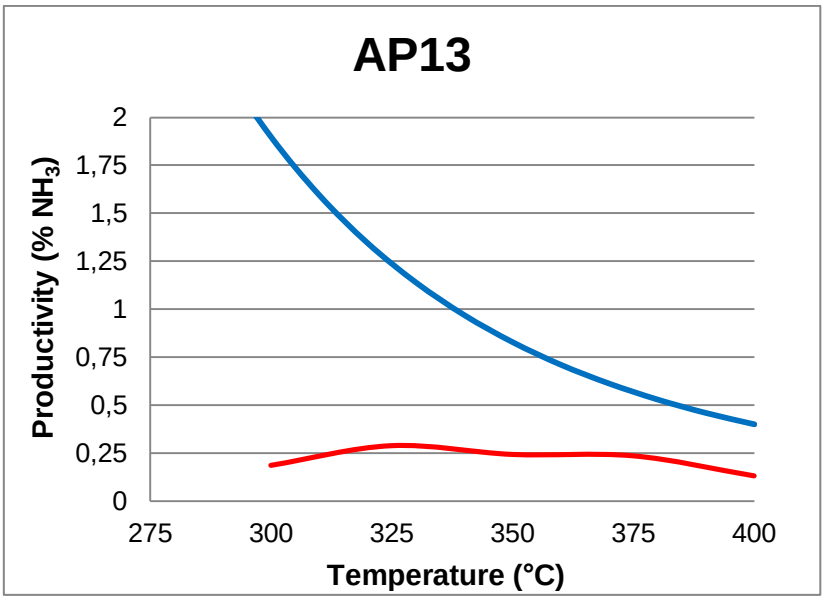

Graph 16.1: productivity of ammonia for AP13

However, by considering the absolute activity of AP13 (Graph 16.2) , the effect of temperature becomes more marked, with an hourly production of ammonia of 0.33 mmol/h per gram of catalyst at the optimal temperature of 325°C.

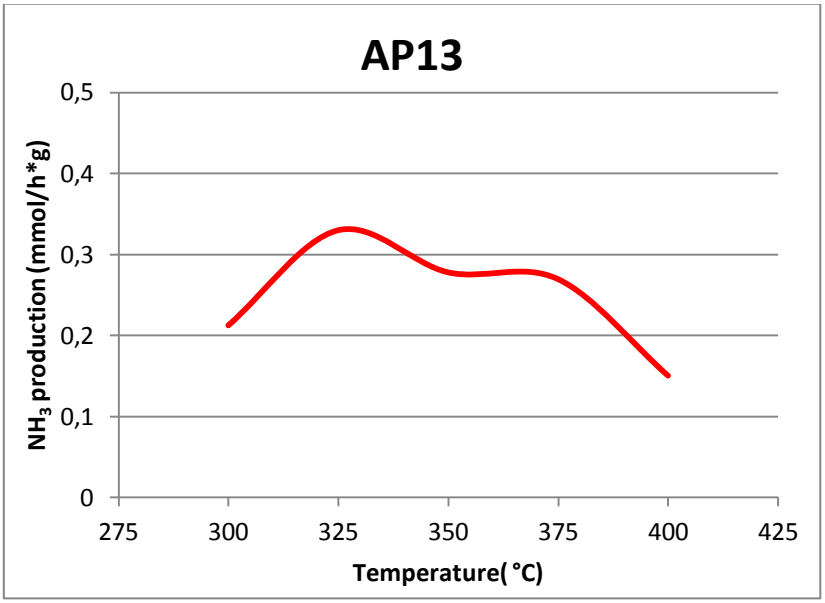

Graph 16.2: absolute production of ammonia for AP13

The productivity curve of AP14 (Graph 16.3) shows that the maximum is reached at 400°C, when the productivity curve is very close to the equilibrium curve.

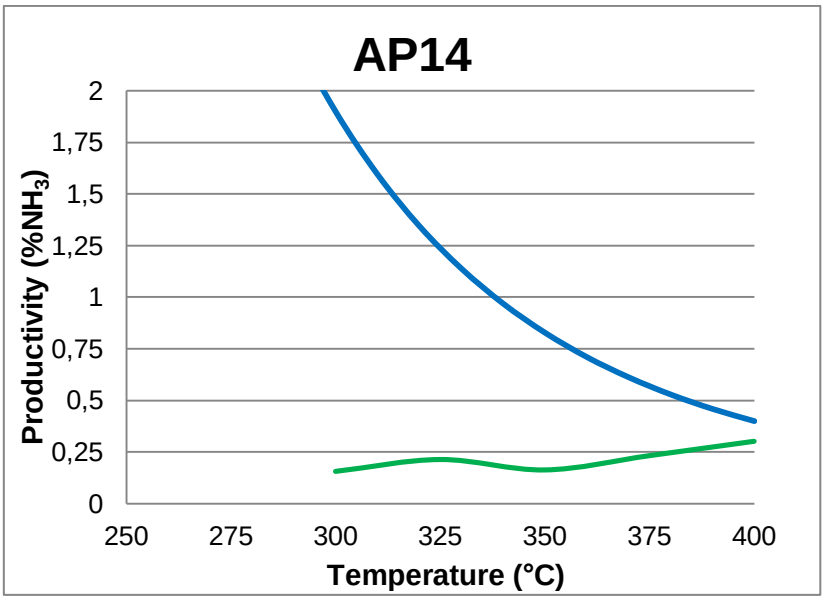

Graph 16.3: productivity of ammonia for AP14

For this catalyst the maximum of absolute ammonia production (Graph 16.4) is 0.4 mmol/h*g at 400°C. Surprisingly, this production results higher than that of AP13.

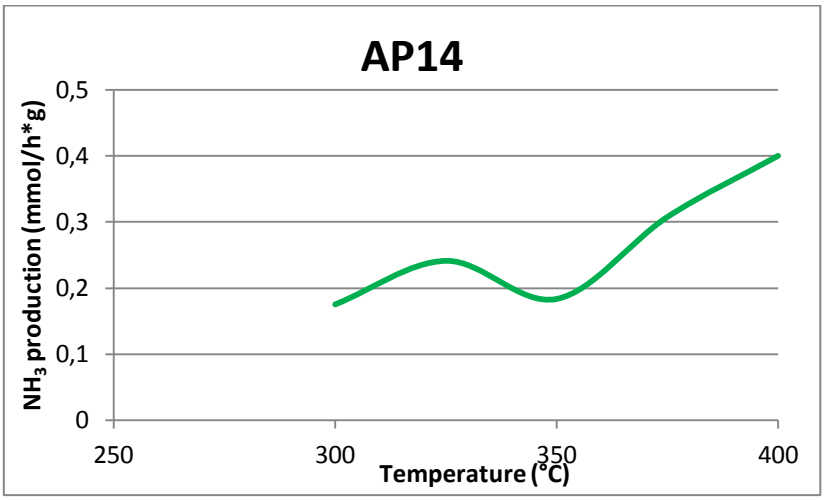

Graph 16.4: absolute production of ammonia for AP14

The last catalyst AP15 (Graph 16.5) shows a curve of ammonia productivity that seems similar to that for AP13.

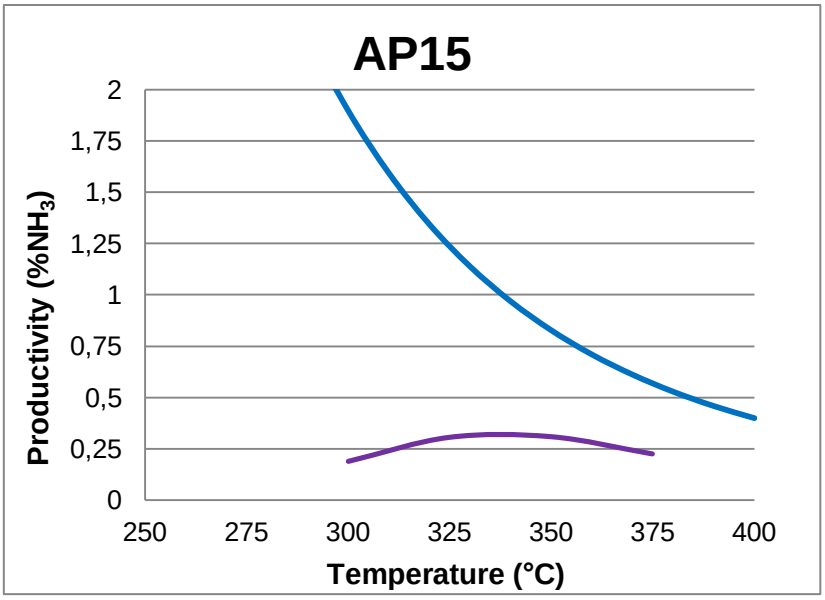

Graph 16.5: productivity of ammonia for AP15

In this case, the maximum production is reached at 350°C. The maximum of ammonia production is slightly higher than 0.35 mmol/h*g.

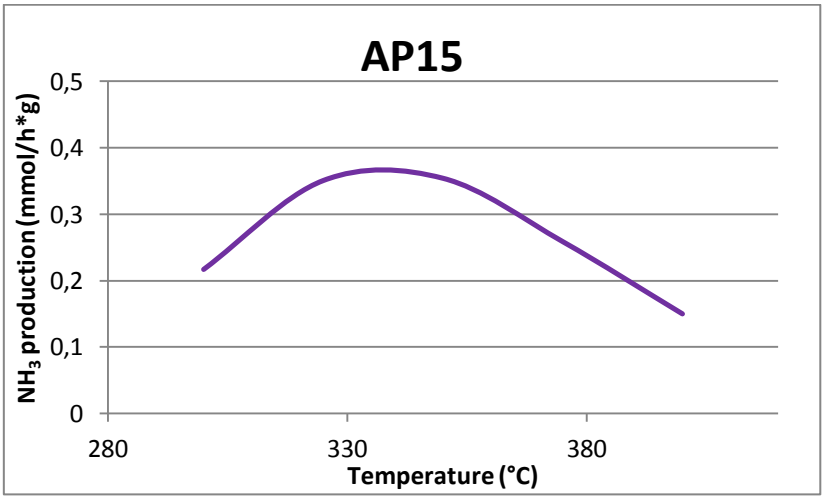

Graph 16.6: absolute production of ammonia for AP15

16.5 Conclusions

The characterizations, in particular the TGA analyses, show that in all cases the activation temperature of 400°C seems sufficient to decompose the precursors of the promoters. The XRD spectra confirm that, as expected, the structure of the catalysts is quite completely amorphous

and the IR spectra confirm the complete activation for all catalysts. Strange results are obtained from the surface area measurements by the B.E.T. method. The value of the surface area of the catalyst promoted with Cs is in the range expected, but the two other catalysts show discordant values. These differences between the observed and the expected data, as already seen, are probably due to the difference in the amount of water used in the gelification step during the sol-gel preparation of these catalysts. The sample AP15, containing Ba, consumes much more water than the other catalysts; the higher amount of water is associated to an higher rate of hydrolysis during the gelification process, that brings to the formation of a network with a lower porosity and, consequently, to a lower value of surface area. On the contrary, during the preparation of the sample AP14 it does not use water for the dissolution of $Li(CH_3COO)$. The gelification process proceeds accompanied by the release of an high amount of volatile compounds. These compounds, released during the thermal treatment, go across the walls of the catalyst particles, by inducing the higher porosity of the sample and the higher values of the surface area.

The results of the catalytic tests show, for all three catalysts, a very similar activity for the ammonia production. The productivity reaches maximum values included between 0.35 and 0.4 mmol/h per gram of catalyst. These values are not so high, as expected for a catalyst supported over alumina. In fact, the alumina was added to give more mechanical stability to the system, but it is known that the acid characteristics of this kind of support does not help the ammonia production. On the contrary, magnesia as basic support shows the opposite characteristics: lower mechanical resistance but higher chemical promotion of the active phase to favour the reaction mechanism involved bythe ammonia synthesis. About the promoters, we expected an increase of activity following the order:

Cs>Ba>Li

corresponding to an opposite order of the electronegativity values of the same elements.

However, this fact is not reflected by the ammonia productivity, since the lithium shows a little more productivity than the other alkaline promoters. The reason is probably in the fact that the alumina partially restrains the activity of all catalysts, then dampingthe role of promoters. Then, the higher activity observed for AP14 is simply connected to its higher surface area.

Bibliography

[1] L. Forni, D. Molinari, I. Rossetti, N. Pernicone; *Applied Catalysis A: General* ***1999.*** *185, 269*

[2] S. R Tennison in: J. R. Jennings (ED), **Catalytic ammonia synthesis**. Plenum Press, New York, 1991.

[3] D. Szmigiel, H. Bielawa, M. Kurtz, O. Hinrichsen, M. Muhler, W. Rarog, S. Jodzis, Z. Kowalczyk, L. Znak, J. Zielinski; *Journal of Catalysis* ***2002.*** *205, 205*

[4] D. Szmigiel, W. Raróg-Pilecka, E. Miskiewicz, M. Glinski, M. Kielak, Z. Kaszkur, Z. Kowalczyk; *Applied Catalysis A: General* ***2004.*** *273, 105*

[5] B. Fastrup; *Catal. Lett.* ***1997.*** *48, 111*

Chapter 17: Egg-shell catalysts

17.1 Introduction

In this chapter we want to evaluate the influence of alkaline promotion[1,2,3] in two catalysts prepared with the egg-shell method, by anchoring a shell of magnesia on a support of alumina[4,5], and to compare their activity with respect to a reference catalyst with the same chemical composition but with the structure of hydrotalcite[6]. The role of the alumina into the core is to give more mechanical stability to the system, while the role of magnesia in the shell is to improve the activity of ruthenium in the ammonia production. For this reason, two catalysts are prepared following the egg-shell method, both with the same composition of 2/1 (molar ratio) magnesium/aluminum, added as oxides in the supporting layers. The active phase is 5% by weight of ruthenium, promoted by an equal molar amount of cesium in the case of AP16 and of lithium in the case of AP17. AP18 is an hydrotalcitic material formed by charged layer of magnesium-aluminum hydroxides, bonded together by ions of ruthenium (added as ruthenium carbonate). Also the preparation procedure of this catalyst provides the impregnation with a solution of precursor of cesium. Table 17.1 summarizes the catalyst compositions.

SAMPLE	ACTIVE PHASE	SUPPORT	PROMOTER	PREPARATION
AP16	5% Ru	MgO/Al_2O_3	Cs	Egg-shell
AP17	5% Ru	MgO/Al_2O_3	Li	Egg-shell
AP18	5% Ru	MgO/Al_2O_3	Cs	Hydrotalcite

Table 17.1: method of preparation and precursors for these catalysts.

17.2 Preparation

AP16

The composition of the catalyst called AP16 is 5% Ru (weight) on a support of MgO/Al_2O_3 promoted with cesium at 1:1 molar ratio with respect to Ruthenium. This catalysts was prepared at a molar ratio between Mg and Al of 2/1. In order to obtain 2.15 g of Al_2O_3, 8.75 g of aluminum isopropoxide ($Al(iPrO)_3$) were dissolved in 175 ml of isopropyl alcohol. 4.6 ml of water were then

added drop by drop to favour the gelification. The gel was finally dried for a week. The obtained powder was used as core of the catalyst. A solution of 2.4 g of $Mg(OEt)_2$ dissolved in 21 ml of ethanol and 1.9 ml of water was added to the alumina powder. The mixture was refluxed for 3h. After cooling, a solution of 0.322g of $Ru_3(CO)_{12}$ dissolved in THF was added and the resulting mixture was left under stirring for 1h. Then, the solution of precursor, in this case 0.265 g of $Cs_2(COO)_2$ in 120 ml of ethanol and 6.75 ml of water was added. The system was maintained under stirring again for 1 h then it was left to gelify for 1 week. The powder obtained was finally dried at 60°C under nitrogen flow.

AP17

The preparation of this catalyst follows exactly the same steps of AP17, but a solution of 0.151 g of $Li(CH_3COO)$ dissolved in 6.7 ml of ethanol was added instead of that of the Cesium precursor.

AP18

AP18 is an hydrotalcitic material prepared by Dott. Maria Bastianini at the Università di Perugia. The molar ratio between Mg and Al is 2/1. The ruthenium was added at around 5% by weight. This hydrotalcite was impregnated with the solution of Cesium precursor.

17.3 Characterization

17.3.1 TPR profiles

The TPR profiles for the catalyst AP16 were collected before (FIG. 17.1) and after the activation treatment (FIG. 17.2). The fresh catalyst shows only a small peak with low intensity at 500°C. The activated catalyst shows indeed a weak peak at 300°C. This fact can be due to the type of preparation, in particular to the incorporation of precursors of ruthenium and cesium inside the magnesia gel, that makes more difficult their decomposition. For this reason, the activation steps occur at higher temperatures and the activation treatment performed at the usual temperature of 400°C cannot be sufficient to activate all the catalyst sample.

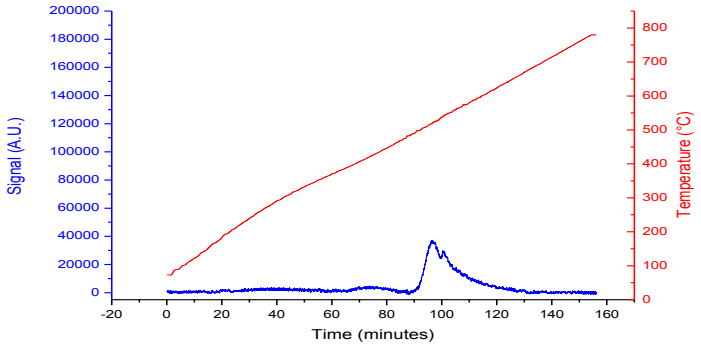

FIG. 17.1: TPR profile for unactived AP16

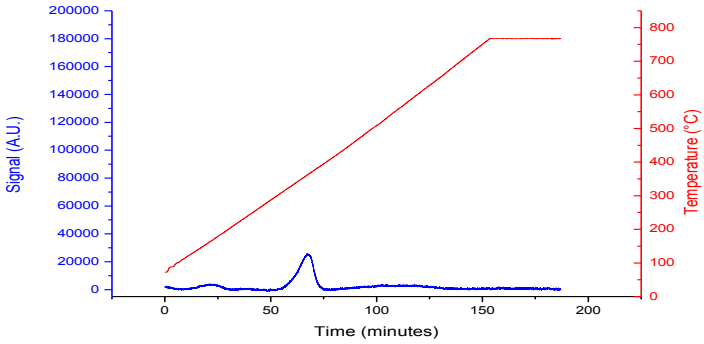

FIG. 17.2: TPR profile for actived AP16

The TPR profile of the unactivated catalyst AP17 (FIG. 17.3) shows only an intense and narrow peak, centered at 350°C, that is assignable to the interaction of hydrogen with the products originated from the decomposition of the precursor of the promoter, in this case the acetate groups CH_3COO-.

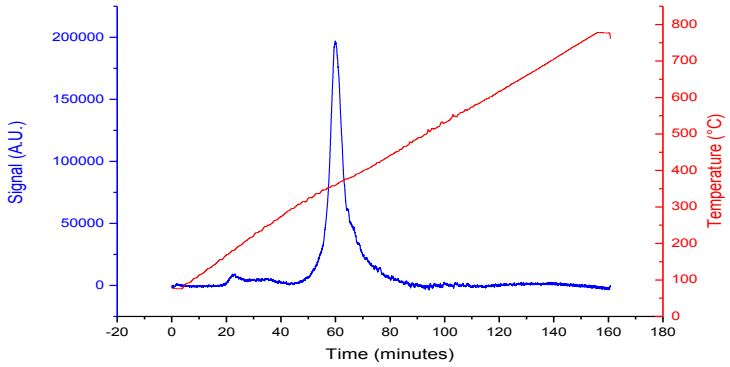

FIG. 17.3: TPR profile for unactived AP17

The analysis of the same catalyst after activation (FIG. 17.4) shows three little peaks of low intensity. These signals are also due to the interaction of hydrogen with products of degradation of species not totally decomposed during the activation procedure.

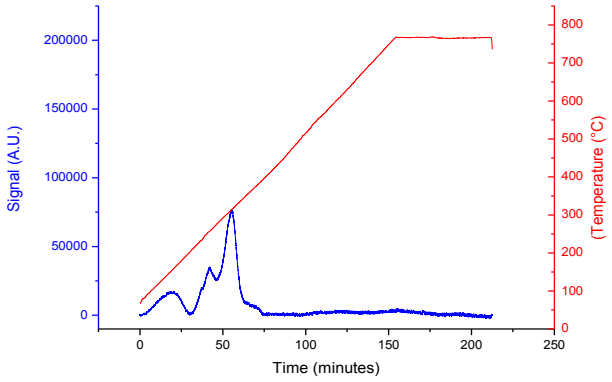

FIG. 17.4: TPR profile for actived AP17

The TPR profile of the catalyst AP18 (FIG. 17.5) shows an intense peak at 350°C. This peak can be originated by the interaction of hydrogen with the CO_2 released by the decomposition of cesium oxalate added as precursor of Cs.

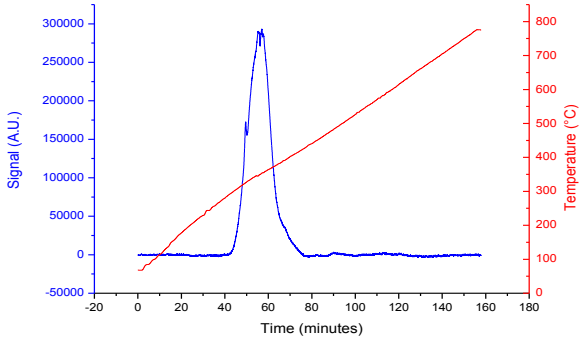

FIG. 17.5 TPR profile for unactived AP18

The TPR analysis of activated AP18 (fig17.6) does not show any peak. This fact is in agreement with a complete activation of the catalyst.

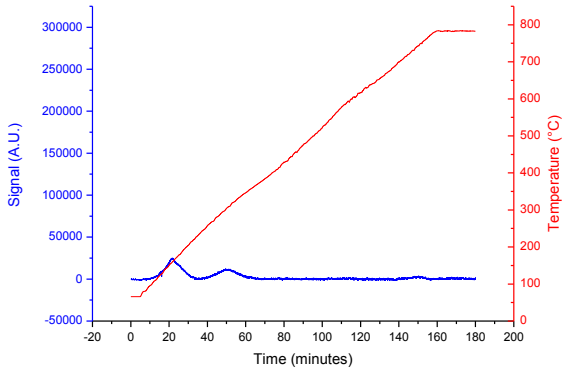

FIG. 17.6: TPR profile for actived AP18

17.3.2 Surface Area

The surface areas of the catalyst are reported in the table 17.2

SAMPLE	SURFACE AREA (m^2/g)
AP16	161
AP17	165
AP18	131

Table 17.2: surface area of the samples

17.3.3 XRD

The XRD spectra collected for the three catalysts (FIG. 17.7, 17.8 AND 17.9) after the activation treatment show that the structure is prevalently amorphous, with only very weak peaks at 2θ = 37°, 43°, 62° and 78° assignables to the periclase[7] form of MgO.

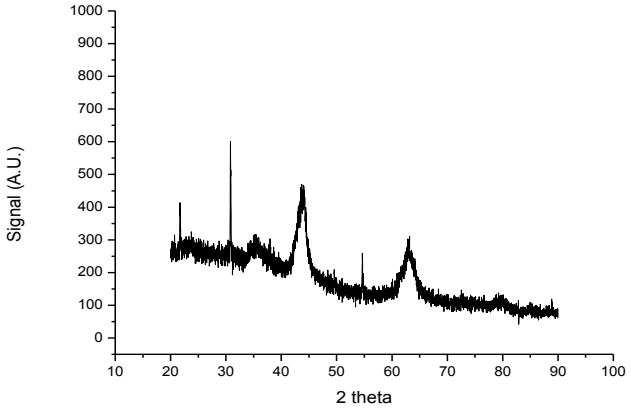

FIG. 17.7: XRD spectrum for AP16

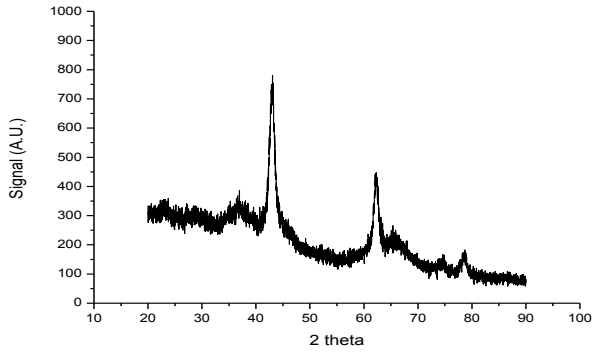

FIG. 17.8: XRD spectrum for AP17

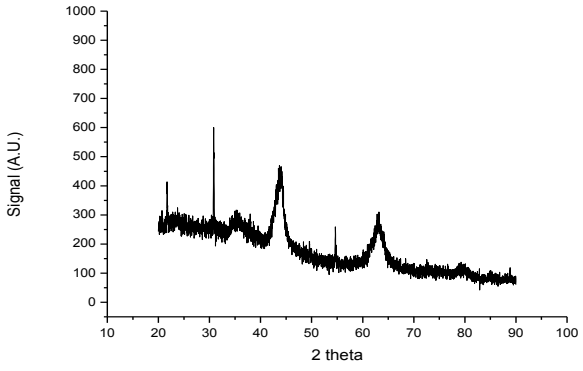

FIG. 17.9: XRD spectrum for AP18

17.3.4 FT-IR

The IR spectra were collected before and after activation (FIG. 17.10, 17.11 and 17.12). The blue lines, that refer to the fresh catalysts, show the usual peaks of water at 3500cm^{-1} and the peaks of precursors of the promoters at 1500 cm^{-1}. These peaks disappear after the activation step, but not completely in the case of AP17. The presence of residual signals means that the activation procedure is not totally performed.

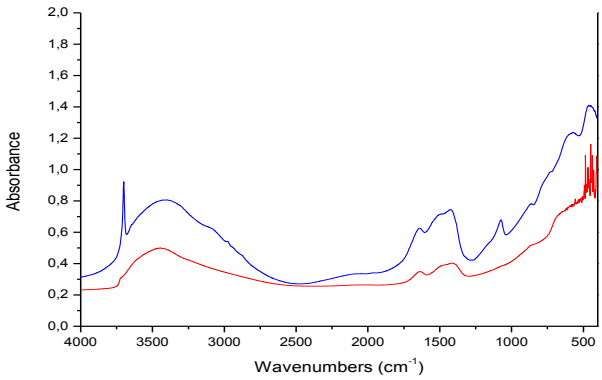

FIG. 17.10: IR spectra for AP16

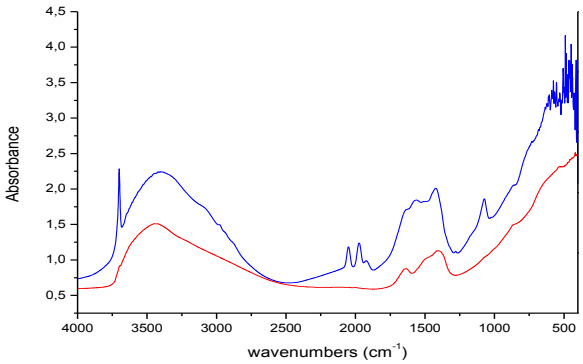

FIG. 17.11: IR spectra for AP17

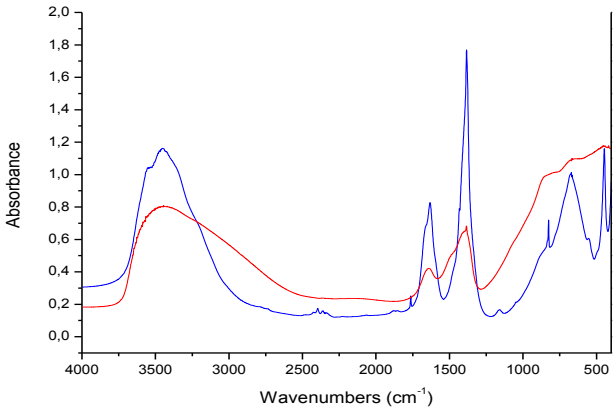

FIG. 17.12: IR spectra for AP18

17.3.5 SEM images

In the SEM images for AP16 (FIG. 17.13), it can be observed the aggregation of spherical particles sized in the range of 10 – 20 nm. The EDX analysis shows values that are different from the expected ones (Al = 34%, Mg = 15%, Ru = 4%, O = 41%). This fact is due to the dishomogeneity usually observed in all catalysts prepared by the sol-gel method.

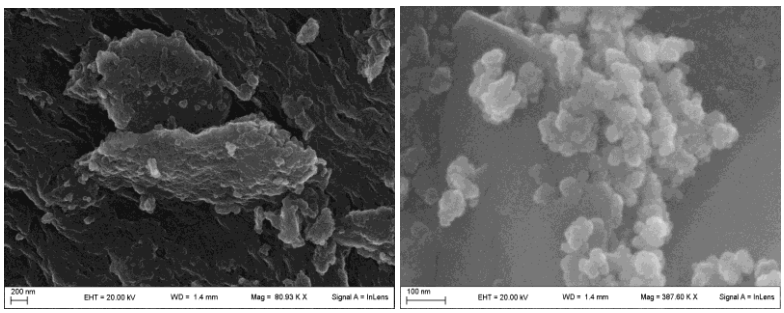

FIG. 17.13: SEM images AP16

The SEM images of AP17 (FIG. 17.14) are very similar to that of AP16. Also in this case, the shape and the size of particles are identical to the previous ones. The dishomogeneity is present also for this catalyst, that gives EDX values quite different from the expected ones.

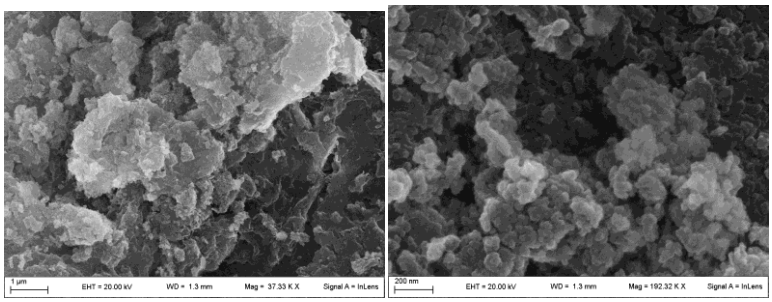

FIG. 17.14: SEM images AP17

From the SEM images collected for the catalyst AP18 (FIG. 17.15), the lamellar structure, typical of hydrotalcite, can be observed. Furthermore, the EDX analysis gives data very similar to the theoretical ones. This means that, in this case, the structure of catalyst is very homogeneous.

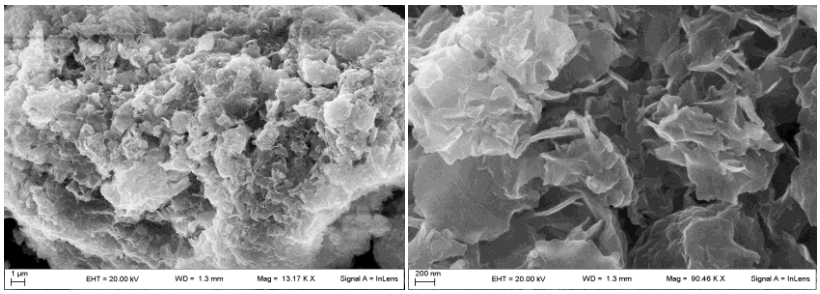

FIG. 17.15: SEM images AP18

17.4 Catalytic tests

The catalytic tests were done in the plant at atmospheric pressure. 1 g of catalyst was charged for each test into the microreactor. The gas was fed at 40 ml/min, with a 3/1 molar ratio between hydrogen and nitrogen.

The ammonia produced was collected in the traps containing hydrochloric acid at known concentration and it was determined by the usual method described for the other cases.

The results obtained for the different catalysts are reported in the following graphs (Graph 17.1, 17.2, 17.3, 17.4, 17.5 and 17.6). The graphs show a similar behaviour for all catalysts: they give the maximum value of absolute productivity of ammonia between 0.30 and 0.35 mmol/h per gram of catalyst. The egg-shell catalyst promoted with Cs shows the highest ammonia production at 375°C, while the Li-promoted catalyst at 325°C and the hydrotalcitic catalyst at 350°C.

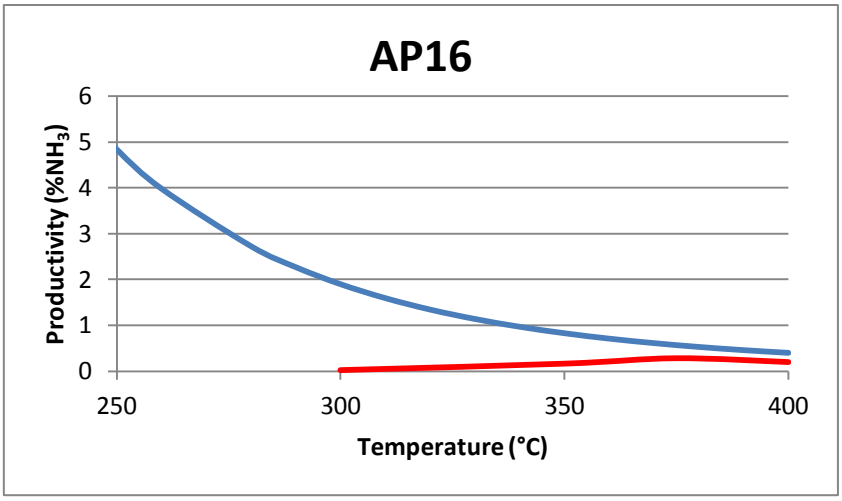

Graph 17.1: productivity of ammonia for AP16

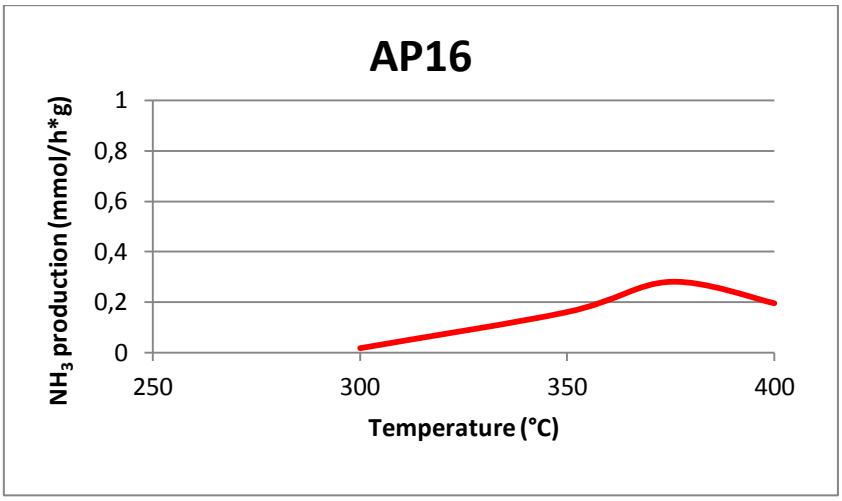

Graph 17.2: absolute production of ammonia for AP16

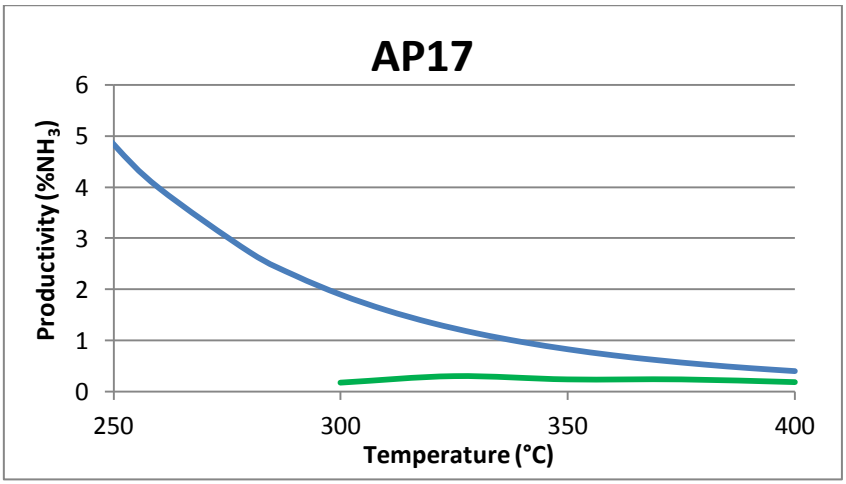

Graph 17.3: productivity of ammonia for AP17

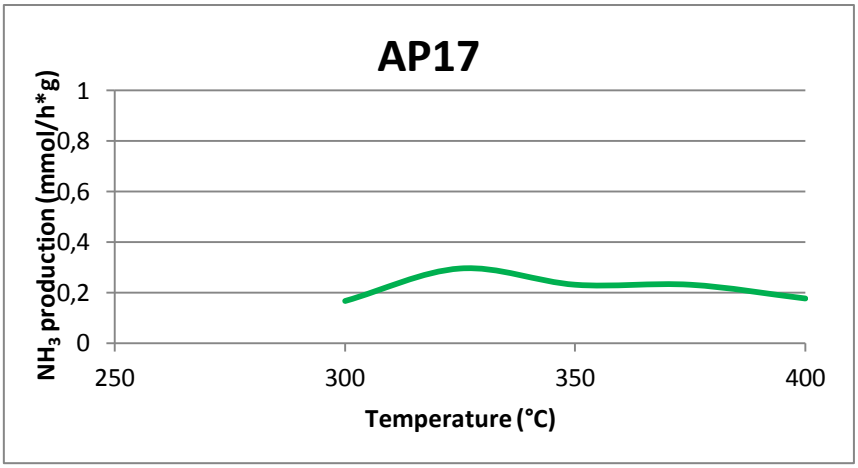

Graph 17.4: absolute production of ammonia for AP17

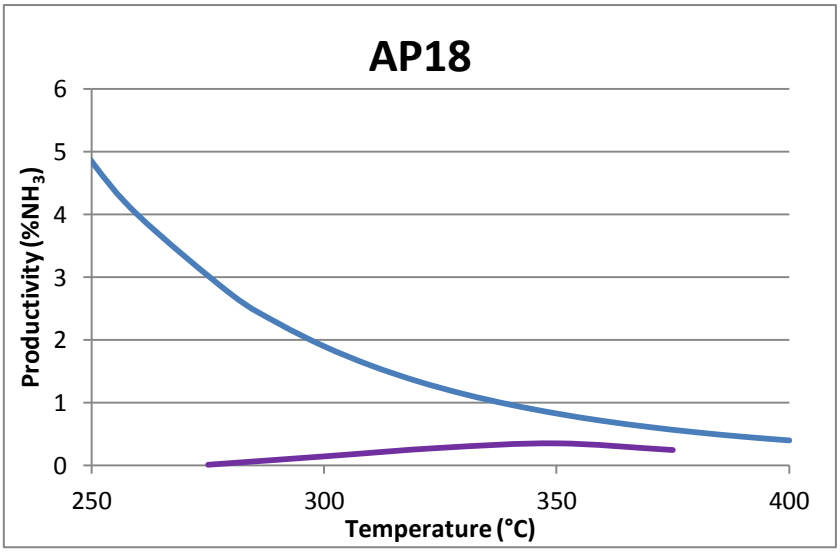

Graph 17.5: productivity of ammonia for AP18

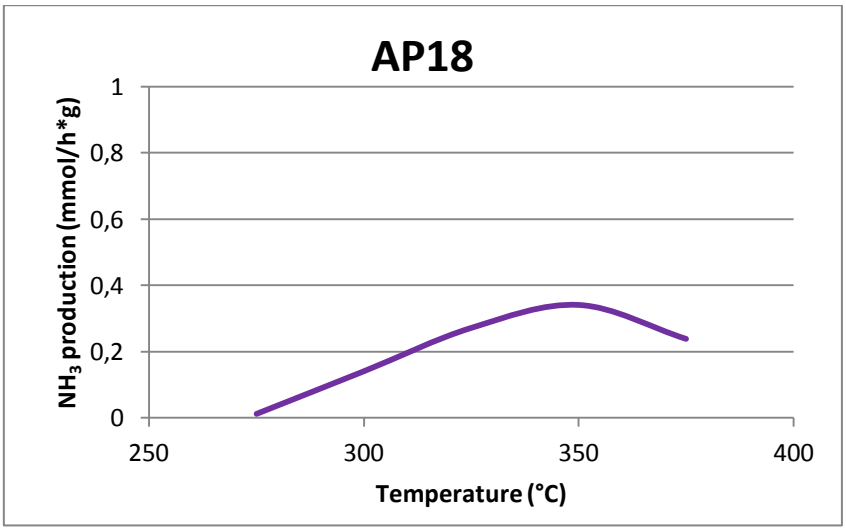

Graph 17.6: absolute production of ammonia for AP18

17.5 Conclusions

The tested catalysts show quite poors results. This could be expected because the use of alumina as support really gives to the catalytic systems more mechanical resistance but it affects negatively the catalytic behaviour.

The values of the surface area are strongly affected by the presence of alumina in the core, because they are higher than those for magnesia alone. The XRD patterns show prevaingly amorphous structures with some small peaks assignable to the presence of periclase as the stable form of magnesia. That is noteworthy for the hydrotalcitic material that was initially obtained from the brucite form .

Despite the catalytic tests do not show high activities, the general behaviour is interesting because the egg-shell catalysts show values of conversion overlapping with those of hydrotalcite. This means that this more simple method of preparation gives comparable results with other onesmore complicated. Furthermore, this method allows to combine different structures for the support of the catalysts, by tuning their different advantages, such as the promoting effect of basic magnesia of the shell with the better mechanical resistance of alumina used only as core.

Bibliography

[1] L. Forni, D. Molinari, I. Rossetti, N. Pernicone; *Applied Catalysis A: General* ***1999.*** *185, 269*

[2] S. R Tennison in: J. R. Jennings (ED), Catalytic ammonia synthesis. Plenum Press, New York, 1991.

[3] D. Szmigiel, H. Bielawa, M. Kurtz, O. Hinrichsen, M. Muhler, W. Rarog, S. Jodzis, Z. Kowalczyk, L. Znak, J. Zielinski; *Journal of Catalysis* ***2002.*** *205, 205*

[4] D. Szmigiel, W. Raróg-Pilecka, E. Miskiewicz, M. Glinski, M. Kielak, Z. Kaszkur, Z. Kowalczyk; *Applied Catalysis A: General* ***2004.*** *273, 105*

[5] B. Fastrup; *Catal. Lett.* ***1997.*** *48, 111*

[6] P. Seetharamulu, V. S. Kumar, A.H. Padmasri, B. D. Raju, K. S. Rama Rao; *Journal of Molecular Catalysis A: Chemical* ***2007.*** *263, 253*

[7] M. A. Aramendia, J. A. Benitez, V. Borau, C. Jiménez, J. M. Marinas, J. R. Ruiz, F. Urbano; *Langmuir* ***1999.*** *15, 1192*

General remarks

By regarding the results obtained for the Fischer-Tropsch catalysts, we can generally observe that silica-supported catalysts show higher activities than the others. Alumina and titania supports procure good mechanical properties to the catalysts, but the chemical characteristics are lower than with silica. Also the selectivity to desired products (higher hydrocarbons) is higher with silica as support. In particular, the use of titania resulted very low attractive, also for its ability to favour the formation of CO_2 instead of the conversion of CO to hydrocarbons.

The catalysts prepared by our egg-shell method are very active and interesting. This method of preparation of solid catalysts is very promising for several reasons. The most important are the practicality of the technique, the large amount of active phase dispersed only at the surface of the catalyst and not inside its bulk and the capability to combine different properties deriving from the core and from the shell of the structure. These abilities are confirmed by the increase of the catalytic activity and of the selectivity to higher hydrocarbons for the egg-shell catalysts with respect to the others. The case of titania as core is typical: the catalytic system shows a good level of activity at temperatures 50°C below when a shell of silica is used to include the active phase. In the case of the use of clusters as precursors of the active phases, and more particularly when cobalt carbonyl is used, the results are the best and become interesting also from an industrial point of view. The observed deactivation of the catalyst due to the formation of waxes inside the pores of its surface could be easily avoided by using a different type of reactor, such as the slurry bed or slurry bubble column reactor.

In the case of the ammonia synthesis, the most active catalyst is resulted that formed by Ruthenium and Cobalt as active phases, supported on carbon nanofibers. However, the use of magnesia as support also gives excellent results nevertheless its poorer mechanical properties. This fact can be corrected by the addition of another supporting material, but titania and alumina cause in this case a strong decrease of the catalytic activity.

Also in this case the egg-shell method can help to obtain catalysts with higher performances, resulting from the synergy between the core and the shell components. The relative amount between these two phases must be yet optimized, and these preliminary studies give a good perspective for further developments.

Finally, we can conclude that our egg-shell technique is a very promising method for the preparation of catalysts based on dispersed metals as the active phase, that gives good results coming from the capability to combine different characteristics by a simple, cheap and easily modifiable method of preparation.

Ringraziamenti

Desidero ringraziare il prof. Moggi Pietro per l'opportunità che mi ha dato; desidero ringraziarlo per la sua disponibilità, la sua competenza e il suo aiuto in ogni fase del lavoro.

Grazie al prof. De Villers e alla prof.ssa Sofie Hermans per avermi accolto ed ospitato nel loro laboratorio di chimica inorganica all'Université Catholique de Louvain-la-Neuve.

Ringrazio il gruppo del prof. Calestani, in particolar modo nella figura della sig.ra Roberta Magnani, per gli spettri XRD.

Un ringraziamento è doveroso anche al Dott. Alessandro Di Michele per le microscopie elettroniche.

Desidero anche ringraziare il gruppo di spettroscopia molecolare del dipartimento di Chimica dell'Università degli Studi di Perugia per l'aiuto negli spettri IR.

Voglio anche salutare quanti in questi anni sono stati miei " compagni di viaggio": Andrea, Fabio, Khalid, Emanuele, Giacomo, Viola, Davide, Nicola, Valentina, Marzia, Niccolò, Elia.

I più grandi ringraziamenti vanno alla mia famiglia che mi ha sempre sostenuto e ad Alessandra, che oltre che sostenermi mi ha aiutato e soprattutto sopportato.

Grazie.